Physiologically-Based Kinetics and Mechanistic Models to Assess Exposure to Chemicals

Julia Pletz

A thesis submitted in partial fulfilment of the requirements of Liverpool John Moores University for the degree of Doctor of Philosophy

January 2020

Acknowledgements

First and foremost, I would like to thank my Director of Studies, Prof. Mark Cronin, for supporting me to obtain the studentship from Liverpool John Moores University, his continuous support and guidance throughout the course of my doctoral studies and for facilitating my attendance at the Lorentz@Snellius Center workshop on e-Resources to Revolutionise Toxicology: Linking Data to Decisions in October 2019.

I would also like to express my deep gratitude to my supervisor Dr. Steven Webb for his generous academic guidance and dedicated support in mathematical modelling, for connecting me to his group of researchers (Webb Lab UK) and facilitating my meeting and fruitful discussion with to Drs. Iain Gardner and Sibylle Neuhoff at Certara.

In addition, I would like to extend my sincere gratitude to my supervisor Dr. Judith Madden for her invaluable input on my research and research communication materials. Nothing escapes her eagle eye.

I would also like to thank Mark and Judith for their encouragement to do a traineeship at the European Commission Joint Research Centre (JRC) in Ispra (Italy), Drs. Stephanie Bopp, Alicia Paini, Nikolaos Parissis and Andrew Worth for their supervision and guidance at the JRC as well as Samantha Blakeman for working with me on the study presented in Chapter 2. My time at the JRC was very inspiring! In the context of this work, we thank the Norwegian Institute for Public Health (especially Catherine Thomsen and Amrit Kaur Sakhi) and the Danish Rigshospitalet, Department of Growth and Reproduction (especially Anna-Maria Andersson; Hanne Frederiksen; Tina Kold Jensen; Katharina Main) for providing the Human Biomonitoring Data used in this study; and Lara Lamon (European Commission Joint Research Centre) for helping to harvest the information on the EDI and TDI in an early stage of this work. Finally, with much appreciation, we would like to thank John F. Wambaugh (US EPA) for providing the Httk model and introducing the model characteristics.

I would also like to thank all of my colleagues at the Chemoinformatics Research Group at Liverpool John Moores University, in particular Drs. David Ebbrell, James Firman and Steve Enoch for helping me to clarify chemistry-related questions, and Dr. Maria Sapounidou, Nicoleta Spinu, Sam Belfield, Antiopi Politi and Michele Assante for the fun and personal enrichment.

I greatly appreciate the studentship provided by Liverpool John Moores University without which this research would not have been possible.

Final thanks go to Drs. Henk Tennekes and Ester Lovšin Barle for encouraging and guiding me in my early years as a toxicologist, my family, capoeira family and friends for their continuous love and positivity.

Abbreviations

3Rs	Replacement, Reduction and Refinement
A_{ABS}	Amount Absorbed from an ACAT Model Compartment (e.g. $A_{ABS(ST)}$ representing the amount absorbed from the stomach lumen compartment)
A_{DEG}	Amount Degraded in an ACAT Model Compartment (e.g. $A_{DEG(ST)}$ representing the amount degraded in the stomach lumen compartment)
A_{DIS}	Amount Dissolved in an ACAT Model Compartment (e.g. $A_{DIS(ST)}$ representing the amount dissolved in the stomach lumen compartment)
A_{UND}	Amount Undissolved in an ACAT Model Compartment (e.g. $A_{UND(ST)}$ representing the amount undissolved in the stomach lumen compartment)
ACAT	Advanced Compartmental Absorption and Transit
ACE	Angiotensin-Converting Enzyme
ACO	Ascending Colon Lumen
AD	Adipose Tissue
ADI	Acceptable Daily Intake
ADME	Absorption, Distribution, Metabolism, Excretion
AKI	Acute Kidney Injury
AO	Adverse Outcome
AOP	Adverse Outcome Pathway
AOP-KB	AOP Knowledge Base
AR	Arterial Blood
ARB	Angiotensin Receptor Blocker
ASA	Aspirin
ATP	Adenosine Triphosphate
BBzP	Butylbenzyl Phthalate
BCL	B-Cell Lymphoma
BE	Biomonitoring Equivalent
BE_{EDI}	Biomonitoring Equivalent based on the EDI
BE_{RfD}	Biomonitoring Equivalent based on the RfD
BE_{TDI}	Biomonitoring Equivalent based on the TDI
BEI	Biological Exposure Index

BL	Bladder
BMA	Bayesian Model Averaging
BMD	Benchmark Dose
BMI	Body Mass Index
BP-3	Benzophenone-3
BPA	Bisphenol A
BPA-glu	Bisphenol A Glucuronide
BR	Brain
BW	Body Weight
C_T	Concentration in Compartment T (e.g. C in the lung translates to C_{LU} or C of the arterial blood to C_{AR})
CAE	Caecum Lumen
CD	Collecting Duct (divided into two sections, CD1-2)
CDB	Collecting Duct Blood (divided into two compartments, CDB1-2)
CDC	Collecting Duct Cells (divided into two compartments, CDC1-2)
CDL	Collecting Duct Lumen (divided into two compartments, CDL1-2)
CEFIC	European Chemical Industry Council
CKD	Chronic Kidney Disease
CL_{hep}	Hepatic Clearance
C_{max}	Maximum Concentration
COX	Cyclooxygenase
CP	Constant representing Conversion from a Metabolite back to Parent
D	Diffusion Coefficient
DDI	Drug-Drug Interactions
DEG	Degraded Amount in an ACAT Compartment (see A_{DEG})
D_{extCC}	External Diameter of the Cellular Compartment (PTC1, PTC2, PTC3, DTC, CDC1, CDC2)
DIS	Dissolved Amount in an ACAT Compartment (see A_{DIS})
D_{LC}	Diameter of luminal compartment of the Henle's loop
DnBP	Di-n-Butyl Phthalate
DUO	Duodenum Lumen
DT	Distal Tubule

DTB	Distal Tubular Blood
DTC	Distal Tubular Cells
DTL	Distal Tubular Lumen
ECVAM	European Centre for the Validation of Alternative Methods
EDI	Estimated Daily Intake
EFSA	European Food Safety Authority
EHR	Enterohepatic Recirculation
EMA	European Medicines Agency
ER	Endoplasmic Reticulum
EtP	Ethyl Paraben
EURL	European Union Reference Laboratory
FAO	Food and Agriculture Organisation of the United Nations
FF_{PT}	Fluid Flow Leaving the Glomerular Space and Proximal Tubules
FF_{HL}	Fluid Flow Leaving the Loop of Henle
FF_{DT}	Fluid Flow Leaving the Distal Tubules and Collecting Ducts
FQ_T	Fractional Tissue Blood Flow in Compartment T (e.g. FQ in the lung translates to FQ_{LU})
$f_{u(p)}$	Fraction Unbound in Plasma
G	Glomerulus
GB	Glomerular Blood
GER	Gastric Emptying Rate
GFR	Glomerular Filtration Rate
GIT	Gastrointestinal Tract
Glucs	Glucuronides
GS	Glomerular Space
GSH	Glutathione
GU	Gut
HA	Hepatic Artery
HBM	Human Biomonitoring
H_{cc}	Height of Cells in the Cellular Compartment (PTC1, PTC2, PTC3, DTC, CDC1, CDC2)
HE	Heart

HI	Hazard Index (for an individual i, i.e. HI(i))
HL	Henle's Loop
HLB	Henle's Loop Blood
HLC	Henle's Loop Cells
HLL	Henle's Loop Lumen
hOAT	Human Organic Anion Transporter
Httk	High-Throughput Toxicokinetics
ICF	IndusChemFate
ICH	International Conference on Harmonisation
IL	Interleukin
IL1/IL2/IL3	Ileum 1 Lumen / Ileum 2 Lumen / Ileum 3 Lumen
IPCS	International Programme of Chemical Safety
IV	Intravenous
IVIVE	*In Vitro* to *In Vivo* Extrapolation
JE1/JE2	Jejunum 1 Lumen / Jejunum 2 Lumen
J_{max}	Maximum Rate of Transport or Flux via a Transporter Protein
k_a	Absorption Rate Constant, with Specific Rates in Stomach ($k_{a(ST)}$) and Gut ($k_{a(GU)}$)
$k_{a\ ACAT}$	Absorption Rate Constant Considering the Paracellular Absorption Rate Constant ($k_{a,p}$) in a specific ACAT compartment
$k_{a,p}$	Paracellular Absorption Rate Constant in an ACAT compartment (e.g. $k_{a,p}$ in the stomach lumen is represented by $k_{a,p,STL}$)
$k_{AT(T)}$	Rate of Active Transport via Transporter Protein T
k_{bil}	Biliary Elimination Rate Constant
K_D	Dissolution Rate Constant
KE	Key Event
$k_{e(r)}$	Renal Elimination Rate Constant
k_{il}	Intestinal Loss Rate Constant
KI	Kidney
KIM	Kidney Injury Molecule
K_m	Michaelis-Menten Constant
$k_{MET(M,i)}$	Rate of Metabolism Forming Metabolite M in Compartment i

K_p	Tissue Partition Coefficient
k_{PT}	Rate of Passive Diffusion
$K_{p,u(T)}$	Unbound Tissue Partition Coefficient in a Tissue T
K_S	Solubility Coefficient corresponding to an ACAT compartment (e.g. K_S in the stomach lumen is represented by $K_{S(STL)}$)
K_t	Transit Rate in Small Intestine ($K_{t(GU)}$) and Colon ($K_{t(CO)}$)
L_c	Length of the Cylinder
L_{CC}	Length of Cellular Compartment (PTC1, PTC2, PTC3, DTC, CDC1, CDC2)
LCN-2	Lipocalin 2
LI	Liver
LRI	Long Range Research Initiative
LU	Lung
MBzP	Monobenzyl Phthalate
MeP	Methyl Paraben
MIE	Molecular Initiating Event
MnBP	Mono-n-Butyl Phthalate
MoA	Mode of Action
MPPGK	Microsomal Protein Per Gram of Human Kidney
MPT	Mitochondrial Permeability Transition
MRA	Mixture Risk Assessment
MSE	Mean Squared Error
MU	Muscle
MW	Molecular Weight
n-BuP	n-Butyl Paraben
n-PrP	n-Propyl Paraben
NGAL	Lipocalin 2
NHANES	National Health and Nutrition Examination Survey
NO	Nitric Oxide
NSAID	Nonsteroidal Anti-Inflammatory Drug
OAT	Organic Anion Transporter
OCT	Organic Cation Transporter

ODE	Ordinary Differential Equation
OECD	Organisation for Economic Co-operation and Development
OEL	Occupational Exposure Limit
Oxy	Oxybenzone
p	Particle Density
PA	Pancreas
P_{app}	Apparent Permeability
PBBK	Physiologically-Based Biokinetic
PBK	Physiologically-Based Kinetic
PBPK	Physiologically-Based Pharmacokinetic
PBTK	Physiologically-Based Toxicokinetic
$P_{diff,u}$	Unbound Passive Diffusion Clearance
P_{eff}	Effective Permeability
PK/PD	Pharmacokinetic-Pharmacodynamic
POD	Point of Departure
PT	Proximal Tubules (divided into three sections, PT1-3)
PTB	Proximal Tubular Blood (divided into three compartments, PTB1-3)
PTC	Proximal Tubular Cells (divided into three compartments, PTC1-3)
PTCPGK	Proximal Tubular Cells Per Gram of Kidney
PTL	Proximal Tubular Lumen (divided into three compartments, PTL1-3)
Q_T	Blood Flow in Compartment T (e.g. Q in the lung translates to Q_{LU})
Q_{HL-CD2}	Blood Flow in Loop of Henle and Collecting Ducts
QC	Cardiac Output
QSAR	Quantitative Structure-Activity Relationship
QSPR	Quantitative Structure-Property Relationship
r	Particle Radius
R	Blood to Plasma Concentration Ratio
R_1	Outer Radius of a Cylinder
R_2	Radius of the Hollow Part of a Cylinder
RAF	Relative Activity Factor
RAS	Renin-Angiotensin System

REACH	Registration, Evaluation, Authorisation and restriction of Chemicals
REF	Relative Expression Factor
RfD	Reference Dose
RMSE	Root Mean Squared Error
ROS	Reactive Oxygen Species
RQ	Risk Quotient (for an individual i at a chemical concentration j, i.e. RQ(ij)
S	Solubility
SA	Salicylic Acid
SAR	Structure-Activity Relationship
SK	Skin
SP	Spleen
ST	Stomach
STL	Stomach lumen
SU	Salicyluric Acid
TCS	Triclosan
TCS-glu	Triclosan Glucuronide
TDI	Tolerable Daily Intake
TH	Thymus
UND	Undissolved amount in an ACAT compartment (see also A_{UND})
U.S. EPA	U.S. Environmental Protection Agency
U.S. FDA	U.S. Food and Drug Administration
V_c	Volume of a Hollow Cylinder
V_{CC}	Volume of the Cellular Compartment (V_{PTC1}, V_{PTC2}, V_{PTC3}, V_{DTC}, V_{CDC1}, V_{CDC2})
VE	Venous Blood
V_{LC}	Volume of Luminal Compartment (V_{PTL1}, V_{PTL2}, V_{PTL3}, V_{DTL}, V_{CDL1}, V_{CDL2})
V_{max}	Maximum Rate of Metabolism
V_T	Volume in a Particular Tissue Compartment T (e.g. V of the lung translates to V_{LU} or V of the arterial blood to V_{AR})
WHO	World Health Organisation

Abstract

In our modern society we are exposed to a myriad of chemical substances. Before these substances can be brought onto the market for use and consumption, their safety – when used as intended – needs to be confirmed in a risk assessment. Typically, a risk assessment comprises a toxicological hazard assessment, the quantification of a dose-response relationship, an exposure assessment and a risk characterisation under the assessed conditions. Traditionally, a toxicological hazard assessment is performed *in vivo* in laboratory animals, and more recently, in targeted *in vitro* testing. However, due to calls for replacement, reduction and refinement of animal testing alternative methods such as *in silico* models are increasingly being used. Also, increasing emphasis is being placed on understanding mechanisms and pathways of toxicity as well as quantifying exposure which leads to an adverse effect in individuals. Physiologically-based kinetic and mechanistic models allow for a mathematical description of causal relationships between an exposure scenario and a toxicological outcome in a biological system.

While much research has been focussed on investigating mechanisms of hepatotoxicity, little is known about adverse effects induced in the kidney and only limited computational models exist to investigate nephrotoxicity. However, the kidney is a major target for toxicity by pharmaceuticals and environmental pollutants. Accumulation is known to play an important role in certain nephrotoxicity pathways. Therefore, physiologically-based kinetic and mechanistic models are considered to offer valuable insights into mechanisms of nephrotoxicity.

This thesis addresses the growing attention given to exposure-based and toxicokinetics-driven toxicity which has resulted in increasing recent application of PBK modelling. The overall aim of this thesis was to propose novel ways to use publicly available data for the quantitative assessment of adverse effects induced in the kidney following chemical exposure. The first part of this thesis examines the suitability of publicly available PBK models for the prediction of urine-level concentrations in the general population following oral doses of various chemicals. Human biomonitoring (HBM) data were used for validation of simulation results and a mixture risk assessment to illustrate how predictions may be used in a risk assessment context. The second part of this thesis shows the development of a

mechanistic kidney model embedded in a full-body PBK model parameterised for aspirin (ASA) and salicylic acid (SA). The research presented herein demonstrates the generation of a novel kidney model which is set up for a young and healthy individual; this was amended to simulate kinetics of elderly individuals and tested for three exposure scenarios. Key challenges in this endeavour revolve around limited data available in the public literature and uncertainties related to scaling *in vitro* data to an *in vivo* setting.

Table of Contents

1.0 INTRODUCTION

1.1 Renal toxicity: a major chemical safety issue

Acute renal failure in critically ill patients, as well as those with chronic kidney disease, was related to drug therapy in about 20% and 35% of cases reported respectively (Mehta et al., 2004; Uchino et al., 2005; Zhang et al., 2005). As a result of such toxicity, six prescription drugs (beta-ethoxy-lacetanilanide, bucetin, phenacetin, suprofen, thiobutabarbitone and zomepirac) were withdrawn from the market between 1983 and 1993, at great cost, due to renal adverse events, solely or in combination with other adverse effects (Fung et al., 2001). Therefore, eliminating drug candidates which cause these adverse effects at early stages of drug design is extremely important to ensure patient safety. However, despite its importance for drug development and for many other industrial sectors, nephrotoxicity is a complex endpoint and often occurs gradually or as a complication related to other pathologies such as diabetes (Zaza et al., 2015) and hypertension (Folli et al., 2010), thus making it difficult to identify even with sophisticated toxicity testing or clinical trials.

In drug research and development, established approaches to identify kidney toxicants have traditionally relied on extensive animal testing. However, the "Toxicity Testing in the 21st Century" paradigm calls for use of alternative testing strategies (National Research Council, 2007). Computational approaches such as (quantitative) structure-activity relationships ((Q)SARs)[1] and structural alerts are currently used to predict a variety of organ toxicities e.g. for hepatic toxicity (Przybylak and Cronin, 2012). In recent years, much emphasis has been placed on understanding the underlying mechanisms of liver toxicity which have led to the development of several Adverse Outcome Pathways (AOPs)[2], many structural alerts and QSARs (Przybylak and Cronin, 2012; Hewitt and Przybylak, 2016; Cronin and Richarz, 2017). The relative progress of the development of alternatives to identify liver toxicants has demonstrated that success can be achieved and it is possible to address other organ level toxicity in a similar manner. Thus, there is a growing movement to investigate

[1]In this thesis, (Q)SAR will be mentioned if both SAR and QSAR are referred to while SAR and QSAR refer to either approach specifically.

[2]An AOP is a conceptual framework that organises scientific knowledge into a sequence of causally linked key events between a molecular initiating event (MIE) and an adverse outcome (AO) which occur at molecular, cellular, organ/tissue, organism and population levels. AOPs are becoming central elements of chemical risk assessment (Ankley et al., 2010; OECD, 2019).

these approaches with reference to other important organs in the body in order to reach the ultimate goal of mapping the toxicological pathways of pharmaceuticals, cosmetics and other chemicals within humans (Sturla et al., 2014).

The kidney is a major target for toxicity elicited by pharmaceuticals but also environmental pollutants. Approximately 20% of acquired acute kidney injury (AKI) cases are associated with the use of drugs (Naughton, 2008). Being burdened with multiple comorbidities, the average patient tends to take several medications which may cause kidney injury (Farooqi and Dickhout, 2016). Environmental chemicals including certain heavy metals, trichloroethylene, and bromobenzene have been known to cause nephrotoxic effects (Van Vleet and Schnellmann, 2003). One of the reasons for the kidney being a key target of toxicity may be related to the kinetics of many xenobiotic substances. High exposures are reached because of a high blood flow in the kidneys and extensive reabsorption, predominantly in the proximal tubule.

Considering that renal toxicity is a major chemical safety issue, standard testing, which often does not investigate underlying mechanisms, has proven not to be an adequate assessment approach. As such, this is an opportunity for the application of computational approaches that utilise the knowledge and structure of existing AOPs (Cronin and Richarz, 2017; Cronin et al., 2017) to provide a weight of evidence on specific mechanisms and dose-response relationships related to nephrotoxicity. In addition, *in silico* approaches using multi-scale data have been demonstrated to provide valuable insight into hepatotoxicity pathways and the assessment of inter-individual variability (Bhattacharya et al., 2012; Diaz Ochoa et al., 2013). Multi-scale models incorporate data which span various biological scales, i.e. population, individual whole body, tissue and multi-cellular and sub-cellular metabolic and signalling pathways (Sluka et al., 2016). As multi-scale modelling has answered some of the pressing questions regarding adverse events in the liver, it is likely to hold the same potential for kidney related toxicity.

In this introductory Chapter, the current scientific landscape related to computational methods for the assessment of pharmaceuticals and other chemicals with regard to their potential to elicit nephrotoxicity was reviewed. Current *in silico*

approaches – more specifically physiologically-based mechanistic models – related to nephrotoxicity were examined and existing knowledge of relevant toxic mechanisms assessed, in order to understand to which extent these have already been covered by existing approaches, including AOPs. The following subchapter summarises key mechanisms of kidney toxicity in order to outline current knowledge which may be used to inform a computational model.

1.2 Mechanisms of kidney toxicity

In order to understand the highly specific adverse effects that may take place in the kidney and associated organs, it is essential to appreciate its function and physiology. The key function of the kidney is to eliminate endogenous waste products, control and maintain blood volume levels, endocrine function, electrolyte content and acid-base balance (Perazella, 2009; Rang et al., 2016). As a major site of elimination of drugs and other chemical compounds, the kidney is a common target for toxicity. Since the kidney is highly vascularised, receiving about 25% of the resting cardiac output, it is exposed to exogenous compounds in large quantities through the systemic circulation (John and Herzenberg, 2009; Perazella, 2009). The functional units of the kidney are nephrons - each kidney contains around one million, which consist of the glomerulus (a ball of capillaries), Bowman's capsule and the tubular element (proximal tubule, loop of Henle, distal tubule and collecting duct). When a substance reaches the glomerulus through the afferent arteriole it is likely to be filtered into the proximal tubules where the vast majority is reabsorbed back into the blood (Boroujerdi, 2015). Compound accumulation and "local" toxic metabolite formation may occur, making the kidney vulnerable to toxicity via various and simultaneously occurring mechanisms (Naughton, 2008; John and Herzenberg, 2009; Perazella, 2009).

As a result of physiology, there are four main mechanisms of drug-induced renal toxicity which are most commonly manifested as acute kidney injury, namely haemodynamic alteration, (proximal and distal) tubular cell toxicity, (tubular, interstitial, tubulo-interstitial and glomerular) nephritis and tubular obstruction (Vaidya et al., 2010; Blatt and Liebman, 2013). An understanding of mechanisms, such as it is, will assist in the development of *in silico* models as well as the

organisation of the associated data. Figure 1.1 shows the sites of the main mechanisms of chemical-induced kidney toxicity.

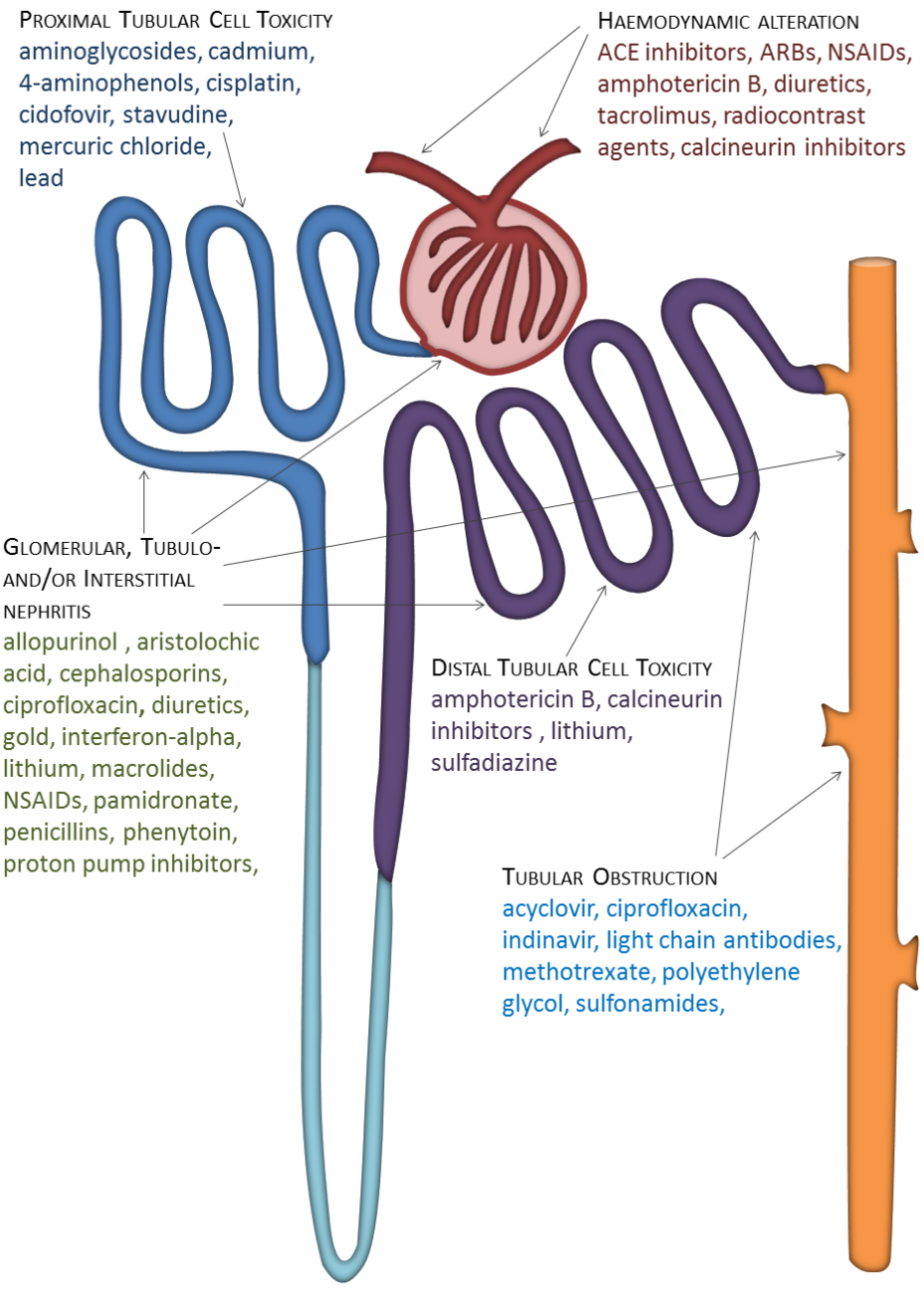

Figure 1.1: Sites and mechanisms of chemical-induced renal toxicity and respective substances potentially causing an effect at each site (adapted from Vaidya et al., 2010).

1.2.1 Nephrotoxicity-related mechanistic knowledge organised as Adverse Outcome Pathways

A consideration of mechanistic toxicology also provides the opportunity to link to relevant AOPs. The AOP framework facilitates the organisation of mechanistic knowledge and grants validity and robustness to data included in the AOP Knowledge Base (AOP-KB), (OECD, 2017; http://aopkb.org), sponsored by the Organisation for Economic Co-operation and Development (OECD). Mechanistic data gathered and organised in the form of AOPs serve as a robust basis for the development of computational toxicology models (Ellison et al., 2016; Cronin and Richarz, 2017). If an MIE and/or Key Events (KEs) have been defined and respective data are available, a predictive approach to estimate a substance's potential to elicit one of more of these may be achieved using the knowledge in the AOP-KB and the public literature. Table 1.1 provides a starting point for *in silico* analyses based around the MIE in particular. Additionally, AOPs may aid the grouping of chemicals for read-across (Cronin and Richarz, 2017). Only a handful of AOPs related to the kidney have been developed and proposed so far which implies that only a small proportion of MIEs and KEs have been defined. Table 1.1 provides an overview of relevant AOPs that existed at the time of the preparation of the thesis, as sourced from the AOP Wiki (OECD, 2019; https://aopwiki.org), one of the key resources for distributing AOPs.

Table 1.1: Mechanisms of kidney toxicity, related (groups of) substances and established and / or proposed MIEs and AOPs directly or indirectly associated with kidney toxicity.

Mechanism	Overview	MIE	AOP	Compounds	Biomarkers
Haemodynamic alteration	Impaired autoregulatory capacity of the renal vasculature to vasodilate or vasoconstrict leading to a reduced GFR	COX-1 and/or COX-2 inhibition leading to reduced prostaglandin synthesis and uncontrolled renal vasoconstriction (aspirin, other NSAIDs, calcineurin inhibitors) (Naesens et al., 2009; Drewe and Surfraz, 2015)	AOP proposed by Lhasa Ltd. (Drewe and Surfraz, 2015)	ACE inhibitors, ARBs, NSAIDs (e.g. aspirin), amphotericin B, tacrolimus, radiocontrast agents, calcineurin inhibitors (cyclosporine, tacrolimus) (Naughton, 2008; Vaidya et al., 2010)	IL-18[I], lipocalin 2 (LCN-2 aka NGAL)[II] (Wilmes et al., 2014)
		Prevention of formation of angiotensin II (ACE inhibitors) (Brown and Vaughan, 1998)	No AOP found		
		Blockage of angiotensin II type 1 (AT1) receptors (ARBs) (Palmer, 2002)	No AOP found		
		Increase endothelin and thromboxane and activation of the renin-angiotensin system (RAS) (vasoconstriction), and reduction prostacyclin, prostaglandin E2 and nitric oxide (NO) (vasodilation) (calcineurin inhibitors) (Naesens et al., 2009)	No AOP found		
		Changing vascular smooth muscle cell permeability, cell depolarization with resultant opening of voltage-dependent calcium channels and muscle cell contraction (potential mechanism for amphotericin B) (Fanos and Cataldi, 2000; Evenepoel, 2010)	No AOP found		

Proximal and distal tubular cell toxicity	Extensive cellular uptake and intra-cellular accumulation inducing compromised mitochondrial respiration, oxidative stress, and the activation of intrinsic apoptotic and necrotic pathways	Metabolism by oxidase in hepatocyte to benzoquinoneimine, followed by formation of GSH S-conjugates (4-aminophenol) (OECD, 2011)	OECD ENV/JM/MONO(2011)8: Nephrotoxicity induced by 4-aminophenols (OECD, 2011)	aminoglycoside antibiotics, amphotericin B, 4-aminophenols, cisplatin, nucleotide and nucleoside antivirals (stavudine, cidofovir) (Vaidya et al., 2010; OECD, 2011; Drewe et al., 2014)	clusterin[III], β2-microglobulin[IV], cystatin C[V], heme oxygenase-1[VI], IL-18[I], lipocalin 2 (LCN-2 aka NGAL)[II], KIM-1[VII], miR-34a[IX] (Ferguson et al., 2008; Bhatt et al., 2010; Bonventre et al., 2010; Zager et al., 2012; Wunnapuk et al., 2013; Schena et al., 2014; Wilmes et al., 2014)
		Mitochondrial toxicity pathways: a) Mitochondrial DNA incorporation (stavudine, cidofovir) (Drewe et al., 2014) b) Mitochondrial DNA polymerase gamma inhibition (stavudine, cidofovir) (Drewe et al., 2014) c) Depletion of SH-groups leading to ROS induction (cisplatin) (Walker and Endre, 2013)	AOP proposed by Lhasa Ltd. (stavudine, cidofovir) (Drewe et al., 2014)		
		Accumulation-induced lysosomal effects: a) accumulation induced lysosomal leakage leading to tubular dysfunction (aminoglycosides) (Mingeot-Leclercq and Tulkens, 1999) b) fusion of compound-containing pinocytic vacuoles and lysosomes causing osmotic nephrosis (contrast agents) (Dickenmann et al., 2008)	No AOP found		
		After moving through cellular membrane, polyunsaturated region participates in auto-oxidation, lipid peroxidation and	No AOP found		

		cell membrane damage; forming pores (amphotericin B) (Fanos and Cataldi, 2000; Evenepoel, 2010)			
Tubular, interstitial, tubulo-interstitial and glomerular nephritis	Inflammatory changes in the glomerulus, interstitial and tubular cells predominantly caused by immune mechanisms resulting in fibrosis and renal scarring	Interaction with hOAT1 and 3, accumulation within proximal tubule cells, followed by uncoupling/inhibition of mitochondrial oxidative phosphorylation and tubular/papillary necrosis (aspirin)* (Drewe and Surfraz, 2015)	AOP proposed by Lhasa Ltd. (Drewe and Surfraz, 2015)	NSAIDs (indomethacin, phenylbutazone, mefenamic acid, aspirin); antibiotics (cephalosporins, ciprofloxacin, ethambutol, isoniazid, macrolides, penicillins, rifampicin, tetracycline); loop (furosemide), potassium-sparing (triamterene) and thiazide diuretics; proton pump inhibitors (omeprazole); allopurinol, lithium, aristolochic acid, phenytoin, propylthiouracil, ranitidine (Kodner and Kudrimoti, 2003; Naughton, 2008; Ursem et al., 2009; Vaidya et al., 2010; Drewe	IL-18[I]; lipocalin 2 (LCN-2 aka NGAL)[II]; osteopontin[VIII] (Hudkins et al., 1999; Vaidya et al., 2008; Bonventre et al., 2010; Schmid et al., 2015)
		Production of inflammatory response triggering TNF-α (cisplatin) (Pabla and Dong, 2008; Walker and Endre, 2013)	No AOP found		
		Formation of immune complex deposits (methicillin, rifampin, allopurinol, phenytoin) (Krishnan and Perazella, 2015)	No AOP found		
		Formation of drug-protein hapten conjugates in renal tissue which elicit an immunogenic response (sulfamethoxazole metabolite = nitrososulfamethoxazole, methicillin) (Krishnan and Perazella, 2015)	No AOP found		
		(Event 244 (AOP 38):Protein alkylation)** (OECD, 2019)	(AOP 38: Protein alkylation leading to liver fibrosis)** (OECD, 2019)		

				and Surfraz, 2015; Krishnan and Perazella, 2015)	
Tubular obstruction	Crystal precipitation within the renal tubule depending on urinary pH and favoured by high concentrations in the urine	OAT interaction causing secretion via proximal tubule cells, accumulation and crystal formation in urine leading to concentration in renal tissue/tubule and obstructive nephropathy (acyclovir) (Drewe et al., 2014)	AOP proposed by Lhasa Ltd. (Drewe et al., 2014)	antibiotics (e.g. ampicillin, ciprofloxacin, vancomycin and sulphonamides), antivirals (e.g. indinavir and acyclovir), methotrexate (Naughton, 2008; Drewe et al., 2014; Luque et al., 2017)	Clusterin[III], lipocalin 2 (LCN-2 aka NGAL)[II], IL-18[I], KIM-1[VII] (Chevalier, 1996; Schmid et al., 2015)

* Interstitial nephritis is not the adverse outcome of these AOPs. However, as NSAIDs have been associated with this mechanism of nephrotoxicity, and KEs, e.g. ROS production and necrosis, are part of this pathway, these AOPs were allocated here.

** This AOP is not directly related to nephrotoxicity but may be relevant for the following pathways:

I) IL-18: inflammatory response, activating NFκB in response to ischemia-reperfusion injury of renal tubules (e.g. after contrast agent exposure)
II) LCN-2, NGAL: maximally expressed in kidney after early ischemic injury, in response to contrast agents; important mediator of innate immune responses
III) Clusterin: associated with membrane recycling, cell repair, ischemic injury in proximal and distal tubule
IV) β2-microglobulin: early marker of tubular injury
V) Cystatin C: related to ischemic injury in proximal tubule
VI) Heme oxygenase-1: changes in response to ischemic and cisplatin-induced injury
VII) KIM-1: found in urine after proximal tubular cell injury
VIII) Osteopontin: associated with accumulation of macrophages, expressed in the distal convoluted tubules, the thick ascending limbs of the loop of Henle and the proximal tubule
IX) miR-34: was upregulated following cisplatin induced acute kidney injury, may play a cytoprotective role for cell survival

Abbreviations:

ACE: angiotensin-converting enzyme; ARB: angiotensin receptor blockers; GFR: glomerular filtration rate; GSH: glutathione; KIM: kidney injury molecule; NSAID: nonsteroidal anti-inflammatory drug; hOAT: human organic anion transporter; ROS: reactive oxygen species.

In the following subchapter, only proximal and distal tubular cell toxicity pathways are discussed in more detail since the mechanistic model of the kidney described in Chapter 4 is applied for this mechanism of nephrotoxicity. More information on the other mechanisms outlined above are included in Pletz et al. (2018b).

1.2.2 Proximal and distal tubular cell toxicity

Renal tubular cells, especially proximal tubule cells, are vulnerable to the toxic effects of drugs. This is because their apical and basolateral transport systems facilitate extensive cellular uptake in their function of re-absorbing glomerular filtrate (Perazella, 2009; Boroujerdi, 2015). Thereby, proximal tubular cells are exposed to a high amount of circulating endogenous and exogenous compounds, including potential nephrotoxicants (Naughton, 2008; Perazella, 2009; Boroujerdi, 2015).

Tubular cell toxicity may be elicited via different pathways which are induced by therapeutic agents such as aminoglycoside antibiotics, cisplatin and amphotericin B (Naughton, 2008; Vaidya et al., 2010). For instance, aminoglycosides are cationically charged and therefore attracted to the anionic phospholipid-rich brush border located at the proximal tubular apical membrane (Perazella, 2010). Accumulation of the aminoglycosides in tubular cells leads to the disruption of endosomal and lysosomal membrane and activation of intrinsic apoptotic pathway (Mingeot-Leclercq and Tulkens, 1999; Markowitz and Perazella, 2005; Lopez-Novoa et al., 2011). This includes impaired mitochondrial respiration and induction of oxidative stress through increased free radical levels within the cell. The kidney is particularly vulnerable to reactive oxygen species (ROS) damage (Ozbek, 2012). Several nephrotoxic compounds, e.g. cisplatin, immunosuppressant drugs, nonsteroidal anti-inflammatory drugs (NSAIDs) and aminoglycosides, exert their toxic effects due to excess ROS production, and depletion of the antioxidant defence mechanism (Ozbek, 2012).

Oxidative injury, inflammation, apoptosis, acute tubular necrosis as well as vasoconstriction have been associated with aminoglycosides as well as exposure to cisplatin (Markowitz and Perazella, 2005; Pabla and Dong, 2008). The extent of

exposure is suggested to determine whether apoptotic or necrotic cell death is induced. High concentrations of cisplatin in the millimolar range were reported to result in necrosis while concentrations in the micromolar range provoked apoptosis – via the intrinsic mitochondrial, extrinsic death receptor and endoplasmic reticulum (ER) stress pathways (Pabla and Dong, 2008).

Experimental data suggested the intrinsic mitochondrial pathway to be the major pathway of cisplatin-induced apoptosis, likely to be induced by sulfhydryl group and mitochondrial glutathione (GSH) depletion (Walker and Endre, 2013). Basolateral uptake by the organic cation transporter OCT2 has been demonstrated to be critical for cisplatin's toxic response to be elicited in the kidney (Pabla and Dong, 2008). Also, different segments (S1, S2, S3) of the nephron demonstrate diverse sensitivities to cisplatin which did not appear to be due to differences in uptake characteristics but intracellular effects (Kröning et al., 1999). S1 cells derived from the early portion of the proximal tubule expressed a considerably lower amount of the anti-apoptotic protein BCL-X_L than S3 cells derived from the late portion of the proximal tubule and distal convoluted tubular cells (Kröning et al., 1999).

The mitochondria of proximal tubular cells also appear to be key targets of nucleotide and nucleoside antiviral drugs stavudine and cidofovir (Drewe et al., 2014). Mitochondrial toxicity induced via mitochondrial DNA incorporation or mitochondrial DNA polymerase gamma inhibition may lead to tubular cell necrosis and acute renal failure (Drewe et al., 2014).

Amphotericin B is also commonly associated with acute tubular necrosis which may be secondary to changes in haemodynamics and cell membrane permeability as described above, and resulting renal tubular acidosis and hypokalemia (Baley et al., 1990; Markowitz and Perazella, 2005; Klaassen, 2008). Unlike aminoglycosides and cisplatin, amphotericin B appears to elicit cellular toxicity predominantly in distal tubular regions as opposed to the proximal tubules (Pabla and Dong, 2008; Vaidya et al., 2010; Blatt and Liebman, 2013).

Another pathway leading to renal tubular necrosis is documented in an AOP related to 4-aminophenol exposure whereby 4-aminophenol cysteine S-conjugates reach

and get concentrated in proximal tubules (OECD, 2011). There, cysteine S-conjugates are metabolised to benzoquinoneimines which cause oxidative stress and necrotic tubular cell death (OECD, 2011).

Ways to use and interpret such mechanistic data quantitatively are described in the following subchapter.

1.3 Physiologically-based mechanistic models to simulate kinetics and toxicity: current state-of-the-art

As noted above, as part of the hazard identification process it is important to be able to predict human nephrotoxicity accurately. The traditional approach for determining safety and toxicity of drug candidates is through histopathological observation from *in vivo* animal studies (Tong et al., 2004; Bonventre et al., 2010; Low et al., 2011; Lee et al., 2013) or, more recently, from targeted *in vitro* testing. However, in recent decades, alternative methods for hazard assessment without the need for testing, such as *in silico* approaches, have been increasingly applied, particularly for the prioritisation of data requirements and identification of chemicals that may require more detailed risk assessment.

Two fundamentally different *in silico* toxicology methods are often applied to assess chemical safety, i.e. chemistry driven (Q)SARs and physiologically-based mechanistic models. The former identify relationships between a structure of a molecule and its toxicity using statistics while the latter simulate the physiologically-based toxicokinetics of a compound in the entire body, a specific organ or tissue or a subset of organs. Mechanistic models are rooted in chemical kinetics and use mathematical equations – typically ordinary differential equations (ODEs) – which reflect causal mechanisms driving input-output behaviours of a biological system (Oates and Mukherjee, 2012; Baker et al., 2018). This allows predictions of whether (and which) effects may be elicited based on the simulation of concentrations at a putative site of toxicity over a defined time period following dosing. More information on nephrotoxicity-related (Q)SARs was included in a recent review (Pletz et al., 2018b) whereas mathematical mechanistic and physiologically-based full-body and kidney-related models are described in more detail here.

In contrast to (Q)SAR methods, mathematical mechanistic and physiologically-based models can be used to simulate the kinetics of a compound through the body and at the site of toxicity. As a vast number and quantity of substances are moving through the kidney, and considering the key principle of toxicology – the dose makes the poison (Paracelsus) – an understanding of a compound's movement and its potential for accumulation at specific sections of the kidney are considered critical. In subchapter 1.2, accumulation is ascertained as playing an important role in certain nephrotoxicity pathways. In order to predict a compound's potential for accumulation within the kidney, in comparison to other organs and tissues, or accumulation at a specific site of the kidney, full-body physiologically-based kinetic (PBK) and kidney-specific mechanistic models may be applied, respectively.

1.3.1 Full-body physiologically-based kinetic models

Physiologically-based kinetic (PBK) models predict the absorption, distribution, metabolism and excretion (ADME) of a chemical in an organism via a series of differential equations, which mathematically represent these ADME processes. PBK models are often synonymously termed physiologically-based pharmacokinetic (PBPK), physiologically-based toxicokinetic (PBTK) or physiologically-based biokinetic (PBBK) models (Paini et al., 2017a). These have gained substantial attention in the field of non-animal methods in toxicology, in particular as more models emerge which increasingly integrate *in vitro* and *in silico* data (Paini et al., 2017a). Pharmaceutical, chemical and consumer goods companies have used PBK models to inform ADME-related decision-making in drug discovery, development and safety assessment, and to derive occupational exposure limits (Kawai et al., 1994; Jones and Rowland-Yeo, 2013; Ferl et al., 2016; Mori et al., 2016; Poet et al., 2016; Punt et al., 2016; Miller et al., 2019). A workshop held recently by the European Union Reference Laboratory European Centre for the Validation of Alternative Methods (EURL ECVAM) on the new generation of PBK models and new guidance by the European Medicines Agency and the U.S. Food and Drug Administration on the format, content and reporting of these models indicate increasing attention and regulatory acceptance (Paini et al., 2017; European Medicines Agency, 2018; U.S. Food and Drug Administration, 2018).

A PBK model consisting of all key organs and tissues of a human body predicts how much of an administered dose accumulates in the kidney over time, in relation to how much is distributed to and cleared from other organs and tissues. This may help to understand whether a certain exposure scenario will lead to toxicity-inducing concentrations in the kidney and/or other organs. Hence, a PBK model supports efforts to differentiate between cases where a compound accumulates in various organs and causes overall non-specific toxicity from kidney-specific accumulation-induced toxicity.

So far, there is a very limited number of publicly available *in silico* tools that incorporate a PBK model to predict target organ concentrations over time coupled to a kidney specific component. This component may be a toxicodynamic model, (Q)SAR or a detailed kinetic model of the kidney that supports organ-level toxicity evaluation. The need for further research in this area is indisputable and future efforts will have a great potential to move non-animal approaches in toxicology a substantial step forward. Kidney-specific mechanistic models will be discussed in further detail in the following subchapter.

Besides commercial packages such as the Simcyp® Simulator provided by Certara and GastoPlus® offered by SimulationsPlus, publicly available PBK models have been developed, such as IndusChemFate and Httk (Jongeneelen and ten Berge, 2011a; Pearce et al., 2017; Madden et al., 2019), and others published ordinary differential equations (ODEs) to facilitate the generation of a new PBK model (Kawai et al., 1994; Peters, 2008a; Jones and Rowland-Yeo, 2013; Hoffman and Hanneman, 2017).

1.3.2 Kidney-specific mechanistic models

As explained above, mechanistic models simulate the kinetics of a compound in a biological system which may be defined as an entire human body, a specific organ or a subset of organs. Some of the early mechanistic models of renal function predict renal clearance while considering passive reabsorption and urine flow (Tang-Liu et al., 1983). These are supplemented by protein binding and glomerular filtration (Hall and Rowland, 1984; Komiya, 1986, 1987; Mayer et al., 1988) and active secretion (Russel et al., 1987b, a; c; Katayama et al., 1990). Of these, Russel et al. (1987a; b)

and Katayama et al. (1990) were the first to differentiate between renal blood, tissue and tubular compartments. Subsequently, Felmlee et al. (2010, 2013) developed a universal mechanistic model predicting renal clearance of substances which were subject to active secretion, active reabsorption or both of these processes, for a broad applicability domain. Here, two ultrafiltrate compartments were included to represent the proximal and distal tubules.

Two of the most detailed mechanistic kidney models were reported by Neuhoff et al. (2013) and Huang and Isoherranen (2018). Both predict renal elimination by accounting for glomerular filtration, active and passive reabsorption, active and passive secretion and renal metabolism. Bypass of parts of the renal blood flow and population variability are considered by Neuhoff et al. (2013). In both models, the nephron is divided into segments representing the glomerulus, proximal and distal tubules, loop of Henle and collecting ducts. Each segment encompasses three compartments, illustrating the blood space, tubular fluid and cellular mass. ODEs describe the movement of a compound between compartments. However, the model developed by Neuhoff et al. (2013) is embedded in the commercial software Simcyp® Simulator and details of the ODEs are not publicly available. The model generated by Huang and Isoherranen (2018) predicts drug renal clearance considering *in vitro* permeability, unbound filtration, active tubular secretion and pH dependent bidirectional passive diffusion. It was validated with data for 46 drugs and can quantify concentrations in each compartment.

In drug development, pharmacokinetic-pharmacodynamic (PK/PD) modelling has been applied to understand which dosing regimens lead to effective or ineffective exposure, or toxic effects in patient populations and investigate inter-individual PK and PD differences. For drugs intended to be used by patients with compromised renal function, such investigations are particularly relevant as pharmacokinetics are likely to be altered in these individuals (Verbeeck and Musuamba, 2009; Eyler and Mueller, 2010). These patients may require an adjusted dosing regimen to reach an effective and nontoxic internal dose which can be selected based on a PK/PD study (Fisher et al., 1999; Skerjanec et al., 2003; Stangier et al., 2010; Chandorkar et al., 2015; Katsube et al., 2017). Furthermore, PK/PD-informed dose adjustments are frequently necessary due to multi-drug therapy-induced drug-drug interactions or

additional treatment such as haemodialysis (Chanu et al., 2010; Eyler and Mueller, 2010; Stangier et al., 2010). In the PK/PD studies mentioned above, the PK are typically described as one- to three-compartment model. Most of these PK/PD analyses are performed using a (linear or nonlinear) mixed-effects modelling approach which incorporates a covariate analysis to understand demographic and (patho-)physiological factors influencing inter-individual variability. Looking beyond pharmaceutical related applications, Diamond et al. (2003) used PK/PD analysis to understand the relationships between environmental or dietary exposures and risks of kidney toxicity.

Overall, there are limited computational toxicity methods available for complex endpoints such as nephrotoxicity – this is likely to be due to the highly intricate mechanisms of toxicity or limitations of the availability of structured, high quality data and a narrow applicability domain of the methods which have been established so far. Also, such models are in part not publicly available. To date, there is no multi-scale nephrotoxicity model available which is embedded in a full-body PBK model, capable of quantifying concentration-time profiles of substances in toxicologically relevant segments of the human kidney and tested for a sensitive population; such a model would be of great benefit in establishing alternatives to *in vivo* testing for these endpoints.

1.4 Context and Aim of this Thesis

For nearly a decade now, AOPs have been considered a key component of the "Toxicity Testing in the 21st Century" paradigm. The fundamental concept of the AOP approach is to evaluate and document a mechanism and/ or pathway spanning from the molecular to the organism level, representing a systems biology/toxicology context. Since mechanistic data organised in the form of an AOP provide a robust basis for the generation of novel *in silico* toxicology methods, these naturally may inform physiologically-based mechanistic models. The aim of this thesis was not to quantify an AOP *per* se, but to attempt to quantify the relationship between an externally applied dose and the induction of an effect that could relate to renal toxicity. It is clear that the data provided in an AOP are not sufficient to provide a full dataset needed to parameterise such a model. It is also important to reiterate that a detailed understanding of many renal toxicity pathways is often lacking. As ever, data

availability and data quality are core issues in the field of computational toxicology, which are addressed throughout this thesis. Approaches to use available data and evaluate their validity will be discussed, in particular in Chapters 3 and 4.

Quantitative approaches, based on human-relevant data, provide a significant opportunity to gain a better understanding of renal mechanisms of toxicity. Many human-relevant parameters to build physiologically-based mechanistic models are available, even though certain parameters are not quantifiable with current testing approaches. However, these may be estimated – partly using computational methods – and further refined when more data become available. Particularly relevant to the fact that renal failure is observed in vulnerable populations, such as patients with decreased renal function, is the possibility to amend specific parameter values within a mechanistic model, which typically differ between healthy and vulnerable individuals. Overall, the physiological basis and human relevance is a core strength of such models, which has not been fully leveraged to date in the field of renal toxicology. Thus, the overall aim of this thesis was to propose novel ways to use publicly available data for the quantitative assessment of adverse effects induced in the kidney following chemical exposure. Data organised in the form of an AOP were focussed on in particular.

This thesis addresses the growing attention that is being given to exposure-based and toxicokinetics-driven toxicity, which is reflected by the increasing application of PBK modelling. The following objectives were addressed in the thesis.

I. First, the suitability and validity of publicly available PBK models was tested for a set of chemicals the general population is exposed to, i.e. phenols, parabens and phthalates (Chapter 2). This work was performed during a traineeship at the European Commission Joint Research Centre under the supervision of Drs. Stephanie Bopp, Alicia Paini, Nikolaos Parissis and Andrew Worth. Two models were used to predict safe urinary concentrations following oral exposure to a safe dose, i.e. a tolerable daily intake (TDI) or reference dose (RfD) value. Moreover, urine-level concentrations were predicted on the basis of estimated daily intakes, which were calculated to include exposure from food, dust and air. These simulated urine concentrations were compared to human biomonitoring (HBM) data which

capture measurements of these compounds or their metabolites present in the urine of cohorts of Norwegian mothers and children and Danish children. These data were kindly provided under respective Data Transfer Agreements. A mixture risk assessment was performed with predicted safe concentrations and measured concentrations to demonstrate how such data may be used in a risk assessment context. The evaluation of results aimed to address uncertainties and limitations of the use of both models selected for this study.

II. In order to guarantee full transparency and flexibility when applying a PBK model, a full-body PBK model was developed based on ordinary differential equations available in the literature (Chapter 3). This model was intended to quantify the relationship between an administered dose and concentrations in various organs over time for a broad range of chemical substances. Therefore, it was validated with nine substances covering a broad physico-chemical space to gauge whether the model predicts well over a wide applicability domain. Even though this PBK model does not represent the sole reproduction of a previously developed model but a product based on various sources, it may not necessarily be considered a scientific novelty. Its use in conjunction with a newly generated mechanistic kidney model formed the core theme and novelty of this thesis.

III. The aim of Chapter 4 was to develop a mechanistic model of the kinetics of drugs in the kidney with specific reference to salicylic acid (SA), a major metabolite of aspirin (ASA). Specific objectives included:
    i. Incorporation of the previously developed sub-compartment kidney model in order to validate it with full-body kinetic data.
    ii. Investigation of whether a quantitative relationship may be established between therapeutic doses of SA, predicted proximal tubular cell concentrations in young and elderly virtual individuals and toxicity events in proximal tubular cells.

Chapters 3 and 4 follow the convention applied in mathematics to present scientific work in the present tense.

2.0 PHYSIOLOGICALLY-BASED KINETIC (PBK) MODELLING AND HUMAN BIOMONITORING DATA FOR MIXTURE RISK ASSESSMENT

Note for Information and Explanation of Contribution to this Chapter

Julia Pletz and Samantha Blakeman worked together on this project under the supervision of Drs. Stephanie Bopp, Alicia Paini, Nikolaos Parissis and Andrew Worth at the European Commission's Joint Research Centre.

As certain tasks were split between both researchers, others were performed simultaneously to compare results afterwards. Tasks which were split included:

- Both researchers sourced parameter values (e.g. density, molecular weight, vapour pressure, log Kow, water solubility, absorption rate constant, hepatic metabolism related V_{max} and K_m values) to inform the IndusChemFate software of eight compounds each.
- In IndusChemFate, Samantha performed a 24-h simulation of EDI-based urine concentrations and predicted BE_{RfD} and BE_{TDI} values for two Norwegian females and children, while Julia performed the simulation of steady state concentrations for BPA and several other compounds for the same individuals. However, only the results for BPA are shown as steady state was not reached for the other compounds.
- While Samantha extended the Httk code so that EDIs could be used as doses in two virtual populations of female adults and children, Julia ran some checks of the code to ensure the accuracy of the results.
- While Samantha generated the results of the number of individuals exceeding calculated BE_{TDI} values, the comparison of measured urine concentrations and BE_{EDI} levels established in Httk, and the mixture assessment, Julia focussed on report writing. However, both contributed to the writing of the report.

Tasks performed simultaneously included:

- Familiarisation with the use of IndusChemFate and Httk,

- Working together on a strategy of how to convert a V_{max} value in "per mg microsomal protein" to "per g liver", and
- Calculation of BE_{TDI} concentrations based on virtual populations, and BE_{EDI} values for Norwegian children and female adults and Danish children.

Julia additionally contributed to the work by proposing a computational model to calculate absorption rate constants used in IndusChemFate and proposed the consideration of steady state concentrations and the 5th of BE_{TDI} distributions for data analysis.

2.1. Introduction

Human biomonitoring (HBM) is a process of evaluating to which degree a human population is exposed to chemicals. It allows assessment of exposure to chemicals by measuring these compounds, their metabolites or other biomarkers present in easily accessible body fluids (blood, urine, saliva, breast milk), or other biological matrices (hair, nails and teeth). Ideally HBM should be performed in conjunction with the monitoring of indoor and outdoor media (air and dust), as well as the collection of information on study participants' age, sex, socioeconomic background and identification of chemical exposure associated with food intake via diet diaries. Thus, HBM allows for the derivation of a complete picture of external and internal exposure. These exposures can be linked to data on sources and epidemiological surveys to attempt to identify trends associated with potential health risks.

There have been numerous HBM programmes across the globe for a number of decades. One of the best and well known examples is the American HBM "National Health and Nutrition Examination Survey" (NHANES) programme. NHANES is the largest ongoing project which has been operational since 1971 (McDowell, 1971). There have been a number of HBM projects in Europe over the years (Choi et al., 2015). In the Democophes project, mother child pairs over large parts of Europe were studied (Den Hond et al., 2015) and in 2017 "The European Human Biomonitoring Initiative" (HBM4EU) project, a joint effort of 28 EU countries, was launched by the European Commission. The aim of the HBM4EU project is to collect and interpret HBM data from across Europe in order to safely manage chemicals and protect

human health (HBM4EU, 2019). The long-time goal of HBM4EU is to build bridges between the research and policy communities and deliver benefits to society in terms of enhanced chemical safety.

Interpretation of HBM data is particularly valuable in the context of combined exposure to multiple chemicals. The environment we live in is made up of an assortment of chemicals, some of these potentially harmful if taken up at sufficiently high concentrations or in conjunction with other chemicals. HBM data provide a measure of internal co-exposure to multiple chemicals and aggregate exposure across routes and sources of exposure. The interpretation of HBM data using internally based reference values is, therefore, one way to improve the assessment of risks from exposure to mixtures of multiple chemicals.

As collection of HBM data is on-going, the challenge and important task is to understand and interpret what those concentrations measured in biological samples, such as human blood and urine, mean in terms of exposure to chemicals and risks to both individual and population health. In terms of practical use, there is a need to determine how to apply this information, how it can be translated into usable knowledge to inform risk assessment for decision making. The best method to interpret HBM data is to compare them to a concentration that is deemed safe. Currently, the majority of these safe values are established as an intake dose, known as acceptable or tolerable daily intakes (ADI or TDI) or reference doses (RfD), referring to how much of one chemical a person can ingest daily over a lifetime without diminishing their health (FAO and WHO, 2009). Only recently have studies begun to look into establishing safe levels in urine or blood against which to compare the measured values. These values are known as biomonitoring equivalents (BE) (Hays et al., 2007) or as HBM Guidance values (HBM4EU, 2019).

Some of the existing BE values have been related to biomonitoring data with the use of physiologically-based kinetic (PBK)[3] models (WHO, 2015). An idealised PBK model is shown in Figure 2.1. These models are based on mathematical descriptions of physiological characteristics (tissue volumes, blood flow, etc.) and biochemical

[3] The term PBK model is synonymous with physiologically-based pharmacokinetic (PBPK), physiologically-based biokinetic (PBBK), and physiologically-based toxicokinetic (PBTK) models.

processes (e.g. metabolism characterised by the maximum rate of a metabolic reaction V_{max} and the Michaelis-Menten constant K_m) (Krishnan et al., 1994). PBK models describe the body as a set of interconnected compartments, which represent the human organs and plasma, describing the absorption, distribution, metabolism, and excretion (ADME) (Krishnan and Andersen, 2007) properties of a chemical or drug within the body. PBK models integrate exposure information (external dose) to predict the time-course of a parent chemical, its metabolite(s) or biomarkers of exposure as target tissue concentrations in an organism.

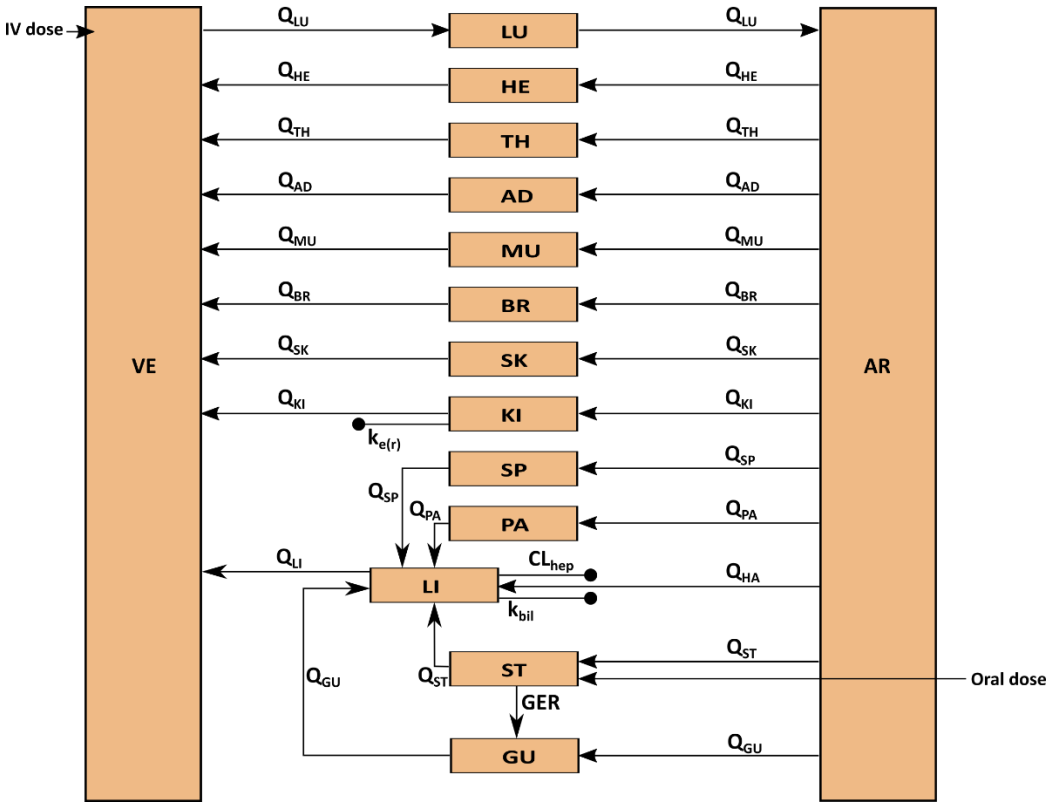

Figure 2.1. Schematic representation of a full-body PBK model, which is illustrated and discussed in full detail in Chapter 3. Q = blood flow rates corresponding to an organ or tissue compartment, namely lung *(LU)*, heart *(HE)*, thymus *(TH)*, adipose tissue *(AD)*, muscle *(MU)*, brain *(BR)*, skin *(SK)*, kidney *(KI)*, spleen *(SP)*, pancreas *(PA)*, liver *(LI)*, hepatic artery *(HA)*, stomach *(ST)*, and gut *(GU)*; blood compartments include the venous blood *(VE)* and the arterial blood *(AR)*; $k_{e(r)}$ = renal elimination rate constant; CL_{hep} = hepatic clearance rate; k_{bil} = biliary elimination rate constant; GER = gastric emptying rate. An intravenous dose is applied to the venous blood compartment, and an oral dose to the stomach compartment.

Results from PBK models can also allow the refinement of the setting of safe levels combining dose–response data. PBK models can be used in two ways, via either forward dosimetry or reverse dosimetry (Hays et al., 2007). The former uses an intake dose and estimates the concentration of a compound in human fluids, whilst the latter uses the measured concentration in a body fluid and identifies the dose the person was subjected to. In addition, PBK models allow comparison of subgroups (gender, age and sensitive populations), inter-individual variation and extrapolations (acute to chronic exposure, route to route, low to high doses) and can support read-across by comparing kinetic profiles of structurally similar substances. A PBK model may be linked to Benchmark Dose (BMD) modelling to derive an occupational exposure limit as proposed for N-methylpyrrolidone (Poet et al., 2016).

PBK models can be chemical specific or generic. A chemical specific PBK model is built using specific knowledge of the physico-chemical properties, mode of action (MoA) and ADME for the specific chemical under study; relevant target organs and specific metabolite formation should be included (Kawai et al., 1994; Abbiati and Manca, 2017; Hoffman and Hanneman, 2017; Moss et al., 2017). A six step approach to build "specific" PBK models was reported by Rietjens et al. (2011). On the other hand, a more generic PBK model has a defined compartmental structure for all chemicals tested. These models are usually built on specific software (see Madden et al., 2019 for an overview of such platforms). This allows for the computation of multiple chemicals with the same type of input data and the same assumptions and limitations. Furthermore, the simulation of more than one chemical can be performed without detailed parameterisation and hence simplifies the task of carrying out a mixture risk assessment. Even though PBK models have been proposed for the derivation of BE values more than 10 years ago (Hays et al., 2007) and this approach has been applied to assess occupational exposures (Droz et al., 1989; Leung, 1992; Thomas et al., 1996; Truchon et al., 2006), little work has been done in the field of exposures of the general population so far. Furthermore, no study exists to this date which uses publicly available PBK models to derive BE values based on which a mixture risk assessment is performed.

The aim of this investigation was to examine the suitability of using generic PBK models to derive BE values based on agreed reference values that can then be used

in a screening level mixture risk assessment using HBM data. The aim was to establish a method to interpret HBM data on multiple chemicals easily, e.g. for prioritisation purposes, which are not intended to be ready for direct uptake in regulatory risk assessment. Two models were considered in this investigation, IndusChemFate and High-Throughput Toxicokinetics (Httk). IndusChemFate (ICF) was developed by IndusTox Consult & Santoxar, funded by the CEFIC Long Range Research Initiative (LRI) and built in an MS excel spreadsheet-file (Jongeneelen and ten Berge, 2011a). The model contains 11 body compartments. The Httk package is available in the CRAN r project (https://cran.r-project.org/web/packages/httk/index.html) and was created by the U.S. Environmental Protection Agency's (U.S. EPA's) National Center for Computational Toxicology. It constitutes a compilation of a one, three and seven-compartment (called PBTK – physiologically based toxicokinetic) models intended to compute concentration vs. time curves (Pearce et al., 2017, more information can be found in methodology).

Both models were used in a forward-dosimetry approach with established TDI or RfD values in order to obtain urinary BE concentrations, i.e. BE_{RfD} and BE_{TDI}. Subsequently, with the information collected a mixture risk assessment was performed using HBM data of Norwegian and Danish cohort studies. This case study presents another example of how HBM data may be used to inform a mixture risk assessment, noting that they should not be regarded as a detailed risk assessment at this time.

2.2. Methods

The overall approach to achieve the aim of this investigation is represented schematically in Figure 2.2. The methods for the HBM analysis reported in Figure 2.2 include the choice of chemicals (parabens, phenols, phthalates), the application of Monte Carlo sampling approach for generation of 'virtual populations' (to be able to capture the response for a representative population) and the steps for the risk assessment. The individual steps are summarised below and described in more detail throughout this study in an iterative manner:

1. HBM data for Norwegian and Danish cohorts (mothers and children) were selected. These contained measured urine concentrations and calculated EDIs for the Norwegian cohort.
2. Review of available PBK model platforms and selection of ICF and Httk. When ICF was applied, steady state was not reached for most chemicals tested. Metabolism is currently not simulated in Httk, therefore, urinary concentrations of phthalate metabolites could not be predicted in Httk.
2.1. Chemicals were selected for simulation, i.e. two phenols and two phthalates for ICF predictions and three phenols and four parabens for Httk predictions.
2.2. TDIs were sourced from the public literature.
2.3. Physiological parameters were selected in both models for women and children to represent the kinetics of both HBM cohorts. In ICF, simulations were performed for four individuals, one normal and one obese woman and one normal and one obese child. In Httk, virtual populations of 4000 mothers aged 32 to 56 and children between the ages of 6 to 11, including 5000 males and females, were created.
3. Forward dosimetry was performed to obtain BE_{TDI}, BE_{RfD} and BE_{EDI} values using available TDIs, RfDs and EDIs as input doses.
4. The performance of PBK models was evaluated by comparing BE_{EDI} with measured urine concentrations and BE_{TDI} / BE_{RfD} with established HBM values.
5. BE_{TDI} / BE_{RfD} values generated with Httk were compared to corresponding measured urine concentrations for each substance.
6. As a case study, a mixture risk assessment was carried out on the basis of BE_{TDI} / BE_{RfD} values generated with Httk.

Figure 2.3 illustrates the process of using TDI, RfD and EDI values as input doses in a forward dosimetry approach to obtain BE_{TDI}, BE_{RfD} and BE_{EDI} values and compare these to measured urine concentrations (Steps 3 to 5).

Chemicals included in the analysis are phenols (bisphenol A, triclosan, benzophenone-3), phthalates (di-n-butyl phthalate/DnBP, butylbenzyl phthalate/BBzP) and parabens (methyl paraben, ethyl paraben, n-propyl paraben, n-butyl paraben).

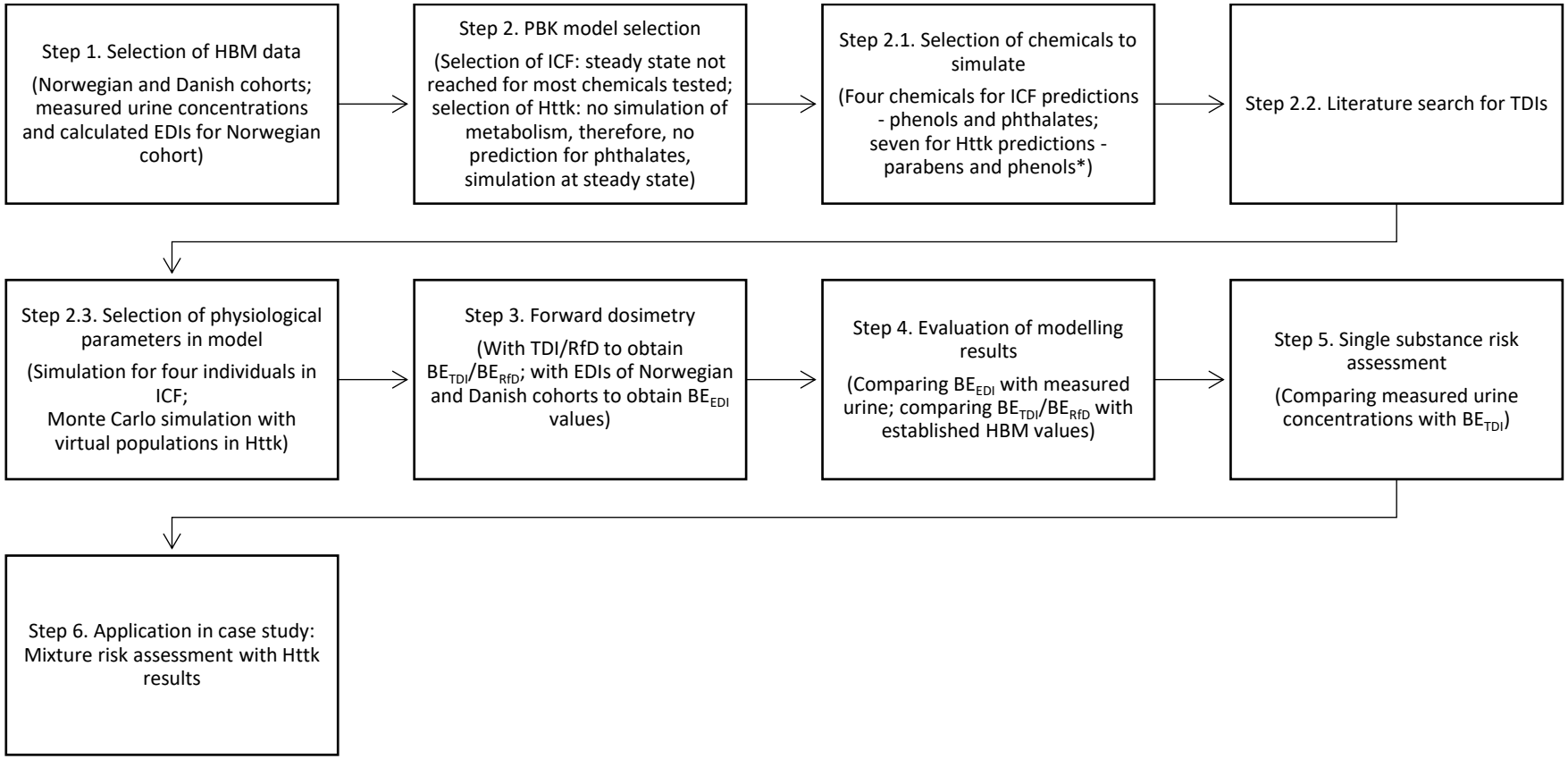

Figure 2.2. The workflow for the application of ICF/excel and the Httk/r highlighting the steps undertaken in the HBM analysis. Only Httk results were used for mixture risk assessment (MRA). HBM: Human biomonitoring, TDI: Tolerable daily intake, EDI: Estimated daily intake, BE: Biomonitoring equivalent.

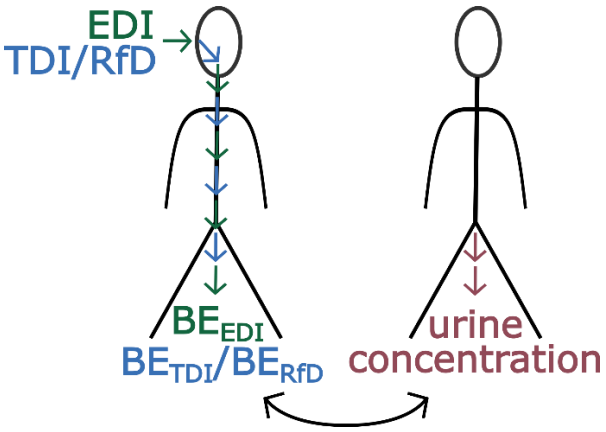

Figure 2.3: Forward dosimetry with TDI, RfD and EDI values as input doses to obtain urine-level BE_{TDI}, BE_{RfD} and BE_{EDI} values and comparison of these to urine concentrations measured in Norwegian and Danish cohorts (Steps 3 to 5).

2.2.1. Step 1: Selection of human biomonitoring data

The HBM data used in this study were of a Norwegian and a Danish cohort population obtained from January to May 2012 and between 2006 and 2007, respectively. They were kindly provided by the Norwegian Institute for Public Health and the Danish Rigshospitalet, Department of Growth and Reproduction under respective Data Transfer Agreements. In these datasets, several classes of chemicals have been included, but for the study presented here, we focused on phthalates and phenols as substance groups.

The Norwegian dataset was based on a mother-child study cohort (48 mothers aged 32-56 years and 48 children aged 6-11 years). Urine samples were taken from 48 mothers and 46 children as 24h morning spot samples as this approach is considered the "gold standard" to assess chemical exposure in the urine (Boeniger et al., 1993; Aprea et al., 2002; Cequier et al., 2017). Concentrations of several chemicals were measured from each of these urine samples; there were missing data for 23 adult females because of interferences or they were below limit of detection (LoD) (two of these women are missing two values whilst the rest are only missing one), 28 children were missing values (one child is missing two values whilst the rest were missing only a single value). Further details about the enrolment, dietary intake (recording of food consumption), sample collection and analysis have been published elsewhere (Cequier et al., 2015, 2017). For some compounds, food, dust and air samples were also analysed to determine external exposure from which estimated daily intakes

(EDIs) were calculated and provided (Haug et al., 2011; Cequier et al., 2014; Sakhi et al., 2014; Liagkouridis et al., 2017).

The study population of Norwegian mothers was divided, based on their body mass index (BMI), into normal, obese and overweight individuals. As reported by the World Health Organisation (WHO), adults are considered overweight if their BMI is equal to or greater than 25 and obese if their BMI is equal to or greater than 30 (WHO, 2019). 28 normal, 12 overweight and 6 obese women with a mean weight of 62.2 kg, 75.2 kg and 100.1 kg, respectively, were part of the Norwegian study. The children in this study had a mean weight of 34.3 kg. Their BMI values were made available, however, as their individual ages and sex are unknown they could not be classified into the normal, overweight or obese categories.

The Danish study population was made up of subsets of two cohort studies: firstly data from spot urine samples of 849 children aged 4 to 9 years from the Copenhagen Mother-Child Cohort (http://www.edmarc.net/mother-child-cohort.html; Boas et al., 2010; Frederiksen et al., 2014), secondly from 24h urine samples of 129 children and adolescents between 6 and 21 years of age from the Copenhagen Puberty Study collected in 2007 (http://www.edmarc.net/puberty-cohort.html; Frederiksen et al., 2013, 2014). For the purpose of this study, only urine measurements in children aged 6-11 years were considered in order to compare the Danish group of children to the same age group of Norwegian children. This sub-group consisted of 725 children in total (660 from the Copenhagen Mother Child cohort and 65 from the Copenhagen Puberty study), with a mean weight of 26.9 kg. Grouping into normal, overweight and obese children would have been possible as individual ages, weights, heights and sex are known. However, this was unnecessary as this dataset was used in the validation of the Httk model chosen to calculate the BE values which included children of all weight categories. The Danish dataset did not include any measurements in mothers.

2.2.2. Step 2: PBK model selection

2.2.2.1. The IndusChemFate (ICF) physiologically-based kinetic model platform

ICF was developed by IndusTox Consult & Santoxar, funded by the CEFIC Long Range Research Initiative (LRI) within the context of the HBM2 project. The ICF version 2.00 which is used here is freely available on the CEFIC-LRI website (Jongeneelen and ten Berge, 2011a; b). The model is distributed in an MS excel spreadsheet, the source

code is written in Visual Basic and is not password protected. The model contains 11 body compartments (i.e. lung, heart, brain, skin, adipose, muscles, bone, bone marrow, stomach & intestines (lumped), liver and kidney) and calculates parent compound and one or more metabolite concentrations in organs over time, as well as the amount excreted in urine. This allows for the study of phthalates as they are rapidly metabolised (Frederiksen et al., 2007) for which the concentration of some of their metabolites is an adequate indicator of exposure to the parent compound (Ramesh Kumar and Sivaperumal, 2016). By default, the model assumes physiological and anatomical parameters of a reference human of 70 kg, however, several different subjects (e.g. male or female adult or child, with normal weight or obese) can be selected.

2.2.2.2. The High-Throughput Toxicokinetics (Httk) physiologically-based kinetic model platform

High-Throughput Toxicokinetics (Httk) is a package found in the CRAN r project (https://cran.r-project.org/web/packages/httk/index.html) which was created by the U.S. EPA's National Center for Computational Toxicology. It constitutes a compilation of a one, three and seven-compartment PBTK (physiologically based toxicokinetic) models intended to compute concentration vs. time curves. A series of additional functions are built in to calculate steady state concentrations, the number of days to reach steady state and uncertainty and variability using a Monte Carlo analysis. The oral - via ingestion - exposure route was selected to make predictions and the seven compartmental model applied. All data used to parametrise the Httk model (physiological, tissue, as well as physico-chemical data sources) are described in Pearce et al. (2017) and Wambaugh et al. (2018). In contrast to ICF, there is no option to simulate the process of a substance being metabolised and consequently predict parent substance and metabolite concentrations in the current version of the Httk. Currently in Httk, only the concentration of the parent substance is predicted following metabolism which is why the model could not be used for phthalates. Httk/r version 1.8 (2018) was used in the current study and the following functions were applied: httkpop_generate, get_httk_params, "solve_pbtk", "calc_css".

2.2.3. Step 2.1: Selection of chemicals to simulate

Nine compounds were selected with measured values in both populations to perform the analysis. The compounds selected are listed in Table 2.1. Several other chemicals and metabolites were available in the cohorts' data sets, but were not considered for this analysis and the MRA due to limitations of both PBK models. For ICF, a steady state was not reached for most chemicals and Httk was limited to compounds measured as parent compounds in urine as it does not include metabolism. Four compounds were selected for the application of ICF, namely two phenols (i.e. bisphenol A and triclosan) and two phthalates (i.e. DnBP and BBzP). For Httk, four of the compounds under consideration were parabens (i.e. methyl paraben, ethyl paraben, n-propyl paraben and n-butyl paraben) along with two phenols (i.e. bisphenol A and triclosan). Furthermore, benzophenone-3 was included in the analysis with Httk to complete the phenol group and therefore improve the MRA.

2.2.4. Step 2.2: Literature search for tolerable daily intakes (TDIs)

The TDIs established by public authorities were collected from databases or the literature and are presented in Table 2.1 including information of the source of the data. Table 2.1 shows all compounds selected for the HBM analysis and MRA, as well as their TDIs and RfD if available. For phthalates, in addition to the parent compound, information on the main metabolite measured in urine as an indicator of exposure is presented.

Table 2.1: Compounds selected for the HBM analysis and MRA, and available TDIs and RfDs.

Parent Compound	Abb.	CAS	TDIs (mg/kg/day)	RfD (mg/kg/day)	Human urine metabolite measured	Abb. of metabolite	CAS of metabolite
Bisphenol A	BPA	80-05-7	0.004[1]	0.05[2]	-/-	-/-	-/-
Triclosan	TCS	3380-34-5	0.047[3]	0.3[2]	-/-	-/-	-/-
Benzophenone-3/ Oxybenzone	BP-3/Oxy	131-57-7	0.1[4]	NA	-/-	-/-	-/-
Methyl paraben	MeP	99-76-3	10[5]	NA	-/-	-/-	-/-
Ethyl paraben	EtP	120-47-8	10[5]	NA	-/-	-/-	-/-
n-Propyl paraben	n-PrP	94-13-3	0.02[6]	NA	-/-	-/-	-/-
n-Butyl paraben	n-BuP	94-26-8	0.02[6]	NA	-/-	-/-	-/-
Di-n-butyl phthalate	DnBP	84-74-2	0.01[7]	0.1[2]	Mono-n-butyl phthalate	MnBP	131-70-4
Butylbenzyl phthalate	BBzP	85-68-7	0.5[8]	0.2[2]	Monobenzyl phthalate	MBzP	2528-16-7

Abb.: abbreviations; NA: not available; -/- : not applicable; References: [1] EFSA, 2015; [2] U.S. EPA, 2019; [3] ITER, 2019; [4] Council of Europe, 2009; [5] Group TDI from EFSA, 2018; [6] Moos et al., 2017; [7] EFSA, 2005b; [8] EFSA, 2005a.

2.2.5. Step 2.3: Selection of physiological parameters in the model

2.2.5.1. IndusChemFate input parameters

Four chemicals were selected initially to test the model. These chemicals were two phthalates (DnBP, BBzP) and two phenols (bisphenol A, triclosan). They were chosen based on the simplicity of their metabolism and the availability of the estimated daily intakes/tolerable daily intakes and measured urine concentrations.

The physico-chemical input parameters needed for each compound and its metabolites included the molecular weight, density, vapour pressure, logarithm of the octanol-water partition coefficient at the pH of blood (pH 7.4) and water solubility. In addition, the model required estimates of the oral absorption rate, resorption in renal tubuli, enterohepatic removal as well as V_{max} and K_m values with respect to each metabolic step that is intended to be considered. All values of these parameters are presented in Table 2.A.1 of Appendix 2.A. Properties of the BPA glucuronide used are those saved in the ICF model.

Based on the conclusions of Pelkonen et al. (1973), Hakooz et al. (2006), Barter et al. (2007) and Zhang et al. (2015), a factor of 40 mg/g was adopted to scale V_{max} values from a value established *in vitro* to an *in vivo* hepatic drug clearance value. The absorption rate (k_a) was calculated using the Winiwarter et al. (1998) model 3b to derive the logarithm of the effective permeability (P_{eff}) and Peters (2008, Eq. 1) to then calculate the k_a.

For more information on how model-inherent parameters were defined or generated, see Jongeneelen and ten Berge (2011a, 2011b). To test the model, two females and two children from the Norwegian population were selected; one of "normal" weight (Woman/ Child 1) and one "obese" (Woman/ Child 2). Respective population scenarios were selected in ICF, i.e. a normal and obese woman, and a normal and obese child at rest. As mentioned previously, to categorise the BMI of a child the age and sex are required. However, a BMI of 16 is a normal weight for a child under 11 regardless of sex and a BMI of 22 is overweight or obese (CDC, 2018). Accordingly, a child with a BMI of 16 was selected for the normal category and a child with a BMI of 22 for the obese category. Their respective weights were entered into the code (via Developer -> VisualBasic) for the corresponding normal/obese woman/child at rest. The duration of simulation was set for an acute oral exposure at 24 hr and for long-term exposure to steady state.

2.2.5.2. Httk input parameters

2.2.5.2.1. Sample size for general population Monte Carlo simulations and generation of virtual population-specific physiological parameters for BE_{TDI} calculation

The urine-related BE_{TDI} values were intended to be applicable to a diverse population, therefore it is more accurate if individual variability is taken into account. This variability can be met in Httk with the creation of a virtual population. Using the function "httkpop_generate", a virtual population with physiological data taken from the NHANES (Johnson et al., 2014) was generated. The gender, age range, weight category, kidney function category and ethnicity may be defined and together they addressed the inter-individual variability. The characteristics of a created virtual population may then be used to generate population-specific parameters to run the PBTK model.

In the present work we used the Yamane formula to define a sample size based on a given population size (Yamane, 1967):

$$n = \frac{N}{[1 + N(e^2)]} \quad \text{(Eq. 2.1)}$$

Where n = sample size, N = population, e = 0.05, error tolerance.

The Yamane formula was used to characterise European Union general population size, based on 508 million inhabitants, a sample size of 400 is estimated. Samples of 400 and 4,000 persons were feasible in Httk, a Yamane-formula-based 400-subject and a 4,000-subject population were created to simulate the BE_{TDI}. As performed for the adult population, two populations, one with a larger sample size than the other, were created for children. The result was a sample size of 1,000 made up of 500 males and 500 females and a sample size of 10,000 made up of 5,000 males and 5,000 females; all between the ages of 6 and 11 years.

These populations constituted a random selection of individuals from all weight categories (underweight, normal, overweight and obese), "non-hispanic white" and

"other" ethnicities, with normal kidney function and from 32 to 56 years of age for female adults and 6 to 11 for children. For each individual in these populations and each chemical, the function "get_httk_params" was used to generate parameters to run the PBK model. When running this function, poor metabolisers were considered.

2.2.5.2.2. Generation of virtual population-based physiological parameters for BE_{EDI} calculation

For the calculation of BE_{EDI} from the EDIs provided for the Norwegian women and children, virtual populations were created which represented both Norwegian groups as accurately as possible. Therefore, the adult females were split into three weight categories based on their BMI. Virtual populations were then created with the same number of individuals in each category. As a result, the three virtual populations were: i) 28 normal weight, ii) 12 overweight and iii) 6 obese individuals.

The Norwegian population of children could not be separated according to weight categories as information of their individual age and sex was not available. A virtual population of children (both male and female) between 6 and 11 years old and of all weight categories was created to visualise the ranges in weight and BMI. The results showed that, in Httk, any child with a BMI over 25 is considered obese, however, with BMIs under 25 the overlap between normal and overweight was too close to compare without the information of age. Therefore, looking at the HBM data of the children with EDIs and corresponding urine measurements, only one child is obese and the other 43 are normal/overweight. For the BE_{EDI} calculation of the obese child, an obese population (200 boys and 200 girls) was simulated and the individual with the closest BMI and weight (weight_adj in Httk) to the child was chosen. For the other individuals, a population of 200 boys and 200 girls with the weight categories normal and overweight was created. Individuals with weights or BMIs outside the limits of those measured in the population were then eliminated. To solve for the same number of individuals as in the data, 43 individuals were randomly selected until the maximum, minimum, median and mean were similar to that of the HBM data.

2.2.6. Step 3: Forward dosimetry

As illustrated in Figure 2.3, the forward dosimetry approach was used in this study to estimate the concentration of a substance in human urine from an oral intake dose, i.e. a BE_{EDI} from an EDI, a BE_{TDI} from a TDI, and a BE_{RfD} from an RfD.

2.2.6.1. Forward dosimetry with ICF

The estimated daily intakes (EDI) measured in the Norwegian HBM project for the chosen individuals, as well as the tolerable daily intakes (TDIs) and reference doses (RfDs) of the chemicals were entered into the model as oral bolus doses (in mg/kg BW) at hour 0. No EDIs were measured for triclosan.

The model was run at 10,000 iterations per hour for 24 hours. The time to reach steady state was assessed using the equation $T_{ss} = 5 \times t_{(1/2)}$, with $t_{(1/2)}$ being the elimination half-life. Of all compounds under consideration, triclosan takes the longest time to reach steady-state, namely 145 hours (6.04 days) if considering the maximum human elimination half-life of 29 hours (European Commission Scientific Committee on Consumer Safety (SCCS), 2009). Therefore, to predict BE values at steady state, all compounds were predicted for seven days to make sure that all reached steady state at the end of simulation time. As results for each BE_{TDI}, BE_{RfD} and BE_{EDI} and individual scenario (Woman/Child 1 and 2), the 24-hour and steady state C_{max} values were recorded.

ICF predicts the concentration of the metabolites, which is directly applicable for the phthalates, where relevant metabolites have been analysed in the urine samples. For TCS and BPA, the ICF model predicts the urinary concentrations of the glucuronidated metabolites (TCS-glu and BPA-glu) while the hydrolysed TCS and BPA forms were analysed in the urine samples. In order to match the results and compare predicted with measured concentrations, the resulting urine concentrations of TCS-glu and BPA-glu were converted from µmol/L to ng/mL based on the molecular weight of the parent compound.

2.2.6.2. Forward dosimetry with Httk to calculate BE_{TDI}

In order to calculate the 'urinary reference values', the TDI was entered as a daily dose. Subsequently, "solve_pbtk" was run for each individual in each population.

When the model was run for the time to reach steady state as defined by the function "calc_css", it was found that the amount excreted in the urine was still increasing at the end of the simulation time. Therefore, simulation times were defined as shown in Table 2.2 to ensure that steady state was reached in the urine by the end of simulation time.

Table 2.2: Times to steady state and selected simulation time for each compound run in Httk

	Calc_css results (days)	**Simulation time (days)**
MeP	1	7
EtP	1	7
PrP	2	7
BuP	2	7
TCS	4	10
BP-3/Oxy	2	7
BPA	11	30

The PBK output table generated for each individual included the amount of the chemicals in the renal tubules. This amount was interpreted as the amount excreted in the urine. The maximum amount excreted was converted from mg/day to ng/day and then divided by the volume of urine expected to be excreted (1600mL for adult females and 820mL for children (Sakhi et al., 2018)) to obtain a value in ng/mL.

BE_{TDI} calculations were performed on two sets of 4,000 and 400 women and two sets of 10,000 and 1,000 children to evaluate whether the BE_{TDI} values would differ considerably based on the different populations. The mean values differed very little between the larger versus the smaller populations but the standard errors of the mean of the larger populations were reduced and therefore populations of 4,000 and 10,000 individuals were used for women and children respectively. When choosing between the two 10,000 and two 4,000 individual populations the 5^{th} percentile and median BE_{TDI} values were compared. The differences were marginal and the one population per age group with the overall lower BE_{TDI} values was chosen.

Of the distribution of 4,000 urine TDI equivalents excreted per day in the adult female population and 10,000 values in the children, the 5^{th} percentile, as a conservative

measure, and the median were used as BE_{TDI} values and compared with measured urine concentrations.

2.2.6.3. Forward dosimetry with Httk to calculate BE_{EDI}

In order to assess potential risks from the exposure information derived from urinary excretion levels, it is common practice to calculate back to the daily intake values. For the current data set and the covered chemicals, many papers were available that had partly already done that for parabens (Asimakopoulos et al., 2014; Moos et al., 2016) and phenols (Frederiksen et al., 2013; Asimakopoulos et al., 2014). In some cases, an EDI is then calculated by multiplying the urinary concentrations with the urine volume over 24h. In reality, in these cases higher exposure was most likely to have occurred.

EDIs derived from ambient air, dust and food concentrations were provided by the Norwegian Institute of Public Health. They were intended to be used for forward dosimetry to obtain a urine level BE_{EDI} which may be compared to measured urine concentrations in order to assess how well simulated and measured values correlate (Step 4 of Figure 2.2).

For the Norwegian populations, the only EDIs available for the chosen chemicals were those for BPA. As discussed in 2.2.5.2.2, virtual populations were created comprising 28 normal weight, 12 overweight and 6 obese women, as well as one obese and 43 normal/overweight children. To calculate the BE_{EDI} values for both Norwegian adults and children, every individual's EDI was used as a daily intake for the individual's corresponding virtual population. Therefore, the same EDI has several BE_{EDI} values, one for each individual in the virtual population (e.g. 28 for the adult female normal weight population). For each EDI the average of its resulting BE_{EDI} values was then compared against the corresponding measured urine concentration. To illustrate this with an example, a normal weight woman having an EDI of 1.40×10^{-4} mg/kg was selected. This value was used as the input for the normal female virtual population of 28 individuals, thus generating 28 BE_{EDI}. The average BE_{EDI} ($\sum BE_{EDI}/28$) was 0.131 ng/mL. The measured urine concentration of the individual woman (with EDI = 1.40×10^{-4} mg/kg) was 1.88 ng/mL, thus an order of magnitude higher than the simulated BE_{EDI} of 0.131 ng/mL.

2.3. Step 4: Evaluation of modelling results

In order to test the model and estimate the quality and validity of the BE_{TDI}, all predicted values – i.e. BE_{EDI}, BE_{TDI}, BE_{RfD} – were contrasted with comparable values. BE_{EDI}, which represent the predicted urine concentration reached at oral exposure to the EDI, were compared to the urine concentration measured in individuals. Under the assumption that EDI values are reliable, the closer BE_{EDI} are to measured urine concentrations, the better the performance of the model. BE_{TDI} and BE_{RfD}, which constitute safe chronic urine concentrations, were compared to previously established BE values.

2.3.1. Deriving BE_{EDI} values with IndusChemFate and comparing these to measured concentrations for four individuals

Using the calculated EDI from external sources for two women and two children from the Norwegian HBM dataset, the corresponding urinary concentrations BE_{EDI} were simulated with ICF and compared to the measured urinary concentrations for these four individuals. For data protection reasons, individual urine concentrations and individual EDI are not shown but the factor of deviation between measured and predicted values are shown (Tables 2.3-2.5).

2.3.1.1. BE_{EDI} predictions with IndusChemFate following 24-hour simulation time

A comparison of urinary concentrations of the two women to simulated BE_{EDI}, BE_{TDI} and BE_{RfD} values for DnBP, BBzP, TCS and BPA is presented in Table 2.3. A comparison of these values related to the two children is included in Table 2.4. For DnBP, the EDI of woman 1 is approximately a factor of two higher than the EDI of woman 2, which is reflected in the corresponding calculated BE_{EDI}. This indicates that predicting urine concentrations for individuals of different weight categories does not necessarily generate substantially different results. The same relationship between the EDI of both women for BBzP and the corresponding BE_{EDI} was observed; the EDI and BE_{EDI} of woman 2 for BBzP is approximately a factor of 2.5 lower than the respective EDI and BE_{EDI} of woman 1. In contrast, for BPA, the EDI of woman 1 - which is similar to the DnBP-related EDI of woman 1 – results in a BE_{EDI} four orders of magnitude higher than the DnBP-related BE_{EDI}. With regard to EDI and the corresponding BE_{EDI} of both children, the same holds for both phthalates and BPA. EDI values of child 1 for DnBP

and BBzP are approximately three times higher than respective EDI values of child 2, which is reflected in all corresponding BE_{EDI}. However, for BPA, the same relationship between EDI and BE_{EDI} is observed as previously seen in both female adults.

When comparing measured urine concentrations (not detailed due to data protection reasons) to calculated BE_{EDI}, they differ by a factor of 3 to just over one order of magnitude for BPA, and three to over four orders of magnitude for both phthalates. For DnBP and BBzB, BE_{EDI} are always lower than measured urine concentrations. The measured urine concentrations of both women and child 1 for MnBP (DnBP metabolite) were very similar, and three to just over four orders of magnitude higher than the calculated BE_{EDI}. Whereas the measured urine concentration of child 2 is a factor of 3.5 higher than the concentration measured in child 1 while the estimated EDI of child 2 is over a factor of three lower than the EDI of child 1. Therefore, corresponding BE_{EDI} of child 2 differs by four orders of magnitude from the measured urine concentration. While for child 1, the measured urine concentrations of MBzP (BBzP metabolite) differ by only three orders of magnitude from the BE_{EDI}, for child 2 and both female adults measured urine concentrations are four orders of magnitude higher than corresponding BE_{EDI}. This could indicate that there are other sources of the selected chemicals that are not covered when calculating the EDI, but it can also indicate that ICF is underpredicting. Overall, it is suspected that total exposure is underestimated for these substances.

In contrast, the BE_{EDI} of BPA for the normal weight adult female and the obese child are higher than measured concentrations in urine by just over an order of magnitude and a factor of three, respectively. Interestingly, the measured urine concentrations of BPA of the obese adult female and the normal weight child were very similar, and a factor of five and nine higher than their respective BE_{EDI} for these individuals. Unfortunately, there were no measurements to estimate EDIs for triclosan so no BE_{EDI} was calculated for this compound.

2.3.1.2. BE_{EDI} predictions with IndusChemFate for steady-state simulations

When running the simulation for all compounds for seven days, only BPA reached a steady-state concentration. The venous blood concentration of all other substances continued to increase steadily, even when the simulation was run for a period

substantially longer than seven days (100-300 days). Therefore, steady state simulation results presented in Table 2.5 are only shown for BPA. Interestingly the steady state BE_{EDI} is very similar to the 24-hour BE_{EDI} for all four individuals. Therefore again, measured urine concentrations and those estimated from the EDI differed by between a factor of three and one order of magnitude.

In conclusion, 24-hour and steady state results suggested that kinetics of BPA were calculated substantially differently to the kinetics of both phthalates included. Predictions for BPA were considered more accurate than predictions for other substances in ICF since steady state was reached only for BPA. This may be related to the fact that the BPA was a test chemical for the development of the ICF model and its data were already provided in ICF when the model was downloaded from the Cefic-LRI website. Uncertainties underlying EDI values were not quantified and further discussed in subchapter 2.3.4.

Table 2.3: Comparison of urinary concentrations of two Norwegian female adults to ICF simulated BE_{EDI} (EDI-based urine concentrations) and predicted BE_{RfD} and BE_{TDI} values after a 24-hour simulation time with IndusChemFate

	Woman	Parent compound	Metabolite	TDI (mg/kg/day)	RfD (mg/kg/day)	BE_{TDI} (ng/mL)	BE_{RfD} (ng/mL)	Factor measured urine conc. / BE_{EDI}	Exceedance of threshold (conc. in urine/BE_{TDI})	Exceedance of threshold (conc. in urine/BE_{RfD})
Phthalates	1	DnBP	MnBP	0.01	0.1	0.14	1.37	8,875	112	11.40
	2	DnBP	MnBP	0.01	0.1	0.13	1.34	18,500	129	12.50
	1	BBzP	MBzP	0.5	0.2	7.8	3.12	7,770	0.67	1.66
	2	BBzP	MBzP	0.5	0.2	7.66	3.06	11,400	0.37	0.92
Phenols	1	TCS	TCS-glu	0.047	0.3	0.44	2.67	NA	0.16	0.04
	2	TCS	TCS-glu	0.047	0.3	0.39	2.36	NA	0.12	0.03
	1	BPA	BPA-glu	4×10^{-3}	0.05	377	4,700	0.1	0.005	4×10^{-4}
	2	BPA	BPA-glu	4×10^{-3}	0.05	437	5,460	9.3	0.025	2×10^{-3}

NA: not available. Up to three significant figures are reported.

Table 2.4: Predicted BE_{EDI} for a variety of chemicals for two Norwegian children after 24-hour simulation time with IndusChemFate

	Child	Parent compound	Metabolite	TDI (mg/kg/day)	RfD (mg/kg/day)	BE_{TDI} (ng/mL)	BE_{RfD} (ng/mL)	Factor measured urine conc. / BE_{EDI}	Exceedance of threshold (conc. in urine/BE_{TDI})	Exceedance of threshold (conc. in urine/BE_{RfD})
Phthalates	1	DnBP	MnBP	0.01	0.1	0.23	2.26	1,510	73.0	7.42
	2	DnBP	MnBP	0.01	0.1	0.23	2.26	17,600	251	25.6
	1	BBzP	MBzP	0.5	0.2	10.9	4.36	1,220	0.25	0.62
	2	BBzP	MBzP	0.5	0.2	10.9	4.36	10,600	0.91	2.27
Phenols	1	TCS	TCS-glu	0.047	0.3	0.73	4.46	NA	0.08	0.02
	2	TCS	TCS-glu	0.047	0.3	0.67	4.11	NA	0.05	0.01
	1	BPA	BPA-glu	4×10^{-3}	0.05	637	7,970	16.2	0.0166	0.0013
	2	BPA	BPA-glu	4×10^{-3}	0.05	736	9,190	0.56	2×10^{-3}	2×10^{-4}

NA: not available. Up to three significant figures are reported.

Table 2.5: Simulated BE_{EDI} of BPA at steady state for four individuals predicted with IndusChemFate

Woman	Parent compound	Metabolite	TDI (mg/kg/day)	RfD (mg/kg/day)	BE_{TDI} (ng/mL)	BE_{RfD} (ng/mL)	Factor measured urine conc. / BE_{EDI}	Exceedance of threshold (conc. in urine/BE_{TDI})	Exceedance of threshold (conc. in urine/BE_{RfD})
1	BPA	BPA-glu	4×10^{-3}	0.05	428	5,350	0.126	4.4×10^{-3}	4×10^{-4}
2	BPA	BPA-glu	4×10^{-3}	0.05	473	5,910	8.59	0.0232	1.9×10^{-3}
Child	**Parent compound**	**Metabolite**	**TDI (mg/kg/day)**	**RfD (mg/kg/ day)**	**BE_{TDI} (ng/mL)**	**BE_{RfD} (ng/mL)**	**Factor measured urine conc. / BE_{EDI}**	**Exceedance of threshold (conc. In urine/BE_{TDI})**	**Exceedance of threshold (conc. In urine/BE_{RfD})**
1	BPA	BPA-glu	4×10^{-3}	0.05	649	8,120	0.063	0.0163	1.3×10^{-3}
2	BPA	BPA-glu	4×10^{-3}	0.05	739	9,240	1.80	2×10^{-3}	2×10^{-4}

Up to three significant figures are reported.

2.3.2. Deriving BE_{EDI} values with Httk and comparing these to measured concentrations of the Norwegian dataset

Similar to the calculation of BE_{EDI} using ICF, as presented in the previous subchapter, EDI values were used in Httk to calculate urine-based BE_{EDI} values which were subsequently compared to measured urine concentrations. For the Norwegian populations, the only EDIs available for the chemicals selected for the use of Httk were those for BPA. Figures 2.4A and 2.4B show the BE_{EDI} values calculated for BPA based on the EDIs of women and children of the Norwegian study group. The horizontal lines in both graphs illustrates the range between the minimum and maximum urine concentrations measured in these individuals. Overall, the difference between the measured and simulated urine concentrations of Norwegian adult females and children is, on average, two to three orders of magnitude, with a minimum of one and a maximum of five orders of magnitude. It is interesting to note is that the higher the EDI value used as the daily dose, the closer the predicted result to the measured urine concentration. This may indicate that either the higher the EDI, the more complete and reliable this value is which results in a more reliable $BE_{EDI,}$ or that Httk performs better with higher oral doses.

A

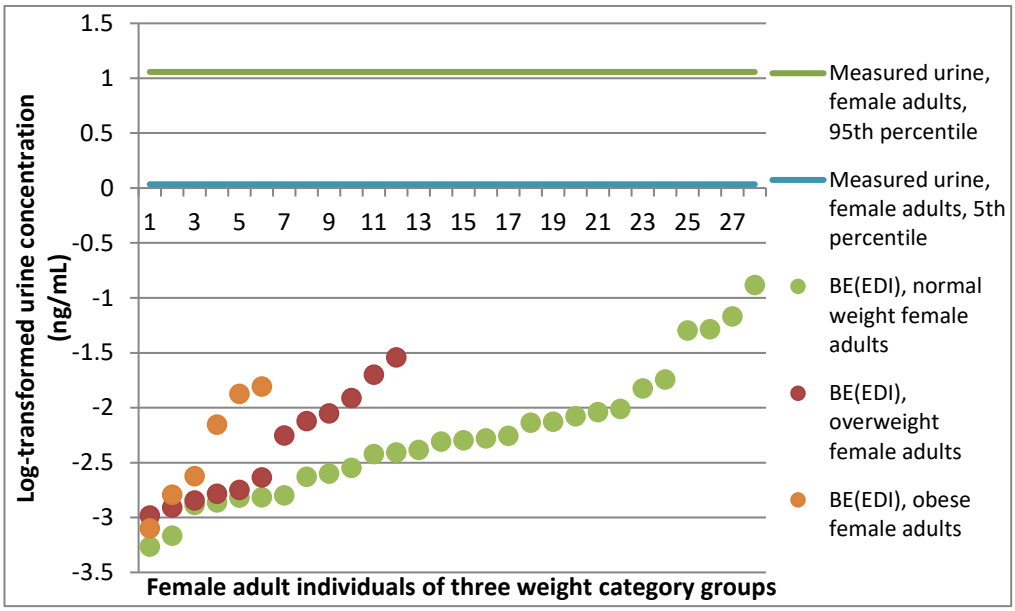

B

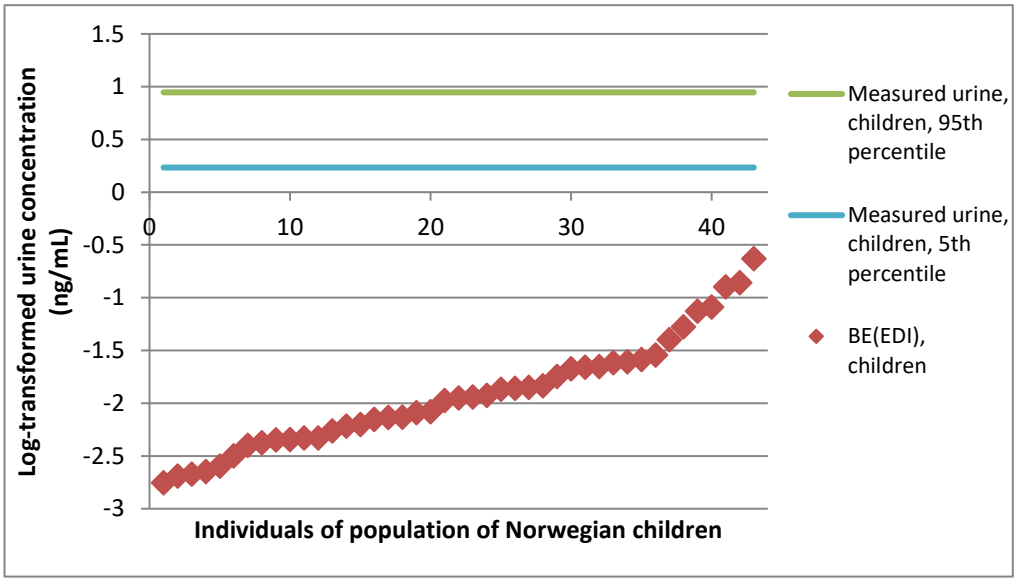

Figure 2.4A. BE_{EDI} concentrations for BPA based on EDIs of 28 normal weight, 12 overweight and 6 obese female adults of the Norwegian group of women in relation to the area between the minimum and maximum measured urine concentration of this study population**. 2.4B**. BE_{EDI} concentrations for BPA based on EDIs of 43 Norwegian children in relation to the area between the minimum and maximum measured urine concentration of this study population.

2.3.3. Deriving BE_{TDI} values with IndusChemFate and Httk and comparing these to previously established BE values

In order to better understand whether the BE_{TDI} values calculated in ICF and Httk are somewhat similar to previously established BE values of the compounds considered here, a search of comparable values was performed. Urine-based BE values were only found in the literature for TCS and BPA. These had been established by the German HBM Commission termed HBM-I values (Angerer et al., 2011) on the basis of TDI values published by Krishnan et al. (2010a, 2010b). The BE values for TCS were 3.000 and 2.000 ng/mL for adults and children, respectively, as well as 200 and 100 ng/mL for BPA.

Table 2.6 shows that for TCS, all BE_{TDI} values obtained from Httk and ICF are comparatively similar to each other and differ from previously established levels by three to four orders of magnitude. It needs to be taken into account, however, that the TDI value used for establishing the HBM-I-values was 0.12 mg/kg/day and therefore higher than the TDI of 0.047 mg/kg/day used in our study. For BPA, however, existing BE values were in the same order of magnitude when considering BE_{TDI} values calculated in ICF for female adults and one order of magnitude different to those simulated for children. The ICF-related values shown here are only based on two individual scenarios offered by the model. Therefore, a range of BE_{TDI} values reflecting inter-individual variability was not obtained with this model. All median-based BE_{TDI} values obtained for BPA from Httk are two orders of magnitude lower than previously established values. Therefore, even the lower BE_{TDI} for BPA based on the 5^{th} percentile may be considered particularly conservative.

Table 2.6: BE_{TDI} values calculated in IndusChemFate and Httk for female adults and children compared to previously proposed BE values (HBM-I-Werte) by the German HBM Commission

		TCS	BPA
BE_{TDI} values established in ICF	**Normal weight female adult (ng/mL)**	0.44[a]	428[b]
	Obese female adult (ng/mL)	0.39[a]	437[b]
	Normal weight child (ng/mL)	0.73[a]	649[b]
	Obese child (ng/mL)	0.67[a]	739[b]
BE_{TDI} values established in Httk	**Female adults, 5th percentile (ng/mL)**	0.89	1.08
	Female adults, median (ng/mL)	2.57	3.08
	Children, 5th percentile (ng/mL)	0.64	0.79
	Children, median (ng/mL)	1.73	2.09
Existing BE values (HBM-I-Werte)	**Adults (ng/mL)**	3,000[c]	200
	Children (ng/mL)	2,000[c]	100

[a] BE_{TDI} values for TCS were derived in ICF using 24h simulations, since a steady state was not reached.

[b] BE_{TDI} values for BPA were derived in ICF using steady state simulations, which is the best comparable to the concept of deriving TDIs as a safe dose based on chronic daily exposure. The difference between 24h simulations and steady state simulations for BPA in ICF are however small (see Table 2.3-2.5).

[c] HBM-I-values for TCS are based on a TDI of 0.12 mg/kg BW and day as opposed to 0.047 mg/kg BW and day which was used for BE_{TDI} values established in this study.

2.3.4. Evaluation of IndusChemFate and Httk modelling results

It is difficult to evaluate the validity of ICF and Httk modelling results as the only exercise undertaken to test both models was the forward dosimetry approach using EDI values of four individuals with ICF and of 46 women and 43 children of the Norwegian study group with Httk.

It is crucial to consider that, besides uncertainties inherent in ICF and Httk predictions, several uncertainties are likely to be associated with the EDI values used. Typically, these uncertainties generally relate to source variability (e.g. changes in exposure rates, sources and duration), variability of model input parameters to calculate the EDI, incomplete capture of precursor compounds, and metabolic variability within a population and with respect to changes in metabolic rate of an individual which are not considered when calculating the intake of precursor compounds (Haug et al., 2011; Hines et al., 2011). The approach used to calculate EDI

values for Norwegian adult females included assumptions of the amount of drinking water consumed and indoor air inhaled as well as three scenarios for dust ingestion in order to achieve sufficiently certain results (see Haug et al., 2011). Another aspect contributing to uncertainty of BE_{EDI} results is related to the use of the EDI value as a whole as an oral dose even though a fraction of it is related to inhalation exposure. Overall, in comparison to other parts of a risk assessment (i.e. hazard identification, dose-response assessment), an even broader range of uncertainties may be involved in exposure assessment due to e.g. incomplete capturing of exposure sources (National Research Council, 2009; Bang et al., 2012; Yao et al., 2018). Therefore, an EDI is assumed to be an estimate of the minimal exposure, while higher exposure has, in reality, most likely occurred.

In conclusion, predictions for BPA are considered more accurate than predictions for other substances in ICF. The reason for this is primarily that steady state was only achieved for BPA. Because of this, ICF results are not considered for single substance risk assessment (Step 5) and mixture risk assessment (Step 6). With regard to the Httk results, simulated urine levels BE_{EDI} differ by, on average, two to three orders of magnitude from measured urine concentrations in 46 adult females and 43 children. This exceeds the conventionally accepted difference of one order of magnitude between predicted and measured results. Interesting to note is that predicted BE_{EDI} concentrations (in ng/mL) follow the same trend as EDIs (mg/kg BW) (data not shown). This indicates linearity between model input and output reflecting linear biological processes. However, metabolism may for instance saturate and therefore be non-linear.

When compared to previously established TDI-based BE concentrations in urine, the BE_{TDI} values obtained with Httk appear to be conservative. Additionally, reference values such as TDIs and RfDs also bear uncertainties (e.g. extrapolation from animal to human populations, see also Hays et al. (2007)) and are continuously updated which indicates, to some degree at least, lack of robustness overall. An overview of limitations and uncertainties of both models is outlined in subchapter 2.3.5.

2.3.5. Uncertainties and assumptions when applying IndusChemFate and Httk to assess HBM data

It is difficult to assess and quantify all uncertainties underlying ICF and Httk modelling results and data interpretation. Table 2.7 summarises assumptions, limitations, and uncertainties identified with regard to the formulated research problem and the workflow of this study (as outlined in subchapter 2.2). Particular regard was given to limitations and uncertainties related to the application of both PBK models, their input parameters, model structure and output since these link strongly to the problem formulation. These aspects are discussed further in the Discussion (subchapter 2.6). Assumptions, limitations and uncertainties related to the presented HBM analysis do not affect the applicability of the selected PBK models but need to be considered when interpreting all simulated results.

Table 2.7: Assumptions, limitations and uncertainties of the IndusChemFate and Httk platforms

	IndusChemFate	**Httk**
Problem formulation	How can PBK models be used to interpret exposure by applying HBM data in the context of assessing the risk of environmental pollutants?	
Limitations and uncertainties related to input parameters	Uncertainty in *in vitro* data (e.g. nominal as opposed to the effective free concentration is recorded). *In vitro* to *in vivo* extrapolation uncertainty (e.g. uncertainty related to the scaling factor used for V_{max} values). Chemical-specific parameters were sourced from different databases and the public literature; therefore, based on a wide variety of techniques. Absorption rate calculated using a QSAR model. Predictions of physiological input parameters based on various QSPRs (blood:air partitioning, tissue:blood partitioning, renal excretion, tubular resorption). The QSPR calculating solubility in blood assumes that human blood consists of 0.7% lipids. 8% of arterial blood is assumed to be turned into primary urine.	Uncertainty in *in vitro* data (e.g. nominal as opposed to the effective free concentration is recorded). *In vitro* to *in vivo* extrapolation uncertainty. Inbuilt chemical-specific parameter values were used. Only the p-value related to the intrinsic clearance of TCS was changed manually. Fewer variety of sources and higher consistency of methodology. High degree of parameters are based on *in vitro* data or QSAR models. Perfusion-limited kinetics. Negligible blood volume fractions in all tissues to justify dividing by the tissue volume without a blood volume fraction and partition coefficient dependency in PBK tissue concentration equations. Allows only for metabolism in liver. Linear, non-saturated metabolism considered. $R_{blood2plasma}$ is constant throughout the body.

	Urinary excretion is driven by the lipophilicity of the molecule. No tubular resorption of very soluble substances with a log K_{ow} < -1.5. Physiological parameters do not change by gender. Lack of detailed consideration of population variability specific protein binding, interaction with intestinal flora, intestinal transport, and excretion by faeces.	Clearance is assumed to be relative to the amount unbound in whole blood instead of plasma, but converted to use with plasma concentration. The function Wetmore.data comprising Wetmore et al. (2012, 2013) and Wetmore (2015) assumed the fraction unbound (f_{ub}) = 0.005 for chemicals with f_{ub} below the limit of detection. Prediction for populations which are based on U.S. NHANES data; degree of variability to European/Scandinavian population unclear.
Model structure	High number of compartments.	Moderate number of compartments. Simulation of metabolite kinetics unavailable.
Model output	Steady state not reached for most compounds. Mass balance can easily be checked but shows errors, especially in children's populations.	Size of adult female population above 4,000 individuals gave error message. Conversion from chemical amount in renal tubule to urine concentration necessary.
Assumptions, limitations and uncertainties related to the presented HBM analysis	Intake is assumed to come from the oral route, although it is known that it can also come from air or dust. Uncertainties underlying EDIs and TDIs. Uncertainties in urine concentration measurements. Only metabolism in liver was considered.	Intake is assumed to come from the oral route, although it is known that it can also come from air or dust. Uncertainties underlying EDIs and TDIs. Uncertainties in urine concentration measurements.

QSPR: Quantitative Structure-Property Relationships.

2.4. Step 5: Single substance risk assessment

In order to interpret the measured urinary concentrations, they can be compared to toxicological and health based reference values. BE_{TDI} and BE_{RfD} values can serve as such reference values to compare to. In this study, the results of BE_{TDI} calculations were applied in Step 5 to assess whether a potential risk may be associated with the concentration of compound measured in urine. The application of the BE_{TDI} values derived here is performed for illustration of the possible use and cannot be considered as detailed risk assessment.

2.4.1. IndusChemFate: Comparison of BE_{TDI} and BE_{RfD} predicted after 24-hour simulation time and at steady state with measured urine concentrations

When considering the 24-hour calculated BE_{RfD} and BE_{TDI} values in comparison to the measured urine concentrations, all four individuals appear to be exposed to concentrations below the BPA and TCS internal RfD or TDI values. For BBzP, urine concentrations measured in all four individuals were below the BE_{TDI}. However, for woman 1 and child 2 their measured urine concentration is higher than that of the BE_{RfD}. For DnBP, all measured urine concentrations are above the calculated BE_{TDI} and BE_{RfD} values for all four individuals; by one to two orders of magnitude for all BE_{TDI} values. Urinary concentrations above BE_{RfD} or BE_{TDI} indicate a potential risk, but have to be interpreted carefully here considering all the uncertainties around the derived BE values. Tables 2.3 and 2.4 summarise BE_{RfD} and BE_{TDI} values for DnBP, BBzP, TCS and BPA of the two adult females and children of the Norwegian study group following a 24-hour simulation time.

Interestingly the steady state BE_{TDI} and BE_{RfD} are very similar to the 24-hour BE_{TDI} and BE_{RfD}. All measured urine concentrations are below the calculated BE_{TDI} and BE_{RfD} values. Table 2.5 includes BE_{RfD} and BE_{TDI} values for DnBP, BBzP, TCS and BPA of the two adult females and children of the Norwegian study group at steady state.

2.4.2. Httk: results of BE_{TDI} calculations and comparing these to measured concentrations

Httk allowed for the creation of virtual populations based on which a distribution of BE_{TDI} were generated. In risk assessment, the 5th percentile of a dose-response distribution (representing the incidence of an adverse effect in 5% of a population; these 5% are considered more sensitive individuals) is often selected as point of departure (POD) (IPCS WHO, 2014; Shao and Gift, 2014; Haber et al., 2018). The POD is typically divided by safety factors (also called adjustment factors), for instance to extrapolate from an animal POD to a human POD, and then applied as safe reference value (e.g. TDI, ADI or RfD) (U.S. Environmental Protection Agency (EPA), 2012; IPCS WHO, 2014). The 5th percentile of the BE_{TDI} distribution was selected as a BE value which is protective of sensitive individuals of the virtual population and the median of the BE_{TDI} distribution was selected to allow comparison. As the TDI itself is considered a protective value, the BE_{TDI} based on the 5th percentile may be over-conservative. In this case, the BE_{TDI} based on the median would be a more adequate value for risk assessment.

Table 2.8 shows the BE_{TDI} values based on the 5th percentile and the median of the distribution of maximum urine concentrations of virtual populations of 4,000 female adults and 10,000 children who ingested daily doses of the TDI until steady state is reached in the urine.

Table 2.8: BE_{TDI} values established in virtual populations of 4,000 female adults and 10,000 children based on daily doses of the TDI.

	BE_{TDI} values (ng/mL)			
	Female adults, 5th percentile	**Female adults, median**	**Children, 5th percentile**	**Children, median**
MeP	1,010	2,970	716	1,940
EtP	1,890	5,390	1,360	3,670
MeP+EtP	1,220	4,050	865	2,690
PrP	4.73	13.9	3.41	9.45
BuP	4.56	12.9	3.19	8.65
TCS	0.89	2.57	0.64	1.73
BP-3/Oxy	11.1	32.1	8.05	21.6
BPA	1.08	3.08	0.79	2.09

Up to three significant figures are reported.

The 5th percentile BE_{TDI} values are all at least half the concentration of the median BE_{TDI} values. For MeP and EtP only a TDI is established for the sum of MeP and EtP. For the calculation of the BE_{TDI} of MeP+EtP, the TDI of 10 mg/kg/day was used to calculate the BE_{TDI} of MeP and EtP individually. From these, the BE_{TDI} for the sum of MeP+EtP was obtained by grouping all the urine TDI equivalents for MeP and EtP together and calculating the 5th percentile and median. Httk contains parameter data for n-propyl and n-butyl parabens but not their isomers. For certain individuals of the Danish dataset only measurements of the sum of n- and i-propyl as well as n- and i-butyl parabens are available. In these cases, data points based on sum measurements are plotted separately in the graph (see Figure 2.5C).

Measured urinary concentrations of Norwegian adult females, and Norwegian and Danish children, were then compared to the simulated BE_{TDI} values, both 5th percentile and median (Figure 2.5A, 2.5B, 2.5C). Measured concentrations greater than BE_{TDI} values indicate a potential risk. However, data need to be interpreted with care and uncertainties around the BE_{TDI} values need to be taken into account.

By and large when identifying urine concentrations higher than the BE_{TDI} values, these data indicate that exposure to BPA is of greatest concern. Over all chemicals and populations and considering both the 5th percentile and median based measures, more that 50% exceed the BE_{TDI} established for BPA. With respect to the 5th percentile based BE_{TDI}, 95%, 100% and over 70% of Norwegian adult females, their children and Danish children, respectively, exceed this level. While TCS exposure only exceeds both BE_{TDI} values in 10-21% of the Norwegian adult and child populations, 63 and 30% of the Danish children exceed the 5th percentile and median based measures, respectively. In both groups of children, both PrP BE_{TDI} values are exceeded by 9 to 26 % of individuals while 34 and 48 % of adult females show higher urine concentrations. Considering the 5th percentile based BE_{TDI} for BP-3/Oxy, approximately 35 to 40 of both Norwegian populations show higher levels of exposure, whereas fewer than 20% (including the Danish group) exceed the median-based value. Exposures to MeP+EtP and BuP appear to constitute the least concern. Up to 6 % of all population groups exceed both 5th percentile and median based BE_{TDI} for these chemicals.

As expected, the 5th percentile based BE_{TDI} may be a rather conservative measure. In the cases of BP-3/Oxy in Norwegian children and female adults, BPA in adult females, and n-PrP and TCS in Danish children, the difference in the number of individuals exceeding the 5th percentile and the median based BE_{TDI} is substantial. In cases where the BE_{TDI} is exceeded by roughly 20% or less of the population, the difference to the median-based BE_{TDI} does not seem to be significant.

A

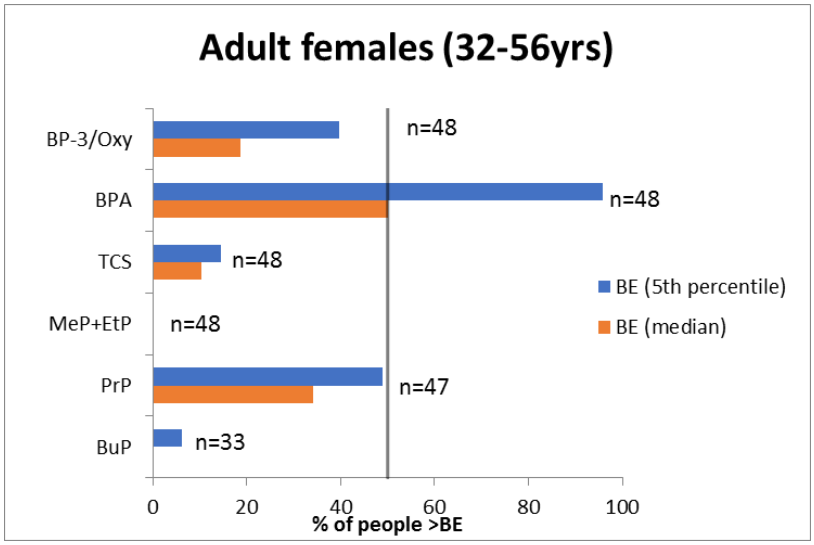

B

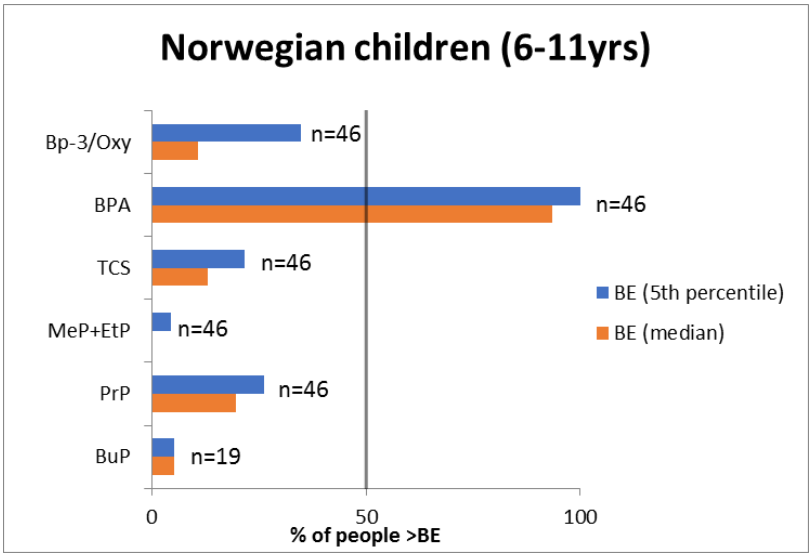

C

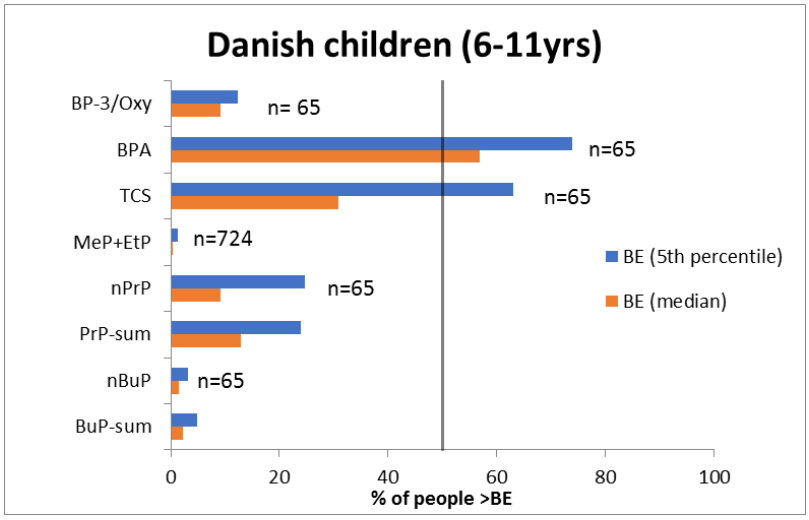

Figure 2.5A. Number of individuals (in %) in the Norwegian adult females' group whose urine concentration exceed the 5th percentile and median based BE_{TDI}. **2.5B**. Number of individuals (in %) in the Norwegian children group whose urine

concentration exceed the 5th percentile and median based BE_{TDI}. **2.5C**. Number of individuals (in %) in the Danish children group whose urine concentration exceed the 5th percentile and median based BE_{TDI}.

Since Httk application and results are considered superior to ICF application and results, as outlined above, Httk results were used for the subsequent mixture risk assessment.

2.5. Step 6: Mixture assessment case study with Httk results

In order to illustrate how the BE_{TDI} values predicted with Httk may be applied, a screening level mixture risk calculation was performed. Some parabens and phenols are known as endocrine disruptors, associated with effects on reproductive hormone and thyroid levels (Aker et al., 2016). In order to assess the risk individuals face from these chemicals as a whole, a Hazard Index (HI) approach was used. The HI is calculated by summing all of the risk quotients (RQ) of an individual, each RQ is the concentration of a chemical (j) found in the urine of an individual (i) divided by the BE_{TDI} values established in this report (see Table 2.8 and Eq. 2.2 and 2.3) (Price and Han, 2011; DG Health & Consumers, 2012; Bopp et al., 2018). Ideally, only chemicals with the same MoA leading to the same adverse outcome should be considered for the combined assessment and in calculating the HI (Kienzler et al., 2016). However, including all chemicals in a first screening level estimate, independent of the detailed MoA and adverse outcome consideration, is a worst-case conservative approach. If the resulting HI is smaller than 1, it indicates that there is low concern. If a potential concern is identified (i.e. if the $HI > 1$), a refinement looking more in depth into grouping chemicals that are expected to contribute to a specific effect should be performed, but this is out of scope of this case study.

$$RQ(ij) = \frac{Urine\ concentration\ (ij)}{BE_{TDI}(j)}$$

(Eq. 2.2)

$$HI(i) = \sum RQ(ij)$$

(Eq. 2.3)

2.5.1. Mixture assessment results

The Hazard Index was calculated for each individual against the two BE_{TDI} values established in subchapter 2.3.3, i.e. 5th percentile BE_{TDI} and median BE_{TDI}. In addition, a HI was determined for each study population in order to represent the risk each one faces. These HIs presented here were calculated using the median measured urine concentration of each chemical against the median BE_{TDI} calculated (Figure 2.6A-C for Norwegian female adults, Norwegian children and Danish children, respectively). The HI for all three study population groups is above the recommended maximum of 1 and is mainly constituted by the RQ for the group of phenols, in particular the RQ related to BPA. It should be noted that the median is estimated for some chemicals with fewer samples than for others (i.e. n-BuP). More information on HIs calculated with the 5th percentile BE_{TDI} and the 95th as well as the median of measured urine concentrations is presented in Appendix 2.B, Figures 2.B.1 and 2.B.2, respectively. In fact, the phenols make up over 95% of the HI for both child populations. In terms of chemicals, BPA has the highest RQ in all of the populations, whilst n-BuP and MeP+EtP have the lowest. In addition, two chemicals of note for the Norwegian mothers are BP-3 and n-PrP. The latter shows that the mothers are more exposed to parabens than their children, however, their HI is lower than both child populations. Finally, although Norwegian children have the highest HI they appear to be less exposed to TCS than the Danish children. In the comparison between the Norwegian and the Danish children, it needs to be taken into account however, that samples were taken in different years (2012 for Norwegian study and 2006/2007 for the Danish study), so that a decrease of external exposure concentrations over time might also play a role.

The risk quotients and HI using the BE_{TDI} values established in this study have to be interpreted with care, taking into account the uncertainties around the BE_{TDI} values and the orders of magnitude difference in them when using different models or comparing to formerly established BE thresholds.

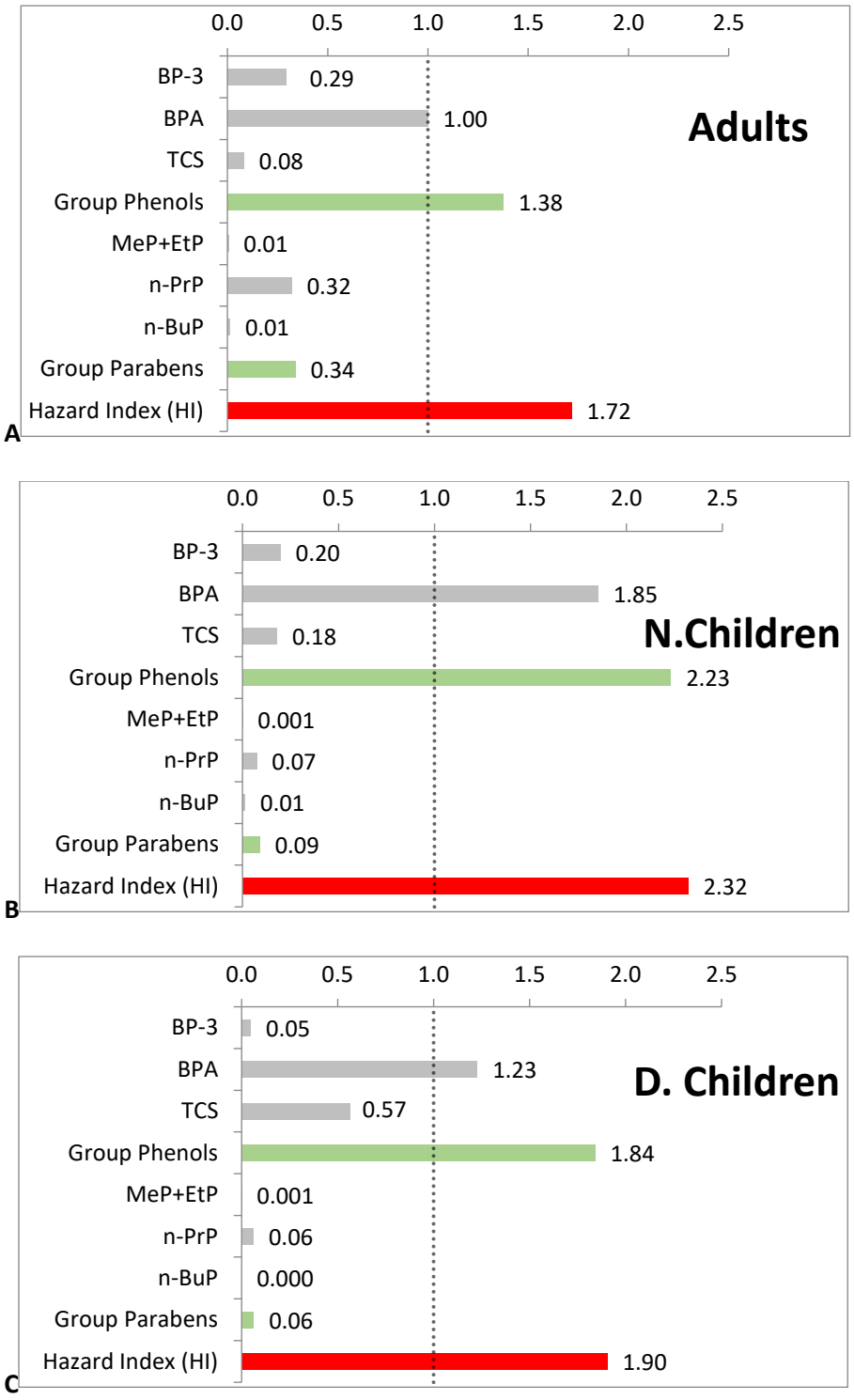

Figure **2.6.** Comparison of median measured urine concentration to the median of the BE_{TDI} distribution established using Httk. Risk Quotients (RQ) for individual chemicals, sum of RQ for the chemical groups phenols and parabens, and the overall Hazard Index (HI) are presented for **A.** Norwegian female adults, **B.** Norwegian children, **C.** Danish children.

2.6. Discussion

According to the "Toxicity Testing in the 21st Century" paradigm, human biomonitoring data provide valuable information on exposure concentrations that may be related to toxicity pathways known to affect human populations (NRC, 2007). With the use of PBK models, these exposure concentrations can be compared to concentrations that caused perturbations of biological pathways *in vitro*. Therefore, the purpose of this study was to examine the suitability of using generic PBK models to derive urine-level BE values considered to be safe based on agreed reference values. Two publicly available PBK models, ICF and Httk, were applied and their performance assessed by comparing BE_{EDI} values with urine concentration data, and BE_{TDI} / BE_{RfD} with established HBM values. Subsequently, a mixture assessment was performed as a case study showing how simulated BE_{TDI} values may be compared to measured urine concentrations.

Both generic and publicly available PBK models provide valuable insights into the application of such models and use of results for HBM data analysis. ICF contains 11 body compartments and by default assumes physiological and anatomical parameters of a reference human of 70 kg. However, several subjects can be selected, such as male, female and child, of normal weight or obese. The model contains algorithms as Quantitative Structure-Property Relationships (QSPRs) for blood:air, tissue:blood partitioning and for urinary excretion in order to estimate concentrations and amounts in body fluids (air excreted, urine and blood) and in organs after inhalation, oral intake or dermal exposure according to user defined exposure scenarios. A detailed analysis of the QSPRs used in ICF exceeded the scope of this study. For further information on these models, please refer to Jongeneelen and ten Berge (2011a). For the present work, various population scenarios were selected, e.g. normal child or obese woman at rest. As organ and tissue volumes and blood flows are scaled relative to the body weight, these are amended for a prediction for a normal or obese woman or child. Besides calculating parent and metabolite concentrations in organs over time, the amount excreted in urine was also predicted. ICF was primarily selected because of its user-friendly qualities. Furthermore, conversion of a parent compound to one or more metabolites may be modelled in parallel. This is particularly relevant for phthalates as they are rapidly metabolised (Frederiksen et al., 2007) and the concentration of some of their

metabolites are an adequate indicator of exposure to the parent compound (Ramesh Kumar and Sivaperumal, 2016). However, a steady-state concentration was only reached for BPA whereas the venous blood concentration of all other substances continued to steadily increase, even when the simulation was performed for a period of 100-300 days. When this issue emerged, initial attempts to resolve it did not improve the results and an email to the developers addressing the problem was unanswered. As the objective of this project was to examine the suitability of applying ICF and Httk, the focus was not placed on investigating issues in the model code or minor adjustments to parameterisation, but on continuing with Httk. This does not mean that this issue cannot be resolved. In fact, it is likely that checking of the model code and parameterisation will clarify the problem which can then be addressed and resolved. At the beginning of the project, the equations applied in ICF were reviewed in the model's documentation, however the model code implemented in the Excel file was not checked. With respect to potential improvements of applied parameter values, it may be worth searching for additional data, potentially considering read-across, to establish a better understanding of ranges of parameter values suitable for the populations of women and children. Of particular interest are ranges of clearance values. Also, as will be shown in Chapter 4, additional scaling factors, such as a relative activity factor (RAF) and a relative expression factor (REF), may be necessary to achieve improved *in vivo* V_{max} values.

The High-Throughput Toxicokinetics (Httk) constitutes a compilation of a one, three and seven-compartment PBK model intended to compute concentration vs. time curves. In this study, the exposure route applied was oral - via ingestion – and the seven compartmental model was used to perform the simulations. The model was used to calculate the number of days to reach steady state and urine concentrations for all compounds selected. Models were parameterised with high-throughput *in vitro* data and structure-derived physico-chemical properties for over 1,300 compounds, and physiological data was taken from the most recent U.S. Centers for Disease Control and Prevention (CDC) NHANES data. At present, there is no option to estimate metabolite concentrations in the current version of the Httk which is why the model could not be used for phthalates. Httk was primarily selected because of the richness of data made available within the model.

Variability of a population is factored into the analysis which is lacking in ICF predictions. Even though population data taken from NHANES represent individuals in the U.S. as opposed to Scandinavian (or other European) populations who are at the centre of this investigation. Among the many functions built into Httk is the code to create a virtual population based on which parameter values are defined. Many different approaches exist to determine the sample size of a virtual population. For simulations considering the general population, Monte Carlo simulations with a sample size of 10,000 is often used (Slob, 2006; Sprandel et al., 2006; Goutelle et al., 2009; Punt et al., 2016). However, a study on the number of replicates required in Monte Carlo simulations found that for all 22 studies considered, the minimum recommended number of replicates (which corresponds to the sample size) is less than 10,000 (Mundform et al., 2011). Overall, 7,500 to 8,000 replicates produce robust results, while in a number of cases 5,000 may be sufficient (Mundform et al., 2011). Others use the Yamane formula to define a sample size based on a given population size (Yamane, 1967). When applying the Yamane formula for the population of the European Union sized 508 million inhabitants, a sample size of 400 people was estimated. Unfortunately, in Httk, a virtual population of 10,000 females could not be created and most attempts to create a population of 5,000 females produced error messages. As samples of 400 and 4,000 are feasible in Httk, a Yamane-formula-based 400-subject and a 4,000-subject population were created to simulate the BE_{TDI} which were compared to urine concentrations measured in mothers. For the population of children, to be similar to the two mother samples, 500 males and 500 females of the same age group was produced. These populations constitute a random selection of individuals from all weight categories (underweight, normal, overweight and obese), "non-hispanic white" and "other" ethnicities, with normal kidney function and from 32 to 56 years of age for female adults and 6 to 11 for children. When the model was run for the time to reach steady state as calculated by “calc_css”, it was found that the amount excreted in the urine was still increasing at the end of simulation time. Therefore, simulation times were extended to ensure that steady state is reached in the urine by the end of simulation time.

Other limitations of the application of ICF and Httk revolve around the use of adequate parameter values, as outlined in Table 2.7. In particular, ICF requires parameter values which may not easily be obtained, such as V_{max} and K_m values.

These are typically established in *in vitro* assays. Uncertainties related to the use of *in vitro* data have been recognised; for instance the discrepancy between the nominal concentration which has been added to the *in vitro* system and the free, bioavailable and actual toxic concentration (Blaauboer, 2010; Kramer, 2010). The free concentration can deviate greatly from the nominal concentration due to binding to the plastic of the culture plate, binding to proteins in the medium or evaporation from the medium. While this aspect was not considered in the data used for ICF, these issues were partly minimised in *in vitro* assays factored in in Httk (Wambaugh et al., 2018). Other inbuilt and sourced parameter values used in ICF were calculated using QSAR and QSPR models which bear uncertainties and may indicate that the model may only be applied for screening level assessments. For example, the human tissue-blood partition coefficient algorithms were specifically established for five tissue types and used for 11 tissue types in ICF (Jongeneelen and ten Berge, 2011a). Tissue-blood partition coefficients are assigned to tissues based on the lipid fraction of the tissue. However, considering the composition of various tissues presented by Woodard and White (1986) a clustering of tissues according to lipid content would not result in the grouping of tissues for tissue:blood partitioning performed by Jongeneelen and ten Berge (2011a). In a similar manner, all other assumptions stated in Table 2.7 may be debated but a more detailed analysis is outside the scope of this study. In terms of applicability, priority was given to the results generated in Httk which were then used for the MRA.

Overall, many factors need to be considered when using generic PBK models. Also, interpretation and use of modelling results require a great degree of care. The great difference in mixture risk assessment results when applying the 5^{th} percentile of the BE_{TDI} distribution compared to the median BE_{TDI} highlights this. In order to add value to the model validation and gain more confidence in model validation results generated in Step 4, confidence in the accuracy of EDI values needs to be increased.

2.7. Conclusions

The aim of the study was to develop a methodology to ultimately assess the risks caused by exposure to multiple chemicals using HBM data, thus taking into account realistic co-exposure scenarios for humans. One straightforward way to facilitate the

use of HBM data in risk assessment focuses on establishing safe levels in urine or blood to which measured HBM values can be compared. These safe levels are known as biomonitoring equivalents (BE) (Hays et al., 2007).

This study applied two generic PBK models to establish such BE values, using different assumptions and virtual populations to cover female adults and 6-11 year old children. HBM data from a Danish and a Norwegian cohort study were used. This is the first study investigating the use of ICF and Httk for HBM data analysis. However, only a limited number of compounds could be simulated, i.e. 4 chemicals in ICF and 7 chemicals using the seven compartmental Httk model. These models were used to assess provisional biomonitoring equivalents (BEs), in a forward dosimetry manner, when applying reference doses (RfDs) or tolerable daily intakes (TDIs). With the preliminary results presented in this study, we can conclude that the performance of the two generic PBK models suggest that these models can help to provide a better understanding and interpretation of HBM results.

The use of a generic PBK model is still supported if BE values are derived for a specific population by adapting the model's physiological parameters to said population. Another option for the future is to use chemical specific PBK models to establish general BE values for children and adults using some more general assumptions about a wider (e.g. European) population to be used as a virtual population.

In the current study, ICF had the advantage of including metabolism features to address chemicals such as phthalates for which usually metabolite concentrations are analysed in urine samples. However, the model seemed to work only for BPA and be less adequate for other tested chemicals. Furthermore, it required a substantial number of input parameters which were not easy to find in the literature or to be simulated, in particular for the metabolites.

The use of Httk is an elegant solution as it has a library of relevant parameters built into the model covering many chemicals, thus being very user friendly and limiting the time needed to gather input parameters. However, in its current version (1.8, 2018), metabolism is only addressed via intrinsic clearance. This means that

metabolite concentration predictions were not included, so that it can only be applied for chemicals where the parent is measured in the urine samples.

The performance of the PBK models for the chemicals under investigation has been evaluated for the Norwegian dataset, estimated daily intakes resulting from external exposure measurements in dust, air and food were used to simulate related urinary concentrations, which were compared to measured urinary concentrations. These EDI were then used in the study models to predict urinary concentrations and to compare to the measured urinary concentrations. The higher BE_{EDI} were predicted, the more conservative may the estimation be considered. Concentrations predicted were mostly by orders of magnitude lower than the measured urinary concentrations. This underprediction indicates that the BE_{TDI} values established in the same way tend to be too low, i.e. too conservative, indicating a risk at very low levels. This was also confirmed when comparing to formerly established HBM-I values by the German HBM Commission which were much higher for TCS and BPA than the BE_{TDI} of this study.

The study shows that establishing safety threshold levels in urine is a difficult and complex task. The approach might be more straightforward for chemicals that are analysed as parent compounds in blood but high uncertainties have to be considered around simulated metabolite concentrations in urine.

Based on the experience gained with this study, the performance of the models for other chemicals could be investigated. From this exercise more could be learned about the uncertainties underlying used input parameter values (including EDIs) and their sources (specified in Table 2.7). However, in order to finally improve the accuracy of the simulations, uncertainties need to be estimated. Also, a generic PBK model may be developed, validated and subsequently applied for the set of phthalates, or other substances, which have not been assessed in Httk. Generating a new PBK model implies incorporating the level of detail needed to perform the HBM analysis. In the case of phthalates, this means including the prediction of metabolite concentrations. Also, challenges such as the inability of ICF to reach steady-state for most substances tested, which seem to be related to an error in the model code, may

be corrected with more ease due to the complete control over the model code and setup.

This study complements efforts to 1) incorporate more human data into chemical risk assessment related to the general population, including vulnerable populations such as children, 2) consider risk posed by chemical mixtures and 3) apply computational methods such as the PBK models used in order to estimate internal exposure. Other researchers investigated the use of PBK models to establish safe internal exposure levels in the context of occupational settings. For example, Droz et al. (1989), Leung 1992, Thomas et al. (1996) and Truchon et al. (2006) used occupational exposure limits (OELs) and the American Conference of Governmental Industrial Hygienists (ACGIH) equivalent Threshold Limit Value (TLV) – which are concentrations of a chemical in the air of a workplace considered safe for workers – to derive acceptable levels of chemicals in biological media called biological exposure indexes (BEIs) in urine. Thomas et al. (1996) and Truchon et al. (2006) also estimated interindividual variability in physiological and ADME-related parameters using Monte Carlo Simulation through which a probability distribution of exposure predictions was obtained. All PBK models used in these studies were comparable in terms of their number of compartments to Httk, even though none of these models had specific kidney and gut compartments. The models used by Leung 1992 and Thomas et al. (1996) calculated metabolite concentrations. Validation of predicted results were not specifically presented in any of these studies discussed above. Perbellini et al. (1990) extended the approach and attempted to validate the model by comparing calculated urine-level BEI values to urine concentrations measured in workers. The only study which used PBK modelling to derive HBM guidance values previously was Arnold et al. (2015) who used a PBK and pharmacodynamic model for chlorpyrifos to predict the impact of age and human variability on levels of target organ and systemic biomarker activation. The work presented here intended to extend this approach to a broad array of chemicals the general population is exposed to. This was not entirely achieved due to the above discussed limitations of both applied models. However, the key lesson learned from this study is that Httk may be used to derive urine-level BE values and evaluate HBM data in a screening-level risk assessment for single substances and mixtures. Further research is needed to validate the modelling results presented.

3.0 PBK MODELLING TO STUDY THE KINETICS OF TOXICOLOGICALLY RELEVANT COMPOUNDS

Physiologically based kinetic (PBK) models are powerful tools in the currently used battery of quantitative computational toxicology approaches. PBK predictions provide insights into i) how much of a given external dose actually arrives at the site of toxicity (typically termed as internal dose), ii) to which extent would exposure at this site differ if the dose is administered via a different route of exposure or formulation, iii) would a similar internal dose be expected in vulnerable populations such as children, elderly individuals or patients. These are all questions which cannot be assessed or are costly to be quantified via current testing methods. Furthermore, PBK results help to explore whether effects observed *in vitro* may be relevant in *in vivo* settings.

Consequently, PBK models have been widely used, for instance to simulate drug-drug interactions (DDIs) (Siccardi et al., 2013; Ferl et al., 2016; Min and Bae, 2017; Rajoli et al., 2019), for reverse dosimetry approaches (Liao et al., 2007; Bartels et al., 2012), species extrapolation (Martin et al., 2015), *in vitro* to *in vivo* extrapolation (IVIVE) (Louisse et al., 2010; Yoon et al., 2012; Martin et al., 2015) and to understand variability in pharmacokinetic outcome when considering vulnerable populations (Ferl et al., 2016; Stader et al., 2019). To evaluate inter-individual human variation in bioactivation and DNA adduct formation, a PBK model has been coupled to Monte Carlo modelling (Punt et al., 2016). Many of these issues have also been investigated using commercial software such as the Simcyp® Simulator and GastroPlus® (Posada et al., 2015; Mori et al., 2016; Polasek et al., 2018; Miller et al., 2019); while others develop their own model. A more comprehensive review of published PBK studies has been compiled by Sager (2015). However, only a small proportion of these include the details and complete set of ODEs associated with their models which may be chemical-specific (Kawai et al., 1994; Hoffman and Hanneman, 2017) or generic (Peters, 2008a; Jones and Rowland-Yeo, 2013). The use of previously developed and fully accessible PBK models, such as Httk, does not allow the full flexibility and transparency which is granted when developing our own model. The most detailed model of Httk, for instance, only compartments for the lung, gut, liver, kidney, blood and the rest of the body (Pearce et al., 2017). A newly generated PBK model based on previously established and validated ODEs provides the transparency needed to

interpret results adequately and may best be tailored to our research needs as outlined in more detail below.

Being based on mathematical descriptions of physiological characteristics and biochemical processes which determine the fate of a compound in a body, PBK models simulate the change in concentration of a compound in defined compartments of a (human or animal) body over time, following administration of a dose intravenously, orally or via other routes (Krishnan and Andersen, 2001; Peters, 2008a). These compartments typically include arterial and venous blood compartments as well as – depending on the research question to answer – specific organs (e.g. liver, kidney, heart) or groups of organs in which a similar kinetic behaviour is observed (e.g. highly versus slowly-perfused compartments) (Krishnan and Andersen, 2001). Reviews of the parameter estimation tools and *in silico* resources to develop and evaluate such models have been discussed elsewhere (Bessems et al., 2014; Madden et al., 2019).

The aim of this Chapter is to develop a human-relevant PBK model which can be used to quantify the relationship between an administered dose and concentrations in various organs over time for a broad range of chemical substances. Similar to the model developed by Peters (2008a), the model is intended to contain the key organs and tissues of the human body and cover a broad applicability domain in order to simulate the kinetics of a broad range of substances reliably. In order to assess the domain of applicability of the model, simulations are performed with a set of substances which are diverse in terms of their physico-chemical and pharmacokinetic characteristics. Subsequently (see Chapter 4), this PBK model is coupled with a newly generated mechanistic kidney model to predict concentration-time profiles in proximal tubular cells.

3.1 Methods

3.1.1 Development of the model

A PBK model is set up using the SimBiology® desktop (version 5.7), an app provided by MATLAB®, version 2017b. SimBiology uses ordinary differential equations (ODEs) and numerical solvers to predict pharmacokinetic and pharmacodynamics processes with outputs of concentration vs. time curves for organ or tissue-specific

compartments (MathWorks, 2019d; c). The ODEs created in SimBiology are then solved by numerical integration using the Matlab solver *ode15s* which integrates the system of stiff differential equations (MathWorks, 2019b).

3.1.1.1 PBK (including ACAT) model structure and physiological parameters

The model consists of 15 somatic compartments including the lungs, eight non-eliminating organs and tissues (i.e. heart, spleen, thymus, pancreas, adipose, muscle, brain, skin), four eliminating and absorbing organs (i.e. liver, stomach, gut, kidney) as well as two blood compartments (venous and arterial) which connect all 13 previously mentioned organs and tissues. As in human physiology, arterial blood at the arteriole level reaches tissues and organs where a substance may leave the blood compartment via passive diffusion. From the tissue, the substance moves into the venous blood compartment from where it flows to the lungs and subsequently back to arterial blood. An intravenous dose is applied as concentration to the venous blood compartment. To predict an oral concentration profile, an oral absorption model is added, i.e. the Advanced Compartmental Absorption and Transit (ACAT) model created by Agoram et al. (2001). The ACAT model consists of the stomach, seven gut sub-compartments, i.e. duodenum, jejunum 1, jejunum 2, ileum 1, ileum 2, ileum 3, caecum and the ascending colon. Here, the volumes of the gut sub-compartments and the colon are taken from Li et al. (2012). As mentioned earlier, contrary to the equations used by Peters (2008a) to express the ACAT model mathematically, the present model does not include ODEs representing degradation in the gastro-intestinal tract (GIT). Figure 3.1 shows the schematic diagram of the PBK model connected to the ACAT model.

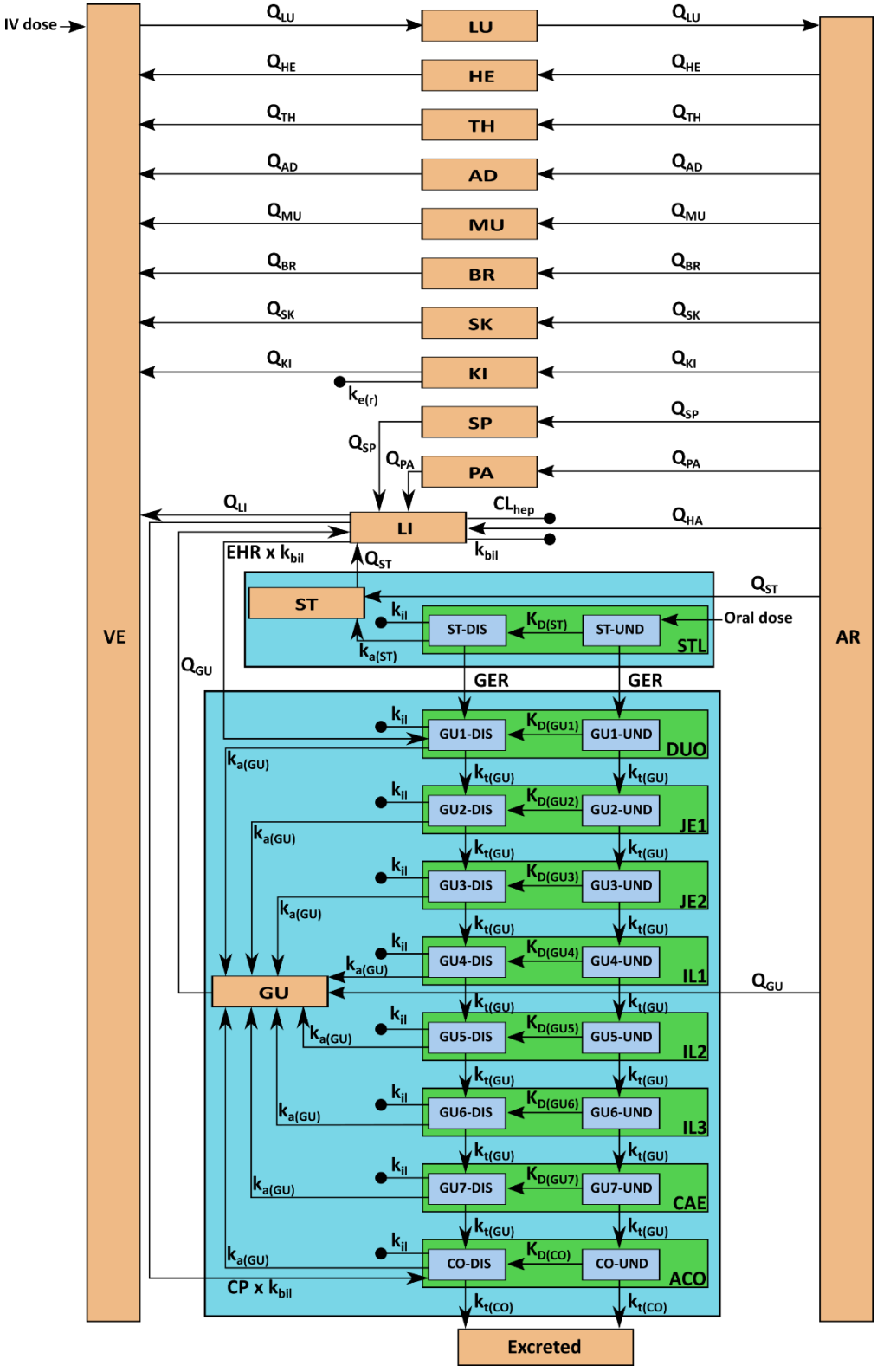

Figure 3.1: Schematic representation of the PBK model illustrating anatomical and physiological characteristics taken into account. Q = blood flow rates corresponding to an organ or tissue compartment, namely lung *(LU)*, heart *(HE)*, thymus *(TH)*, adipose tissue *(AD)*, muscle *(MU)*, brain *(BR)*, skin *(SK)*, kidney *(KI)*, spleen *(SP)*, pancreas *(PA)*, liver *(LI)*, hepatic artery *(HA)*, stomach *(ST)*, and gut *(GU)*; blood

compartments include the venous blood *(VE)* and the arterial blood *(AR)*; $k_{e(r)} =$ renal elimination rate constant; $CL_{hep} =$ hepatic clearance rate; $EHR =$ enterohepatic recirculation; $k_{bil} =$ biliary elimination rate constant; $CP =$ conversion of the metabolite to the parent compound; the undissolved *(UND)* and dissolved *(DIS)* amounts of all ACAT compartments, namely stomach lumen *(STL)*, duodenum lumen *(DUO)*, jejunum 1 lumen *(JE1)*, jejunum 2 lumen *(JE2)*, ileum 1 lumen *(IL1)*, ileum 2 lumen *(IL2)*, ileum 3 lumen *(IL3)*, caecum lumen *(CAE)*, ascending colon lumen *(ACO)*; $k_a =$ absorption rate constant in stomach *($k_{a(ST)}$)* and gut *($k_{a(GU)}$)*; $k_{il} =$ intestinal loss rate constant; $K_D =$ dissolution rate constant; $GER =$ gastric emptying rate; $k_t =$ transit rate in small intestine *($k_{t(GU)}$)* and colon *($k_{t(CO)}$)*. An intravenous dose is applied to the venous blood compartment, and an oral dose to the undissolved stomach *(ST-UND)* compartment.

The basics of mathematical representations of PBK models have been described extensively elsewhere (O'Flaherty, 1981; Krishnan and Andersen, 2001; Jones et al., 2006, 2011; Peters, 2008a; Thompson and Beard, 2011; Jones and Rowland-Yeo, 2013; Ferl et al., 2016). All ODEs used in this study are based on those published by Peters (2008a) and are compiled in Appendix 3.A. The ODE of the arterial blood compartment [Eq. (3.1)] is slightly amended from that used in Peters (2008a) in order to preserve mass balance, thus it becomes:

$$\frac{dC_{AR}}{dt} = \frac{Q_{LU}}{V_{AR}}\left(\frac{C_{LU} \times R}{K_p}\right) - \sum_i \frac{Q_i \times C_{AR}}{V_{AR}}$$

(Eq. 3.1)

where $i =$ heart *(HE)*, hepatic artery *(HA)*, stomach *(ST)*, gut *(GU)*, spleen *(SP)*, kidney *(KI)*, thymus *(TH)*, pancreas *(PA)*, adipose tissue *(AD)*, muscle *(MU)*, brain *(BR)*, skin *(SK)*.

The change of arterial and venous blood concentrations as described by Eqs. 3.1 and 7 in Appendix 3.A.1) represent plasma concentrations (Jones and Rowland-Yeo, 2013; Ye et al., 2016).

Also, ODEs representing amounts degraded *(A_{DEG})* from any GIT compartment are simplified to the following term:

$$\frac{dA_{DEG(j)}}{dt} = k_{il} \times A_{DIS(j)}$$

(Eq. 3.2)

where $j = ST, GU1\text{-}7, CO$.

The change in concentration of a compound within each somatic compartment over time is expressed by a differential equation. Each somatic and ACAT compartment is associated to a tissue or organ volume and a blood flow rate whose values characterise a healthy human body of 70 kg. The same blood flow rates are used in Peters (2008a) and expressed here as function of the cardiac output and fractional tissue blood flow:

$$Q_T = QC \times FQ_T \quad \text{(Eq. 3.3)}$$

with $Q_T =$ blood flow of a tissue compartment, $QC =$ cardiac output and $FQ_T =$ fractional tissue blood flow. Somatic organ and tissue volumes are also taken from Peters (2008a). Further physiological parameters incorporated are the pHs of each ACAT compartment, GIT transit rates and the radius of the small intestine. These values are used to estimate oral absorption besides compound-specific parameters explained in subchapter 3.1.1.2. Table 3.1 contains all physiological parameters used which are average values for a 70 kg human body and kept constant for all compounds.

Table 3.1: Physiological parameters used in the PBK and ACAT model

Physiological parameters		References
Organ and tissue volumes	**mL**	
Lung (V_{LU})	1172	Peters, 2008a
Heart (V_{HE})	310	Davies and Morris, 1993; Peters, 2008a
Liver (V_{LI})	1690	Bernareggi and Rowland, 1991; Davies and Morris, 1993; Peters, 2008a
Stomach (V_{ST})	154	Peters, 2008a
Gut (V_{GU})	1650	Bernareggi and Rowland, 1991; Davies and Morris, 1993; Peters, 2008a
Spleen (V_{SP})	192	Bernareggi and Rowland, 1991; Davies and Morris, 1993; Peters, 2008a
Kidney (V_{KI})	280	Davies and Morris, 1993; Peters, 2008a
Thymus (V_{TH})	29	Peters, 2008a
Pancreas (V_{PA})	77	Peters, 2008a
Adipose tissue (V_{AD})	10'000	Bernareggi and Rowland, 1991; Davies and Morris, 1993; Peters, 2008a

Muscle (V_{MU})	35'000	Davies and Morris, 1993; Peters, 2008a
Brain (V_{BR})	1450	Bernareggi and Rowland, 1991; Davies and Morris, 1993; Peters, 2008a
Skin (V_{SK})	7800	Bernareggi and Rowland, 1991; Davies and Morris, 1993; Peters, 2008a
Venous blood (V_{VE})	3396	Peters, 2008a
Arterial blood (V_{AR})	1698	Peters, 2008a
ACAT compartment volumes (mL)	**mL**	
Stomach lumen (V_{STL})	50	Li et al., 2012
Duodenum lumen (V_{DUO})	48	Li et al., 2012
Jejunum 1 lumen (V_{JE1})	175	Li et al., 2012
Jejunum 2 lumen (V_{JE2})	140	Li et al., 2012
Ileum 1 lumen (V_{IL1})	108	Li et al., 2012
Ileum 2 lumen (V_{IL2})	79	Li et al., 2012
Ileum 3 lumen (V_{IL3})	56	Li et al., 2012
Caecum lumen (V_{CAE})	53	Li et al., 2012
Ascending colon lumen (V_{ACO})	57	Li et al., 2012
pH in ACAT compartments		
Stomach lumen	1.3	Dressman et al., 1998; Li et al., 2012
Duodenum lumen	6	Dressman et al., 1998; Li et al., 2012
Jejunum 1 lumen	6.2	Dressman et al., 1998; Li et al., 2012
Jejunum 2 lumen	6.4	Dressman et al., 1998; Li et al., 2012
Ileum 1 lumen	6.6	Dressman et al., 1998; Li et al., 2012
Ileum 2 lumen	6.9	Dressman et al., 1998; Li et al., 2012
Ileum 3 lumen	7.4	Dressman et al., 1998; Li et al., 2012
Caecum lumen	6.4	Dressman et al., 1998; Li et al., 2012
Ascending colon lumen	6.8	Dressman et al., 1998; Li et al., 2012
Blood flow rates	**mL/min (fraction of QC)**	
Lung (Q_{LU})	6.338×10^3 (1)	Peters, 2008a[1]
Heart (Q_{HE})	150 (0.024)	Bernareggi and Rowland, 1991; Peters, 2008a
Hepatic artery (Q_{HA})	300 (0.047)	Bernareggi and Rowland, 1991; Davies and Morris, 1993
Liver (total) (Q_{LI})[2]	1.650×10^3 (0.260)	Bernareggi and Rowland, 1991; Peters, 2008a
Gut (Q_{GU})	1.10×10^3 (0.174)	Bernareggi and Rowland, 1991; Peters, 2008a
Spleen (Q_{SP})	77 (0.012)	Bernareggi and Rowland, 1991; Peters, 2008a
Stomach (Q_{ST})	38 (0.006)	Kawai et al., 1994; Peters, 2008a

Kidney (Q_{KI})	1.10×10^3 (0.174)	Bernareggi and Rowland, 1991; Peters, 2008a
Thymus (Q_{TH})	80 (0.013)	Bernareggi and Rowland, 1991; Peters, 2008a
Pancreas (Q_{PA})	133 (0.021)	Kawai et al., 1994; Peters, 2008a
Adipose tissue (Q_{AD})	260 (0.041)	Bernareggi and Rowland, 1991; Peters, 2008a
Muscle (Q_{MU})	750 (0.118)	Bernareggi and Rowland, 1991; Peters, 2008a
Brain (Q_{BR})	700 (0.110)	Bernareggi and Rowland, 1991; Peters, 2008a
Skin (Q_{SK})	300 (0.047)	Bernareggi and Rowland, 1991; Peters, 2008a
Other physiological parameters		
Cardiac output (QC) (mL/min)	6.338×10^3	Peters, 2008a[1]
Gastric emptying rate (GER) (min^{-1})	0.066	Oberle et al., 1990
Small intestine transit rate $(k_{t(GU)})$ (min^{-1})	0.035	Yu and Amidon, 1998
Colon transit rate $(k_{t(CO)})$ (min^{-1})	0.0007	Peters, 2008a
Radius of the small intestine (cm)	1	Oh et al., 1993

[1]Peters (2008a) used 5.233×10^3 mL/min as lung blood flow while the sum of all the tissue blood flows is 6.338×10^3. However, to make sure that the sum of all tissue blood flows equals the lung blood flow (which is equal to QC) (see (IPCS WHO, 2010)), the lung blood flow is set to 6.338×10^3 mL/min. This value is within the normal ranges of QC values established for the age groups 18-19.9, 30-59.9 and 60+ (Cattermole et al., 2017). The QC confidence intervals are 3.06-9.00, 2.51-7.77 and 2.97-7.49 L/min, respectively.

[2]Flows of the hepatic artery and portal vein which collects the blood leaving the gut, spleen, stomach, pancreas and gallbladder (gallbladder not included in the model) (Eipel et al., 2010).

Principle assumptions of the model include well-stirred compartments and perfusion-limited (as opposed to permeability-limited) kinetics, which implies instantaneous and homogenous absorption of a compound into, and distribution within, a compartment (Wilkinson and Shand, 1975; Yang et al., 2007; Peters, 2008a). The kinetics of metabolism are assumed to be similarly homogeneous within a compartment. Active transport and diffusion delay are disregarded (Yang et al., 2007). Perfusion rate-limited kinetics applies to small lipophilic compounds for which the blood flow towards the tissues represents the rate-limiting process (Peters, 2008a; Jones and Rowland-Yeo, 2013).

3.1.1.2 Literature search and estimation of compound-specific parameters to simulate the pharmacokinetics of nine drugs

Similar to Peters (2008a), the model is used to simulate and validate against the venous blood concentration-time profiles of nine drugs, i.e. atenolol, bisoprolol, chlorpropamide, cimetidine, diazepam, hexobarbital, ivermectin, mebendazole and theophylline. These drugs are diverse in terms of their physico-chemical and pharmacokinetic profiles, in particular regarding their solubility and permeability. While atenolol and cimetidine show high solubility and low permeability, mebendazole has low solubility and high permeability properties and ivermectin both low solubility and low permeability (Peters, 2008a). The remaining five compounds – theophylline, hexobarbital, diazepam, chlorpropamide and bisoprolol – demonstrate high solubility and high permeability. For these compounds, minor or no impact of enterohepatic recirculation, gut wall metabolism, gastric emptying or transporter-driven absorption and intestinal efflux is reported (Peters, 2008a). Compound-related physico-chemical and biochemical (related to the binding and metabolising capacities in tissues) parameters needed for the model are explained below and the values used are shown in Tables 3.4 and 3.5. In cases where more than one parameter value is sourced from the literature, the mean of all values is determined and used for simulation. Given the variability in the values found, the mean, in contrast to the median, is considered acceptable.

- K_p is a multiplicative factor used by Peters (2008a) to increase or reduce the tissue distribution coefficients of all tissue compartments. It is referred to as the tissue partition coefficient and, mathematically, it is defined as follows:

$$K_p = f_{u(p)} \times K_{p,u(T)} \qquad \text{(Eq. 3.4)}$$

  where $f_{u(p)}$ is the fraction unbound in plasma, which is, in fact, dependent upon the drug affinity to human serum albumin and the individual's albumin level in plasma (Peters, 2008a; Jamei et al., 2009). Only the fraction unbound or freely circulating in the plasma penetrates cell membranes and interacts with cellular receptors (Boroujerdi, 2015). $K_{p,u(T)}$ is the unbound tissue partition coefficient which may be defined for individual tissues and organs. However, in the present model only one K_p value is applied to all compartments. Peters (2008a) set the value of K_p for each compound

through fitting to an observed intravenous curve. These and all $f_{u(p)}$ values are taken from Peters (2008a).

- R is the whole blood to plasma concentration ratio; an additional drug distribution parameter (Hinderling, 1997; Peters, 2008a). If a substance binds to, or distributes into, erythrocytes, plasma clearance exceeds blood clearance. This needs to be taken into account besides $f_{u(p)}$ when considering behaviour of a compound in the blood compartment. R values are sourced from the public scientific literature and, if not available, assumed to be 1.
- k_a is the absorption rate constant which feeds into the oral absorption part of the model and describes the rate of absorption from the GIT (represented by ACAT compartments) into the systemic circulation. k_a values are sourced from clinical/PK studies, and in cases where no clinical data are available, calculated using the approach proposed by Winiwarter et al. (1998), namely:

$$\log \mathrm{P_{eff}} = -3.067 + 0.162\ \mathrm{CLOGP} - 0.010\ \mathrm{PSA} - 0.235\ \mathrm{HBD}$$

(Eq. 3.5)

with $CLOGP =$ calculated log P, $PSA =$ polar surface area, $HBD =$ number of hydrogen bond donors. These parameter values for all nine compounds are sourced from Peters (2008a, Table II).

P_{eff} is then used to calculate k_a with Eq. 3.6 (Yu and Amidon, 1999; Peters, 2008a):

$$k_a = \frac{P_{eff} \times 2}{Radius\ of\ small\ intestine}$$

(Eq. 3.6)

If a value is available from a clinical/PK study, it is compared to the calculated k_a of that compound. For atenolol, the calculated value is one to two orders of magnitude lower than the two absorption rates sourced from Mason et al.'s (1979) 3-compartment model of which one is used for gastric absorption and the other for intestinal absorption. However, Mason et al. (1979) does not specifically assign any of them to absorption from the stomach or the gut which contributes to the level of uncertainty associated with these values. The higher value is used as the intestinal absorption rate constant of atenolol, while the lower value is used as a gastric absorption rate constant.

For cimetidine, the calculated absorption rate constant is, by slightly more than an order of magnitude, lower than the value established in a group of volunteers (Veng Pedersen and Miller, 1980). No obvious aspect of that study is identified which might contribute to the uncertainty inherent in the experimental value. Interestingly, both atenolol and cimetidine are absorbed via paracellular pathways. Calculated absorption rate constants for chlorpropamide, diazepam, hexobarbital and ivermectin differ up to one order of magnitude from their respective literature values.

An absorption rate constant may also be derived from an *in vitro* Caco-2 apparent permeability value (P_{app}) (often given in $10^{-6} cm\, s^{-1}$) by a) conversion to $cm\, min^{-1}$, b) if needed applying a scaling factor to convert from an *in vitro* apparent permeability value to *in vivo* P_{eff} and c) applying Eq. 3.6 to obtain k_a (Peters, 2008a; Fabian et al., 2019). However, as *in vitro* Caco-2 data are not obtained for all nine compounds, this approach is not applied here and the QSAR model explained above is chosen instead. If available, *in vitro* Caco-2 permeability data are typically preferred over a QSAR model to derive k_a as Caco-2 cells are considered an adequate model to mimic the transport of substances through the human intestinal epithelium (Van Breemen and Li, 2005; Yang et al., 2017).

Oral bioavailability (F) is a parameter tightly connected to the oral absorption rate constant as well as stability, and considered crucial for drug candidate selection and formulation strategies in drug development. Mathematically, F may be expressed as product of the fraction of drug absorbed (f_a), the fraction that escapes metabolism in the GIT (f_g) and the fraction that enters the liver and escapes first-pass hepatic metabolism (f_h) (Jamei et al., 2009; Yang et al., 2017) or as a function of P_{eff} (Yu and Amidon, 1999). Many PBK models are set up to investigate various aspects related to oral drug absorption and biovailability (Peters and Dolgos, 2019) and oral bioavailability may be predicted and compared to a measured oral bioavailability value or used to calculate the area under the concentration vs. time curve (AUC) as part of the model validation. However, this study did not specifically assess oral bioavailability.

- k_{il} is the intestinal loss rate constant which accounts for chemical degradation in the lumen, gut wall metabolism and/or P-glycoprotein efflux

from the GIT compartments (Peters, 2008a; b). All initial k_{il} values are estimated to be 1×10^{-7} min^{-1} if no data are found in the public literature and intestinal loss is assumed to be negligible. A higher value is estimated if experimental data indicate that intestinal loss may occur.

- k_{bil} refers to a first-order biliary elimination rate constant taking into account the excretion of a compound from the liver compartment into the bile from where it is transported to the duodenal compartment (Peters, 2008a). Enterohepatic recirculation *(EHR)* occurs when, after its excretion from the liver into the bile and via the bile into the GIT, a compound is reabsorbed from the intestinal compartment and re-distributed to the liver (Abbiati and Manca, 2017). If EHR takes places, a value of $k_{bil} = 1$ min^{-1} is selected, while it is 0 if no EHR takes place (Peters, 2008a). k_{bil} values are sourced from the literature and estimated if no data are available. A value of 0 is selected if no indication of enterohepatic recirculation is identified.
- $k_{e(r)}$ is the linear first-order renal elimination rate constant which determines the amount of a compound being excreted in the urine (Peters, 2008a). $k_{e(r)}$ values are either sourced from the literature or derived from renal clearance and volume of distribution values or the renal elimination half-life. See Table 3.3 for more information.
- CL_{hep} represents the hepatic clearance rate. We use hepatic clearance as opposed to intrinsic clearance as used by Peters (2008a), as our values are measured in clinical settings rather than intrinsic clearance values obtained from *in vitro* experiments. CL_{hep} accounts for the linear first-order process in which the parent compound is converted to a metabolite (Peters, 2008a). For chlorpropamide and diazepam, plasma clearance values are used as liver specific metabolic clearance data are not available (Huupponen and Lammintausta, 1981; Herman and Wilkinson, 1996). The value sourced for hexobarbital is predicted from rat data (Sawada et al., 1985).
- MW is the molecular weight and is taken from PubChem (National Center for Biotechnology Information, 2018; https://pubchem.ncbi.nlm.nih.gov) and DrugBank (Wishart et al., 2018; www.drugbank.ca). MW is used when converting an oral or intravenous dose given in mg or mg/mL (or equivalent) to µmol or µmol/mL, respectively. Also, MW is needed to calculate the paracellular absorption rate constant $k_{a,p,ACAT}$ as outlined in Eq. 3.8.

- $Log\ P$ is used to calculate k_a as stated above (see Eq. 3.5) and $k_{a,p,ACAT}$ (see Eqs. 3.8 and 3.9).
- CP is a constant representing the conversion from a metabolite back to the parent compound (Peters, 2008a). In cases where no data are available, indicating that this process takes place with a particular compound, this value is set to 0.
- Since the solubility of a substance depends on the pH present in a compartment, solubility values corresponding to the pHs of each ACAT model compartment are generated with the ACD/Percepta 14.0.0 (Build 2726) software. According to Li et al. (2012), the pHs in the stomach, duodenum, jejunum1, jejunum2, ileum1, ileum2, ileum3, caecum and ascending colon lumen are 1.3, 6, 6.2, 6.4, 6.6, 6.9, 7.4, 6.4, and 6.8 respectively. These eight different pH values may induce up to eight different solubility values. The generated solubility value at pH 6.4 is used in the model as solubility parameter S. In order to account for solubility values different to S, a solubility coefficient corresponding to each ACAT compartment (i.e. $K_{S(STL)}$, $K_{S(DUO)}$, $K_{S(JE1)}$, $K_{S(JE2)}$, $K_{S(IL1)}$, $K_{S(IL2)}$, $K_{S(IL3)}$, $K_{S(CAE)}$, $K_{S(ACO)}$) is multiplied by S.
- The diffusion coefficient (D), particle density (p), particle radius (r) and diffusion layer thickness (T) are used to calculate the dissolution rate constant K_D of a drug in a gastrointestinal compartment (i) using Eq. 3.7 (Peters, 2008a).

$$K_D = \frac{3D}{p\ r\ T}\left(S \times K_{S(i)} - C_i\right)$$

(Eq. 3.7)

where $K_{S(i)}$ is the solubility coefficient and C_i the concentration in the respective compartment.

Small, hydrophilic compounds, including atenolol, cimetidine and theophylline, are subject to paracellular absorption. In order to account for this, a paracellular absorption rate constant for each ACAT compartment $(k_{a,p,ACAT})$ is calculated using Eq. 3.8 and 3.9 as proposed by Peters (2008a) and Leahy et al. (1989, 1994). Namely,

$$k_{a,p,ACAT} = \frac{ø \times J_{ms}}{V_{ACAT}}$$

(Eq. 3.8)

where J_{ms} is the physiological flux of water from the mucosal to the serosal side of the lumen. The mean of five J_{ms} values (8.6, 8.2, 19.7, 20.6, 8.1 $cm^3\ hr^{-1}$) published by Leahy et al. (1994) is used, i.e. $J_{ms} = 0.2173$ mL/min.

V_{ACAT} defines the volume of the ACAT compartment under consideration, e.g. the stomach (V_{ST}) etc.

ø is a compound-dependent fraction ranging from 0 to 1, depending on the lipophilicity, represented by the $Log\ P$, and the molecular weight (MW) of the molecule (Leahy et al., 1989, 1994; Peters, 2008a). Following Eq. 3.9, large lipophilic compounds are assigned a $ø$ value of 0, while small hydrophilic compounds a $ø$value approaching 1:

$$Log\ P > 0.7: ø = 0$$
$$Log\ P < 0.7:$$
$$MW > 200 \text{ but } < 360: ø = 0.1$$
$$MW < 200: ø = -0.0045 \times MW + 1.$$

(Eq. 3.9)

For atenolol, cimetidine and theophylline the following $k_{a,p,ACAT}$ values are calculated as proposed in Peters (2008a) using the approach established by Leahy et al. (1989, 1994) (see Table 3.2).

Table 3.2: Paracellular absorption rate constants for each ACAT compartment

$k_{a,p,ACAT}$ parameter	Atenolol, Cimetidine (min^{-1})	Theophylline (min^{-1})
$k_{a,p,STL}$	4.347×10^{-4}	8.226×10^{-4}
$k_{a,p,DUO}$	4.528×10^{-4}	8.569×10^{-4}
$k_{a,p,JE1}$	1.242×10^{-4}	2.350×10^{-4}
$k_{a,p,JE2}$	1.552×10^{-4}	2.938×10^{-4}
$k_{a,p,IL1}$	2.012×10^{-4}	3.808×10^{-4}
$k_{a,p,IL2}$	2.751×10^{-4}	5.206×10^{-4}
$k_{a,p,IL3}$	3.881×10^{-4}	7.345×10^{-4}
$k_{a,p,CAE}$	4.101×10^{-4}	7.670×10^{-4}
$k_{a,p,ACO}$	3.813×10^{-4}	7.216×10^{-4}

STL= stomach, DUO= duodenum, JE1= jejunum 1, JE2= jejunum 2, IL1= ileum 1, IL2= ileum 2, IL3= ileum 3, CAE= caecum, ACO= ascending colon

These $k_{a,p,ACAT}$ values are added to the k_a value used in each ACAT compartment so that for these compounds:

$$k_{a_{ACAT}} = k_a + k_{a,p.ACAT}.$$

(Eq. 3.10)

Initial oral and IV doses which are based on clinical study data sourced from the public literature (Mason et al., 1979; Leopold et al., 1986; Huupponen and Lammintausta, 1981; Somogyi and Gugler, 1983; Kaplan et al., 1973; van der Graaff et al., 1986, and Breimer, 1977; Okonkwo et al., 1993; Dawson et al., 1985; Aslaksen et al., 1981) are presented in Table 3.3. For ivermectin, only oral data are available. Apart from the data presented by van der Graaff et al. (1986), all experimental data applied here are also used by Peters (2008a) to evaluate the performance of their PBK model.

An IV dose is applied directly to the venous blood compartment as initial venous blood concentration while typically the initial concentration in any other compartment is zero. An oral dose is applied as an amount to the undissolved stomach compartment, from which the dissolved amount of the substance is calculated. The amount absorbed over time into the stomach and intestinal tissues depends on the amount dissolved and the absorption rate constant in each ACAT compartment:

$$\frac{dA_{ABS(i)}}{dt} = k_{a(i)} \times A_{DIS(i)}$$

(Eq. 3.11)

where i= gastrointestinal tract compartments 1 to 7, colon and stomach.

In general, the kinetics of a substance in non-eliminating organs and tissues are described by Eq. 3.12. The ODE represents the change in concentration within that tissue compartment over a concentration gradient between the capillary and tissue ($C_{blood} - C_{tissue}$; Boroujerdi, 2015). The binding to fatty acids (e.g. in plasma proteins or erythrocytes) as well as the perfusion rate (expressed as the tissue blood flow rate over the tissue volume; Arundel, 1997), are considered:

$$\frac{dC_T}{dt} = \frac{Q_T}{V_T}\left(C_{AR} - \frac{C_T \times R}{K_p}\right)$$

(Eq. 3.12)

where T represents all organs and tissues, except for the stomach, gut, kidney, liver and lung.

In eliminating tissues such as the kidney, terms representing for instance renal clearance are subtracted:

$$\frac{dC_{KI}}{dt} = \frac{1}{V_{KI}} \times \left[Q_{KI}\left(C_{AR} - \frac{C_{KI} \times R}{K_p}\right)\right] - \frac{C_{KI} \times k_{e(r)}}{K_p} \times f_{u(p)}$$

(Eq. 3.13)

Venous blood concentrations, which are compared to blood or plasma concentrations in patients, are calculated using Eq. 3.14.

$$\frac{dC_{VE}}{dt} = \frac{1}{V_{VE}}\left(\sum \frac{Q_T \times C_T \times R}{K_p} - Q_{LU} \times C_{VE}\right)$$

(Eq. 3.14)

where T stands for all tissues and organs excluding the gut, pancreas, spleen, stomach, and lung.

Table 3.3: Initial oral and IV doses to generate PK simulations for all nine compounds

Doses	Atenolol (Mason et al., 1979)	Bisoprolol (Leopold et al., 1986)	Chlorpropamide (Huupponen and Lammintausta, 1981)	Cimetidine (Somogyi and Gugler, 1983)	Diazepam (Kaplan et al., 1973)	Hexobarbital (Breimer, 1977; van der Graaff et al., 1986)	Ivermectin (Okonkwo et al., 1993)	Mebendazole (Dawson et al., 1985)	Theophylline (Aslaksen et al., 1981)
Oral (µmol)	188	31	225	800	35	2,100	12.2	4.01×10^{-3}	1,400
IV (µmol/mL)	0.0553	0.0091	0.0663	0.236	0.0103	0.742	NA	1.18×10^{-6}	0.569

NA= not available. Reported up to three significant figures.

Table 3.4: Physico-chemical and kinetic parameters used in the PBK model which are subject to fitting and their experimental[a], calculated[c] and, where applicable, fitted[b] values

Parameter	Atenolol	Bisoprolol	Chlorpropamide	Cimetidine	Diazepam	Hexobarbital	Ivermectin	Mebendazole	Theophylline
K_p factor[a]	1.7 [1]	2.5 [1]	50 [1]	1.2 [1]	K_p:2 [1]; $K_{p(AD)}$:12.5[1]	1.7 [1]	1*	5 [1]	1.3 [1]
K_p factor[b]	3.43×10^{-3}	NA	1.81×10^{-3}	NA	K_p: 0.533	NA	1×10^{-7}*	0.301	0.345
K_p factor[b] SE	6.14×10^{-4}	NA	3.30×10^{-4}	NA	K_p: 0.453	NA	NA	0.067	0.047
R[a]	1.11 [2]	1.1 [7]	1*	0.98 [10]	0.5587 [12]	1.0 [15]	1*	1*	0.83 [2]
R[b]	1.74×10^{-3}	0.569	0.024	0.741	1.180	0.323	0.348	0.081	NA
R[b] SE	1.98×10^{-4}	0.068	3.46×10^{-3}	0.093	0.912	0.137	0.071	0.016	NA
$f_{u(p)}$[a]	0.96 [1]	0.7 [1]	0.04 [1]	0.835 [1]	0.013 [1]	0.53 [1]	0.069 [1]	0.073 [1]	0.44 [1]
$f_{u(p)}$[b]	NA	NA	NA	NA	NA	NA	NA	NA	NA
$f_{u(p)}$[b] SE	NA	NA	NA	NA	NA	NA	NA	NA	NA
k_a (min^{-1}) (literature)[a]	0.0363 [3] 0.175 [4]	NA	0.0967 [8]	0.0478 [11]	0.0319 [13]	0.015[16]	7.7×10^{-3} [16]	NA	NA
k_a (min^{-1}) (calculated)[c]	0.0013	0.0159	0.0119	0.0033	0.1622	0.0216	2.8×10^{-3}	0.0160	0.0142
k_a (min^{-1})[b]	NA	NA	NA	NA	NA	NA	NA	NA	NA
k_a (min^{-1})[b] SE	NA	NA	NA	NA	NA	NA	NA	NA	NA
k_{il}(min^{-1})[a]	3×10^{-3}*	1×10^{-7}*	1×10^{-7}*	1×10^{-7}*	1×10^{-7}*	1×10^{-7}*	1×10^{-4}*	1×10^{-7}*	1×10^{-7}*
k_{il}(min^{-1})[b]	NA	NA	NA	NA	NA	NA	NA	NA	NA
k_{il}(min^{-1})[b] SE	NA	NA	NA	NA	NA	NA	NA	NA	NA
k_{bil}(min^{-1})[a]	1×10^{-3}*	0*	0*	1×10^{-3}[10]	1×10^{-4} [14]	1×10^{-4} [17]	0.0859 [18]	4.6×10^{-3} [19]	7.2×10^{-4} [20]
k_{bil}(min^{-1})[b]	NA	NA	NA	NA	NA	NA	NA	NA	NA

k_{bil} (min^{-1})[(b)] SE	NA	NA	NA	NA	NA	NA	NA	NA	NA
$k_{e(r)}$ (min^{-1})[(a)]	1.8×10^{-3} [5]	7.08×10^{-4} [5]	2.383×10^{-4} [5]	5.4×10^{-3} [5]	3.75×10^{-4} [13]	2.1×10^{-3} [5]	1×10^{-7} [18]	4.6×10^{-3} [19]	7.2×10^{-4} [5]
$k_{e(r)}$ (min^{-1})[(b)]	NA	NA	NA	NA	NA	NA	NA	NA	NA
$k_{e(r)}$ (min^{-1})[(b)] SE	NA	NA	NA	NA	NA	NA	NA	NA	NA
CL_{hep} (mL/min)[(a)]	1.0×10^{-7} [6]	91 [6]	1.5 [9]	147 [10]	21.5 [14]	249 [15]	140 [1]	650 [19]	76 [21]
CL_{hep} (mL/min)[(b)]	NA	NA	NA	NA	NA	NA	NA	NA	NA
CL_{hep} (mL/min)[(b)] SE	NA	NA	NA	NA	NA	NA	NA	NA	NA

[(a)]sourced from literature

[(b)]fitted in SimBiology

[(c)]calculated using Winiwarter et al. (1998, model 3b), with data provided by Peters (2008a) and Eq. 3.5

SE= standard error; NA= not available; *estimated

[1]Peters (2008a): K_p is fitted value; diazepam has two K_p values, i.e. $K_{p(AD)} = 12.5$ which is used for adipose tissue and $K_p = 2$ for all other tissues; p (µmol/mL) is based on $p = 1\frac{g}{mL}$

[2]Rodgers and Rowland (2007)

[3]$k_{a(ST)}$ derived from k_{13} in Mason et al. (1979), used for the ACAT stomach compartment

[4]$k_{a(GU)}$ derived from k_{12} in Mason et al. (1979), used for all ACAT compartments from duodenum to ascending colon

[5]calculated using $k_{e(r)} = \frac{CL_r}{V_d} = \frac{\ln(2)}{t_{1/2(elim)}}$, while CL_r is the renal clearance, V_d the volume of distribution and $t_{1/2(elim)}$ the elimination half-life; parameter values for atenolol are sourced from Mason et al. (1979); for bisoprolol from Leopold et al. (1986); for chlorpropamide from Neuvonen et al. (1987); for cimetidine from Somogyi and Gugler (1983) (weighted mean CL_r value); for hexobarbital from the OCHEM database (Sushko et al., 2011; www.ochem.eu/home/show.do); for mebendazole from Dawson et al. (1985), CL_r is estimated at 400 mL/min; for theophylline from Antal et al. (1981)

[6]McGinnity et al. (2004); also for atenolol: Kirch and Görg (1982)

[7]Li et al. (2012): CP is assumed to be 0 as either non-metabolised form of bisoprolol is excreted via the urine or it is metabolised in the liver to inactive metabolites

[8]Danlami et al. (2011)

[9]Huupponen and Lammintausta (1981): plasma clearance value is used as CL_{hep}, comparable value, 3.15 mL/min, in Obach et al. (2008); evidence for enterohepatic circulation is discussed in this paper

[10]Somogyi and Gugler (1983): k_{bil} is estimated, biliary excretion of cimetidine accounts for only 2% of the dose; CL_{hep} is based on weighted mean CL_p – weighted mean CL_r

[11]Veng Pedersen and Miller (1980)

[12]Jones and Larsson (2004): R derived from plasma/blood distribution

[13]Kaplan et al. (1973): k_a is mean value; $k_{e(r)}$ is mean elimination rate constant

[14]Herman and Wilkinson (1996): k_{bil} and EHR are estimated based on evidence provided; CL_{hep} is approximated mean of the two age groups

[15]Sawada et al. (1985): CL_{hep} is predicted from rat data

[16]$k_a = \frac{\ln(2)}{t_{1/2(abs)}}$: for hexobarbital the absorption half-life ($t_{1/2(abs)}$) is derived from Lagas et al. (1980, Figure 6), digitized acid pure, acid and sodium data; for ivermectin mean $t_{1/2(abs)}$ is calculated from González Canga et al. (2008)

[17]Drew et al. (1977): k_{bil} is estimated based on altered PK in rats after 72-hour bile duct ligation

[18]González Canga et al. (2008, 2009): for ivermectin the main route of elimination is via bile, k_{bil} is estimated based on the value fitted for atenolol; $k_{e(r)}$ is estimated to be close to 0 as urinary excretion of ivermectin is very low (1%); $CP = 0$ is assumed as ivermectin is extensively metabolised in the liver and hardly excreted via urine

[19]Dawson et al. (1985): k_{bil} is estimated based on assumption that 50% of the mebendazole dose is eliminated via urine and 50% via bile (see also Dayan, 2003), therefore $k_{bil} = k_{e(r)}$ is assumed; $k_{e(r)}$ is calculated, see [5]; $CP = 0$ is assumed as AUCs of metabolites are higher than the AUC of the parent compound; CL_{hep} is an estimate based on data in Dawson et al. (1985) and Dayan (2003)

[20]$k_{bil} = k_{e(r)}$ is assumed, $k_{e(r)}$ is calculated, see [5]

[21]Antal et al. (1981)

Table 3.5: Physico-chemical and kinetic parameters used in the PBK model which are not subject to fitting

Parameters (not subject to fitting)	Atenolol	Bisoprolol	Chlorpropamide	Cimetidine	Diazepam	Hexobarbital	Ivermectin	Mebendazole	Theophylline
MW(g/mol)	266.34 [22]	325.45 [22]	276.74 [22]	252.34 [22]	284.74 [22]	236.27 [22]	875.11 [22]	295.30 [22]	180.17 [22]
$Log\ P$	-0.11 [1]	1.83 [1]	2.35 [1]	0.19 [1]	3 [1]	1.63 [1]	5.4 [1]	3.08 [1]	-0.03 [1]
EHR	1 [23]	0*	1 [9]	0 [10]	0 [14]	0*	1 [26]	1 [27]	0*
CP	0*	0 [7]	0*	0*	0*	0 [25]	0 [18]	0 [19]	0*
S(µmol/mL)	4,600 [24]	3,070 [24]	31.4 [24]	43.5 [24]	0.02 [24]	1.31 [24]	0.002 [24]	0.04 [24]	79.8 [24]
$K_{S(STL)}$	1	1	0.0156	55.6	136.5	0.985	1	42.7	0.995
$K_{S(DUO)}$	1	1	0.408	2.067	1	0.992	1	1	0.998
$K_{S(JE1)}$	1	1	0.637	1.41	1	0.992	1	1	0.999
$K_{S(JE2)}$	1	1	1	1	1	1	1	1	1
$K_{S(IL1)}$	0.941	0.922	1.58	0.740	1	1.02	1	1	1.00
$K_{S(IL2)}$	0.783	0.717	3.13	0.520	1	1.05	1	1	1.01
$K_{S(IL3)}$	0.539	0.424	8.18	0.366	1	1.18	1	1	1.05
$K_{S(CAE)}$	1	1	1	1	1	1	1	1	1
$K_{S(ACO)}$	0.835	0.782	2.49	0.577	1	1.03	1	1	1.01
D (cm²/min)	1×10^{-4} [1]	1×10^{-4} [1]	1×10^{-4} [1]	1×10^{-4} [1]	1×10^{-4} [1]	1×10^{-4} [1]	1×10^{-4} [1]	1×10^{-4} [1]	1×10^{-4} [1]
p (µmol/mL)	3,754 [1]	3,687 [7]	3,613 [1]	3,962 [1]	3,511 [1]	4,232 [1]	1,142 [1]	3,386 [1]	5,550 [1]
r (cm)	5×10^{-4} [1]	2.5×10^{-3} [7]	5×10^{-4} [1]	5×10^{-4} [1]	5×10^{-4} [1]	5×10^{-4} [1]	5×10^{-4} [1]	5×10^{-4} [1]	5×10^{-4} [1]
T (cm)	3×10^{-3} [1]	2.5×10^{-3} [7]	3×10^{-3} [1]	3×10^{-3} [1]	3×10^{-3} [1]	3×10^{-3} [1]	3×10^{-3} [1]	3×10^{-3} [1]	3×10^{-3} [1]

*estimated; $Log\ P$ = logarithm of the octanol-water partition coefficient; K_S = solubility coefficient; STL = stomach lumen; DUO = duodenum lumen; $JE1$ = jejunum1 lumen; $JE2$ = jejunum2 lumen; $IL1$ = ileum1 lumen; $IL2$ = ileum2 lumen; $IL3$ = ileum3 lumen; CAE = caecum lumen; ACO = ascending colon lumen

For [1-21], please refer to captions of Table 3.4

[22]PubChem (U.S. National Center for Biotechnology Information, 2018) (https://pubchem.ncbi.nlm.nih.gov)

[23]Mofenson et al. (2016): enterohepatic recirculation is observed which is why a value of 1 is assigned;

[24]sourced from ACD/Percepta 14.0.0 (Build 2726) software

[25]CP is assumed 0 as hexobarbital is completely metabolised by the human liver (Breimer et al., 1975)

[26]Baraka et al. (1996)

[27]Braithwaite et al. (1982)

3.1.1.3 Fitting of parameters based on sensitivity analysis

Simulations are initially performed with literature sourced and estimated parameters as identified in Tables 3.1-3.5. In order to explore whether the simulated oral and IV concentration-time curves may be approximated to their respective experimental data points, typically fitting of 2-3 selected parameters is undertaken. A parameter is selected for fitting if a local sensitivity analysis performed in SimBiology indicated that the modelling outcome is highly sensitive to the value of this parameter.

3.1.1.3.1 Sensitivity analysis: theory and application

Calculating sensitivities allows for the determination of a specific condition (e.g. change in hepatic clearance), defined by a model parameter (e.g. CL_{hep}), which has the most impact on an output in a model (e.g. concentration of a substance in the venous blood compartment, C_{VE}). In other words, this method determines to which extent a model output is sensitive to a slight change of a specific parameter value. To do this, a time-dependent sensitivity coefficient $\mathrm{C_q(t)}$ for a model parameter q is calculated to denote the parameter's sensitivity to $\mathrm{C_{VE}(t)}$, namely:

$$C_q(t) = \frac{q}{C_{VE}(t)} \frac{\partial(C_{VE}(t))}{\partial(q)}$$

$$= \frac{(q + \Delta q/2)}{\big(C_{VE}(t, q + \Delta q) + C_{VE}(t, q)\big)/2} \frac{\big(C_{VE}(t, q + \Delta q) - C_{VE}(t, q)\big)}{\Delta q}$$

(Eq. 3.15)

Here, q represents the model parameters $K_p, R, f_{u(p)}, k_a, k_{il}, k_{bil}, k_{e(r)}$ and CL_{hep}. Each $\mathrm{C_q}$ is normalised so that each sensitivity calculation output is dimensionless. This helps to assess the relative sensitivity of each parameter to the model output. From these, the corresponding time-integral sensitivity coefficients (S_q) are calculated, which give an indication of the total sensitivity of the model parameter to C_{VE} over a pre-defined timecourse of simulation.

The timespan over which a sensitivity analysis is run, is set to be equal to the time span the compound's experimental data are based on (e.g. 1450 minutes in the case of atenolol):

$$S_q = \int_{t=0}^{t=1450\ mins} \left|C_q(t)\right| \, dt.$$

(Eq. 3.16)

Full details of this method can be found, for example, in Martins et al. (2000, 2001) and Ingalls and Sauro (2003). The end result, however, is a number for each parameter indicating how sensitive the venous blood concentration is to perturbations to this parameter. The larger the value indicates a higher sensitivity and, therefore, small changes in this model parameter would cause large changes to venous blood concentrations, and vice-versa. Both oral and IV experimental data are considered for sensitivity analysis.

3.1.1.3.2 Fitting method

Subsequent to a sensitivity analysis for each compound, all fittings are performed in SimBiology using fminsearch as an estimation method to minimise the distance between the model output and experimental data points. Lagarias et al. (1998) provide further information on this method.

IV and oral curves are fitted simultaneously to their respective experimental data. The parameters subject to sensitivity analysis and fitting include those presented in Table 3.4, i.e. K_p, R, f_{up}, k_a, k_{il}, k_{bil}, $k_{e(r)}$, and CL_{hep}. Fitted values and their standard errors (SE) are given in Table 3.4 with subscript $^{(b)}$.

3.1.1.4 Goodness-of-fit statistics to evaluate the performance of the PBK model quantitatively

In order to quantify how well the model describes the clinical data used for testing the model, several goodness-of-fit statistics are calculated. These are R-squared (R^2), the adjusted R^2, the mean squared error (MSE) and the root mean squared error (RMSE). To understand quantitatively to which degree fitting improved the representation of clinical data, goodness-of-fit measures are calculated for each simulation before fitting, with all initial parameters, and after fitting. R-squared is

only applicable to linear models with an intercept term (Kvalseth, 1985; Spiess and Neumeyer, 2010) and the PBK model output does not meet these requirements. Therefore, the majority of R-squared and adjusted R-squared values calculated are negative (data not shown) while an R-squared value useful for the interpretation of a fit is any value between 0 and 1 (Kvalseth, 1985; MathWorks, 2019a). The MSE and RMSE are common statistics to measure model accuracy, which is defined as the overall distance between the true value and estimated values (Bainbridge, 1985; Walther and Moore, 2005). The MSE is calculated by dividing the summed squares of residuals (SS_{res}) by the degree of freedom (DF) (Walther and Moore, 2005; MathWorks, 2019a) (Eq. 3.17-3.21).

$$SS_{res} = \sum_{i=0}^{n} (y_i - f_i)^2$$

(Eq. 3.17)

where n is the number of oral and IV experimental data points ($n = n_{oral} + n_{IV}$), y_i the value of the ith experimental data point and f_i the value of the corresponding estimation.

$$DF = n - m$$

(Eq. 3.18)

where m is the number of fitted parameters.

The MSE values specific to the oral data fit (MSE_{oral}), the IV data fit (MSE_{IV}) and both fittings overall (MSE_{total}) are calculated using Eq. 3.19-3.21.

$$MSE_{oral} = \frac{SS_{res}^{oral}}{DF}$$

(Eq. 3.19)

where SS_{res}^{oral} is the summed squares of residuals between the oral measured data points and their corresponding estimated data points.

$$MSE_{IV} = \frac{SS_{res}^{IV}}{DF}$$

(Eq. 3.20)

where SS_{res}^{IV} is the summed squares of residuals between the IV measured data points and their corresponding estimated data points.

$$MSE_{total} = \frac{SS_{res}^{oral} + SS_{res}^{IV}}{DF}$$

(Eq. 3.21)

While the MSE equals the variance of estimates plus the squared mean error, the RMSE is calculated as the square root of the MSE (Eq. 3.22) and is therefore defined as the standard deviation of the random component in the data (Walther and Moore, 2005; MathWorks, 2019a).

$$RMSE = \sqrt{MSE}$$

(Eq. 3.22)

The closer both statistics are to 0, the better is the predictive accuracy of the model. However, there is no well-defined threshold for both MSE and RMSE distinguishing an acceptable from a non-acceptable quality of predictions (Roy et al., 2016). Veerasamy et al. (2011) noted that an RMSE of <0.3 may indicate a good predictive model. Besides considering the statistical value, the data underlying it need to be taken into account. For example, the robustness of the RMSE and other statistics are likely to be compromised if the sample size is small ($n < 10$) (Chai and Draxler, 2014). The datasets used for testing consist of 7 to 18 data points as shown in Table 3.6. RMSEs and MSEs based on fewer than 10 data points, i.e. the oral data based statistics of bisoprolol, chlorpropamide and theophylline and the IV data based measures of hexobarbital, need to be interpreted with care.

Table 3.6: Number of data points used to test the PBK model performance

	Oral	**IV**
Atenolol	14	12
Bisoprolol	9	13
Chlorpropamide	7	10
Cimetidine	18	13
Diazepam	14	18
Hexobarbital	11	7
Ivermectin	10	NA
Mebendazole	10	11
Theophylline	7	12

NA = not available

3.2 Results

The aim of this Chapter is to generate a human-relevant PBK model which can quantify the relationship between an administered dose and concentrations in various organs over time for a broad range of chemical substances. The PBK model consists of 15 somatic compartments including the lungs, eight non-eliminating organs and tissues (i.e. heart, spleen, thymus, pancreas, adipose, muscle, brain, skin), four eliminating and absorbing organs (i.e. liver, stomach, gut, kidney) as well as two blood compartments (venous and arterial). It also includes the ACAT model to simulate oral absorption from the stomach and seven gut sub-compartments. Organ/tissue-specific blood flow determines the rate a substance flows between the arterial blood, venous blood, and organ/tissue compartments. Rate constants determine the rate of absorption, renal elimination, hepatic clearance, intestinal loss, biliary elimination, gastric emptying and gut transit. In order to evaluate whether the model is able to simulate the kinetics of a broad range of substances reliably, simulated venous blood concentration-time profiles and compared to measured profiles of nine drugs.

3.2.1 Results of sensitivity analyses and simulations with initial and fitted values

Simulations are initially performed with literature sourced and estimated parameters. Subsequently, a sensitivity analysis is undertaken to identify which parameters have a major impact on the predicted venous blood concentration. Results of the sensitivity analyses for bisoprolol, diazepam and theophylline are illustrated in Appendix 3.B, while a summary of the findings for the other compounds is given below. For all compounds, the parameters identified as having a major impact (shown in sensitivity matrices of Appendix Figures 3.B.1, 3.B.4 and 4.B.7 as yellow bars) are included in fitting, as outlined in subchapter 3.1.1.3.

For each substance, simulations before and after fitting are inspected visually to make sure that simulations with fitted parameters represent clinical data a) better than simulations with initial parameters and b) predicted values and clinical data are in close proximity (within the same order of magnitude) to each other over the entire data set. Appendix 3.B contains plots of the fitted simulated output and observed data of bisoprolol, diazepam and theophylline, as well as the residual plots of these

fitted plots. For all sensitive parameters, fitted values and their standard errors (SE) are presented in Table 3.4 with superscript [(b)] and discussed in more detail in the following.

In the case of atenolol, the sensitivity analysis performed to determine parameters which have the most impact on C_{VE} identified K_p and R as sensitive factors. With initial values of 1.7 and 1.11 (see also Table 3.4), fitting for these parameters achieves a good fit according to visual inspection with K_p of 3.43×10^{-3} ($\pm$ 6.14×10^{-4}) and R of 1.74×10^{-3} ($\pm$ 1.98×10^{-4}). Both fitted values are three orders of magnitude lower than their initial values. As K_p is a fitted value by itself, this is not considered an issue. It is interesting to note that both are in the same order of magnitude before and after fitting.

For bisoprolol, primarily R and to a lower extent K_p are identified as sensitive parameters. However, fitting for both parameters produces high standard errors. Good results are achieved when R is fitted on its own. The fitted value of 0.569 (± 0.068) differs by less than an order of magnitude from the experimental value of 1.1.

In the case of chlorpropamide, K_p and R are identified as sensitive parameters. As K_p is a fitted value and $R = 1$ is estimated, it is considered acceptable that their fitted values of 1.81×10^{-3}($\pm 3.30 \times 10^{-4}$) and 0.024 ($\pm 3.46 \times 10^{-3}$), respectively, are more than two orders of magnitude smaller than the initially set values. Also, the initial value of 50 for K_p is an order of magnitude or more higher than all the other K_p values proposed by Peters (2008a).

For cimetidine, the two oral experimental data sets of Somogyi and Gugler (1983) are available, i.e. where the compound is administered with and without food. For fitting, data based on administration without food are used. Also, two plasma concentration-time profiles following IV administration established in two patients are available (Somogyi and Gugler, 1983). Mean values of both profiles are used for fitting. R is identified as most sensitive parameter at the initial input parameter value of 0.98 and fit to 0.741 (± 0.093). The new value is within the acceptable one order of magnitude difference. Less sensitive parameters are K_p and $f_{u(p)}$. In order to assess whether the oral fitted curve may be improved, fitting is performed with R and K_p, and R and $f_{u(p)}$ (data not shown) but does not result in a significantly better fit.

With the data considered for diazepam, R is identified as most sensitive parameter followed by K_p with initial values of 0.5587 and 2, respectively. Fitted values of both R and K_p, i.e. 1.180 ± 0.912 and 0.533 ± 0.453, are less than one order of magnitude different to the initial values. These and both fitted curves are considered acceptable. Two concentration-time profiles following two oral doses administered to the same individual are available (van der Graaff et al., 1986). Mean values of both profiles are calculated and used for fitting.

A sensitivity analysis for hexobarbital-related data reveals that R is the most sensitive parameter followed by K_p. Fitting attempts of R on its own, and R and K_p show that the latter does not generate better results than the former. Therefore, fitting results are adopted for R only. Its initial value of 1.0 is amended to 0.323 ± 0.137.

As mentioned above, only oral data are available for ivermectin. The initial simulation using literature and estimated parameter values differs substantially from experimental data points. A sensitivity analysis identifies R, k_{bil} and K_p as virtually equally sensitive parameters. Neither fitting with all three parameters simultaneously, nor fitting of k_{bil} on its own, produce acceptable results. k_{bil} on its own is mostly fit to zero while the fitted curve is less adjusted to given experimental data than the initial simulation. When R and K_p are fitted together, they are estimated to be 0.348 ± 0.071 and zero, respectively. Subsequently, R is set to the proposed value and K_p is fitted on its own. A most adequately fitted curve is achieved with K_p set to zero which is why this parameter is proposed to be $1.0\ x\ 10^{-7}$ (approaching 0).

For mebendazole, again, R and K_p are identified as sensitive parameters. Their initial values of 1 and 5 for R and K_p are fitted to 0.081 ± 0.016 and 0.301 ± 0.067, respectively. Both estimated values are more than an order of magnitude smaller than their initial values. However, as the initial K_p is fitted and R is estimated, this difference is not considered an issue. Both IV and oral clinical theophylline profiles are taken from Aslaksen et al. (1981). The IV data Peters (2008a) used are based on a single individual presented by Chrzanowski et al. (1977). It is considered that IV data from an experiment on six individuals as presented in Aslaksen et al. (1981) are more robust than using the data assessed from a single individual. The most sensitive parameter for this compound is R, followed by K_p. When fitting is performed for both parameters, R is estimated to be its initial value of 0.83. Therefore, K_p is fitted on its own resulting in 0.345 ± 0.047 which differs less than an order of magnitude from

its initial value of 1.3. Results of the fitted simulated concentration-time profiles and observed data points of bisoprolol, diazepam and theophylline are included in Appendix 3.B.

3.2.2 Results of goodness-of-fit statistics

Goodness-of-fit statistics are calculated as presented in subchapter 3.1.1.4, before and after fitting to evaluate if simulated output (i.e. venous blood concentration) curves with fitted values are closer to observed data points than output curves simulated with initial input values (before fitting). Overall, MSEs and RMSEs after fitting are lower than those calculated with initial parameter values (see Table 3.7). Yet, this is not the case for the oral data based MSE and RMSE of hexobarbital, and the IV and total data based MSEs and RMSEs of atenolol, bisoprolol, cimetidine and diazepam. While the oral data based MSE and RMSE of hexobarbital after fitting are slightly higher than before fitting, the IV data based MSE and RMSE values improved considerably (by one order of magnitude) as well as the total data based MSE and RMSE values. Similarly, the oral data based MSEs and RMSEs of atenolol, bisoprolol, cimetidine and diazepam are improved substantially at the slight expense of the IV and total data based values. Generally, RMSE values that are higher after fitting than their corresponding MSE and RMSEs calculated before fitting are lower than the proposed 0.3 threshold.

Table 3.7: Goodness-of-fit parameters for oral, IV and total data, before and after fitting, of all compounds studied

	MSE						RMSE					
	Oral		**IV**		**Total**		**Oral**		**IV**		**Total**	
	BF	**AF**	**BF**	**AF**	**BF**	**AF**	**BF**	**AF**	**BF**	**AF**	**BF**	**AF**
Atenolol	8.14×10^{-7}	1.11×10^{-7}	1.70×10^{-6}	2.52×10^{-6}	2.51×10^{-6}	2.63×10^{-6}	9.02×10^{-4}	3.33×10^{-4}	1.30×10^{-3}	1.60×10^{-3}	1.60×10^{-3}	1.60×10^{-3}
Bisoprolol	1.81×10^{-9}	5.60×10^{-10}	3.14×10^{-8}	4.39×10^{-8}	3.32×10^{-8}	4.45×10^{-8}	4.26×10^{-5}	2.37×10^{-5}	1.77×10^{-4}	2.10×10^{-4}	1.82×10^{-4}	2.11×10^{-4}
Chlorpropamide	1.37×10^{-4}	1.96×10^{-6}	1.70×10^{-4}	1.95×10^{-6}	3.07×10^{-4}	3.91×10^{-6}	0.0117	1.40×10^{-3}	0.0130	1.40×10^{-3}	0.0175	2.00×10^{-3}
Cimetidine	8.21×10^{-6}	4.25×10^{-6}	4.53×10^{-6}	6.14×10^{-6}	1.27×10^{-5}	1.04×10^{-5}	2.90×10^{-3}	2.10×10^{-3}	2.10×10^{-3}	2.50×10^{-3}	3.60×10^{-3}	3.20×10^{-3}
Diazepam	2.64×10^{-8}	8.27×10^{-9}	8.29×10^{-8}	1.64×10^{-7}	1.09×10^{-7}	1.72×10^{-7}	1.62×10^{-4}	9.09×10^{-5}	2.88×10^{-4}	4.05×10^{-4}	3.31×10^{-4}	4.15×10^{-4}
Hexobarbital	1.56×10^{-5}	2.15×10^{-5}	6.24×10^{-5}	6.19×10^{-6}	7.80×10^{-5}	2.77×10^{-5}	3.90×10^{-3}	4.60×10^{-3}	7.90×10^{-3}	2.50×10^{-3}	8.80×10^{-3}	5.30×10^{-3}
Ivermectin	6.52×10^{-10}	1.11×10^{-10}	NA	NA	6.52×10^{-10}	1.11×10^{-10}	2.55×10^{-5}	1.05×10^{-5}	NA	NA	2.55×10^{-5}	1.05×10^{-5}
Mebendazole	9.35×10^{-18}	2.34×10^{-18}	2.77×10^{-17}	7.12×10^{-18}	3.71×10^{-17}	9.46×10^{-18}	3.06×10^{-9}	1.53×10^{-9}	5.27×10^{-9}	2.67×10^{-9}	6.09×10^{-9}	3.08×10^{-9}
Theophylline	1.13×10^{-4}	8.47×10^{-6}	0.0136	0.0134	0.0137	0.0134	0.0106	2.90×10^{-3}	0.117	0.116	0.117	0.116

BF= before fitting, AF= after fitting, NA= not available.

3.3 Discussion

With an indisputable lack of mechanistic and quantitative understanding of renal toxicity pathways, it is important to know how much of a dose reaches the kidney and potentially accumulates there. PBK models provide these insights. A newly generated PBK model based on previously established and validated ODEs is judged to provide the transparency and flexibility needed for its use in conjunction with a mechanistic kidney model. For example, as shown in Chapter 4, to simulate the kinetics of aspirin and salicylic acid, ODEs of the PBK model are extended, amongst other things to incorporate metabolism of aspirin to salicylic acid in the liver compartment. Therefore, a newly generated PBK model, as opposed to using a previously established one, best fulfils the requirements addressed in the study described in Chapter 4. In comparison to the amount of studies published on PBK models, only a small proportion of these studies include full details on the model structure and ODEs. Of these, Peters (2008a) presents a comprehensive description which is why it is used as key source for the development of the PBK model presented here. Nevertheless, the model published by Peters (2008a) cannot be reproduced as such, due to missing details and minor errors. Therefore, the study presented here proposes a unique PBK model, and the extensive level of detail used to describe the model's structure adds value to the scientific literature.

This study presents the development of a generic human-data-based PBK model, which simulates the kinetics of a broad range of chemical substances. In order for the model to be robust, i.e. representing the physiology of the human body, 15 major human organs and tissues are included as compartments and key physiological processes such as tissue permeation, hepatic and renal elimination, oral absorption including paracellular absorption and gastro-intestinal dissolution, enterohepatic recirculation and biliary elimination, intestinal loss as well as the conversion of the metabolite to the parent compound, are incorporated. In order to evaluate whether the model may be used for a broad range of chemicals, the model is parameterised and validated against nine compounds which possess diverse physico-chemical and pharmacokinetic characteristics. Following each simulation, a local sensitivity analysis is performed in order to assess which parameters influence the concentration-time curve the most. Parameters identified as most sensitive are fitted so that the model output best represents clinical data. Overall, when fitted

simulations are compared to clinical data via visual inspection, simulations are found to provide a good representation of experimentally established data. Also, all RMSE values, a goodness-of-fit parameter measuring model accuracy, are below the critical 0.3 threshold, indicating a good fit to the data in each case.

The level of confidence in a PBK model may be characterised on the basis of three criteria outlined in the WHO/IPCS Guidance on the Characterisation and Application of Physiologically Based Pharmacokinetic Models in Risk Assessment (IPCS WHO, 2010). These criteria are

1) biological basis of the model structure and parameters,
2) comparison of model simulations with experimental data and
3) reliability of model predictions of dose metrics relevant to risk assessment (model testing, uncertainty analysis and sensitivity analysis).

The model structure and parameters are considered to have a reasonable biological basis as

1.1) the cardiac output is equal to the sum of all tissue blood flow rates (see Table 3.1),
1.2) the blood flow rates and tissue volumes applied are within the documented range for a human weighing 70 kg (see Table 3.1),
1.3) the vast majority of chemical-specific parameter values are based on human data established in clinical studies (see 3.1.1.2, particularly Table 3.4), and
1.4) key physiological processes outlined above have been mathematically expressed and incorporated into the model (see 3.1. and Appendix 3.A).

The only parameter values that are based on animal data are CL_{hep} of hexobarbital and J_{ms} to calculate the paracellular absorption rate constant of atenolol, cimetidine and theophylline. Considering the amount of parameters based on human data, this is judged to be acceptable.

Another aspect supporting the confidence in the model is that fitting of typically one or two parameters resulted in an acceptable representation of experimental data. In six of nine compounds, K_p, a previously fitted value, had to be re-fitted. In cases where an experimental value of R is not found in the literature, a value of R=1 is assumed, namely in the cases of chlorpropamide, ivermectin and mebendazole. The value of R may have a substantial impact on predicted blood concentrations as

confirmed by the sensitivity analysis results. Based on these results, the value of R is fitted for 8 of the 9 substance profiles selected (including chlorpropamide, ivermectin and mebendazole). Therefore, potential flaws related to the assumption of R=1 are corrected. Assuming R=1 while the actual value of R<1 implies that the predicted plasma concentration suggests a higher blood concentration than actually exists since the majority of the compound is located in the plasma. Fitted values of R for hexobarbital differ by a factor of three from the initially used experimental value. Even though this is by far higher than the factor of two proposed by the WHO/IPCS guidance for adequate PBK predictions, it is within acceptable limits of common modelling practice. The only value that differs by more than an order of magnitude from its experimentally established value is atenolol-related R. Underlying uncertainties may compromise the validity of the experimental value. Overall, assuming a value of 1 may produce suboptimal results and may be corrected in a future refined version by using QSARs to estimate R (Peyret et al., 2010; Peyret and Krishnan, 2011; Najafi et al., 2013).

According to criterion 2) of the WHO/IPCS guidance, confidence in a PBK model will be high if a variety of data are reproduced. The nine compounds chosen cover a broad chemical space and a wide spectrum of PK profiles in terms of solubility and permeability. For each of the studied compounds, oral and IV data generated in one human PK study following a single dose are used for validation – apart from the validation of ivermectin since only oral data are available for this compound.

It is appreciated that the consideration of additional PK data would benefit the validation of the model further. Since only one set of PK study data is considered for each route of administration, it remains unknown whether the model performs equally well for higher or lower dose levels or for datasets established in different young and healthy individuals or with different measurement techniques. At higher doses, certain metabolism or excretion processes may be saturated so that the hepatic clearance or renal elimination rate constant is lower overall (and no longer proportional to the drug concentration) in comparison to these elimination processes when non-saturated. To model saturated elimination processes, an elimination rate constant or clearance parameter is replaced by a Michaelis-Menten term (as explained in Chapter 4).

Including additional data established in groups of young and healthy individuals and by using a range of measurement techniques would help understanding

interindividual and interstudy variability and uncertainty underlying certain parameter values. Moreover, in order to use this PBK model to quantitatively assess mechanisms and dose-response relationships related to renal toxicity, physiological parameters need to be modified to simulate the PK of elderly and/or patient individuals or even elderly/patient populations. The reason for this is, as discussed in Chapter 1, that renal toxicity is predominantly observed in elderly patients with various comorbidities. In addition, since the vast majority of renal adverse effects are recorded after repeated drug exposure and often associated with accumulation in renal tissues, PK after repeated doses need to be assessed. Both latter aspects, prediction of renal kinetics in elderly individuals and repeated dose administration, are considered in the study in Chapter 4. Except for cardiac output, all physiological parameters modified in Chapter 4 to simulate kinetics in elderly individuals are kidney-related. However, in drug development, PBK models aim to predict the PK in the intended patient population early in the development process so that a PBK model based on an average young and healthy individual is of limited value. In order to account for age- and/or disease-related changes in the human body overall, various physiological characteristics are typically adapted; these include modifications of enzyme and transporter activity and abundance (mainly in the liver and intestines), organ size (according to anthropometric data), organ blood flow, circulating levels of erythrocytes and plasma proteins, intestinal surface area, gastro-intestinal pH as well as intestinal and stomach motility (Rostami-Hodjegan and Tucker, 2007; Jamei et al., 2009; Bosgra et al., 2012). For instance, organ volumes and blood flows may be derived from distributions of anthropometric parameters – such as body weight, height, body surface area and body mass index – which represent interindividual variability of a population (Price et al., 2003; Willmann et al., 2007; Bosgra et al., 2012). Open-source or proprietary virtual populations have been created to facilitate population-based predictions (Willmann et al., 2007; Jamei et al., 2009; Pearce et al., 2017; Sarigiannis et al., 2020). Considering such additional data would help to adequately predict PK in elderly individuals and/or patient populations. However, at this stage the focus of this model validation is given to the coverage of a broad range of physicochemical and PK properties.

For all nine chemicals used here, both oral and IV data are simulated and fitted simultaneously. Therefore, both routes of exposure are taken into account. Visual inspection is applied to evaluate in a qualitative manner if the simulated curve

reproduces the general trend of experimental observations. For all nine compounds, reproduction of the general trend of clinical concentration-time curves is found to be adequate when assessed via visual inspection. The ability of the model to replicate experimental data is assessed quantitatively using the goodness-of-fit statistics MSE and RMSE which indicate a good fit to clinical data for each substance. The validation approach taken here may be further extended by quantifying additional simulation-based dose metrics and PK parameters (e.g. AUC, C_{max}, trough concentration C_{trough} and $t_{1/2}$) and comparing these to their measured equivalents as proposed by PBK guidance and best practice documents (IPCS WHO, 2010; EMA, 2018) and recent case studies (Fàbrega et al., 2016; Moss et al., 2017; Rajoli et al., 2019). C_{max} and C_{trough} values characterise upper and lower bound values and the AUC quantifies exposure over a defined time span. Comparing simulated and measured AUC, C_{max} and C_{trough} values, in addition to predicted and measured venous blood concentrations, would help to quantitatively assess whether the model reproduces a variety of measured data adequately which are typically generated to characterise the PK of a compound.

One limitation of this study relates to simulations of whole blood concentrations. As stated above, predicted arterial and venous blood concentrations represent plasma concentrations. For six of the tested compounds (atenolol, bisoprolol, cimetidine, hexobarbital, ivermectin and mebendazole), experimental observations are presented as plasma concentrations. For chlorpropamide and theophylline, clinical measurements are given as serum concentrations which is comparable to plasma concentrations. However, diazepam related clinical data are recorded as whole blood concentrations which are not corrected for in the present study. Though this explains the discrepancy between the experimentally derived and the fitted value of R for diazepam (measured R=0.5587; fitted R=1.180 with a standard error of 0.912). In future studies considering measured concentrations in whole blood, ODEs similar to those presented by Krishnan et al. (1994, 2009) may be applied to predict blood concentrations.

With regard to criterion 3) of the WHO/IPCS guidance, a detailed assessment of uncertainty inherent in experimental data considered here goes beyond the scope of this study. However, apart from one study taken into account for hexobarbital, all other studies considered here have previously been accepted by Peters (Peters, 2008a) for the evaluation of model performance. Local sensitivity analyses are performed for each chemical which highlight that overall, K_p and R are the most

sensitive parameters. Interestingly, CL_{hep}, the parameter that Peters (2008a) fitted in the first instance, is not found to be sensitive for any dataset tested.

Further limitations of this study include that transporter-driven (permeability rate-limited) kinetics are ignored. Permeability rate-limited kinetics, implying that distribution into tissue is limited by drug-specific membrane permeability, are predominantly observed with larger (MW > 300 Da) polar molecules (Jones and Rowland-Yeo, 2013; Cheng and Ng, 2017). Also, interaction between compounds and transporters may be significantly altered in a specific patient population, potentially attributed to DDIs, so that PK studies in healthy volunteers may be not provide transferable results (Evers et al., 2018). In general, a PBK model may benefit from incorporating active transport terms in specific compartments if these are necessary to express the kinetics of a substance to the required degree of accuracy in an individual or population. An increasing number of *in vitro* data characterising the rate of active transport are being generated and protein expression data provide an opportunity to account for interindividual variability. Examples of such models applying active transporter terms in the gut, liver, kidney, lung, brain and vascular compartments are presented by Thompson and Beard (2011), Ball et al. (2013), Gaohua et al. (2015), Emami Riedmaier et al. (2016) and Cheng and Ng (2017). Even though transporter-driven absorption and intestinal efflux are confirmed to have minimal impact *in vivo* (Peters, 2008a), it is appreciated that all compounds tested above may show permeability rate-limited kinetics (ivermectin due to its MW and remaining compounds due to polarity) to some extent in certain compartments. Overall, active transport processes are considered to have low impact on the PK of the group of compounds studied. However, to simulate the PK of compounds which are significant transported via active processes, the model's code needs to be amended accordingly. For instance, active transport is considered in the mechanistic kidney model discussed in the following Chapter.

Furthermore, for the purpose of this study, no tissue-specific partition coefficients are used but a compound-specific partition coefficient is applied to each compartment even though it is known that partitioning of a chemical differs from tissue to tissue (Brown et al., 1997; Björkman, 2002). Also, differences in transit rates through the gastrointestinal tract have not been investigated. Li et al. (2012) showed that stomach transit time may be a sensitive parameter. Furthermore, the lungs and

skin have not been considered as portals of entry which is why inhalation and dermal exposures may not be simulated at this point. Additionally, metabolism is solely incorporated in the liver compartment. However, metabolism can take place for some chemicals in various tissues including the kidneys, gut, lungs, skin, testis and bone marrow (Brown et al., 1997; Krishnan and Andersen, 2001; Boroujerdi, 2015). Moreover, since this PBK model is tested and validated with small molecule drugs, its validity to predict the kinetics of substances which are not classified as small molecule drugs – e.g. nanoparticles or large biopharmaceuticals – would have to be reassessed. Lastly, this model does not include certain organs which may be target organs of toxicity such as reproductive organs or the bone marrow. All these aspects may be added in the future.

Overall, the level of confidence in this model for a broad chemical applicability domain and the organs and tissues taken into account is considered to be good.

In Chapter 4, the PBK model is applied in conjunction with a newly developed mechanistic model of the kidney which simulates the kinetics of SA in that particular organ. When applied in conjunction, both the PBK model and the mechanistic kidney model provide a novel way to evaluate dose-response relationships in the context of renal toxicology, as discussed in more detail in Chapter 4. As mentioned in 1.4, the PBK model on its own may not necessarily be considered a scientific novelty. However, besides being used in conjunction with the mechanistic kidney model, it may be used in different ways for quantitative risk assessment approaches. For example, concentration-time profiles from the PBK may feed into a variety of organ or tissue-specific mechanistic toxicokinetic, toxicodynamic or (Q)SAR models. In contrary to the more costly and time-consuming pharmacokinetic studies in animals and humans, this PBK model not only provides information on blood, urine and other easily accessible biological matrices but also organ-level concentrations. Hence, it bridges the knowledge gap between external and internal exposure in a transparent way for a broad range of substances and helps to better interpret *in vitro* toxicity testing results.

4.0 A MECHANISTIC MODEL TO STUDY THE KINETICS OF SALICYLIC ACID IN THE KIDNEY

4.1 Introduction

The costs of chronic kidney disease (CKD) constitute a major and increasing challenge for national health care systems worldwide, with expenditures in England reaching £1.45 billion in 2009 and taking up close to 30% of general medical care (Medicare) costs in the U.S. in 2011 (Kerr et al., 2012; Collins et al., 2015; Eriksson et al., 2016). The kidney is a major target of drug-induced toxicity, particularly in vulnerable individuals such as patients who are critically ill and or have chronic kidney disease (Mehta et al., 2004; Uchino et al., 2005; Zhang et al., 2005). Some of the pharmaceuticals responsible for nephrotoxicity have been on the market for decades. Whilst much is known about some classes of drugs, a detailed understanding of the mechanisms and toxicity pathways of all drugs is lacking (Pletz et al., 2018b).

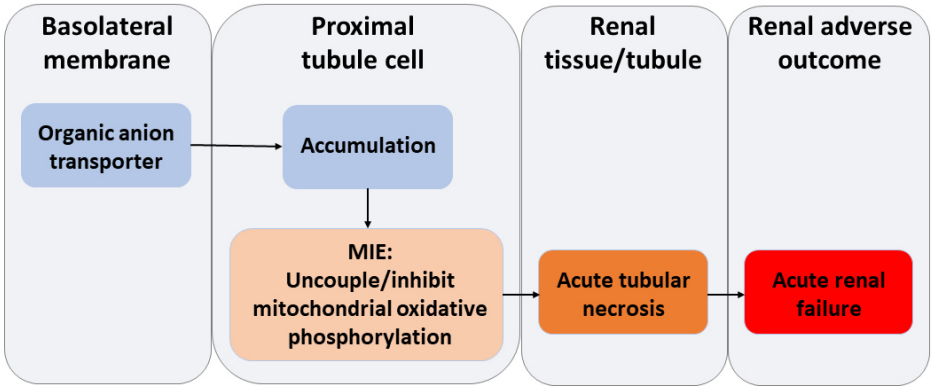

Figure 4.1: Summary of a proposed AOP for the nephrotoxicity of NSAIDs via the uncoupling/inhibition of mitochondrial oxidative phosphorylation (adapted from Drewe and Surfraz, 2015)

The role mitochondrial dysfunction plays in renal disease has been well, and increasingly, researched over the last few decades (You, 1983; Ishimoto and Inagi, 2016; Eirin et al., 2017; Guo et al., 2018). It has been known for many years that therapeutic concentrations of salicylic acid (SA) in serum – 0.5 to 2.2 mM – are high enough to induce mitochondrial swelling if the cytosolic concentration of an exposed cell is at the same level as the plasma concentration (You, 1983). SA is the major metabolite of the NSAID aspirin (acetyl salicylic acid; ASA). Despite the importance of

this effect, a quantitative evaluation of the concentration reached in proximal tubular cells at therapeutic and toxic exposures is still lacking. Such a quantitative assessment would help with the interpretation of mechanistic *in vitro* data and add clarity to the current understanding of nephrotoxic effects observed in individuals at different dosing levels.

Previously developed mechanistic models (formerly introduced in subchapter 1.3.2) to simulate renal kinetics consider urine flow and passive reabsorption (Tang-Liu et al., 1983), complemented by glomerular filtration and protein binding (Hall and Rowland, 1984; Komiya, 1986, 1987; Mayer et al., 1988) and active secretion (Russel et al., 1987a; b; c; Katayama et al., 1990). Most of these early models (Tang-Liu et al., 1983; Hall and Rowland, 1984; Komiya, 1986, 1987; Mayer et al., 1988) derive quantitative relationships between renal clearance and urine flow, renal reabsorption, glomerular filtration and protein binding in various species and for a selection of substances, without compartmentalising the kidney. Hence, these models do not facilitate the quantification of a substance's concentration (i.e. internal exposure) in a particular compartment of renal tissue. Russel et al. (1987a; b) and Katayama et al. (1990) differentiate between renal blood, tissue and tubular compartments. Felmlee et al. (2010, 2013) generated a universal mechanistic model for a broad applicability domain predicting renal clearance driven by active secretion, active reabsorption or both of these processes. The authors separate a proximal tubule from a distal tubule compartment, besides including a renal blood and urine compartment but do not consider metabolism and passive reabsorption.

Two of the most sophisticated mechanistic models to predict kinetics of chemicals in the kidney are reported by Neuhoff et al. (2013) and Huang and Isoherranen (2018). The structure of their models represents a nephron divided into segments illustrating the glomerulus, proximal and distal tubules, loop of Henle and collecting ducts. Each segment contains three compartments, characterising the cellular mass, blood space and tubular fluid. Both models predict renal elimination by accounting for active and passive reabsorption, active and passive secretion, glomerular filtration and renal metabolism. Bypass of parts of the renal blood flow and population variability are considered by Neuhoff et al. (2013). In both models, ODEs describe the movement of a compound between compartments so that the concentration of a substance can

be quantified in each compartment. However, the model developed by Neuhoff et al. (2013) is embedded in the commercial software Simcyp® Simulator and details of the ODEs are not publicly available. Applications of this model are reported (Hsu et al., 2014; Posada et al., 2015; Burt et al., 2016; Emami Riedmaier et al., 2016; Scotcher et al., 2017; Hsueh et al., 2018). Limitations of this model revolve around missing data, e.g. on proximal tubular cells per gram of kidney (PTCPGK) and absolute renal transporter abundances at different parts of the nephron. The model generated by Huang and Isoherranen (2018) predicts drug renal clearance considering *in vitro* permeability, unbound filtration, active tubular secretion and pH dependent bidirectional passive diffusion. It is validated with data from 46 drugs and can quantify concentrations in each compartment, even though it is not used in this way.

In addition to models simulating drug or chemical compound related kinetics, Layton (2013) reviewed mathematical models on (patho-)physiological processes of the kidney. Among others, these processes include the regulation of renal oxygen transport. Incorporating intrarenal oxygen transport and consumption into a toxicokinetic kidney model may be valuable since hypoxia in renal tissue has been argued to drive kidney dysfunction (Palm and Nordquist, 2011; Fu et al., 2016).

In summary, there are limited computational models which quantify concentration-time profiles of substances in toxicologically relevant segments of the human kidney. To date, a publicly available kidney model is lacking which is embedded in a full-body PBK model and has been tested for a sensitive population.

The aim of the study undertaken in this Chapter is to develop a mechanistic model of renal kinetics with specific reference to SA, the major metabolite of ASA. Specific objectives included:

1) Incorporation of this sub-compartment kidney model in our previously developed PBK model in order to validate it with full-body kinetic data.
2) Investigation whether a quantitative relationship may be established between therapeutic doses of SA, predicted proximal tubular cell concentrations in young and elderly virtual individuals and toxicity events in proximal tubular cells. Since ASA is rapidly metabolised to SA, the

mechanistic kidney model is set up to simulate the kinetics of SA only while the PBK model is parameterised to simulate the kinetics of both ASA and SA.

4.2 Methods

4.2.1 Development of the model

A mechanistic model of the kidney is created using the SimBiology® desktop (version 5.8.1), an app provided by MATLAB®, version R2018b. SimBiology uses ordinary differential equations (ODEs) and numerical solvers to predict biokinetic and biodynamic processes with outputs of concentration vs. time curves for tissue or organ-specific compartments (MathWorks, 2019d). The ODEs created in SimBiology are solved using the Matlab solver *ode15s* which integrates the system of stiff differential equations (MathWorks, 2019b). A principal assumption of the model is that compartments are well-stirred, which implies instantaneous and homogenous distribution of a compound within a compartment.

As the nephron is the functional unit of a kidney, we assume that the core element of the kidney submodel is that of a nephron, connecting to a collecting duct. In the scientific literature, the latter is not considered part of the nephron (Fenton and Praetorius, 2015). The main components of a nephron include the glomerulus, proximal tubules, loop of Henle and distal tubules as shown in Figure 4.2. In a human kidney, 85% of the nephrons are predominantly located in the cortex, the outer region of the kidney, with short loops of Henle reaching the outer medulla (Feher, 2017). The remaining 15% are juxtamedullary nephrons which originate close to the corticomedullary boundary with long loops of Henle extending into the inner medulla (Fenton and Praetorius, 2015; Feher, 2017). Figure 4.2 shows a longitudinal cross-section of the kidney depicting key anatomic structures including the cortex and medulla.

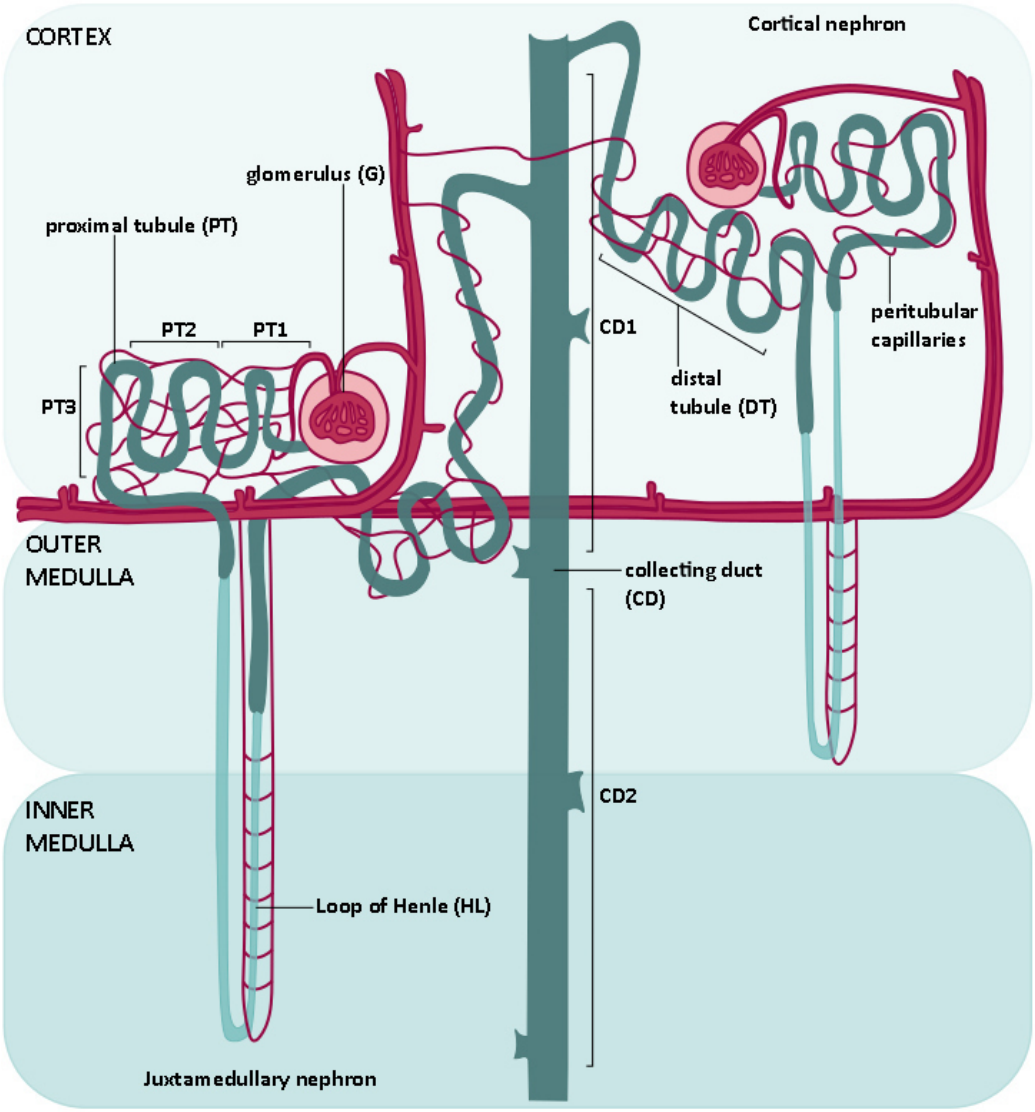

Figure 4.2: A schematic diagram of the structure of nephrons and their cortical and juxtamedullary locations relevant for the development of a mechanistic model (adapted from Feher, 2017). The main components of the mechanistic model developed here are the glomerulus (G), proximal tubules divided into three sections (PT1-3), loop of Henle (HL), distal tubules (DT) and collecting ducts divided into two sections (CD1-2).

A substance reaches the nephrons via arterial blood vessels, so-called afferent arterioles which connect to the glomerulus where approximately 120 mL of water along with small, unbound substances are filtered per minute into the glomerular space. From there, the filtrate flows through the proximal tubule, subsequently the loop of Henle, distal tubule and collecting duct through which the filtrate reaches the bladder where it is excreted as urine. Compounds that are not filtered at the

glomerulus move through peritubular capillaries which surround the proximal and distal tubules and *vasa recta* surrounding the loop of Henle and collecting ducts from where they may be absorbed into the tubular cells and from there into the tubular lumen via active and passive transport. Active and passive reabsorption from the tubular lumen may also occur back into tubular cells. The kinetic processes of SA reaching and moving through a nephron are described in subchapter 4.2.2.

Since tubular cells in the early proximal tubule (PT) section differ in morphology to those in later sections and the same holds for cells in collecting ducts, these parts of the nephron are divided into three (PT1-3) and two (CD1-2) sections, respectively. The model comprises eight blood compartments, representing arterial and venous blood vessels at different locations of the nephron (glomerular blood, proximal tubular blood sections 1-3, loop of Henle blood, distal tubular blood, collecting duct blood sections 1-2), and eight corresponding luminal compartments (i.e. glomerular space, proximal tubular lumen sections 1-3, loop of Henle lumen, distal tubular lumen, collecting duct lumen sections 1-2). Seven cellular compartments (proximal tubular cells sections 1-3, loop of Henle cells, distal tubular cells, collecting duct cells sections 1-2) connect to site-equivalent luminar and blood compartments via passive diffusion and active transport. Metabolism is incorporated in all cellular compartments. Figure 4.3 shows a schematic diagram of the mechanistic kidney model including all compartments, flows and metabolism that are taken into account.

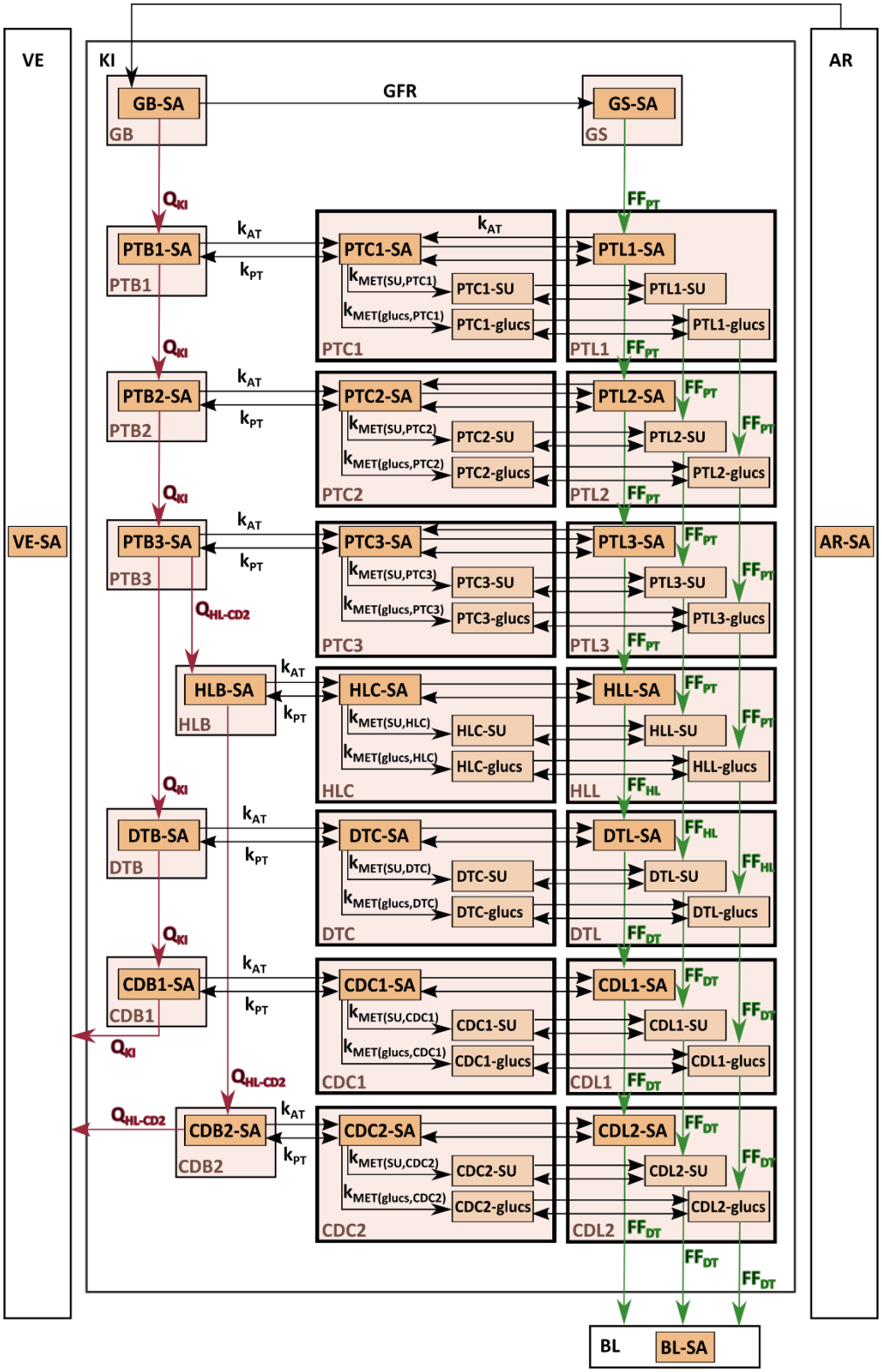

Figure 4.3: Schematic representation of the mechanistic kidney model. The white central box stands for the kidney compartment (KI). The light orange boxes represent the compartments of the kidney model while the darker orange boxes represent concentrations of SA, SU and glucuronides. **Compartments**: GB = glomerular blood; GS = glomerular space; PTB1-3 = proximal tubular blood 1-3; HLB

= loop of Henle blood; DTB = distal tubular blood; CDB = collecting duct blood 1-2; PTC1-3 = proximal tubular cells 1-3; HLC = loop of Henle cells; DTC = distal tubular cells; CDC1-2 = collecting duct cells 1-2; PTL1-3 = proximal tubular lumen 1-3; HLL = Loop of Henle lumen; DTL = distal tubular lumen; CDL1-2 = collecting duct lumen 1-2; **Concentrations**: -SA = SA concentration in respective compartment; -SU = SU concentration in respective compartment; -glucs = glucuronide concentration in respective compartment; **Blood and fluid flows**: $GFR =$ glomerular filtration rate; $Q_{KI} =$ renal blood flow rate; $Q_{HL-CD2} =$ blood flow in loop of Henle and collecting ducts; $FF_{PT} =$ fluid flow leaving the glomerular space and proximal tubules; $FF_{HL} =$ fluid flow leaving the loop of Henle; $FF_{DT} =$ fluid flow leaving the distal tubules and collecting ducts; **Active transport**: single-sided arrows between blood and cellular, and between cellular and luminal concentrations with rate k_{AT}, equations presented in Appendix 4.A show that k_{AT} represents added Michaelis-Menten terms of relevant active transport processes in the respective compartment; **Passive diffusion**: double-sided arrows between blood and cellular, and between cellular and luminal concentrations with rate k_{PT}; **Metabolism**: $k_{MET} =$ rate of metabolism to form SU or glucuronides in a subcompartment, Eq. 9-20 of Appendix 4.A.2 show that k_{MET} represents added Michaelis-Menten terms of relevant metabolic reactions in the respective compartment; exposure is entering the kidney compartment from the arterial blood compartment (AR) and moves from the kidney compartment into the bladder (BL) or the venous blood compartment (VE).

4.2.1.1 Compartment volumes

Each compartment is assigned a physiologically-based volume. For this, a gross estimate of the volumes of renal tubules (comprising cellular and luminal compartments) and blood vessels is performed as described in subchapter 4.2.1.1.1. Glomerular blood and glomerular space compartment volumes are discussed subsequently in subchapter 4.2.1.1.2. The volume of each compartment for a single nephron is calculated based on values sourced from the literature. For the cellular and luminal compartments, the external diameter of the tubular section, the cell height and compartment length are used to derive cylindrical compartmental volumes. For estimates of cell height of collecting duct cells, measurements of histological images of the collecting duct are utilised to derive these values whereas

all other cell height estimates are taken from text sources. All these calculations are presented in subchapter 4.2.1.1.3. Subsequently, compartmental volumes per nephron and collecting duct are scaled to those present in a human, i.e. in both kidneys containing one million nephrons each totalling 280 mL (Davies and Morris, 1993; Peters, 2008a).

4.2.1.1.1 Gross estimation of cellular, luminal and blood compartments

The composition of the tissue in the renal cortex differs greatly from the tissue composition in the renal medulla. While the cortex contains virtually all components of all nephrons, with the exception of the parts of loops of Henle, it is assumed that the cortex volume comprises all glomeruli, proximal tubules and distal tubules. The volume of peritubular capillaries, the blood vessels surrounding renal tubules, has previously been estimated to be 7% of the total kidney volume (Neuhoff et al., 2013), so whether capillaries are equally distributed in the cortex and medulla had to be defined. According to animal and human data of the architecture of the renal medulla (Knepper et al., 1977; Wei et al., 2015), the medullary peritubular capillary volume is estimated at 7% of the medulla volume, and the same fraction is set for the cortical capillary volume. The *vasa recta* which arises from efferent arterioles of juxtamedullary nephrons and forms a capillary network in the renal medulla, takes up 15% of the volume of the medulla (Pallone and Cao, 2013; Feher, 2017). It is known that the *vasa recta* interacts with the loop of Henle and collecting duct to exchange urea and NH_4^+, respectively (Feher, 2017). While the *vasa recta* appears to exchange substances mainly with the loop of Henle (Alpern et al., 2013; Fenton and Praetorius, 2015), the volume of the collecting ducts significantly exceeds the volume of the loop of Henle, even though a quantitative estimation is not retrieved from the literature. Therefore, it is assumed that the medullary blood compartments, taking up 22% of the medullary volume, as they comprise capillary and *vasa recta* volumes, are equally distributed around the loop of Henle and collecting ducts.

The interstitial volume in the cortex has been estimated at 4% of the cortical volume (Eaton and Pooler, 2013; Neuhoff et al., 2013) while animal and human data indicate that the interstitium occupies between 15 and 25% of the renal medulla (Knepper et al., 1977; Wei et al., 2015). Hence, a fraction of 23% of medullary volume is estimated

for the interstitium. This fraction is added to the tubular cell fractions of the loop of Henle and collecting ducts, and concurrently 4% of the cortical volume assigned for the interstitium is added to the tubular cell fraction of the cortex. Since the volume ratio of cortex/medulla is found to be 0.92 in healthy subjects (Kojima et al., 2001), 133 and 147 mL are assigned to the cortex and medulla, respectively, adding up to a total kidney volume of 280 mL. Table 4.1 summarises the volumes of cortex and medulla and fractional distribution of tubular, blood and interstitial volumes.

Table 4.1: Fraction between cellular and luminal, blood and interstitial volumes in the renal cortex and medulla

	Cortex	**Medulla**
Volume (mL)	133	147
Tubular fraction (%) (cellular and luminal)	89	55
Blood fraction (%)	7	22 (7 – capillaries; 15 – *vasa recta*)
Interstitial fraction (%)	4	23

4.2.1.1.2 Glomerular blood and glomerular space compartment volumes

Since the volume of one million glomeruli is estimated to be 4.2 mL (Rouiller, 1969), 8.4 mL is assigned to the entire glomerular blood compartment accounting for two million glomeruli in both kidneys. The volume of the glomerular (or Bowman's) space, the urinary cavity that connects to the lumen of the proximal tubule, is derived from the volume of the Bowman's capsule which represents the total glomerular volume minus the volume of the glomerular blood compartment (Rouiller, 1969; Fenton and Praetorius, 2015). As the volume of the Bowman's capsule has been estimated to be 0.044 mL per gram of kidney, the total Bowman's capsule volume per person yields 12.32 mL, which results in 3.92 mL for the glomerular space.

4.2.1.1.3 Calculation of cellular and luminal compartment volumes for a single nephron

We assume that a renal tubule and collecting duct have the shape of a hollow cylinder, where the volume of the hollow cylinder (V_c) represents volume of tubular or collecting duct cells and the inner space (V_l) constitutes the tubular or collecting duct lumen. Figure 4.4A illustrates the parameter values relevant to calculate the volume of a hollow cylinder:

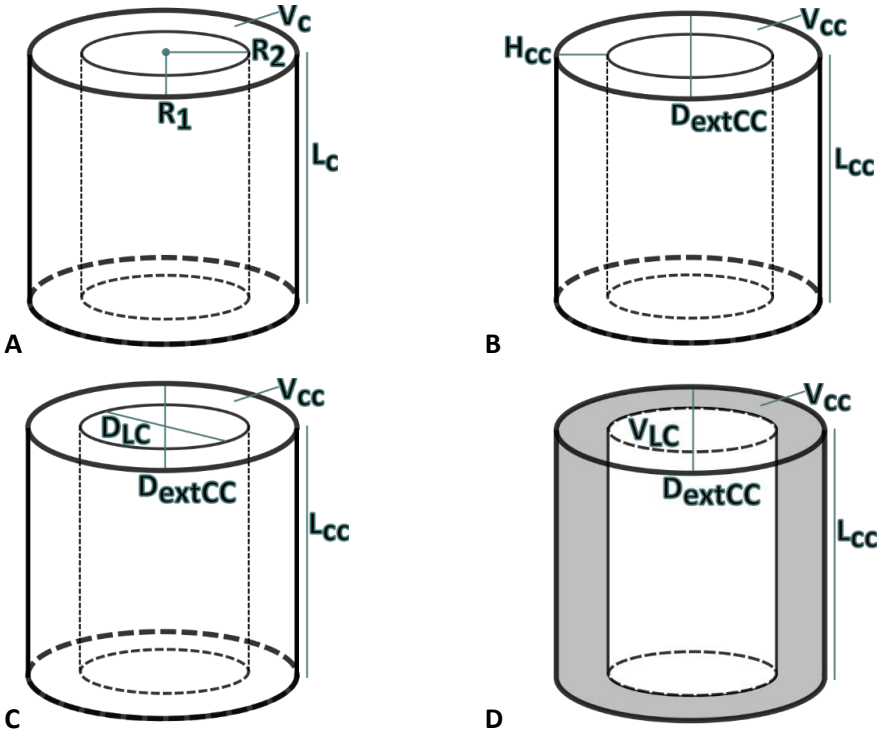

Figure 4.4: **A**. Illustration of the values necessary to calculate the volume of a hollow cylinder, where V_c = volume of a hollow cylinder; R_1 = outer radius of a cylinder; R_2 = radius of the hollow part of a cylinder; L_c = length of the cylinder. **B**. Parameter values available to calculate the volumes of the cellular compartments of proximal and distal tubules and collecting ducts, where V_{CC} = volume of cellular compartment (V_{PTC1}, V_{PTC2}, V_{PTC3}, V_{DTC}, V_{CDC1}, V_{CDC2}); D_{extCC} = external diameter of the cellular compartment; H_{CC} = height of cells in the compartment; L_{CC} = length of cellular compartment. **C**. Parameter values available to calculate the volume of the cellular compartment of the loop of Henle (V_{HLC}), where D_{LC} = diameter of the luminal compartment of the loop of Henle. **D**. Volume of luminal compartments of proximal and distal tubules and collecting ducts (V_{LC} = V_{PTL1}, V_{PTL2}, V_{PTL3}, V_{DTL}, V_{CDL1}, V_{CDL2}).

Eq. 4.1 calculates the volume of a hollow circular cylinder by subtracting the volume of the inner cylinder with radius R_2 from the volume of the outer cylinder with radius R_1:

$$V_c = \pi \left(R_1^2 - R_2^2\right) L_c$$

(Eq. 4.1)

Where $V_c =$ volume of the hollow cylinder; $R_1 =$ outer radius of the cylinder; $R_2 =$ radius of the hollow part of the cylinder; $L_c =$ length of the cylinder.

For proximal and distal tubules and collecting ducts, instead of the radii of renal tubules, the external diameters and the average height of the cells present in these tubular sections are available. Figure 4.4B shows the parameter values available to calculate the volumes of cellular compartments of proximal tubules (PTC1-3), the distal tubule (DTC) and collecting ducts (CDC1-2), i.e. V_{PTC1}, V_{PTC2}, V_{PTC3}, V_{DTC}, V_{CDC1}, V_{CDC2}. Therefore, Eq. 4.1 is translated to Eq. 4.2 to derive the volume of a cellular compartment:

$$V_{CC}\ (mL)\ = \pi \left(\left(\frac{D_{extCC}}{2}\right)^2 - \left(\frac{D_{extCC}}{2} - H_{CC}\right)^2\right) L_{CC} \times 0.001$$

(Eq. 4.2)

With $V_{CC} =$ volume of cellular compartment (V_{PTC1}, V_{PTC2}, V_{PTC3}, V_{DTC}, V_{CDC1}, V_{CDC2}) (mL); $D_{extCC} =$ external diameter of the cellular compartment (mm); $H_{CC} =$ height of cells in the compartment (mm); $L_{CC} =$ length of cellular compartment (mm); $0.001 =$ factor to convert from mm^3 to mL.

Instead of the cell height, the diameter of the loop of Henle lumen is available and used to derive the volumes of the cellular and luminal compartments of the loop of Henle. Figure 4.4C shows the parameter values available to calculate the volume of the loop of Henle cellular compartment. In this case, Eq. 4.2 is amended to Eq. 4.3 to calculate the cellular volume of the loop of Henle:

$$V_{HLC}\ (mL) = \pi \left(\left(\frac{D_{extCC}}{2}\right)^2 - \left(\frac{D_{LC}}{2}\right)^2\right) L_{CC} \times 0.001$$

(Eq. 4.3)

Where $V_{HLC} =$ volume of the cellular compartment of the loop of Henle (HLC) (mL); $D_{LC} =$ diameter of the luminal compartment of the loop of Henle (mm).

Figure 4.4D illustrates the values used to calculate the volumes of luminal compartments of proximal tubules (PTL1-3), the distal tubule (DTL) and collecting ducts (CDL1-2), i.e. V_{PTL1}, V_{PTL2}, V_{PTL3}, V_{DTL}, V_{CDL1}, V_{CDL2}.

Eq. 4.4 shows that these are calculated by subtracting the volume of the cellular compartment (V_{CC}) from the volume of the outer cylinder with diameter D_{extCC}:

$$V_{LC}\ (mL) = \left(\pi\left(\frac{D_{extCC}}{2}\right)^2 L_{CC} \times 0.001\right) - V_{CC}$$

(Eq. 4.4)

Where V_{LC} = volume of luminal compartment of proximal tubules (PTL1-3), the distal tubule (DTL) and collecting ducts (CDL1-2), i.e. V_{PTL1}, V_{PTL2}, V_{PTL3}, V_{DTL}, V_{CDL1}, V_{CDL2} (mL).

In parallel to the amendment to Eq. 4.2, Eq. 4.4 is modified to Eq. 4.5 to calculate the luminal volume of the loop of Henle (HLL):

$$V_{HLL}\ (mL) = \pi\left(\frac{D_{LC}}{2}\right)^2 L_{CC} \times 0.001$$

(Eq. 4.5)

Where V_{HLL} = volume of the luminal loop of Henle compartment (mL).
All values used to calculate tubular and luminal volumes are presented in Table 4.2.

Table 4.2: Parameters applied to derive tubular and luminal volumes using Eq. 4.2 to 4.5. Part **A** considers volumes of the proximal and distal tubules (PT1-3 and DT) and the collecting ducts (CD). Part **B** considers volumes of the loop of Henle (HL).

A

Compartments	**External diameter (mm)[1]**	**Cell height (mm)[2]**	**Compartment length (mm)[3]**	**References**
PTC1 and PTL1	0.06	0.011	6	[1,3] Neuhoff et al., 2013; [2] estimates based on Pitts, 1968; and Maunsbach and Christensen, 2011
PTC2 and PTL2	0.06	0.011	6	
PTC3 and PTL3	0.06	0.008	6	
DTC and DTL	0.05	0.006	5.5	[1,3] Neuhoff et al., 2013; [2] estimate based on Ericsson et al., 1965; Rouiller, 1969; Fenton and Praetorius, 2015
CDC1 and CDL1	0.04	0.009	11	[1] Rouiller, 1969; [2] estimate based on Ericsson et al., 1965; [3] Neuhoff et al., 2013
CDC2 and CDC2	0.2	0.02	11	[1] Rouiller, 1969; Neuhoff et al., 2013; [2] estimate based on Madsen et al., 1988; [3] Neuhoff et al., 2013

B

Compartments	**External diameter (mm)[1]**	**Luminal diameter (mm)[2]**	**Compartment length (mm)[3]**	**References**
HLC and HLL	0.018	0.0125	7	[1,3] Neuhoff et al., 2013; [2] estimate based on Rouiller, 1969

4.2.1.1.4 Scaling of cellular, luminal and glomerular blood volumes per nephron to volumes per person

4.2.1.1.4.1 Cortical compartments

Equations 4.2-4.5 give volumes per single tubule or collecting duct. In order to obtain the volumes of each compartment per person, having one million nephrons per kidney and two kidneys (Nyengaard and Bendtsen, 1992; Hoy et al., 2003; Bertram et al., 2011), the cellular and luminal volumes of proximal and distal tubular compartments are multiplied by 2×10^6. When summed up, the volumes of all cortical cellular and luminal as well as glomerular blood and space compartments amount to 135.11 mL which is considered to be fairly close to the intended value of 123.47 mL (93% of the cortical volume since 7% of it are assigned to capillary blood). Subsequently, all cortical cellular and luminal, as well as glomerular blood and space, compartments are scaled down to yield 123.47 mL. Interestingly, the scaled glomerular blood value is in line with the volume of the glomerulus proposed by Nyengaard and Bendtsen (1992).

4.2.1.1.4.2 Medullary compartments

Scaling up the cellular and luminal volumes of CD1 and CD2 per collecting duct (as obtained with Eq. 4.2-4.5) to volumes per person is not as straightforward as scaling up cortical compartments from one to two million nephrons. This is because on average 11 nephrons drain into a cortical collecting duct and approximately 2,570 into a terminal inner medullary collecting duct (Kaissling and Kriz, 2011). Estimating average quantities of collecting ducts in CD1 and CD2 compartments and multiplying these with cellular and luminal volumes per collecting duct produced values which are nearly a factor of 20 lower than the gross estimates shown in subchapter 4.2.1.1.1. Also, since the interstitium takes up a substantial proportion of the medulla and it is not considered in the calculated cellular and luminal volumes obtained from Equations 4.2-4.5, the interstitium needs to be taken into account specifically. Therefore, 23% of the total medulla volume allocated to the medullary interstitium (see Table 4.1) is proportionally assigned to cellular compartments of the medulla, i.e. HLC, CDC1 and CDC2. These volumes of medullary cellular and luminal compartments are then scaled up proportionally so that they add up to 115 mL in total (78% of medullary volume, see Table 4.1).

Table 4.3: Compartment volumes of the kidney model

Compartment volumes	**Parameter value (mL)**	**References; derivation of parameter value**
Glomerular blood (V_{GB})	7.64	Rouiller, 1969; scaling see 4.2.1.1.4.1
Proximal tubular blood 1 (V_{PTB1})	2.56	27.5 % of cortical peritubular blood
Proximal tubular blood 2 (V_{PTB2})	2.56	27.5 % of cortical peritubular blood
Proximal tubular blood 3 (V_{PTB3})	2.56	27.5 % of cortical peritubular blood
Loop of Henle blood (V_{HLB})	11.78	36.36 % of medullary blood
Distal tubular blood (V_{DTB})	1.63	17.5 % of cortical peritubular blood
Collecting duct blood 1 (V_{CDB1})	6.55	20.21 % of medullary blood
Collecting duct blood 2 (V_{CDB2})	14.07	43.42 % of medullary blood
Proximal tubular cells 1 (V_{PTC1})	18.49	See Table 4.1 and Eq. 4.2; scaling see 4.2.1.1.4.1
Proximal tubular cells 2 (V_{PTC2})	18.49	See Table 4.1 and Eq. 4.2; scaling see 4.2.1.1.4.1
Proximal tubular cells 3 (V_{PTC3})	14.27	See Table 4.1 and Eq. 4.2; scaling see 4.2.1.1.4.1
Loop of Henle cells (V_{HLC})	26.80	See Table 4.1 and Eq. 4.3; scaling see 4.2.1.1.4.2
Distal tubular cells (V_{DTC})	8.30	See Table 4.1 and Eq. 4.2; scaling see 4.2.1.1.4.1
Collecting duct cells 1 (V_{CDC1})	22.60	See Table 4.1 and Eq. 4.2; scaling see 4.2.1.1.4.2
Collecting duct cells 2 (V_{CDC2})	29.16	See Table 4.1 and Eq. 4.2; scaling see 4.2.1.1.4.2
Glomerular space (V_{GS})	3.57	Rouiller, 1969; $V_{G\_total} - V_{GB}$; for a total glomerular volume (V_{G_total}) averaging 44 mm^3 per g kidney; scaling see 4.2.1.1.4.1
Proximal tubular lumen 1 (V_{PTL1})	12.38	See Table 4.1, Eq. 4.2 and Eq. 4.4; scaling see 4.2.1.1.4.1
Proximal tubular lumen 2 (V_{PTL2})	12.38	See Table 4.1, Eq. 4.2 and Eq. 4.4; scaling see 4.2.1.1.4.1
Proximal tubular lumen 3 (V_{PTL3})	16.60	See Table 4.1, Eq. 4.2 and Eq. 4.4; scaling see 4.2.1.1.4.1
Loop of Henle lumen (V_{HLL})	14.20	See Table 4.1, Eq. 4.3 and Eq. 4.5; scaling see 4.2.1.1.4.2
Distal tubular lumen (V_{DTL})	11.35	See Table 4.1, Eq. 4.2 and Eq. 4.4; scaling see 4.2.1.1.4.1
Collecting duct lumen 1 (V_{CDL1})	3.51	See Table 4.1, Eq. 4.2 and Eq. 4.4; scaling see 4.2.1.1.4.2
Collecting duct lumen 2 (V_{CDL2})	18.57	See Table 4.1, Eq. 4.2 and Eq. 4.4; scaling see 4.2.1.1.4.2

Bladder (V_{BL})	350	Lukacz et al., 2011; average value
Arterial blood (V_{AR})	1698	Peters, 2008a
Venous blood (V_{VE})	3396	Peters, 2008a

4.2.1.1.5 Determination of blood compartments

Since capillaries surround renal tubules, the volume of each cortical peritubular blood compartment is assigned in proportion to the volume of the respective cellular and luminal sections (see Figure 4.2). This also applies to medullary blood compartments since medullary blood including capillaries and *vasa recta* are assumed to be distributed equally around the loop of Henle and collecting ducts. Cortical peritubular blood compartments, i.e. PTB1-3 and DTB, total 9.2937 mL which is 7% of the overall cortical volume. Medullary blood compartments, i.e. HLB and CDB1-2, amount to 32.3914 mL, which is 22% of the medullary volume (see Table 4.1). Table 4.3 summarises all compartment volumes of the kidney model.

4.2.1.2 Blood flow, fluid flow and glomerular filtration rates

The change in concentration of a compound within each renal compartment over time is represented by ODEs that conserve mass balance. All ODEs are compiled in Appendix 4.A. The change in concentration within each compartment is driven by physiological flow rates and compound-specific parameters. Physiological flow rates such as the blood flow or fluid flow at different sections of the tubular lumen are presented in Table 4.4.

The renal blood flow determines the movements of the compound from the glomerular blood to consecutive blood compartments. The selected value of 1100 mL/min for the renal blood flow is used in a previously established PBK model in which the mechanistic kidney model will be embedded. The renal blood flow value is within the range of 800-1200 mL/min and 1100-1200 mL/min presented by Hallow and Gebremichael (2017) and Boroujerdi (2015), respectively, and within an order of magnitude of the value of 1000 mL/min selected by Neuhoff et al. (2013) and Hallow and Gebremichael (2017).

Table 4.4: Physiological flow rates at different sections of the tubular lumen

Flow rates	**Parameter value (mL/min)**	**References**
Renal blood flow $(Q_{KI} = QC \times FQ_{KI})$	1100	Bernareggi and Rowland, 1991; Peters, 2008a; Boroujerdi, 2015
Blood flow in loop of Henle and collecting ducts 2 (Q_{HL-CD2})	100	Eaton and Pooler, 2013
Glomerular filtration rate (GFR)	120	Neuhoff et al., 2013; mL of water/min
Fluid flow leaving glomerular space and proximal tubules (FF_{PT})	45	Neuhoff et al., 2013
Fluid flow leaving loop of Henle (FF_{HL})	25	Neuhoff et al., 2013
Fluid flow leaving distal tubules and collecting ducts (FF_{DT})	12	Neuhoff et al., 2013

QC = cardiac output (6338 mL/min); FQ_{KI} = fractional tissue blood flow in the kidney (0.174)

Medullary blood flow occurs predominantly through the *vasa recta* which connects the loop of Henle and the inner medullary collecting duct (CDB2) and is slower than cortical blood flow (Eaton and Pooler, 2013). Shunt vessels bypassing juxtamedullary glomeruli are considered to have a minor impact on renal kinetics (Alpern et al., 2013; Calzavacca et al., 2014; Munger et al., 2015) and a quantitative estimation of periglomerular shunting has not been obtained from the literature. Thomas et al. (1998) suggest that shunts are formed in the aging kidney. One of the consequences of periglomerular shunting is a decreased glomerular filtration rate (GFR) which will be taken into account in subchapter 4.4, within the modelling scenario reflecting an elderly individual. Fluid flows determine the rate at which the filtrate (forming urine) flows from the glomerular space through lumen compartments of the nephron and collecting ducts. Parameter values for the fluid flows leaving the glomerular space and collecting ducts are not identified in the scientific literature, instead fluid flows leaving the proximal tubules, loop of Henle and distal tubules are obtained from Neuhoff et al. (2013). For glomerular space and collecting duct luminal compartments, the same flow rates are assumed as those leaving the proximal tubules and distal tubules, respectively. Compound-specific parameters relate to active and passive transport between the cellular, blood and luminal compartments, and metabolic activities. As mentioned earlier, this mechanistic model is developed to explore the kinetics of SA at the kidney level. The following section describes the

kinetics of SA and all compound-specific parameters used in this model to simulate active and passive transport, as well as metabolic activity.

4.2.2 Prediction of SA-specific kinetics in the kidney: GFR, active and passive transport, and metabolic activity

The key kinetic processes of SA incorporated in the kidney model include glomerular filtration, active secretion and reabsorption, passive secretion and reabsorption, and metabolism. The key metabolites of SA include salicyluric acid (SU) and acyl and phenolic glucuronides (glucs) which are all considered in this kidney model.

4.2.2.1 Glomerular filtration rate of SA

SA reaches the kidney via the renal artery represented by the glomerular blood compartment. From there, compounds with a molecular weight of about 60,000 Dalton and lower are filtered into the glomerular space from where they flow into the proximal tubular lumen and later luminal compartments as part of the urinary filtrate (Boroujerdi, 2015). Clearance of substances from glomerular blood (CL_{GB}) by glomerular filtration is typically presented as the product of the glomerular filtration rate (GFR) and the fraction of the compound unbound in the plasma ($f_{u(p)}$) (Tucker, 1981; Rowland, 1984; Janků, 1993; Fenton and Praetorius, 2015) as shown in Eq. 4.6:

$$CL_{GB} = GFR\, f_{u(p)} \qquad \text{(Eq. 4.6)}$$

Please refer to Table 4.4 for the value of GFR. About 20% of SA is free in plasma (therefore $f_{u(p)} = 0.2$), indicating approximately 80% of SA is bound to plasma proteins, such as albumin, and therefore is not readily filtered (Navar, 2009; Tojo and Kinugasa, 2012). The fraction not undergoing glomerular filtration passes onto peritubular capillaries surrounding the proximal tubules. Through active transport and passive diffusion, SA may be secreted from the proximal tubular blood into proximal tubular cells, and from there into the proximal tubular lumen or reabsorbed from there back into the blood.

4.2.2.2 Active transport of SA in the kidney

Active transport is a saturable process and typically expressed as a Michaelis-Menten term (Felmlee et al., 2010, 2013; Ménochet et al., 2012a; Boroujerdi, 2015) as presented in Eq. 4.7:

$$k_{AT(T)} = \frac{J_{\max\,(T)}\, C_i}{K_{m(T)} + C_i}$$

(Eq. 4.7)

where $k_{AT(T)}$ is the rate of active transport via transporter protein T, $J_{\max\,(T)}$ is the maximum rate of transport or flux via transporter T, $K_{m(T)}$ is the Michaelis-Menten constant which represents the affinity of the transporter T for its substrate and C_i the concentration of SA in compartment i in which a drug concentration increases or decreases due to active transport.

Membrane proteins responsible for active transport through the basolateral membrane of proximal tubular cells include OATP4C1, OCT2, OAT1, OAT2, OAT3, while OAT4, URAT1, PEPT1, PEPT2, MRP2, MRP4, MATE1, MATE2-K, P-gp, OCTN1, OCTN2 are found on the apical (luminal) membrane (Giacomini et al., 2010). All membrane protein terms used here are explained below[4].

For SA, transporter inhibition and kinetics studies have been performed for OAT1, OAT2, OAT3, OAT4, MRP2, MRP4, BCRP, URAT1 and NPT1 (Sekine et al., 1998; Cha et al., 2000; Deguchi et al., 2002; Takeda et al., 2002; Khamdang et al., 2002; El-Sheikh et al., 2007; Matsson et al., 2007; Nozaki et al., 2007; Iharada et al., 2010; Ohtsu et al., 2010; Sedykh et al., 2013). Various techniques exist to measure J_{max} and K_m values characterising the rate of active transport, such as uptake by kidney slices, kidney cell lines or cell lines expressing a specific transporter (Kusuhara and Sugiyama, 2009; Felmlee et al., 2013). Generally, data on active transport rates are scarce. A SA-specific K_m value established in human cells is identified only for URAT1 (Ohtsu et al., 2010). Neither a J_{max} is obtained from this study, nor a URAT1-related J_{max} of another NSAID. A URAT1 associated J_{max} value of perfluorooctanoate is

[4] **OATP4C1** = organic anion transporter polypeptide 4C1; **OCT2/OCTN1/OCTN2** = organic cation transporter 2/N1/N2; **OAT1/OAT2/OAT3/OAT4** = organic anion transporter 1-4; **URAT1** = urate transporter 1; **PEPT1/PEPT2** = peptide transporter 1-2; **MRP2/MRP4** = multidrug resistance-associated protein 2/4; **MATE1/MATE2-K** = multidrug and toxin extrusion protein 1/2-K; **P-gp** = P-glycoprotein; **BCRP** = breast cancer resistance protein; **NPT1** = sodium-dependent phosphate transport protein

sourced and utilised (Yang et al., 2010). Salicylate has been observed to be transported by the human OAT1 (hOAT1) and hOAT3 (Cha et al., 2001; Khamdang et al., 2002). However, since no SA-specific J_{max} and K_m values are identified for these transporters, values established for *para*-aminosalicylic acid are incorporated in the present model. J_{max} and K_m values for OCT2 are found for *para*-aminosalicylic acid and used for the OCT2-mediated active transport of SA. The remaining active transport related parameter values used are established either with non-salicylates and non-NSAIDs in human embryonic kidney (HEK) cells or with SA in animal cells.

When SA-specific animal data are available, these are preferred to data established with different substances in human cells, even though interactions between SA and other NSAIDs with rat OAT2 (rOAT2) appear to differ significantly from their interactions with the hOAT2 (Morita et al., 2001; Khamdang et al., 2002). SA is found to be transported by hOAT2 to a lesser extent than hOAT1 and hOAT3 (Khamdang et al., 2002) which would be reflected in a lower J_{max} or higher K_m for the OAT2 term compared to parameters used for the OAT1 and OAT3 terms. However, the equally high K_m established with SA in rat liver and higher creatinine-specific J_{max} are likely to overestimate the transport of SA via OAT2. For NPT1, SA-specific J_{max} and K_m values are obtained, established with mouse NPT1 protein (Iharada et al., 2010). For hOAT4, low and no inhibitory potency data are identified but no data on the rate of transport of salicylates or other NSAIDs (Cha et al., 2001; Khamdang et al., 2002). While SA is classified as a non-substrate for transport via MRP2 and MRP4, and ASA a non-substrate for MDR1 (a P-gp) (Sedykh et al., 2013; University of Cambridge, 2019), no data are obtained for the active transport of SA or other NSAIDs via these transporters. Similarly, no data are obtained for all the other transporters present in proximal tubular cells. In order to account to some degree for uncertainty associated with this lack of data, active transport of the bi-directional transporter OAT4 is incorporated using J_{max} and K_m values of perfluorooctanoate (Yang et al., 2010). Apart from the J_{max} of the URAT1 term, all J_{max} values are given in µmol/mg protein/min. These values are scaled from a per-mg-protein-of-a-HEK-cell level to their equivalence of whole kidney mass for a 70 kg person. The scaling factor (SF_{AT}) applied to J_{max} values comprises of the following components:

$$SF_{AT} = proteinHEK293 \times \frac{PTCPGK}{3} \times weight_{KI}$$

(Eq. 4.8)

where $proteinHEK293$ is the mass of protein per HEK 293 cell, $PTCPGK$ is the number of proximal tubular cells per gram of kidney which is set at 60×10^6 (Neuhoff et al., 2013) one third of which accounts for the number of proximal tubular cells per PTC compartment; $weight_{KI}$ is the total kidney weight per person; $proteinHEK293$ is calculated as the sum of membrane protein, nuclear protein and cytoplasmic protein (as presented by Han and Ni, 2004, in mg protein/g HEK 293 cell) multiplied by the weight of a HEK 293 cell (Ho et al., 2004). The values of these parameters are summarised in Table 4.5.

Table 4.5: Components and value of the scaling factor (SF_{AT}) applied to transporter-related J_{max} values

Parameter (unit)	Value	References
$proteinHEK293\ \left(\frac{mg}{HEK293\ cell}\right)$	1.09×10^{-7}	Han and Ni, 2004; Ho et al., 2004
$PTCPGK\ (\frac{cells}{g})$	60×10^6	Neuhoff et al., 2013
$weight_{KI}\ (g)$	280	Fenton and Praetorius, 2015; weight of human kidney ranges from 115 g to 170 g; average weight of one kidney is estimated to be 140 g
$SF_{AT}\ \left(\frac{mg\ protein}{cells\ in\ PTC\ compartment}\right)$	611	Calculated with Eq. 4.8

Since the J_{max} associated with transport via URAT1 is given in µmol/well/min, it is scaled on the basis of 2×10^5 HEK 293 cells per well (Yang et al., 2010) and $\frac{SF_{TP}}{proteinHEK293}$. Neuhoff et al. (2013) proposed a similar scaling of renal transporter data including a relative activity factor (RAF) which accounts for *in vitro-in vivo* differences or differences between animal and human activity. Since the majority of J_{max} and K_m values are established in human cells and details related to *in vitro-in vivo* differences are unknown, no RAF is applied. As plasma protein binding is found to affect active (as well as passive) drug transport in the Caco-2 cell model (Neuhoff et al., 2006), only the unbound fraction of drug concentration is considered to be relevant for active transport from blood to cellular compartments. Table 4.6 shows

the transporter proteins which are taken into account in this model, i.e. OCT2, OAT1, OAT2, OAT3, OAT4, URAT1 and NPT1, their direction, $J_{\max}$ and K_m values used, whether these are established for SA or another compound, in human or animal cells. Active transport with all these transporters is factored in in all proximal tubular compartments. Other models (Neuhoff et al., 2013; Huang and Isoherranen, 2018) only consider active transport in the proximal tubules. However, evidence exists indicating the presence of active transport mechanisms in the renal medulla and collecting ducts (Madsen et al., 1988; Pearce et al., 2015). Also, when validating the performance of the model with excretion data reported by Levy (1965), initial simulations show that passive diffusion is insufficient to achieve the almost complete excretion of SA within 39 hours. Therefore, the OAT1 active transport term is included at each level of the nephron to reach the rate of excretion observed in healthy volunteers.

Table 4.6: Transporter proteins considered, their location and direction, and J_{max} and K_m values utilised in this model

Transporter (T)	**$J_{\max(T)}$ (µmol/min)**	**$K_{m(T)}$ (µM)**	**Compound**	**Cells/ species**	**Direction**	**Reference**
OCT2	0.0432	28.7	*Para*-amino-salicylic acid	HEK	PTB → PTC	Parvez et al., 2017
OAT1	1.16	78	*Para*-amino-salicylic acid	HEK	PTB → PTC	Parvez et al., 2017
OAT2	15.3 [1]	88.8 [2]	Creatinine[1] / SA[2]	HEK[1]/ rat liver cells[2]	PTB → PTC	[1] Shen et al., 2015 / [2] Sekine et al., 1998
OAT3	0.961	100	*Para*-amino-salicylic acid	HEK	PTB → PTC	Parvez et al., 2017
OAT4	22.4	172	Perfluoro-octanoate	HEK	PTC → PTL PTL → PTC	Yang et al., 2010
NPT1	78.2	1.9×10^3	SA	Mouse protein	PTC → PTL	Iharada et al., 2010
URAT1	8.96 [1]	25.3 [2]	Perfluoro-octanoate [1] / SA [2]	HEK	PTL → PTC	[1] Yang et al., 2010 / [2] Ohtsu et al., 2010

HEK = human embryonic kidney; PTB = proximal tubular blood; PTC = proximal tubular cells. Up to three significant figures reported.

4.2.2.3 Passive diffusion of SA and metabolites in the kidney

Passive diffusion is a bidirectional, non-saturable process and of particular relevance to the reabsorption of substances from the tubular lumen rather than secretion from renal blood and tubular cells (Ménochet et al., 2012a; Felmlee et al., 2013; Ducharme, 2016). In this kidney model, passive diffusion is included between blood and cellular, and cellular and luminal compartments of all parts of the nephron and collecting ducts. The pH of the urine and the pK_a of a compound affect the extent of reabsorption from the urine, as both factors determine the degree of ionisation of the compound (Ducharme, 2016). An unionised species is more lipid soluble and therefore permeates the phospholipid bilayer of tubular membranes more easily than ionised species. Ménochet et al. (2012b) present a QSAR for logarithm of the unbound passive diffusion clearance ($P_{diff,u}$) observed in human hepatocytes based on the pH 7.4-based logarithm of the distribution coefficient ($log\ D_{7.4}$) as shown in Eq. 4.9. In the absence of any additional kidney specific data, it is assumed that the unbound passive diffusion clearance in human hepatocytes and human renal cells is the same. Therefore, Eq. 4.9 is used to account for passive diffusion of SA between all blood and cellular, as well as cellular and luminal compartments.

$$Log\ P_{diff,u} = 0.632 \times log\ D_{7.4} - 0.314$$

(Eq. 4.9)

Log D values of SA and its metabolites, i.e. salicyluric acid, SA acyl glucuronide and SA phenolic glucuronide, are calculated in the ACD/Percepta 14.0.0 (Build 2726) software and presented in Table 4.6. An average $P_{diff,u}$ value for all glucuronides ($P_{diff,u_{glucs}}$) is calculated with the average of log D values of SA acyl glucuronide and SA phenolic glucuronide. Since the resulting $P_{diff,u}$ is given in $\frac{\mu L}{min \times 10^6\ cells}$, scaling to the PTC cell population of 20×10^6 per g of kidney is needed for all substances. The scaled $P_{diff,u}$ values for SA, SU and glucuronides are 0.3297, 0.0313 and 2.03×10^{-3} mL/min, respectively. Table 4.7 summarises all Log D and $P_{diff,u}$ values of SA, SU and SA glucuronides at pH 7.4.

Table 4.7: Log D and resulting $P_{diff,u}$ values of SA and its glucuronide and salicyluric acid metabolites at pH 7.4

Substance (S)	**Log D at pH 7.4**	$\boldsymbol{P_{diff,u(S)}}$ **(mL/min)**
SA	-1.45	0.330
Salicyluric acid (SU)	-3.07	0.0313
SA acyl glucuronide	-4.36	NA
SA phenolic glucuronide	-5.54	NA
Glucuronide average (glucs)	-4.95	2.03×10^{-3}

The passive diffusion term, in which the SA and metabolite $P_{diff,u}$ values are applied, is defined in Eq. 4.10.

$$k_{PT} = P_{diff} C_i - P_{diff} C_j \quad \text{(Eq. 4.10)}$$

where C_i and C_j are concentrations subject to passive diffusion , e.g. C_{PTB1} and C_{PTC1}, or C_{PTC1} and C_{PTL1}. All k_{PT} terms are included in detail in ODEs presented in Appendix 4.A.

4.2.2.4 Active transport of SA metabolites

As described above for SA, active secretion terms are added on all levels of the nephron and collecting ducts since including active secretion only at proximal tubular segments is insufficient to achieve a nearly complete excretion of SA within 39 hours. Similar to these observations on SA, initial simulations indicated that active secretion is necessary for SA metabolites to achieve excretion rates similar to those reported by Levy (1965).

Glucuronides are reported to interact with hOAT3 (Weiner et al., 1960; Lien, 1975; Wolff et al., 2007) and SA shows a high affinity to hOAT1 (Motojima et al., 2002). Since SU and SA glucuronides appear to share the same mechanism of active secretion as SA, an active secretion term is included for SA metabolites from PTC1-3 to PTL1-3, HLC to HLL, DTC to DTL, CDC1 to CDL1 and CDC2 to CDL2 with estimated K_m and J_{max} values similar to those of OAT transporters, i.e. $K_{m(OATmets)} = 0.07$ µmol/mL and $J_{\max\,(OATmets)} = 20$ µmol/min.

4.2.2.5 Metabolism of SA in the kidney

Many phase I and phase II enzymes expressed in hepatocytes are also found in proximal tubular cells. However, levels in proximal tubular cells typically reach only 5-20 % of those in hepatocytes (Jakobsson and Cinti, 1973; Lash et al., 2008). This is also true for UGT enzymes, whereas UGT1A9, UGT2B7 and, to a lesser extent, UGT1A6 are found to be significantly expressed in the kidney (Knights and Miners, 2010; Margaillan et al., 2015). These enzymes are considered in an IVIVE study of renal clearance previously (Knights et al., 2016) and are taken into account here. In the kidney, SA is metabolised to salicyluric acid, salicyl acyl glucuronide and salicyl phenolic glucuronide (Levy, 1965; Needs and Brooks, 1985). Similar to the mathematical representation of active transport, the Michaelis-Menten equation, as defined in Eq. 4.11, is used to express a metabolic reaction (Felmlee et al., 2010; Boroujerdi, 2015; Cornish-Bowden, 2015):

$$k_{MET(M,i)} = \frac{V_{\max\,(M,i)}\, C_i}{K_{m(M)} + C_i}$$

(Eq. 4.11)

where k_{MET} is the rate of metabolism, M represents the metabolite resulting from this reaction, C_i stands for the concentration in the compartment in which metabolism takes place, $V_{\max\,(M,i)}$ is the maximum rate of metabolism for the formation of metabolite M in compartment i, $K_{m(M)}$ for the Michaelis-Menten constant for the formation of metabolite M.

While some evidence shows that glucuronidation catalysing enzymes, UGT2B7 and UGT1A, are relatively evenly distributed across the tubular parts of the kidney (excluding the vasculature, glomeruli and the proximal straight tubule) (Gaganis et al., 2007), other sources report the contrary (Boroujerdi, 2015). In line with this, it might be appropriate to assume slightly higher concentrations of UGT1A enzymes in the proximal tubule than in subsequent compartments, however, since specific data on metabolism rates in these subsequent compartments are lacking, an even distribution across all cellular compartments of the proximal and distal tubule, loop of Henle and collecting duct is assumed.

Similar to the scaling of transporter related J_{max} values, V_{max} values given in µmol/mg protein/min are scaled to the whole kidney level by multiplying these with

a metabolism related compartment-specific scaling factor (SF_{metCPT}) as defined in Eq. 4.12:

$$SF_{metCPT} = MPPGK \times weight_{KI} \times fracCPT \quad \text{(Eq. 4.12)}$$

where CPT is the compartment in which the scaling factor is applied, i.e. PTC1-3, HLC, DTC, CDC-2; $MPPGK$ is the weighted mean microsomal protein per gram of human kidney; $weight_{KI}$ is the kidney weight as discussed above, and $fracCPT$ is the fraction of the compartment volume in relation to the entire kidney volume.

A $MPPGK$ of 13.6 mg homogenate protein/g kidney tissue is calculated by Scotcher (2016) from values presented by Jakobsson and Cinti (1973), Pacifici et al. (1988), Al-Jahdari et al. (2006) and Knights et al. (2016). Table 4.8 outlines all $fracCPT$ and resulting SF_{metCPT} values used to scale above mentioned V_{max} values:

Table 4.8: $fracCPT$ and resulting SF_{metCPT} values used to scale V_{max} values from µmol/mg protein/min to kidney-level metabolism (i.e. µmol/min) for each cellular compartment

Compartment ($\boldsymbol{CPT}$)	$\boldsymbol{fracCPT}$	$\boldsymbol{SF_{metCPT}}$
PTC1	0.134	510
PTC2	0.134	510
PTC3	0.103	393
HLC	0.194	739
DTC	0.060	229
CDC1	0.164	623
CDC2	0.211	804

Since the V_{max} of SU is based on clinical data, no scaling is necessary for this value, while for all other V_{max} values scaling is applied. It turns out that initial simulations indicated that the amounts of glucuronides excreted were particularly low (approx. 5%) compared to amounts reported by Levy (1965). Therefore, all glucuronidation-related V_{max} values are increased accordingly to reach the rate of excretion observed in humans (see results in subchapter 4.3; we find that an order of magnitude increase is necessary). For all three metabolism reactions – conjugation with glycine to form salicyluric acid (SU) and conjugation with glucuronic acid catalysed by UGT1A6,

UGT1A9 and UGT2B7 to form the salicyl phenolic and salicyl acyl glucuronides (SAPG and SAAG) – V_{max} and K_m values are presented in Tables 4.9 and 4.10.

In order to place the results of the kidney model in the context of whole-body kinetics, the kidney model is incorporated into a full-body PBK model parameterised for ASA and SA predicting ASA and SA concentrations. For this, several additional parameters are required to run the PBK model. All additional SA- and ASA-specific parameters are defined in the following subchapter.

Table 4.9: V_{max} and K_m values sourced from the literature to account for SA conjugation with glycine to form SU in cellular compartments

Metabolite	**Parameter designation (M)**	**$V_{max(M)}$ (µmol/min)**	**$K_{m(M)}$ (µM)**	**Reference**
SU	SU	6.3 [1,2] (a)	103.5 [2]	[1] Levy and Tsuchiya, 1972; [2] Bochner et al., 1981

(a)average of V_{max} cited from Levy and Tsuchiya (1972) and Bochner et al. (1981)

Table 4.10: V_{max} and K_m values applied to account for SA glucuronidation in cellular compartments

Metabolite (catalysing enzyme)	**Parameter designation (M)**	**$K_{m(M)}$ (µM)**	**$V_{max(M,PTC1)}$ (µmol/min)**	**$V_{max(M,PTC2)}$ (µmol/min)**	**$V_{max(M,PTC3)}$ (µmol/min)**	**$V_{max(M,HLC)}$ (µmol/min)**	**$V_{max(M,DTC)}$ (µmol/min)**	**$V_{max(M,CDC1)}$ (µmol/min)**	**$V_{max(M,CDC2)}$ (µmol/min)**
SAPG (UGT1A6)	$PhenUGT1A6$	40.7	9.69×10^{-4}	9.69×10^{-4}	7.48×10^{-4}	1.40×10^{-3}	4.35×10^{-4}	1.18×10^{-3}	1.53×10^{-3}
SAAG (UGT1A6)	$AcylUGT1A6$	78.0	9.18×10^{-4}	9.18×10^{-4}	7.08×10^{-4}	1.33×10^{-3}	4.12×10^{-4}	1.12×10^{-3}	1.45×10^{-3}
SAPG (UGT1A9)	$PhenUGT1A9$	94.2	0.0762	0.0762	0.0588	0.1105	0.0342	0.0932	0.1202
SAAG (UGT1A9)	$AcylUGT1A9$	334.3	0.0162	0.0162	0.0125	0.0235	0.0073	0.0198	0.0256
SAPG (UGT2B7)	$PhenUGT2B7$	1242	0.0145	0.0145	0.0112	0.0210	0.0065	0.0177	0.0228
SAAG (UGT2B7)	$AcylUGT2B7$	1640	0.0094	0.0094	0.0072	0.0136	0.0042	0.0115	0.0148

Reference for values presented in Table 4.10: Kuehl et al., 2006.

4.2.3 Mechanistic model coupled to a PBK model

The development and validation of the PBK model used here, including sensitivity analysis and fitting of sensitive parameters of nine drugs, are fully described in Chapter 3. Here, we now describe how the PBK model developed in Chapter 3 is parameterised for ASA and extended with metabolism (i.e. hydrolysis) to and kinetics of SA. Since hydrolysis of ASA to SA is incorporated in the gut, liver, arterial and venous blood compartments, the ODEs of these compartments are amended as shown in Appendix 4.B1. After performing a sensitivity analysis and fitting for plasma concentrations of ASA and SA in the extended PBK model, we embed and validate the mechanistic kidney model in subchapter 4.3.

4.2.3.1 Initial fit of ASA parameter values to simulate ASA plasma concentration

As a first step, the PBK model is parameterised for ASA, without including SA, with the values presented in Tables 4.11 and 4.12. As outlined in Chapter 3, to account for metabolic clearance and renal elimination, a hepatic clearance and renal elimination rate are typically used in the PBK model. However, for ASA, instead of these rates, a total plasma clearance value of SA is used to account for the clearance of ASA via both, hepatic and renal, processes. This clearance value is incorporated into the renal compartment while the hepatic clearance is set to zero for the fitting to ASA data only. With these parameters, the simulated venous blood concentration-time curve resulting from an oral dose of 6,720 µmol (1.2 g) of ASA is compared to the plasma concentration of ASA reported by Roberts et al. (1983) in six young individuals. A sensitivity analysis of parameters included in Table 4.11 identifies R, the K_p factor and k_a as parameters which have a significant influence on the venous blood concentration curve of ASA. The results of the sensitivity analysis are shown in Figure 4.5. Through a fitting of the simulated curve to the observed concentration-time profile, fitted values of R, the K_p factor and k_a are obtained, as shown in Table 4.11.

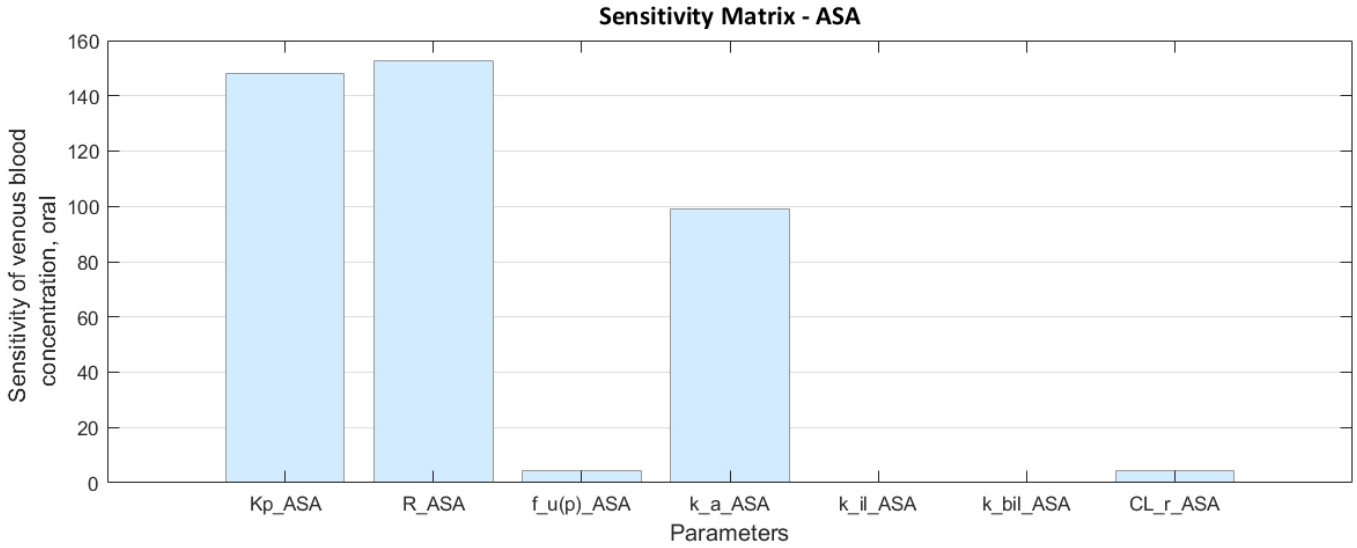

Figure 4.5: Time-integral sensitivity coefficients (S_q), giving an indication of the total sensitivity of the model parameters $K_{p_{ASA}}$, R_{ASA}, $f_{u(p)_{ASA}}$, $k_{a_{ASA}}$, $k_{il_{ASA}}$, $k_{bil_{ASA}}$ and $CL_{r_{ASA}}$ on the predicted venous blood concentrations following oral administration of ASA. Sensitivity analysis of model parameters and fitting of simulated ASA venous blood concentration to pharmacokinetic data reported by Roberts et al. (1983, Figure 1). $K_{p_{ASA}} =$ tissue partition coefficient of ASA, $R_{ASA} =$ whole blood to plasma concentration ratio of ASA, $f_{u(p)_{ASA}} =$ fraction unbound in plasma of ASA, $k_{a_{ASA}} =$ absorption rate constant of ASA, $k_{il_{ASA}} =$ intestinal loss rate constant of ASA, $k_{bil_{ASA}} =$ first-order biliary elimination rate constant of ASA and $CL_{r_{ASA}} =$ renal clearance rate of ASA.

Table 4.11: Kinetic parameters of ASA which are subject to fitting to observed ASA plasma concentrations, and their experimental, calculated and, where applicable, their fitted values

Parameter	ASA	References
$K_{p_{ASA}}$ factor[(a)]	1.19	[(a)] U.S. National Center for Biotechnology Information, 2019a
$K_{p_{ASA}}$ factor[(b)]	3.21×10^{-4}	
$K_{p_{ASA}}$ factor[(b)] SE	3.79×10^{-4}	
R_{ASA}[(a)]	1.0*	*estimated value
R_{ASA}[(b)]	3.11×10^{-3}	
R_{ASA}[(b)] SE	8.82×10^{-4}	
$f_{u(p)_{ASA}}$[(a)]	0.417	[(a)] Ghahramani et al., 1998
$f_{u(p)_{ASA}}$[(b)]	NA	
$f_{u(p)_{ASA}}$[(b)] SE	NA	
$k_{a_{ASA}}$ (min^{-1}) (literature)[(a)]	0.014	[(a)] Ijaz et al., 2003
$k_{a_{ASA}}$ (min^{-1}) (calculated)[c)]	0.022	
$k_{a_{ASA}}$ (min^{-1})[(b)]	0.033	
$k_{a_{ASA}}$ (min^{-1})[(b)] SE	0.016	
$k_{il_{ASA}}$ (min^{-1})[(a)]	0*	*estimated value
$k_{il_{ASA}}$ (min^{-1})[(b)]	NA	
$k_{il_{ASA}}$ (min^{-1})[(b)] SE	NA	
$k_{bil_{ASA}}$ (min^{-1})[(a)]	1×10^{-7}*	*estimated value based on Brune et al., 1993
$k_{bil_{ASA}}$ (min^{-1})[(b)]	NA	
$k_{bil_{ASA}}$ (min^{-1})[(b)] SE	NA	
$CL_{r_{ASA}}$(mL/min)[(a)]	33.6	[(a)] Miners et al., 1986
$CL_{r_{ASA}}$ (mL/min)[(b)]	NA	
$CL_{r_{ASA}}$ (mL/min)[(b)] SE	NA	
$CL_{hep_{ASA}}$(mL/min)[(a)]	0	[(a)] see text above, CL_r value includes hepatic clearance
$CL_{hep_{ASA}}$(mL/min)[(b)]	NA	
$CL_{hep_{ASA}}$ (mL/min)[(b)] SE	NA	

[(a)]sourced from the literature

[(b)]fitted in SimBiology

[(c)]calculated using Winiwarter et al. (Winiwarter et al., 1998), model 3b, with data provided by Peters (2008a) and Eq. 3.5

SE=standard error; K_p factor = multiplicative factor to increase or reduce tissue distribution coefficients; R = whole blood to plasma concentration ratio; $f_{u(p)}$ = fraction unbound in plasma; k_a = absorption rate constant; k_{il} = intestinal loss rate constant; k_{bil} = biliary elimination rate constant; CL_r = renal clearance; CL_{hep} = hepatic clearance

Figure 4.6 presents the fitted simulated plot of the venous blood concentration over time in comparison to the plasma concentration profile for ASA observed by Roberts et al. (1983, Figure 1). In Figure 4.7, the residual distribution of the ASA fit is shown indicating that the residuals are evenly distributed around the zero line.

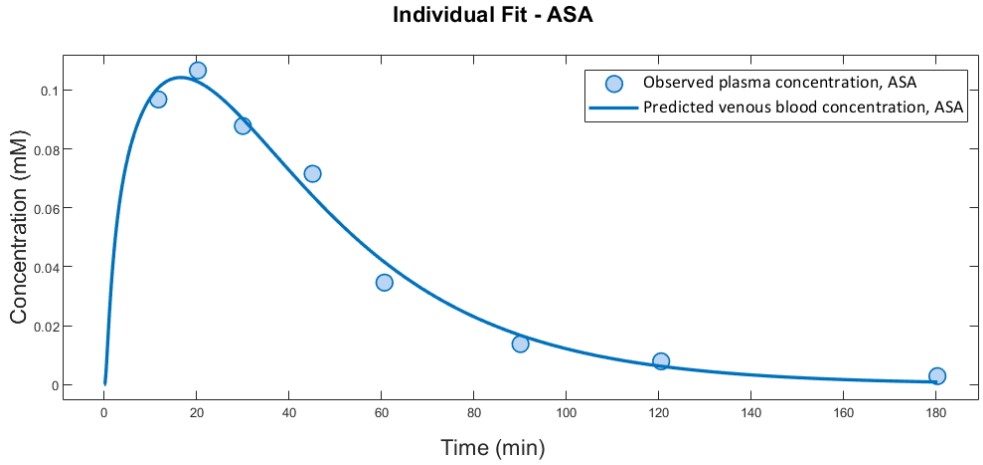

Figure 4.6: ASA simulated venous blood concentration curve fitted to observed pharmacokinetic data reported by Roberts et al. (1983, Figure 1)

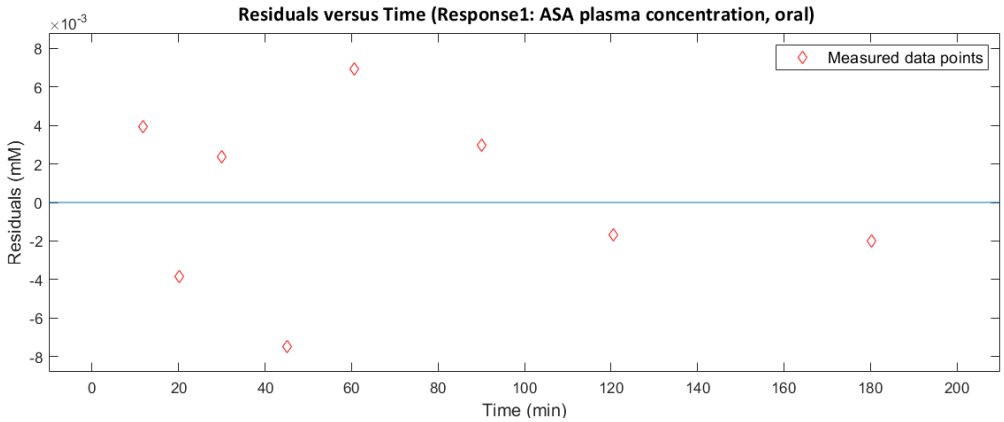

Figure 4.7: Residual distribution of aspirin fit (blue line) in relation to data points measured by Roberts et al. (1983, Figure 1)

Table 4.12 includes ASA-specific parameters used in the PBK model which are not subject to fitting. These parameters are, with the exception of enterohepatic recirculation (EHR), all used in the oral absorption part of the model.

Table 4.12: Physico-chemical and kinetic parameters of ASA which are not subject to fitting

Parameters (not subject to fitting)	ASA	References
MW (g/mol)	180.16	U.S. National Center for Biotechnology Information, 2019a
$Log\ P$	1.19	U.S. National Center for Biotechnology Information, 2019a
PSA	63.6	U.S. National Center for Biotechnology Information, 2019a
HBD	1	U.S. National Center for Biotechnology Information, 2019a
EHR	0	Brune et al., 1993
CP	0*	*estimated value
S (µmol/mL)	2,170	sourced from ACD/Percepta 14.0.0 (Build 2726) software, pH 6.4
$K_{S(STL)}$ (dimensionless)	0.0057	based on S for ASA at pH 1.3
$K_{S(DUO)}$	0.664	based on S for ASA at pH 6.0
$K_{S(JE1)}$	0.825	based on S for ASA at pH 6.2
$K_{S(JE2)}$	1	based on S for ASA at pH 6.4
$K_{S(IL1)}$	1.19	based on S for ASA at pH 6.6
$K_{S(IL2)}$	1.50	based on S for ASA at pH 6.9
$K_{S(IL3)}$	2.06	based on S for ASA at pH 7.4
$K_{S(CAE)}$	1	based on S for ASA at pH 6.4
$K_{S(ACO)}$	1.40	based on S for ASA at pH 6.8
D (cm^2/min)	1×10^{-4}	Peters, 2008a
p (µmol/mL)	5'550.7	Peters, 2008a
r (cm)	5×10^{-4}	Peters, 2008a
T (cm)	3×10^{-3}	Peters, 2008a

*estimated; MW = molecular weight; $Log\ P$ = logarithm of the octanol-water partition coefficient; PSA = polar surface area; HBD = number of hydrogen bond donors; EHR = enterohepatic recirculation; CP = conversion from metabolite back to parent compound; S = solubility; K_S = solubility coefficient; STL = stomach lumen; DUO = duodenum lumen; $JE1$ = jejunum1 lumen; $JE2$ = jejunum2 lumen; $IL1$ = ileum1 lumen; $IL2$ = ileum2 lumen; $IL3$ = ileum3 lumen; CAE = caecum lumen; ACO = ascending colon lumen; D = diffusion coefficient; p = particle density; r = particle radius; T = diffusion layer thickness

These parameters are utilised for the extended PBK model which simulates concentrations of both ASA and SA, as explained in the following.

4.2.3.2 Extension of the PBK model to include ASA and SA concentrations

ASA is rapidly hydrolysed to SA in the gut, liver and plasma (Yelland et al., 1991; Summerbell, 1992; Grešner et al., 2006; Imai et al., 2006; Tang et al., 2006). Therefore, in the extended version of the PBK model, hydrolysis reactions expressed as Michaelis-Menten terms are included in the gut, liver, arterial blood and venous blood compartments to generate SA concentrations. The amendments to gut, liver, arterial blood and venous blood compartment ODEs are shown in Appendix 4.B.1.

4.2.3.2.1 ASA parameters to account for ASA hydrolysis to form SA and renal elimination

All V_{max} and K_m values for ASA hydrolysis reactions are presented in Table 4.13. An estimated renal elimination rate ($k_{e(r)_{ASA}}$) replaces the previously used CL_r for ASA which represented a total plasma clearance value. Since hepatic clearance is now reflected by all hydrolysis terms, a specific ASA renal elimination rate with the estimated value of 1×10^{-4} mL/min is inserted.

Table 4.13: Kinetic parameters of ASA which are subject to fitting to observed ASA and SA plasma concentrations and their experimental, calculated and, where applicable, their fitted values.

Parameter	ASA	Reference / conversion factor[1]
$K_{m_{hydro(AR-VE)}}$ (mM)[a]	4.5	[a] Summerbell, 1992
$K_{m_{hydro(AR-VE)}}$ (mM)[b]	2.95	
$K_{m_{hydro(AR-VE)}}$ (mM)[b] SE	0.33	
$V_{max_{hydro(AR)}}$ (µmol/min)[a]	1,015	[a] Summerbell, 1992; 1698 mL (V_{AR})
$V_{max_{hydro(AR)}}$ (µmol/min)[b]	NA	
$V_{max_{hydro(AR)}}$ (µmol/min)[b] SE	NA	
$V_{max_{hydro(VE)}}$ (µmol/min)[a]	2,030	[a] Summerbell, 1992; 3396 mL (V_{VE})
$V_{max_{hydro(VE)}}$ (µmol/min)[b]	NA	
$V_{max_{hydro(VE)}}$ (µmol/min)[b] SE	NA	
$K_{m_{hydro(GU)}}$ (mM)[a]	0.36	[a] Tang et al., 2006; HCE2 value as HCE2 is predominantly expressed in the gut
$K_{m_{hydro(GU)}}$ (mM)[b]	NA	
$K_{m_{hydro(GU)}}$ (mM)[b] SE	NA	
$V_{max_{hydro(GU)}}$ (µmol/min)[a]	1.62	[a] Imai et al., 2006; 2977 mg
$V_{max_{hydro(GU)}}$ (µmol/min)[b]	NA	
$V_{max_{hydro(GU)}}$ (µmol/min)[b] SE	NA	
$K_{m_{hydro(LI)}}$ (mM)[a]	1.20	[a] Tang et al., 2006; average of HCE1 and HCE2 values as both are expressed in the liver
$K_{m_{hydro(LI)}}$ (mM)[b]	NA	
$K_{m_{hydro(LI)}}$ (mM)[b] SE	NA	
$V_{max_{hydro(LI)}}$ (µmol/min)[a]	28.6	[a] Imai et al., 2006; 56000 mg
$V_{max_{hydro(LI)}}$ (µmol/min)[b]	NA	
$V_{max_{hydro(LI)}}$ (µmol/min)[b] SE	NA	
$k_{e(r)_{ASA}}$ (min^{-1})[a]	1×10^{-4}*	*estimated value
$k_{e(r)_{ASA}}$ (min^{-1})[b]	NA	
$k_{e(r)_{ASA}}$ (min^{-1})[b] SE	NA	

[a]sourced from literature

[b]fitted in SimBiology

[1] The derivation of *in vitro* to *in vivo* conversion factors to scale the $V_{max_{hydro(LI)}}$ and $V_{max_{hydro(GU)}}$ from nmol/min/mg protein to µmol/min is outlined in detail in Appendix 4.B.2.

$K_{m_{hydro(AR-VE)}} = K_m$ for hydrolysis of ASA in the arterial and venous blood compartments;

$V_{max_{hydro(AR)}} = V_{max}$ for hydrolysis of ASA in the arterial blood compartment;

$V_{max_{hydro(VE)}} = V_{max}$ for hydrolysis of ASA in the venous blood compartment;

$K_{m_{hydro(GU)}} = K_m$ for hydrolysis of ASA in the gut compartment;

$V_{max_{hydro(GU)}} = V_{max}$ for hydrolysis of ASA in the gut compartment;

$K_{m_{hydro(LI)}} = K_m$ for hydrolysis of ASA in the liver compartment;

$V_{max_{hydro(LI)}} = V_{max}$ for hydrolysis of ASA in the liver compartment;

$k_{e(r)_{ASA}}$ = renal elimination rate for ASA

4.2.3.2.2 SA parameters used for the extended PBK model

The mechanistic kidney model is embedded in the PBK model described in Chapter 3 to predict the kinetics of SA in the human body, providing greater detail for kinetics within the kidney. All SA-specific parameter values inserted to predict SA concentrations in PBK compartments are presented in Table 4.14. SA is assumed to be formed in the gut tissue after ASA is absorbed from the gut lumen. Equivalent to ASA, the intestinal loss rate (k_{il}) and enterohepatic recirculation (EHR) are assumed to be 0 for SA, and the biliary excretion rate (k_{bil}) is set to 1×10^{-7} min^{-1}. Since SA is predominantly removed from the body by renal excretion and metabolism in the kidney (Needs and Brooks, 1985), hepatic clearance (CL_{hep}) is set to 0. All additional initial parameter values used for SA and ASA subject to fitting are presented in Tables 4.13 and 4.14, respectively.

Table 4.14: Physico-chemical and kinetic parameters of SA which are subject to fitting to observed ASA and SA plasma concentrations and their experimental, calculated and, where applicable, their fitted values.

Parameter	SA	References
$K_{p_{SA}}$ factor[(a)]	2.26	[(a)]U.S. National Center for Biotechnology Information, 2019b
$K_{p_{SA}}$ factor[(b)]	1.57	
$K_{p_{SA}}$ factor[(b)] SE	1.16	
R_{SA} [(a)]	1.0*	*estimated value
R_{SA} [(b)]	0.997	
R_{SA} [(b)] SE	0.892	
$f_{u(p)_{SA}}$ [(a)]	0.20*	[(a)]estimated based on Milne et al., 1958; Ghahramani et al., 1998
$f_{u(p)_{SA}}$ [(b)]	0.601	
$f_{u(p)_{SA}}$ [(b)] SE	0.376	
$k_{bil_{SA}}$ (min^{-1})[(a)]	1×10^{-7}*	*estimated value
$k_{bil_{SA}}$ (min^{-1})[(b)]	NA	
$k_{bil_{SA}}$ (min^{-1})[(b)] SE	NA	

[(a)]sourced from literature

[(b)]fitted in SimBiology

4.2.3.2.3 Sensitivity analysis and fitting for ASA and SA plasma concentrations in the extended PBK model

A sensitivity analysis of non-kidney related parameters which influence the plasma concentrations of ASA and SA is performed including $V_{max_{hydro}}$ and $K_{m_{hydro}}$ values which determine the hydrolysis rate metabolising ASA to SA in the gut, liver and blood, the $k_{e(r)}$ of ASA, and K_p, R, $f_{u(p)}$ and k_{bil} for SA. The analysis is performed with a dose of 6.72×10^3 µmol and over the course of 1,440 minutes as in Roberts et al. (1983, Figures 1 and 3). Results shown in Figure 4.8 show that slight changes to $f_{u(p)}$, K_p and R of SA have the most impact on SA blood concentration even though the impact is still relatively low (since the bar colour for these parameters is only slightly lighter than the bar colour of the other parameters, indicating higher impact of $f_{u(p)}$, K_p and R of SA in comparison to the other parameters). When the sensitivity analysis is run with slightly different initial values and a less elaborated kidney model included (i.e. active transporter terms only included on proximal tubular level and only for SA, data not shown), $f_{u(p)_{SA}}$, $K_{p_{SA}}$ and R_{SA} of SA show a much greater impact on SA blood concentration. Also, results of the sensitivity analysis illustrate that slight changes to $K_{m_{hydro(AR-VE)}}$ have a great impact on the blood concentration of ASA. Therefore, $f_{u(p)_{SA}}$, $K_{p_{SA}}$ and R_{SA} and $K_{m_{hydro(AR-VE)}}$ are included in the fitting. Values of these parameters fitted to Roberts et al. (1983, Fig. 1 and 3) are shown in Tables 4.13 and 4.14. Figure 4.9 presents the fitted simulated plot of the venous blood concentration over time in comparison to the plasma concentration profiles for ASA and SA observed by Roberts et al. (1983, Figures 1 and 3). The distribution of residuals of the ASA and SA fit is shown in Figure 4.10, indicating that the residuals are relatively evenly distributed around the zero line.

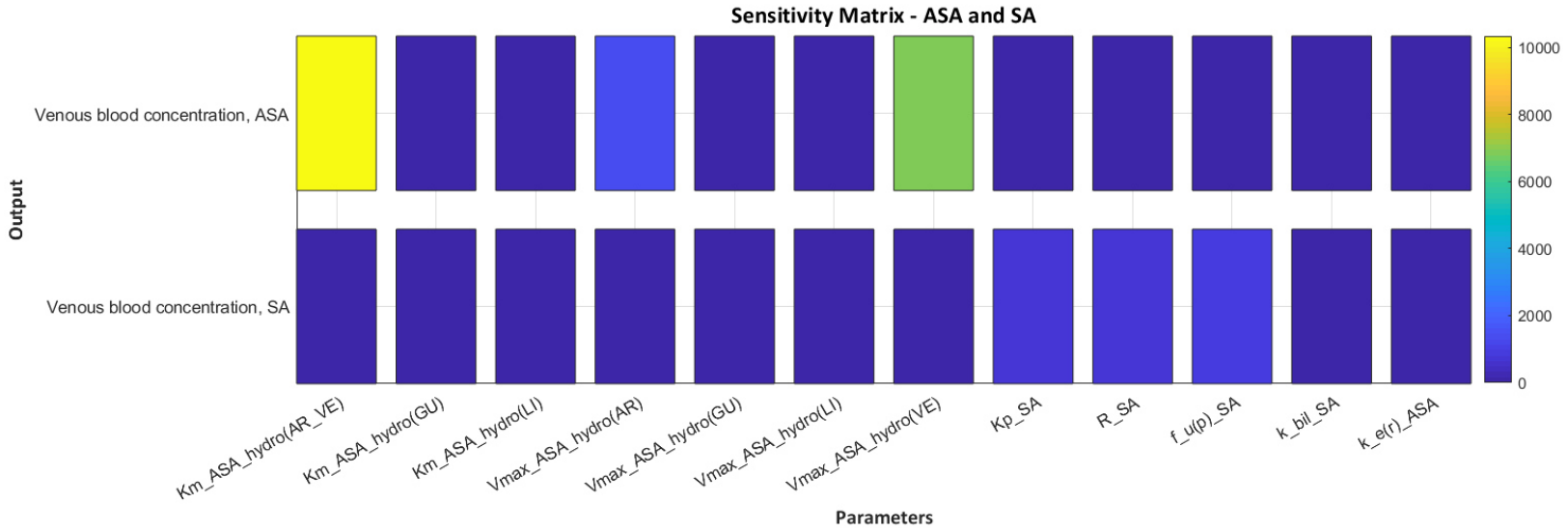

Figure 4.8: Time-integral sensitivity coefficients (S_q), giving an indication of the total sensitivity of the model parameters $K_{m_{hydro(AR-VE)}}$, $K_{m_{hydro(GU)}}$, $K_{m_{hydro(LI)}}$, $V_{max_{hydro(AR)}}$, $V_{max_{hydro(GU)}}$, $V_{max_{hydro(LI)}}$, $V_{max_{hydro(VE)}}$, $K_{p_{SA}}$, R_{SA}, $f_{u(p)_{SA}}$, $k_{bil_{SA}}$, $k_{e(r)_{ASA}}$ on the predicted venous blood concentrations of ASA and SA following oral administration of ASA. For more details on the parameters included here please refer to the captions of Tables 4.11 and 4.13.

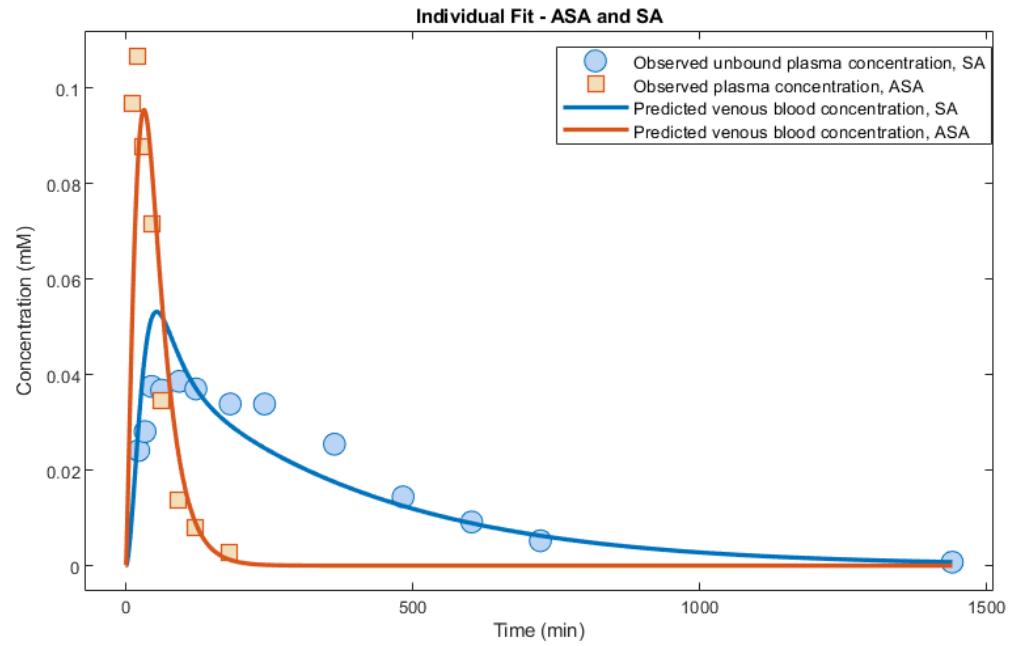

Figure 4.9: ASA and SA fitted simulated venous blood concentration curve fitted to observed pharmacokinetic data reported by Roberts et al. (1983, Figures 1 and 3)

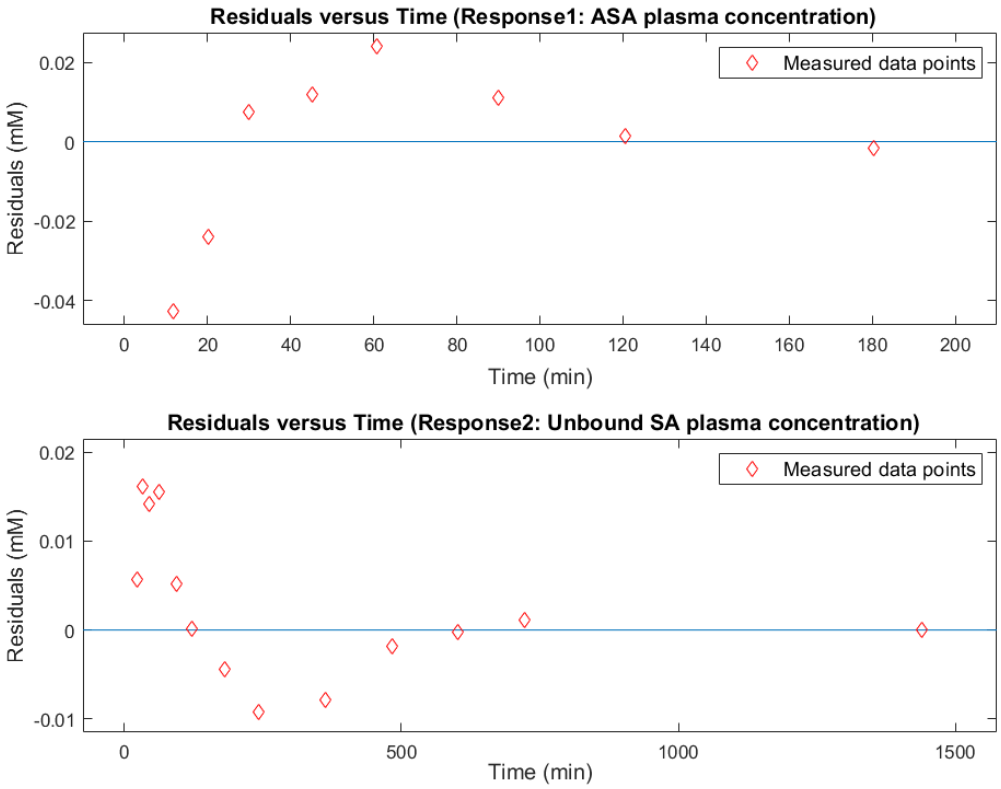

Figure 4.10: Residual distribution of ASA and SA fit (blue line) in relation to data points measured by Roberts et al. (1983, Figures 1 and 3)

The fitted values of the $K_{p_{SA}}$ factor, R_{SA} and the $K_{m_{hydro(AR-VE)}}$ value for ASA are close to the initially proposed values of 2.26, 1.0 and 4.5, respectively. The fitted value of $f_{u(p)_{SA}}$ is 0.6013, which is higher than unbound fractions that have typically been reported for SA, namely between 0.07 to 0.27 (Milne et al., 1958; Furst et al., 1979; Verbeeck et al., 1984). However, the fraction unbound of salicylic acid is reported to reach about 0.6 in plasma when the total concentration is very high and clearly toxic (Alvan et al., 1981). Therefore, the fitted value of $f_{u(p)}$ may be slightly too high for therapeutic concentrations but adequate for toxic blood concentrations. All fitted parameters are subsequently incorporated in the model.

4.3 Validation of the mechanistic kidney model

In order to assess whether the mechanistic kidney model simulates the excretion of ASA, SA and SA metabolites as reported in individuals, the percentage of an orally administered dose excreted in the urine as SA, SU, glucuronides and ASA is predicted. Experimental data on these values are obtained from Levy (1965). Predicted percentages of four orally administered doses, i.e. 1,400, 5,600, 8,400 and 11,200 µmol, excreted in the urine after 2,340 minutes (39 hours) are reported in Table 4.15.

Table 4.15: Predicted fractions of an orally administered dose excreted in the urine as SA, SU, glucuronides and ASA

Oral dose (µmol)	**% of dose excreted in urine as SA**	**% of dose excreted in urine as SU**	**% of dose excreted in urine as glucs**	**% of dose excreted in urine as ASA**
1,400	6.89	81.1	11.5	0.40
5,600	11.5	77.2	10.8	0.41
8,400	15.2	73.9	10.4	0.41
11,200	18.7	70.8	9.95	0.42

For the recovery of SU, a slightly wider range, from 59.2 to 91.4%, is reported by Levy (1965) for four individuals at the same doses used for prediction. However, Roberts et al. (1983) reported similar percentage recoveries for SU in young and elderly individuals as predicted, i.e. between about 70 and 80%. SA recoveries reported by Levy (1965) and Roberts et al. (1983), ranging from 2 to 5.1% for the lowest dose

level, from 3.6 to 10.3% for both mid-range doses and 17.1% for the highest dose level, are on average slightly lower but comparable to the predicted excretion percentages. The reason for the slightly increased predicted SA excretion may be that the rates of glucuronide formation are still too low even though glucuronidation related V_{max} values sourced from the literature had already been increased by an order of magnitude, as discussed earlier. The percentage recoveries of glucuronides recorded by Levy (1965) range from 4.7 to 33.4%. Overall, the PBK coupled mechanistic kidney model simulates the rates of metabolism of SA to SU and glucuronides and excretion of these compounds well, for the doses and excretion time considered. It is of interest to note that SA and SU concentrations found in the urine of people not taking salicylate drugs are in the nano to micromolar range, respectively, and are assumed to stem from the intake of salicylate-containing plants (Baxter et al., 2002).

4.4 Application of the kidney model to predict renal tubular concentrations of drugs in three virtual individuals: young and healthy, elderly at risk of CDK and elderly with signs of renal dysfunction

4.4.1 Setting parameter values characterising an elderly person at risk of CDK and an elderly person with signs of renal dysfunction

The mechanistic kidney model described above is set up with parameter values representing a young and healthy individual. However, acute renal failure or other adverse effects observed in the kidney are typically observed in elderly individuals or persons who have been diagnosed with a compromised renal function (Zhang et al., 2005). In order to establish to what degree renal tubular concentrations predicted for a young and healthy adult differ from those predicted for the elderly, two virtual elderly individuals are defined. For this, key parameters whose values are known to be decreased in the elderly at risk of CKD and with signs of renal dysfunction are set accordingly. These parameters are the GFR, cardiac output, cortical renal blood flow, rates determining the flow of urinary filtrate in the tubular lumen and the number of nephrons. Also, urinary pH is decreased in one individual, since pH influences urinary excretion of SA.

4.4.1.1 Glomerular filtration rate in elderly individuals

GFR is a key parameter of kidney function. The GFR observed with normal kidney function ranges from 110 to 140 mL/min/1.73 m^2 body surface area of an adult (Weinstein and Anderson, 2010; Delanaye et al., 2012) and is set at 120 mL/min in the kidney model. Glomerular filtration has been observed to decrease in elderly people (Denic et al., 2016; Abdulkader et al., 2017). Once the GFR falls below 60 mL/min for more than three months and in the presence of an increased quantity of proteins in the urine (proteinuria), chronic kidney disease (CKD) is typically diagnosed in an individual (Delanaye et al., 2012). For both cases of elderly people, one at risk of CKD and the second with signs of renal dysfunction, the GFR is decreased to 60 and 50 mL/min, respectively.

4.4.1.2 Cardiac output and cortical renal blood flow in elderly individuals

Cortical renal blood flow is set at 1,100 mL/min for the young and healthy (Bernareggi and Rowland, 1991; Peters, 2008a) while it may reach about 440 to 600 mL/min for adults up to the age of 70 (Weinstein and Anderson, 2010). Renal blood flow is dependent on the cardiac output (as discussed in the PBK notes in Chapter 3). In the elderly, a cardiac output of 2,970 mL/min is set, a value reported by Cattermole et al. (2017) for a group of 60 to 89-year olds. With a QC of 2,970 mL/min and the fractional tissue blood flow to the kidney of 0.174, as previously set in the PBK model, Q_{KI} for both elderly cases is 515 mL/min (according to Eq. 3.3). Therefore, in both elderly individuals, the renal blood flow in the cortex is set at 515 mL/min. Blood flow in the medulla is decreased less in the aging kidney (Weinstein and Anderson, 2010) and remains therefore unchanged in the model.

4.4.1.3 Flow rate of the urinary filtrate in elderly individuals

Besides the blood flow, the filtrate flow in the tubular lumen may decrease due to tubular epithelial cell swelling, crystal precipitation forming obstructive casts and adversities in the lower urinary tract (Sutaria and Staskin, 2000; Fogo et al., 2017; Mulay and Anders, 2017). In the elderly with signs of renal dysfunction, the luminal flows FF_{PT}, FF_{HL} and FF_{DT} are decreased from 45, 25 and 12 mL/min to 30, 18 and 8 mL/min, respectively.

4.4.1.4 Urinary pH influencing the rate of passive diffusion

Urinary pH and SA excretion are positively correlated, so at a low urine pH SA urinary excretion is relatively low while SU and glucuronide excretion is less affected (Levy, 1965). Urine pH may range from 4.6 to 8.0 (Cook et al., 2007). In the elderly with signs of renal dysfunction, the pH is set to 5.3 since 5.3 is the lowest pH recorded by Levy (1965) when recording the pharmacokinetics of ASA and its metabolites. At a low urine pH, a higher proportion of ionised substances will be present which cannot be passively diffused. Calculations of the unionised fractions and amended rates of passive diffusion for SA, SU and glucuronides are outlined in subchapter 4.4.1.5, since passive diffusion is also affected by a decreased number of nephrons. Table 4.16 summarises physiological parameters changed in both elderly individuals.

Table 4.16: Physiological parameters determining three cases, a young and healthy adult, an elderly person at risk of CKD, and an elderly individual with signs of renal dysfunction

Parameter	**Young and healthy adult**	**Elderly, at risk of CKD**	**Elderly with signs of renal dysfunction**
GFR (mL/min)	120	60	50
QC (mL/min)	$6{,}338$	$2{,}970$	$2{,}970$
Q_{KI} (mL/min)	1100	515	515
$FF_{PT}, FF_{HL}, FF_{DT}$ (mL/min)	$45, 25, 12$	$45, 25, 12$	$30, 18, 8$
Urinary pH	7.4	7.4	5.3
Number of nephrons	1×10^6	5×10^5	5×10^5

4.4.1.5 Number of nephrons influencing the active transporter and metabolic activity

The number of nephrons within an individual may vary from 200,000 to 2.5 million nephrons per kidney while an average of about 1 million nephrons per kidney is generally expected (Nyengaard and Bendtsen, 1992; Hoy et al., 2003; Bertram et al., 2011). With increasing age, the number of nephrons decreases, with an average loss of approximately 6,000 to 7,000 nephrons per year (Hoy et al., 2003; Denic et al., 2017). This implies that the number of functional renal tubular cells and consequently the overall transporter and metabolism function of both kidneys decreases. In a group of 70 to 75-year olds, roughly 500,000 nonsclerotic glomeruli are found per kidney (Denic et al., 2017). Hence, the number of functional nephrons in both elderly

populations, and tubular cell numbers to scale transporter J_{max} and $P_{diff,u}$ values are halved, and the metabolism-related parameter $MPPGK$ is halved to scale SU and glucuronide V_{max} values accordingly. All elderly-based J_{max}, $P_{diff,u}$ and V_{max} values are presented in Tables 4.17, 4.18 and 4.19.

Table 4.17: Transporter J_{max} values for both elderly cases

Transporter (T)	$J_{\mathbf{max(T)_{elderly}}}$ **(µmol/min)**
OCT2	0.0216
OAT1	0.580
OAT2	7.64
OAT3	0.480
OAT4	11.2
NPT1	39.1
URAT1	4.48
OAT_{mets}	10

Table 4.18: $P_{diff,u}$ values of SA and its glucuronide metabolites and SU at pH 7.4 for both elderly cases, and fractions unionised at a urine pH of 5.3.

Substance (S)	$P_{diff,u(S)_{elderly}}$ **(mL/min)**	$frac_{unionised(S)}$
SA	0.165	4.66×10^{-3}
Salicyluric acid (SU)	0.0156	0.0124
Glucuronide average (glucs)	1.01×10^{-3}	3.54×10^{-3}

Eq. 4.9, the calculation of $Log\ P_{diff,u}$, is established on the basis of a log D at a pH of 7.4. To calculate the unbound passive diffusion clearance of SA and its metabolites at a urinary pH of 5.3, the $P_{diff,u(S)_{elderly}}$ is multiplied with the Henderson-Hasselbalch equation-based term (Ducharme, 2016; Huang and Isoherranen, 2018) presented in Eq. 4.13 to calculate the fraction of the unionised substance at a pH of 5.3. This results in a $P_{diff,u(S)_{elderly(unionised)}}$ as shown in Eq. 4.14:

$$frac_{unionised(S)} = \frac{1}{1 + 10^{pH - pK_a}}$$

(Eq. 4.13)

$$P_{diff,u(S)_{elderly(unionised)}} = P_{diff,u(S)_{elderly}} \times frac_{unionised(S)}$$

(Eq. 4.14)

At a urinary pH of 5.3 and with the pK_a of SA of 2.97 (U.S. National Center for Biotechnology Information, 2019b), this fraction for SA ($frac_{unionised(SA)}$) is 4.66×10^{-3}. For salicyluric acid, SA acyl glucuronide and SA phenolic glucuronide, the pKa is calculated in the GALAS module of the ACD/Percepta 14.0.0 (Build 2726) software at 3.4, 2.9 and 2.8, respectively. At a glucuronide pK_a average of 2.85, the unionised fraction of SA glucuronides ($frac_{unionised(glucs)}$) is 3.54×10^{-3}, and the unionised fraction of SU ($frac_{unionised(SU)}$) at a urinary pH of 5.3 is 0.0124. The fractions of SA, SU and glucuronides unionised at a pH of 5.3 are presented in Table 4.18. Since the pH in renal tubular cells and the blood is assumed to be 7.4, the $P_{diff,u(S)_{elderly(unionised)}}$ is only relevant for passive diffusion from luminal to cellular compartments.

Table 4.19: V_{max} values applied to account for SU formation and SA glucuronidation in cellular compartments of both elderly individuals

Metabolite (catalysing enzyme)	**Parameter designation (M)**	$V_{\mathrm{max(M)PTC1_{elderly}}}$ **(µmol/min)**	$V_{\mathrm{max(M)PTC2_{elderly}}}$ **(µmol/min)**	$V_{\mathrm{max(M)PTC3_{elderly}}}$ **(µmol/min)**	$V_{\mathrm{max(M)HLC_{elderly}}}$ **(µmol/min)**	$V_{\mathrm{max(M)DTC_{elderly}}}$ **(µmol/min)**	$V_{\mathrm{max(M)CDC1_{elderly}}}$ **(µmol/min)**	$V_{\mathrm{max(M)CDC2_{elderly}}}$ **(µmol/min)**
SU	SU	3.15	3.15	3.15	3.15	3.15	3.15	3.15
SAPG (UGT1A6)	$PhenUGT1A6$	4.84×10^{-4}	4.84×10^{-4}	3.74×10^{-4}	7.02×10^{-4}	2.17×10^{-4}	5.92×10^{-4}	7.64×10^{-4}
SAAG (UGT1A6)	$AcylUGT1A6$	4.59×10^{-4}	4.59×10^{-4}	3.54×10^{-4}	6.65×10^{-4}	2.06×10^{-4}	5.61×10^{-4}	7.24×10^{-4}
SAPG (UGT1A9)	$PhenUGT1A9$	0.0381	0.0381	0.0294	0.0552	0.0171	0.0466	0.0601
SAAG (UGT1A9)	$AcylUGT1A9$	0.0081	0.0081	0.0063	0.0117	0.0036	0.0099	0.0128
SAPG (UGT2B7)	$PhenUGT2B7$	0.0072	0.0072	0.0056	0.0105	0.0033	0.0088	0.0114
SAAG (UGT2B7)	$AcylUGT2B7$	0.0047	0.0047	0.0036	0.0068	0.0021	0.0057	0.0074

4.4.2 Sensitivity analysis for simulations with all three individuals

4.4.2.1 Parameters included in the sensitivity analysis

Sensitivity analyses are performed on the impact of parameters used in the mechanistic kidney model, including GFR, $f_{u(p)}$, blood and filtrate flow rates (QC, FQ_{KI}, Q_{HL-CD2}, FF_{PT}, FF_{HL}, FF_{DT}), passive diffusion parameters ($P_{diff,u(SA)}$, $P_{diff,u(SU)}$, $P_{diff,u(glucs)}$), active transporter parameters ($J_{\max}$ and K_{m} values for OAT_{mets} and the transporters OCT2, OAT1-4, NPT1 and URAT1) and metabolism parameters ($V_{\max}$ and K_{m} values for the formation of SU and salicyl phenolic and salicyl acyl glucuronides catalysed by UGT1A6, UGT1A9 and UGT2B7). The method underlying the sensitivity analysis approach used here is outlined in Chapter 3 (subchapter 3.1.1.3.1). The aim of the sensitivity analysis is to identify parameters which, when perturbed (i.e. changed to a minor degree), have a high impact on the predicted SA and SU concentrations in PTC compartments. This is relevant since a certain degree of uncertainty underlies each of these parameters. Also, there will be inter-individual differences in blood flows, transporter expression or the rate of metabolism. Since it is important to understand how the behaviour of a model changes with a wide range or parameter values (representing for instance a variety of individuals), the parameters which are identified to have the most impact on predicted PTC concentrations will be changed over a biologically plausible range. As a result, a range of PTC concentrations is predicted which may reflect exposure levels in a variety of individuals with respect to the dosing scenarios defined. Since one of the aims of this study is to compare predicted proximal tubular cell concentrations to toxicity events observed *in vitro*, only concentrations in the PTC1-3 compartments are evaluated. Besides SA, concentrations for SU are taken into account, since about 70 to 80% of an oral dose of ASA is excreted in the form of SU as discussed in subchapter 4.3.

4.4.2.2 Dosing scenarios considered for all three individuals

For the three individuals – a young and healthy adult, an elderly person at risk of CKD and an elderly person with signs of renal dysfunction – three different scenarios are set which differ in the dose applied daily and the length of exposure. In the first scenario, a common low dose of 420 µmol/day (75 mg/day) (Petersen et al., 1989; The Salt Collaborative Group, 1991; Wallentin, 1991; Hansson et al., 1998; The Medical Research Council's General Practice Research Framework, 1998; Derry, 2000; NHS, 2018; Mayo Clinic, 2019; MedicineNet, 2019) is applied to prevent cardiovascular events. In the second scenario, a venous blood concentration of 2.2 µmol/mL is used as initial concentration, since at therapeutic doses, a SA steady state concentration of up to 2.2 µmol/mL is reached (Furst et al., 1979; Needs and Brooks, 1985). The first two scenarios are simulated for a period of two weeks representing chronic exposure. Even though an exposure duration of two weeks with a dose applied once per day would be classified as sub-acute rather than chronic, the maximum concentration (C_{max}) reached in the proximal tubular cells on the first day is equal to the C_{max} values reached on subsequent days. Also, under constant exposure, the steady state in the proximal tubular cells is reached after approximately 7 minutes. Therefore, a two-week simulation period is judged to be adequate to represent chronic exposure. The third scenario represents a case of intoxication which requires therapeutic intervention at a salicylate plasma (in the model as venous blood) concentration of 3.24 µmol/mL (450 mg/L, mean of 400-500 mg/L as reported by Wood et al., 2005). The simulation period for this case is one day. All scenario data are shown in Table 4.20.

Table 4.20: Exposure levels, duration and simulation times used in three different exposure scenarios

Scenario	**Dose (compartment, in which substance is applied)**	**Exposure time**	**Simulation time (min)**
Low therapeutic dose, chronic	420 µmol (ASA, stomach undissolved)	Once a day	20,160 (14 days)
High therapeutic dose, chronic	2.2 µmol/mL (SA, venous blood)	Constant	20,160 (14 days)
Intoxication, acute	3.24 µmol/mL (SA, venous blood)	Constant	1,440 (1 day)

4.4.2.3 Sensitivity analysis results: chronic, low therapeutic dose of ASA

For all three individuals, both parameters determining the formation of SU, $V_{\max\,(SU)}$ and $K_{\mathrm{m}\,(SU)}$, are predicted to have moderate impact on the concentration of SA in the PTC1 compartment, high impact in PTC2 and highest impact in PCT3. The concentration of SU in all PTC compartments is highly influenced by parameters defining the rate of active transport of all metabolites, $J_{\max\,(OATmets)}$ and $K_{\mathrm{m}\,(OATmets)}$, in all three individuals. In the young, all PTC concentrations of SA and SU are highly sensitive to the fraction unbound of SA ($f_{u(p)}$) and to a lesser extent $J_{\max\,(OAT2)}$ and $K_{\mathrm{m}\,(OAT2)}$. In both elderly individuals, $f_{u(p)}$ has a moderate impact on all PTC concentrations. For the young and healthy adult and the elderly person at risk of CKD, the sensitivity analysis results for this dose are illustrated in Figures 4.11 and 4.12, respectively.

4.4.2.4 Sensitivity analysis results: chronic upper therapeutic dose reaching a SA venous blood concentration of 2.2 mM

At a constant SA venous blood concentration of 2.2 mM of SA, sensitivity analyses are identical for all three individual cases tested. Sensitivity analysis results are shown in Figure 4.13 for the elderly individual with signs of renal dysfunction. Parameters determining the rate of the active transport of SA via NPT1, $J_{\max\,(NPT1)}$ and to a lesser extent $K_{\mathrm{m}\,(NPT1)}$, as well as $f_{u(p)}$ moderately influence SA concentrations in all PTC compartments. SU concentrations are highly sensitive to the V_{max} of SU formation ($V_{\max\,(SU)}$) and to the active transport of metabolites ($J_{\max\,(OATmets)}$ and to a lower extent $K_{\mathrm{m}\,(OATmets)}$).

4.4.2.5 Sensitivity analysis results: acute intoxication at 3.24 mM SA venous blood concentration

Results of sensitivity analyses related to a constant SA venous blood concentration of 3.24 mM for 24 hours are equal to results outlined above for a 14-day constant SA venous blood concentration of 2.2 mM. Results are specifically shown in Figure 4.14 for the elderly person at risk of CKD.

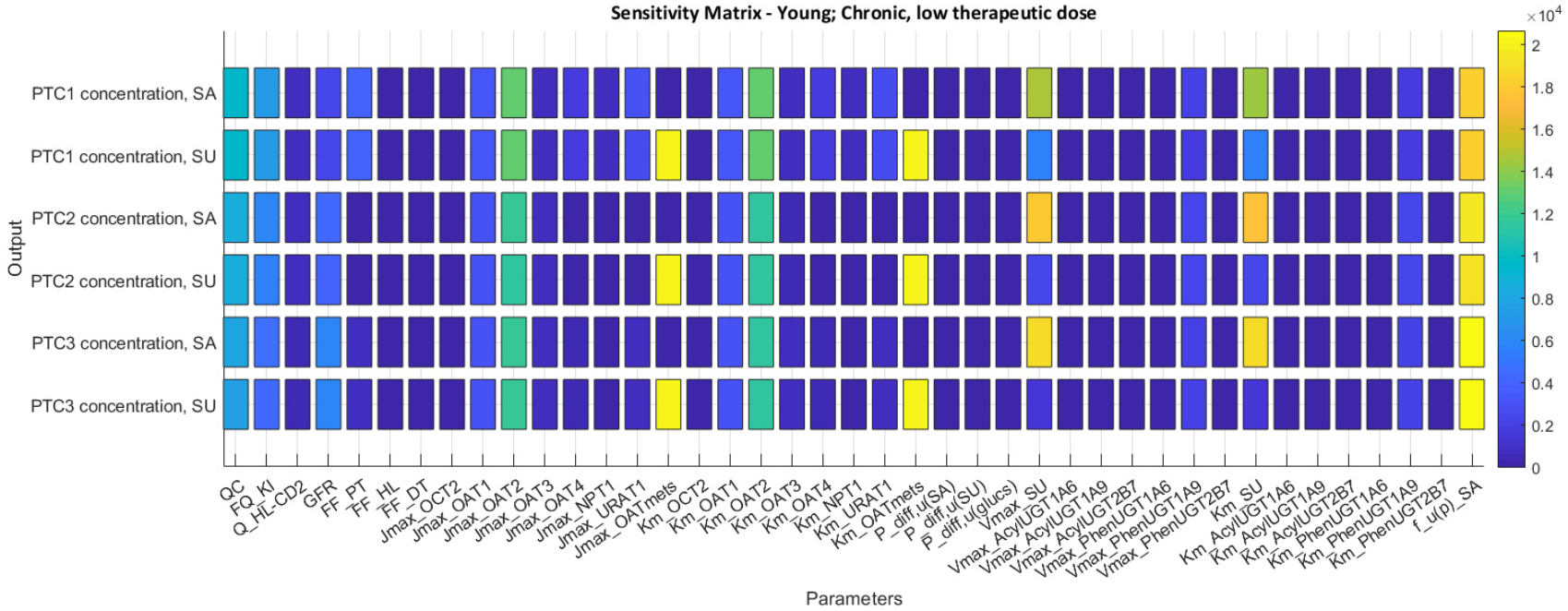

Figure 4.11: Time-integral sensitivity coefficients (S_q), giving an indication of the total sensitivity of the model parameters QC, FQ_{KI}, Q_{HL-CD2}, GFR, FF_{PT}, FF_{HL}, FF_{DT}, $Jmax_{(OCT2)}$, $Jmax_{(OAT1)}$, $Jmax_{(OAT2)}$, $Jmax_{(OAT3)}$, $Jmax_{(OAT4)}$, $Jmax_{(NPT1)}$, $Jmax_{(URAT1)}$, $Jmax_{(OATmets)}$, $Km_{(OCT2)}$, $Km_{(OAT1)}$, $Km_{(OAT2)}$, $Km_{(OAT3)}$, $Km_{(OAT4)}$, $Km_{(NPT1)}$, $Km_{(URAT1)}$, $Km_{(OATmets)}$, $P_{diff,u(SA)}$, $P_{diff,u(SU)}$, $P_{diff,u(glucs)}$, $V_{\max(SU)}$, $V_{\max(AcylUGT1A6)}$, $V_{\max(AcylUGT1A9)}$, $V_{\max(AcylUGT2B7)}$, $V_{\max(PhenUGT1A6)}$, $V_{\max(PhenUGT1A9)}$, $V_{\max(PhenUGT2B7)}$, $K_{m(SU)}$, $K_{m(AcylUGT1A6)}$, $K_{m(AcylUGT1A9)}$, $K_{m(AcylUGT2B7)}$, $K_{m(PhenUGT1A6)}$, $K_{m(PhenUGT1A9)}$, $K_{m(PhenUGT2B7)}$, $f_{u(p)_{SA}}$ on the predicted PTC concentrations of SA and SU following the oral administration of a chronic, low therapeutic dose of ASA in the young and healthy adult

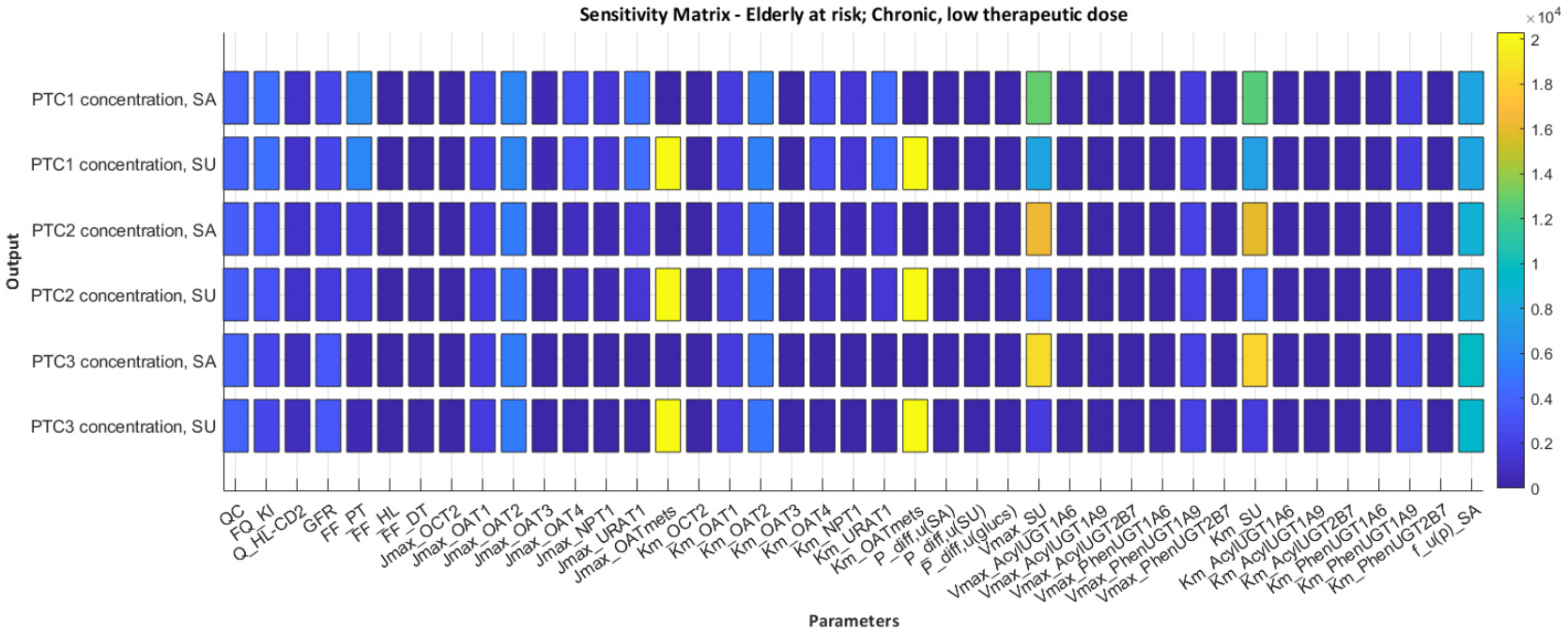

Figure 4.12: Time-integral sensitivity coefficients (S_q), giving an indication of the total sensitivity of the model parameters QC, FQ_{KI}, Q_{HL-CD2}, GFR, FF_{PT}, FF_{HL}, FF_{DT}, $J_{max_{(OCT2)}}$, $J_{max_{(OAT1)}}$, $J_{max_{(OAT2)}}$, $J_{max_{(OAT3)}}$, $J_{max_{(OAT4)}}$, $J_{max_{(NPT1)}}$, $J_{max_{(URAT1)}}$, $J_{max_{(OATmets)}}$, $K_{m_{(OCT2)}}$, $K_{m_{(OAT1)}}$, $K_{m_{(OAT2)}}$, $K_{m_{(OAT3)}}$, $K_{m_{(OAT4)}}$, $K_{m_{(NPT1)}}$, $K_{m_{(URAT1)}}$, $K_{m_{(OATmets)}}$, $P_{diff,u(SA)}$, $P_{diff,u(SU)}$, $P_{diff,u(glucs)}$, $V_{\max(SU)}$, $V_{\max(AcylUGT1A6)}$, $V_{\max(AcylUGT1A9)}$, $V_{\max(AcylUGT2B7)}$, $V_{\max(PhenUGT1A6)}$, $V_{\max(PhenUGT1A9)}$, $V_{\max(PhenUGT2B7)}$, $K_{m(SU)}$, $K_{m(AcylUGT1A6)}$, $K_{m(AcylUGT1A9)}$, $K_{m(AcylUGT2B7)}$, $K_{m(PhenUGT1A6)}$, $K_{m(PhenUGT1A9)}$, $K_{m(PhenUGT2B7)}$, $f_{u(p)_{SA}}$ on the predicted PTC concentrations of SA and SU following the oral administration of a chronic, low therapeutic dose of ASA in the elderly at risk of CKD

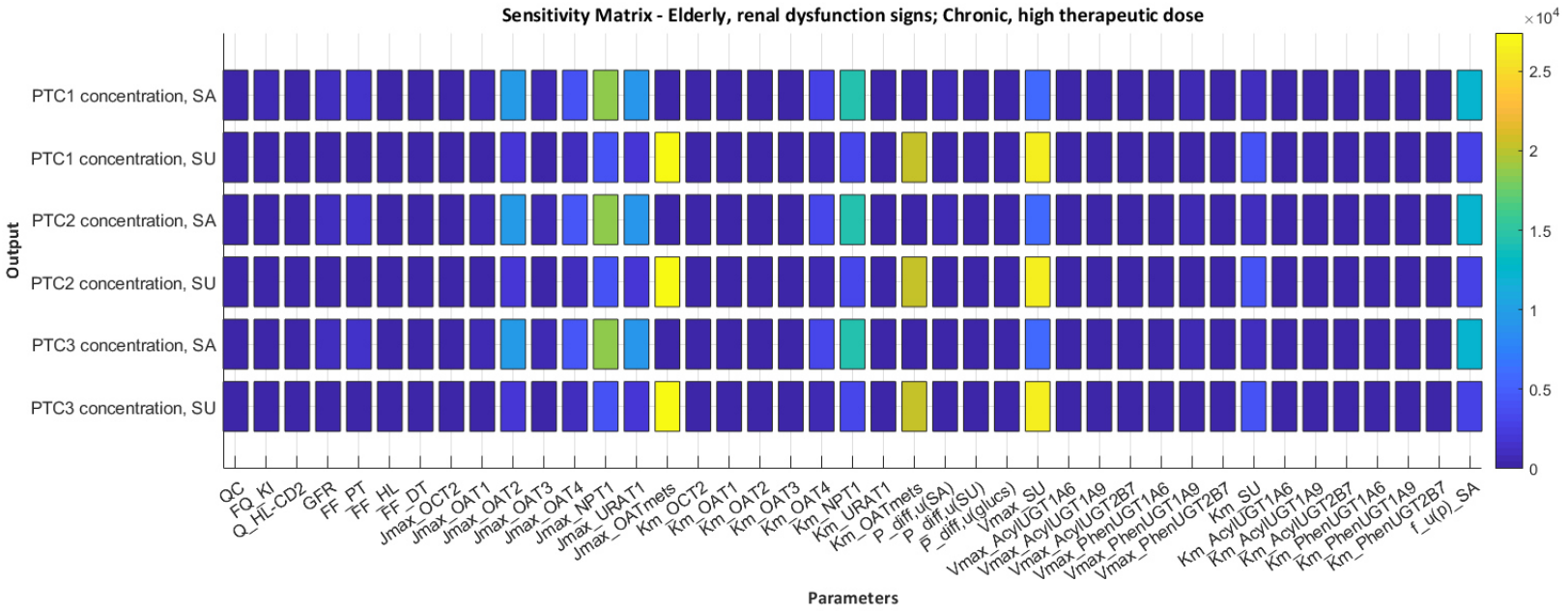

Figure 4.13: Time-integral sensitivity coefficients (S_q), giving an indication of the total sensitivity of the model parameters QC, FQ_{KI}, Q_{HL-CD2}, GFR, FF_{PT}, FF_{HL}, FF_{DT}, $J_{max_{(OCT2)}}$, $J_{max_{(OAT1)}}$, $J_{max_{(OAT2)}}$, $J_{max_{(OAT3)}}$, $J_{max_{(OAT4)}}$, $J_{max_{(NPT1)}}$, $J_{max_{(URAT1)}}$, $J_{max_{(OATmets)}}$, $K_{m_{(OCT2)}}$, $K_{m_{(OAT1)}}$, $K_{m_{(OAT2)}}$, $K_{m_{(OAT3)}}$, $K_{m_{(OAT4)}}$, $K_{m_{(NPT1)}}$, $K_{m_{(URAT1)}}$, $K_{m_{(OATmets)}}$, $P_{diff,u(SA)}$, $P_{diff,u(SU)}$, $P_{diff,u(glucs)}$, $V_{\max(SU)}$, $V_{\max(AcylUGT1A6)}$, $V_{\max(AcylUGT1A9)}$, $V_{\max(AcylUGT2B7)}$, $V_{\max(PhenUGT1A6)}$, $V_{\max(PhenUGT1A9)}$, $V_{\max(PhenUGT2B7)}$, $K_{\mathrm{m}(SU)}$, $K_{\mathrm{m}(AcylUGT1A6)}$, $K_{\mathrm{m}(AcylUGT1A9)}$, $K_{\mathrm{m}(AcylUGT2B7)}$, $K_{\mathrm{m}(PhenUGT1A6)}$, $K_{\mathrm{m}(PhenUGT1A9)}$, $K_{\mathrm{m}(PhenUGT2B7)}$, $f_{u(p)_{SA}}$ on the predicted PTC concentrations of SA and SU following the oral administration of a chronic, low therapeutic dose of ASA in the elderly with signs of renal dysfunction

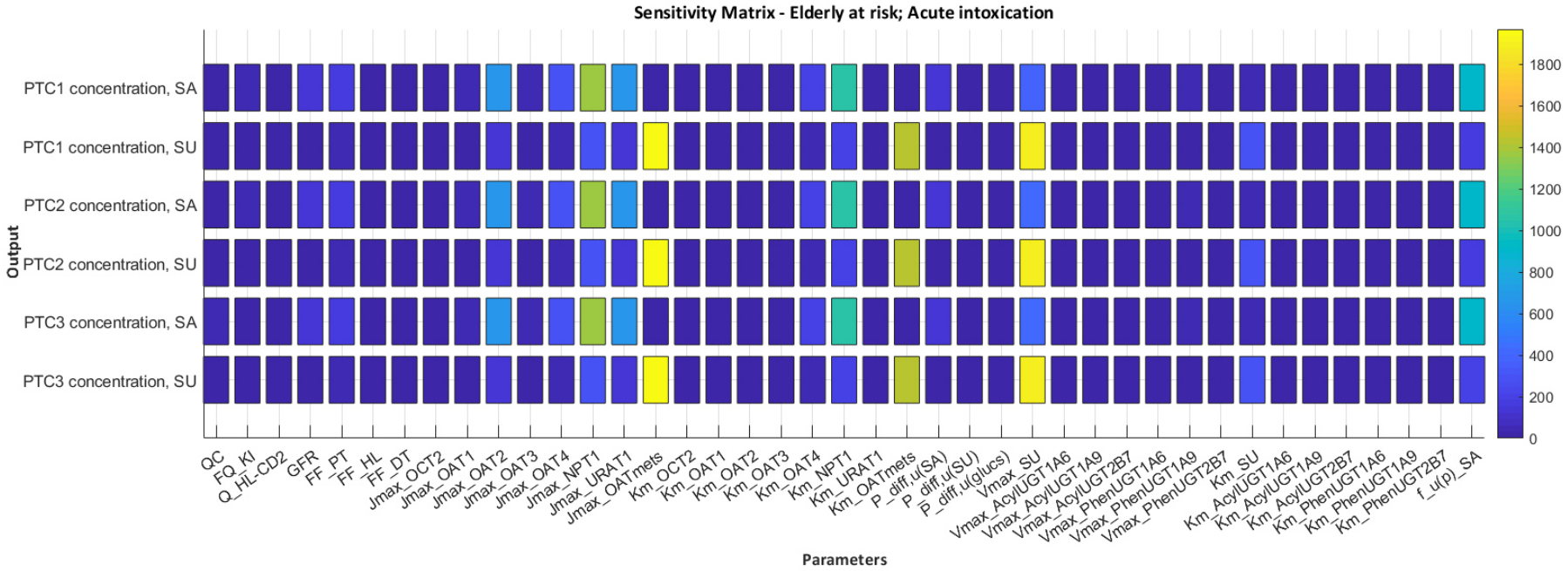

Figure 4.14: Time-integral sensitivity coefficients (S_q), giving an indication of the total sensitivity of the model parameters QC, FQ_{KI}, Q_{HL-CD2}, GFR, FF_{PT}, FF_{HL}, FF_{DT}, $J_{max_{(OCT2)}}$, $J_{max_{(OAT1)}}$, $J_{max_{(OAT2)}}$, $J_{max_{(OAT3)}}$, $J_{max_{(OAT4)}}$, $J_{max_{(NPT1)}}$, $J_{max_{(URAT1)}}$, $J_{max_{(OATmets)}}$, $K_{m_{(OCT2)}}$, $K_{m_{(OAT1)}}$, $K_{m_{(OAT2)}}$, $K_{m_{(OAT3)}}$, $K_{m_{(OAT4)}}$, $K_{m_{(NPT1)}}$, $K_{m_{(URAT1)}}$, $K_{m_{(OATmets)}}$, $P_{diff,u(SA)}$, $P_{diff,u(SU)}$, $P_{diff,u(glucs)}$, $V_{\max(SU)}$, $V_{\max(AcylUGT1A6)}$, $V_{\max(AcylUGT1A9)}$, $V_{\max(AcylUGT2B7)}$, $V_{\max(PhenUGT1A6)}$, $V_{\max(PhenUGT1A9)}$, $V_{\max(PhenUGT2B7)}$, $K_{\mathrm{m}(SU)}$, $K_{\mathrm{m}(AcylUGT1A6)}$, $K_{\mathrm{m}(AcylUGT1A9)}$, $K_{\mathrm{m}(AcylUGT2B7)}$, $K_{\mathrm{m}(PhenUGT1A6)}$, $K_{\mathrm{m}(PhenUGT1A9)}$, $K_{\mathrm{m}(PhenUGT2B7)}$, $f_{u(p)_{SA}}$ on the predicted proximal tubular concentrations of SA and SU following acute ASA intoxication in the elderly at risk of CKD

All parameters which have been identified to have the most impact on predicted proximal tubular concentrations are presented in Table 4.22 and included in scans over a predefined range in subchapter 4.4.4. In order to understand which concentration of SA may be considered to be toxic, relevant toxicity data are reviewed in the following subchapter.

4.4.3 Pathway of SA toxicity and concentrations at which SA is hypothesised to be toxic

SA has been shown to act as a mitochondrial swelling and uncoupling agent at concentrations of approximately 0.25 mM and above in rat liver and kidney mitochondria (Brody and Fouts, 1956; Whitehouse and Dean, 1965; Thompkins and Lee, 1969; You, 1983; Gutknecht, 1992; Mingatto et al., 1996; Al-Nasser, 1999). At 0.25, 0.5 and 0.75 mM, oxidative phosphorylation decreases by roughly 30, 45 and 55% in rat liver mitochondria, respectively (Thompkins and Lee, 1969). At a concentration of 1 to 2 mM, sodium SA and SA uncouple oxidative phosphorylation completely, abolish inorganic phosphate uptake and the aerobic synthesis of adenosine triphosphate (ATP) in the mitochondria (Brody and Fouts, 1956; Thompkins and Lee, 1969; You, 1983).

With a lag time of approximately 7-8 minutes, 90 µM of SA causes large-amplitude swelling in rat liver mitochondria (Martens et al., 1986). Since liver and kidney mitochondria in rats show similar sensitivity to mitochondrial effects (Brody and Fouts, 1956), the delayed large-amplitude swelling observed at 90 µM in rat liver mitochondria is expected to occur in rat kidney mitochondria as well at that concentration. Large-amplitude swelling indicates permeability transition and compromised integrity of the inner mitochondrial membrane (Al-Nasser, 1999; Armstrong, 2006). Mitochondrial swelling, mitochondrial permeability transition (MPT) and assessment of ATP levels are common endpoints to assess mitochondrial toxicity (Broom, 2015). However, it is unclear which endpoint is most relevant, and when a change or perturbation may be considered a true toxic effect that could lead to functional impairment of an organ. MPT implies free access of small solutes to the mitochondrial matrix, dissipation of the mitochondrial membrane potential, suspension of ATP synthesis and structural breakdown of the organelle (Bernardi et

al., 2015; Bonora et al., 2015; Izzo et al., 2016). This effect is inhibited by cyclosporine A suggesting that the pathway relies on cyclophilin D which has been linked to apoptosis and more commonly necrosis (Al-Nasser, 1999; Kim et al., 2003; Zamzami et al., 2005; Izzo et al., 2016). Mitochondrial permeability transition (MPT) occurs in several pathways of necrotic cell death, including pH-dependent ischemia/reperfusion injury and oxidative stress and has been suggested to be a key event in SA-induced in rat hepatocyte cytotoxicity (Trost and Lemasters, 1997; Lemasters et al., 1998; Armstrong, 2006).

However, at the current state of science, it is not possible to define the threshold concentration, and duration of exposure in human proximal tubular cells, above which an inhibition of mitochondrial oxidative phosphorylation is expected which will cause acute tubular necrosis on the renal tissue level, with the potential to ultimately induce acute renal failure. However, in line with the Martens et al. (1986) study referenced above, for the purposes of this study, it is hypothesised that a SA PTC concentration of 90 µM which causes large-amplitude swelling in rat liver mitochondria induces the same effect in human PTC mitochondria followed by MPT, acute tubular necrosis and clinical signs of renal dysfunction. The key assumptions underlying this hypothesis are that:

1) predicted PTC concentrations are achieved in all nephrons at the same time,
2) large-amplitude swelling induces MPT in all PTCs at the same time which enables the development of acute tubular necrosis across both kidneys and manifestation of clinical signs as a linear, non-reversible process.

In contrast, SU is reported to have no uncoupling effect (Whitehouse and Dean, 1965; Thompkins and Lee, 1969; Gutknecht, 1992) nor is SU a mitochondrial swelling agent (You, 1983). However, in opossum kidney cells, SU inhibits cell proliferation and stimulates the production of free radicals at cellular concentration of 2.5 mM or higher (Motojima et al., 2002). Since the predicted concentrations of SA in PTC compartments significantly exceed predicted SU concentrations (by up to a factor of 24 for the scenarios tested), results presented in the following section will focus on SA concentrations only.

Glucuronides in general are not considered of toxicological concern. Even though the acyl glucuronide metabolite of diclofenac, another NSAID, has been found to bind covalently to endogenous serum albumin in man, an immune-mediated adverse reaction has not been associated with the acyl glucuronide (Regan et al., 2010; Hammond et al., 2014). No evidence is found associating SA glucuronides exposure with mitochondrial dysfunction.

In the following subchapters, simulated PTC concentrations of SA are compared to the hypothesised threshold of 90 µM.

4.4.4 Results of predictions with initial parameter values and scans over predefined ranges

Table 4.21 shows the highest predicted C_{max} across PTC1-3 compartments when the model is simulated with the parameter values sourced from the literature. Generally, for any of the scenarios, the C_{max} in PTC1 is very similar to the C_{max} in PTC2 and PTC3. Therefore, only the highest C_{max} across all PTC compartments is presented in Table 4.21 but for each scenario, all C_{max} values are detailed below.

Table 4.21: C_{max} concentrations (in mM) predicted with initial parameters for the three individual cases exposed at three different dose levels

	Maximum PTC concentration at chronic, low therapeutic dose (mM) (compartment)	**Maximum PTC concentration at chronic, high therapeutic dose (mM) (compartment)**	**Maximum PTC concentration at acute intoxication (mM) (compartment)**
Young and healthy adult	0.0090 (PTC1)	0.6079 (PTC3)	0.6534 (PTC3)
Elderly, at risk of CKD	0.0124 (PTC1)	0.5575 (PTC3)	0.5970 (PTC2)
Elderly with signs of renal dysfunction	0.0133 (PTC1)	0.5467 (PTC3)	0.5734 (PTC2)

As mentioned in subchapter 4.4.2, the parameter values highlighted in sensitivity analyses performed for each of the nine exposure scenarios (3 individuals and 3 dosing conditions) are changed over five steps spread over a predefined range. All

parameter values selected for each scenario are presented in Table 4.22 and ranges designated for these parameters are shown in Table 4.23.

Table 4.22: Parameters identified to have the most impact on SA concentrations in PTC compartments for the scenarios tested

	Chronic, low therapeutic dose	**Chronic, high therapeutic dose**	**Acute intoxication**
Young and healthy adult	$f_{u(p)}$, $V_{\max\,(SU)}$, $K_{\mathrm{m}\,(SU)}$	$J_{\max\,(NPT1)}$	$J_{\max\,(NPT1)}$
Elderly, at risk of CKD	$V_{\max\,(SU)}$, $K_{\mathrm{m}\,(SU)}$	$J_{\max\,(NPT1)}$	$J_{\max\,(NPT1)}$
Elderly with signs of renal dysfunction	$V_{\max\,(SU)}$, $K_{\mathrm{m}\,(SU)}$	$J_{\max\,(NPT1)}$	$J_{\max\,(NPT1)}$

Table 4.23: Ranges over which parameter values will be changed using the scans function in SimBiology

Parameter	**Initial value, young and healthy adult**	**Initial value, elderly individuals**	**Range**
$f_{u(p)}$ (dimensionless)	0.601	NA	0.07 – 0.601
$V_{\max\,(SU)}$ (µmol/min)	6.3	3.15	3.15 – 12.6
$K_{\mathrm{m}\,(SU)}$ (mM)	0.104	0.104	0.0109 – 0.197
$J_{\max\,(NPT1)}$ (µmol/min)	78.2	39.1	0.0432 – 782

The fraction unbound of salicylic acid is fitted to 0.6013 which may be higher than expected for therapeutic concentrations, as indicated earlier, but adequate for toxic SA blood concentrations. Since the lower bound of reported $f_{u(p)}$ values lies at approximately 0.07 (Furst et al., 1979), the range for $f_{u(p)}$ is set between 0.07 and 0.6013. For the rate of SU formation, the widest range (mean ± standard deviation) of V_{max} and K_m values is found in Roberts et al. (1983) who included values for both young adults and elderly individuals. The maximum K_m and V_{max} values are based on the young group and the minimum K_m is based on the elderly group. Since the minimum V_{max} of both groups is 3.8 µmol/min and therefore slightly higher than the $V_{\max\,(SU)}$ for both elderly cases set at 3.15 µmol/min, the lower bound of the $V_{\max\,(SU)}$ range is set at 3.15 µmol/min. The $J_{\max\,(NPT1)}$ value taken from the literature is established with mouse protein which implies a high degree of

uncertainty underlying this value. It is difficult to estimate a biologically adequate range for this parameter. Since the $J_{\max}$ of NPT1 is the highest $J_{\max}$ value used in this model, the higher bound is selected an order of magnitude higher than the literature value. The lower bound is set at 0.0432 µmol/min which is the lowest $J_{\max}$ value used in this model (for OCT2).

4.4.4.1 Detailed simulation and scan results: chronic, low therapeutic dose of ASA

When the model is simulated with the initial $f_{u(p)}$, $V_{\max\,(SU)}$ and $K_{\mathrm{m}\,(SU)}$ values for the young and healthy adult, PTC1, PTC2 and PTC3 concentrations plateau at 0.0090, 0.0068 and 0.0056 mM, respectively.

In the elderly at risk of CKD and initial $V_{\max\,(SU)}$ and $K_{\mathrm{m}\,(SU)}$ values, maximum PTC1, PTC2 and PTC3 concentrations are predicted at 0.0124, 0.110 and 0.0091, respectively. For the elderly with signs of renal dysfunction, maximum PTC1, PTC2 and PTC3 concentrations are predicted at 0.0133, 0.0113 and 0.0090 mM, respectively, when simulated with initial $V_{\max\,(SU)}$ and $K_{\mathrm{m}\,(SU)}$ values. With any of the values included in the scan, no maximum concentration in PTC1-3 compartments exceeds 0.02 mM for all three individuals. Figures 4.15 and 4.16 show C_{max} values predicted for the elderly individual with signs of renal dysfunction in each PTC compartment over the scan ranges of $V_{\max\,(SU)}$ and $K_{\mathrm{m}\,(SU)}$ values, respectively. When performing the scans for two and three parameters simultaneously over 20,160 minutes, as defined in subchapter 4.4.2.2, an error occurred in SimBiology. Therefore, scan performance times are amended for the young and healthy individual and both elderly individuals to 7,200 and 10,080 minutes, respectively.

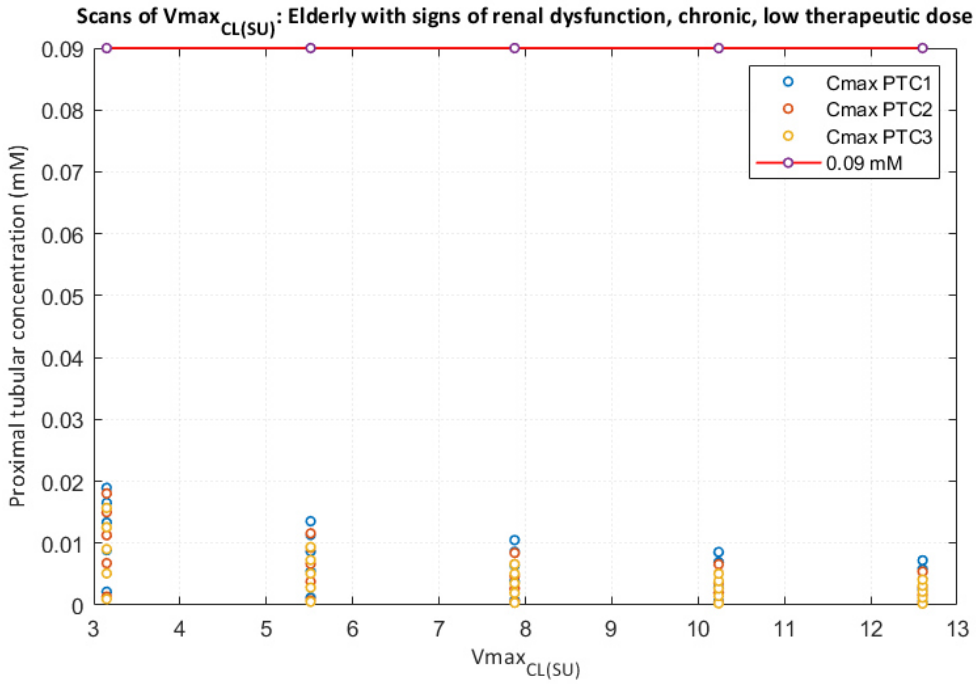

Figure 4.15: C_{max} values predicted for the elderly individual with signs of renal dysfunction in each PTC compartment over the scan ranges of $V_{\max\,(SU)}$ values, in relation to the defined threshold of toxicity at 0.09 mM.

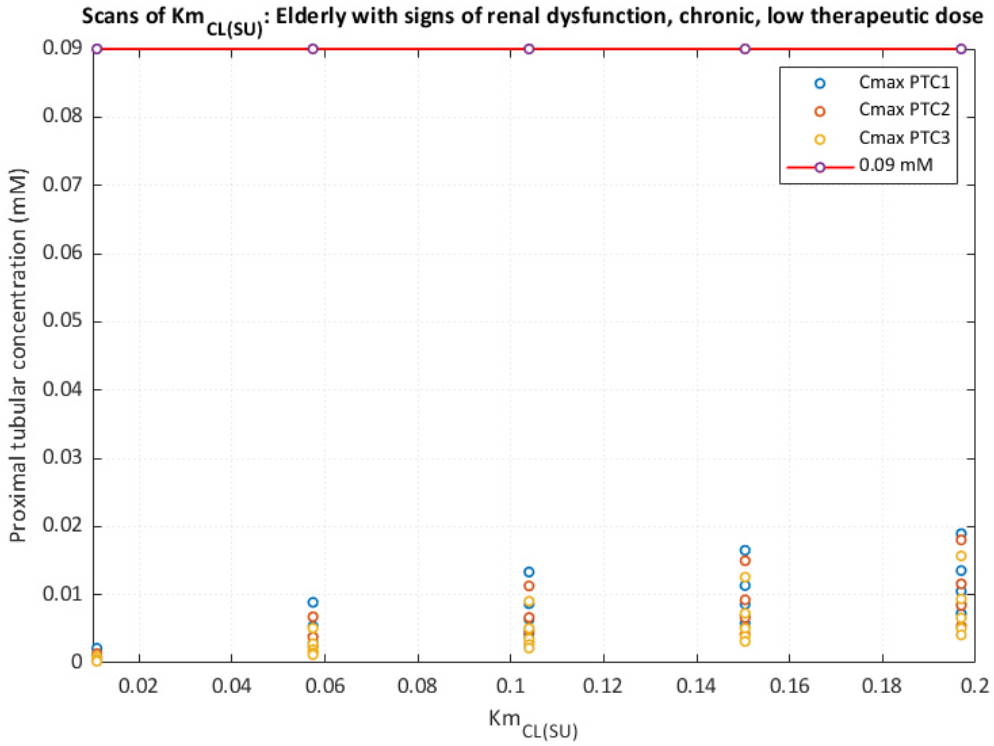

Figure 4.16: C_{max} values predicted for the elderly individual with signs of renal dysfunction in each PTC compartment over the scan ranges of $K_{\mathrm{m}\,(SU)}$ values, in relation to the defined threshold of toxicity at 0.09 mM.

4.4.4.2 Detailed simulation and scan results: chronic, upper therapeutic dose reaching a SA venous blood concentration of 2.2 mM

For the young and healthy adult, PTC1, PTC2 and PTC3 concentrations plateau at 0.602, 0.6035 and 0.6079 mM, respectively, when the model is run with the initial $J_{\max\,(NPT1)}$ at 78.2316 µmol/min. A scan including five steps over the range of 0.0432 to 782.3160 µmol/min for $J_{\max\,(NPT1)}$ shows that for a value close to 700 µmol/min, PTC1-3 concentrations reach their maxima at around 0.09 mM. At lower $J_{\max\,(NPT1)}$ values PTC concentrations plateau at a level exceeding the 0.09 mM threshold, and at higher $J_{\max\,(NPT1)}$ values maximum PTC concentrations are below it. For the elderly individual at risk of CKD, maximum concentrations in PTC1, PTC2 and PTC3 with the initial $J_{\max\,(NPT1)}$ are at 0.5549, 0.5564 and 0.5575 mM, respectively. The scan for the elderly individual at risk of CKD indicates that at a $J_{\max\,(NPT1)}$ of 391.18 µmol/min and higher maximum PTC1-3 concentrations are below 0.09 mM while at 195.61 µmol/min and lower PTC1-3 concentrations plateau at a level above the threshold. The scan for the elderly individual with signs of renal dysfunction gives the same results as described for the elderly at risk of CKD. When simulated with initial parameter values for the elderly with signs of renal dysfunction, PTC1, PTC2 and PTC3 concentrations reach 0.5452, 0.5462 and 0.5467 mM, respectively. Figure 4.17 shows C_{max} values predicted for the elderly individual at risk of CKD in each PTC compartment over the scan ranges of $J_{\max\,(NPT1)}$.

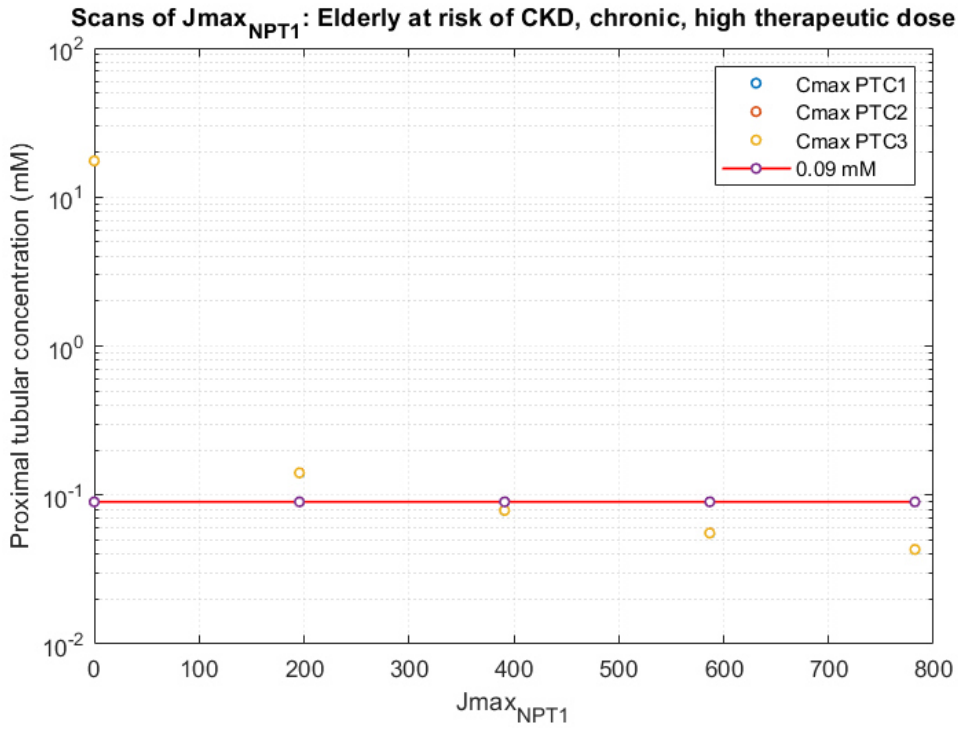

Figure 4.17: C_{max} values predicted for the elderly individual at risk of CKD in each PTC compartment over the scan ranges of $J_{\max\,(NPT1)}$, in relation to the defined threshold of toxicity at 0.09 mM. Predicted C_{max} values for PTC3 are superimposed on the predicted C_{max} values for PTC1 and PTC2.

4.4.4.3 Detailed simulation and scan results: acute intoxication at 3.24 mM SA venous blood concentration

When the model is simulated with the initial $J_{\max\,(NPT1)}$, PTC1, PTC2 and PTC3 concentrations of the young and healthy adult are 0.6482, 0.6496 and 0.6534 mM. A scan including five steps over the range of 0.0432 to 782.32 µmol/min for $J_{\max\,(NPT1)}$ shows slightly higher but very similar results as generated with the chronic upper therapeutic dose. At a SA venous blood concentration at 3.24 mM and a $J_{\max\,(NPT1)}$ value at 695 µmol/min, PTC1, PTC2 and PTC3 concentrations reach their maxima at 0.0944, 0.0945 and 0.096 mM, respectively. Only the highest $J_{\max\,(NPT1)}$ value generates PTC values below 0.09 mM. For the elderly individual at risk of CKD, maximum concentrations in PTC1, PTC2 and PTC3 with the initial $J_{\max\,(NPT1)}$ are at 0.5959, 0.5970 and 0.5964 mM, respectively. The scan results for both elderly individuals at a SA venous blood concentration of 3.24 mM are similar to those

obtained at a constant SA venous blood concentration of 2.2 mM. At a $J_{\max\,(NPT1)}$ of 391.18 µmol/min and higher maximum PTC1-3 concentrations are below 0.09 mM while at 195.61 µmol/min and lower PTC1-3 concentrations plateau at a level above the threshold. When the model is simulated with the initial $J_{\max\,(NPT1)}$ for the elderly individual with signs of renal dysfunction, maximum concentrations in PTC1, PTC2 and PTC3 are at 0.5730, 0.5734 and 0.5721 mM, respectively. Figure 4.18 shows C_{max} values predicted for the elderly individual with signs of renal dysfunction in each PTC compartment over the scan ranges of $J_{\max\,(NPT1)}$.

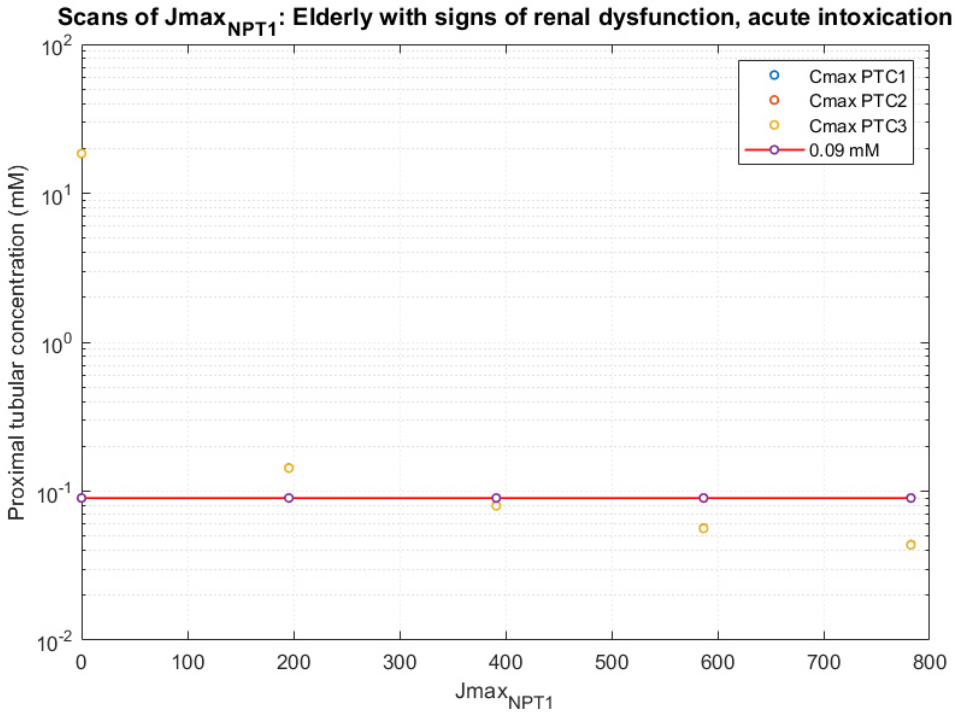

Figure 4.18: C_{max} values predicted for the elderly individual with signs of renal dysfunction in each PTC compartment over the scan ranges of $J_{\max\,(NPT1)}$, in relation to the defined threshold of toxicity at 0.09 mM. Predicted C_{max} values for PTC3 are superimposed on the predicted C_{max} values for PTC1 and PTC2.

4.5 Key results

This subchapter summarises those results, presented in subchapters 4.4.2.3 to 4.4.4.3, that are most relevant to the quantitative assessment of toxicity in the proximal tubules, induced by SA. For the three virtual individuals and the chronic, low therapeutic dose scenario, parameter values determining the rate of formation of SU, i.e. $V_{\max\,(SU)}$ and $K_{\mathrm{m}\,(SU)}$, have a significant impact on the SA concentration in PTC compartments. $V_{\max\,(SU)}$ is the maximum rate of metabolism for the formation of SU, the main metabolite of SA formed in the kidney, and $K_{\mathrm{m}\,(SU)}$ is the Michaelis-Menten constant which represents the affinity of the metabolising enzyme for SA. For the chronic, high therapeutic dose and acute intoxication scenarios and all three individuals, the maximum rate of transport via the transporter protein NPT1, i.e. $J_{\max\,(NPT1)}$, predominantly influences SA concentrations in all PTC compartments. $V_{\max\,(SU)}$, $K_{\mathrm{m}\,(SU)}$ and $J_{\max\,(NPT1)}$ are parameters which contribute to the decrease of SA in PTC compartments.

Results of prediction with initial parameter values show that a hypothesised toxicity threshold of 90 µM PTC concentration is not exceeded for any individual at the chronic, low therapeutic dose. However, PTC concentrations reached in any individual at the chronic, high therapeutic dose and acute intoxication exposure are above the hypothesised toxicity threshold, with highest C_{max} values reaching between 0.547 and 0.653 mM.

For each parameter identified in the sensitivity analyses, scans are performed over five steps over a predefined range. For the chronic, low therapeutic dose scenario and all three individuals, no maximum concentration in PTC compartments exceeds 0.02 mM with any of the values included in the scans for $V_{\max\,(SU)}$ and $K_{\mathrm{m}\,(SU)}$. For the young and healthy adult exposed to the chronic, high therapeutic dose, the scan for $J_{\max\,(NPT1)}$ shows that at a value close to 700 µmol/min and higher, maximum PTC concentrations are below 0.09 mM. For both elderly individuals at this exposure, the turning point is at a $J_{\max\,(NPT1)}$ value of approx. 390 µmol/min. This means that at this level and higher maximum PTC concentrations are below the hypothesised toxicity threshold. For the acute intoxication scenario, results are very similar to those predicted for the chronic, high therapeutic dose scenario. While for both

elderly individuals the toxicity threshold is exceeded at $J_{\max\,(NPT1)}$ values below 390 µmol/min, the threshold is exceeded at 695 µmol/min and lower for the young and healthy adult.

4.6 Discussion

In accordance with the first aim defined in subchapter 4.1., this study offers a detailed description of the development of a mechanistic kidney model predicting the kinetics of SA through eight renal blood and luminal, and seven cellular, compartments. Major kinetic processes included in this model comprise blood and luminal fluid flows, glomerular filtration, active and passive secretion and reabsorption processes, and metabolism to SU and glucuronides. With regard to the first objective (i) defined in subchapter 4.1, this study shows how the mechanistic kidney model is embedded into a full-body PBK model parameterised for ASA and SA and validated with data on the fractions of a dose excreted in urine as SA, ASA, SU and glucuronides. In accordance with the second objective (ii) set out subchapter 4.1, an example is presented of how the PBK-coupled kidney model may be applied. For this, key parameters of this model, which is initially set up for a young and healthy adult, are adjusted to simulate kinetics of two virtual elderly individuals, one at risk of CKD and one with signs of renal dysfunction. For these three individuals three exposure scenarios are defined, including a chronic, low therapeutic dose, a chronic high therapeutic dose and acute intoxication. For these three individuals and three exposure scenarios defined, sensitivity analyses are performed to understand which parameter values, when changed slightly, have the most impact on the predicted proximal tubular concentrations. To account for inter-individual variability and to some degree to account for uncertainty underlying parameter values, parameters identified in sensitivity analyses are changed over a predefined range. Then, simulations are run for five steps spanning this predefined range.

To sum up the results of the sensitivity analyses, values for the $V_{\max\,(SU)}$ and $K_{\mathrm{m}\,(SU)}$ significantly influence PTC concentrations at the chronic, low therapeutic dose, and $J_{\max\,(NPT1)}$ has the most impact on PTC concentrations at the two higher exposure scenarios. $V_{\max\,(SU)}$, $K_{\mathrm{m}\,(SU)}$ and $J_{\max\,(NPT1)}$ are parameters which contribute to the

decrease of SA in PTC compartments – as opposed to parameters contributing to the increase of SA such as rates of SA transport into PTC compartments. This indicates that in comparison to SA influx processes into PTC compartments, processes driving efflux and metabolism of SA are less saturated. However, this interpretation only holds for the current set of parameter values since a sensitivity analysis with different parameter values may produce different results. Important to note is that among all the transporter related $J_{\max}$ values applied here, $J_{\max\,(NPT1)}$ has by far the highest value which may explain why this value has a significant impact on PTC concentrations. Even though this value is established with SA while most other transporter parameter values are generated with other substances other than SA, it is not based on a human but mouse protein system. Therefore, there may be a higher uncertainty underlying this value in comparison to the much lower $J_{\max}$ values.

The results of simulations with initial parameter values indicate that for all three individuals (young and healthy adult, elderly person at risk of CKD and elderly person with signs of renal dysfunction) only the chronic, low therapeutic dose leads to proximal tubular concentrations below the previously set toxic concentration threshold of 0.09 mM. Interestingly, at the two higher exposure levels, proximal tubular concentrations predicted for both elderly individuals are lower than those predicted in the young and healthy adult. Further data may be required to validate these results.

The results of scans for the chronic, low therapeutic dose show that for any value included in the scan, predicted proximal tubular concentrations are below 0.02 mM, so well below the hypothesised toxic threshold. Results of the scans for the two higher exposure scenarios re-emphasise that active transport J_{max} values impact proximal tubular concentrations greatly and that interindividual variability in transporter expression may determine whether an adverse effect is experienced by an individual or not. As discussed earlier, there are uncertainties underlying all active transporter J_{max} values which is a limitation of this study. A reliable quantification of these uncertainties is crucial to the development of a robust model. Interesting to note is that for the two higher exposure scenarios the hypothesised toxicity threshold is exceeded at a $J_{\max\,(NPT1)}$ of approx. 390 µmol/min and lower for the two elderly individuals while the threshold is reached at approx. 700 µmol/min for the young and

healthy adult. This discrepancy reflects the difference in transporter activity between the young and both elderly individuals initially set due to the difference in the number of nephrons among them.

Overall, this study adds to the knowledgebase of mechanistic models related to kinetic processes and IVIVE approaches to increase the common understanding of nephrotoxicity induced by pharmaceutical compounds. All major kinetic factors (e.g. protein binding) and processes (i.e. glomerular filtration, urine flow, active and passive secretion and reabsorption) included in early models (Tang-Liu et al., 1983; Hall and Rowland, 1984; Komiya, 1986, 1987; Russel et al., 1987a; b; Mayer et al., 1988; Katayama et al., 1990) are taken into account in this model. Similar to the two most sophisticated mechanistic model to predict renal kinetics (Neuhoff et al., 2013; Huang and Isoherranen, 2018), the present model has the structure of a nephron divided into segments illustrating the glomerulus, proximal and distal tubules, loop of Henle and collecting ducts. These segments are divided into vascular, cellular and luminal compartments. While the present model has the same number of compartments overall, the model presented by Huang and Isoherranen (2018) has two segments for the loop of Henle and five for the collecting duct, instead of one and two in the model presented here, respectively. These differ in the tubular flow rate entering each tubular segment and the tubular pH. Even though no references are given by Huang and Isoherranen (2018) to explain the choice of pH values, the values applied may be a good starting point to incorporate different pHs in each luminal compartment. Since luminal pH has an impact on the extent of passive reabsorption, one of the major kinetic processes in the kidney, it needs to be considered if the available data allow for it. Huang and Isoherranen (2018) address the issue of lacking factors to scale from *in vitro* to *in vivo* system activity, and propose a factor to scale the surface area of the *in vitro* systems to the real intrinsic permeability by considering microvilli expression. The model is validated with data from 46 drugs so it covers a comparatively wider applicability domain while the model presented here is specific to SA.

Also, it may be valuable to re-assess the volumes assigned to each compartment in both models. As outlined in subchapter 4.2.1.1, all compartment volumes of the mechanistic kidney model presented here add up to a total kidney volume of 280 mL.

This volume is used in PBK models generated in the past (Davies and Morris, 1993; Peters, 2008a). In contrast, the volumes of all subsegments defined by Huang and Isoherranen (2018) add up to approx. one litre which may exceed the typical physiological volume of a kidney. The volumes which may have to be revised in the model developed here are those of the loop of Henle since they seem to be high in comparison to how volumes of the loop of Henle are described qualitatively or semi-quantitatively in the literature. The discrepancy between the approach to scale up volumes calculated from the external diameter, cell height and compartment length and the gross estimates of medullary compartments (discussed in subchapter 4.2.1.1.4.2) may also indicate that these volumes need to be re-assessed. A nephrologist's expert opinion is needed to further refine these volumes. Since the present investigation focusses on proximal tubular cell concentrations, potential inaccuracies in subsequent compartment volumes do not have a significant impact on the results of this study. Furthermore, the models presented by Neuhoff et al. (2013) and Huang and Isoherranen (2018) only incorporate renal metabolism and active transport processes at proximal tubular level. However, in this study metabolism is included on all levels starting from the proximal tubule since glucuronidation catalysing enzymes are reported to occur in latter tubular segments (Gaganis et al., 2007). Also, evidence indicates that active transport mechanisms exist in the renal medulla and collecting ducts (Madsen et al., 1988; Pearce et al., 2015). Furthermore, when validating the performance of the model with excretion data reported by Levy (1965), initial simulations show that active transport is needed to achieve the almost complete excretion of SA within 39 hours. In contrast to the model developed by Neuhoff et al. (2013), all data applied to generate this model are presented in this study.

This study contributes to the field of *in silico* toxicology since it is the first mechanistic model of the kidney which is embedded in a full-body PBK model whose data and ODEs used to generate both models are comprehensively reported. Additionally, in contrast to Huang and Isoherranen (2018), we amended certain physiological parameters of the model to simulate the physiology of two sensitive elderly individuals to address issues of variability.

The model presented here may be extended by making active transport processes from cellular to blood or luminal compartments only accessible to the fraction unbound. Due to a lack of information on protein binding of SA and metabolites in tubular cells, this component is not added to this model. However, it may be necessary to make active transport from cellular compartments only accessible to the fraction unbound in order to increase passive reabsorption of SA from cellular compartments. This process has currently a minor influence, but salicylic acid has been proposed to be reabsorbed in the distal renal tubule in the physiological range of urine pH, however to a lower extent at a high pH (Proudfoot et al., 2003). Also, in order to reach the renal tissue/tubule level of the AOP proposed in Figure 4.1., reliable data explaining a quantitative relationship between an exposure level and acute tubular necrosis in humans are needed. However, these data do not exist to this date. As soon as these become available, a quantitative dose-response relationship may be established between a dose or exposure scenario and necrosis observed at renal tubular level.

4.7 Conclusions

There are several lessons learned from this study. The results of the sensitivity analyses performed for all individuals and exposure scenarios highlight that it is of major importance to use active transporter and metabolism data that are of good quality. Also, $f_{u(p)}$ may have a major impact on the predicted concentration in proximal tubules. The need for an accurate estimate of renal active transporter V_{max} values is highlighted previously (Felmlee et al., 2013). Since it is not necessarily straight forward to assess the quality of such data, using and comparing data from various sources helps to find an adequate value to inform the model (Min and Bae, 2017). Also, the application of a relative expression factor (REF) or a RAF is proposed to scale from *in vitro* to *in vivo* transporter expression or activity, respectively, but such values are typically lacking (Neuhoff et al., 2013; Scotcher et al., 2016). The fact that glucuronidation V_{max} values have to be increased in order to predict similar fractions of the dose excreted as glucuronides as observed in individuals indicates that a REF or RAF is needed to scale these V_{max} values to *in vivo* activity. Overall, more human-based compound-specific data are needed to simulate kinetic

processes. This holds in particular for active transport J_{max} and K_m data since most of these values used are generated with substances other than SA and/or in animal cell systems. IVIVE approaches to predict hepatic clearance are more advanced than IVIVE to simulate renal processes (Houston and Galetin, 2008; Obach, 2011; Chen et al., 2012; Scotcher et al., 2016; Min and Bae, 2017). The value of using certain extrapolation factors established for hepatic drug elimination for the prediction of renal drug elimination has not been assessed comprehensively but may hold potential to move the field of IVIVE for renal processes forward.

In summary, a lot of high-quality data are needed in order to generate a reliable mechanistic model. Some of the data gaps may be bridged with read-across or other approaches but these add to the uncertainty associated with predicted results. As with any new method, the more mechanistic models are used the more their weaknesses are understood and potential unlocked.

5.0 DISCUSSION

In this final Chapter, a summary of the findings and conclusions with respect to this thesis's relevance for the field of chemical risk and drug safety assessment is presented. A full discussion of the study results is included within each of Chapters 2 to 4. Overall, this Chapter attempts to address how the quantitative methods developed in this thesis may be leveraged to answer pressing questions in nephrotoxicology and how the work performed within this thesis may help the progress of *in silico* toxicology in general. The final subchapter will focus on the future work required to ensure further progress with the use of PBK and organ-level mechanistic models and adequate interpretation of results.

These efforts respond to the "Toxicity Testing in the 21st Century" paradigm (NRC, 2007) and the principles of the 3Rs (replacement, reduction and refinement) (Tannenbaum and Bennett, 2015) which call for the use of non-animal methods for toxicity testing where feasible. These calls have been taken up by European regulatory frameworks such as the European REACH (Registration, Evaluation, Authorisation and Restriction of Chemicals) Regulation which promotes the use of alternative methods and the European Cosmetics Regulation which prohibits using animal testing to prove the safety of ingredients, formulations or final cosmetic products for human health (European Commission, 2006, 2009). Also, emphasis has been given to quantifying and using human exposure data, including HBM data, to guide and inform toxicity testing and assessment (NRC, 2007). The use of HBM data in the *in silico* toxicology context is specifically addressed in Chapter 2 and, in the broader sense, this thesis responds to the increasing demand to focus on human-based toxicity assessment. This means that human health hazard assessments are increasingly based on human-based data, computational models or *in vitro* systems based on human cell lines. Last, but foremost, with regard to the aims of this thesis, toxicology has been moving from a semi-quantitative endpoint-focussed science towards a more quantitative human pathway-based science. PBK modelling and mechanistic understanding have played a central role in the vision and strategy set out by ECVAM and the U.S. National Research Council to advance chemical risk assessments (NRC, 2007; Coecke et al., 2013). How this thesis contributed to the progress of quantitative human pathway-based toxicology is discussed in the summary of findings.

5.1 Summary of findings

As a major organ of elimination and therefore subject to high exposure of compounds, the kidney has been recognised as a significant target for drug and chemical induced toxicity. As adverse renal effects typically occur in patients who take several medications and as many chemicals are suspected to elicit toxicity via unspecific cytotoxicity (Judson et al., 2011; Thomas et al., 2012; Vinken and Blaauboer, 2017), supersaturation of parts of the renal system may be an important mechanism of inducing renal toxicity. Therefore, accounting for toxicokinetics and the potential of a substance to accumulate at organ-level or at a specific site within the kidney is considered to be vital. Also, a detailed mechanistic understanding of nephrotoxicity pathways is often lacking and clearly needs effort for improvement.

For the registration of many chemicals and pharmaceuticals, adverse effects to the kidney are currently assessed through traditional toxicological approaches, involving *in vitro* and *in vivo* animal studies (WHO, 1991). However, a standardised test specifically designed to investigate a substance's potential and mechanisms to elicit nephrotoxicity does not exist to date; normally repeat dose toxicity testing is used. In drug development, whilst safety pharmacology studies on the kidney are not part of the core required animal study battery, supplemental safety pharmacology studies on the renal and urinary system may be performed if there is cause for concern (International Conference on Harmonisation (ICH), 2000). Furthermore, clinical studies of drug compounds in humans cover endpoints related to renal toxicity but their efficacy to assess this pathology adequately has been challenged because of the high number of drug-induced acute renal failure cases in critically ill and chronic kidney disease patients.

In silico methods, in particular multiscale models that incorporate data spanning various biological scales, have the capacity to provide vital insights into nephrotoxicity mechanisms. As highlighted in Chapter 1, this thesis addresses the growing attention given to exposure-based and toxicokinetics-driven toxicity. In this context, PBK modelling has been regarded as the most appropriate approach to integrate *in vitro* data for the assessment of dose-response relationships for adverse

effects observed in humans (Coecke et al., 2013). Therefore, the aims and key results of this study were

I. To examine the suitability of publicly available generic PBK models to derive BE values based on agreed reference values that can then be used in a screening level mixture risk assessment using HBM data (Chapter 2). The aim was to establish a method to interpret HBM data on multiple chemicals easily, e.g. for prioritisation purposes. Two models were used to predict safe urinary concentrations following oral exposure to a safe dose, i.e. a TDI or RfD value. Safe urinary-level concentrations are termed BE_{RfD} and BE_{TDI} values. In order to test the performance of both PBK models, urine-level concentrations were predicted on the basis of estimated daily intakes of the chemicals considered, which were provided with other HBM data from cohorts of Norwegian mothers and children and Danish children. These simulated urine concentrations were compared to HBM data which capture measurements of these compounds or their metabolites present in the urine of these cohorts. A single substance and mixture risk assessment were performed with predicted safe concentrations, BE_{RfD} and BE_{TDI}, and measured concentrations to demonstrate how such data may be used in a risk assessment context.

   It was demonstrated that, despite the limitations of both models applied, IndustChemFate (ICF) and Httk, PBK models help to evaluate HBM data in a risk assessment context. The limitations of ICF related mainly to the inability of the model to reach steady-state concentrations for most compounds tested and the substantial number of input parameters required to perform simulations. Limitations of the current version of Httk were associated with the inability to simulate metabolite concentrations; this explains why the model could not be used to predict urine concentrations of phthalates. As Httk has recently been developed (Pearce et al., 2017), studies such as the comparison of urine-level EDI (BE_{EDI}) to measured urine concentrations presented in this thesis can help to validate this model. However, more studies are needed to validate this model fully and adequately interpret the results obtained here. High confidence data, such as EDI and measured urine

concentrations for which key uncertainties have been quantified are necessary, as well as increasing use of *in vitro* data in which the free and actual toxic concentration is measured. Although the comparison of BE_{EDI} to measured urine concentrations showed a difference of, on average, two to three orders of magnitude, this may not only be as a result of the performance of Httk performance but also due to uncertainties underlying input values (i.e. EDI, TDI and RfD).

These input values, in particular EDI, but also the accuracy of urine measurements, need to be challenged to explain the differences between predicted BE_{EDI} and measured urine concentrations. Uncertainties underlying these values were acknowledged; such uncertainties underlying EDI may relate to source variability, variability of input parameters to calculate EDI, incomplete capture of precursor compounds etc. However, their quantification, even though necessary in order to interpret predicted results with higher confidence, exceeded the scope of this study. Therefore, one of the main conclusions from this Chapter was that future efforts are needed to quantify uncertainties related to EDI and urine concentration measurements. This may be achieved by using probabilistic methods and a range of EDI and urine concentration values which have been established with a variety of methods (National Research Council, 2009). The uncertainties underlying the reference values (i.e. TDI, RfD) relate to the periodic reassessment of these values in which new data may be considered and may result in the derivation of a reference value lower than the previously adopted one.

Predicted BE_{RfD} and BE_{TDI} values were considered to be conservative, particularly since previously established BE values were three to four orders of magnitude higher than those derived here. This was also reflected and taken into account when comparing the results of the mixture risk assessment based on the 5^{th} percentile of the BE_{TDI} distribution to those based on the median BE_{TDI}.

A refined mixture risk assessment only groups substances leading to the same adverse outcome via the same mechanism of action (MoA). Since the approach

taken here grouped substances according to their structural similarity (i.e. phenols and parabens) independent of their MoA, the mixture risk assessment results were to be interpreted as worst-case scenarios (most conservative). In cases where the crude risk assessment indicates an unacceptable risk, a more refined risk assessment is needed before taking risk management measures. Overall, the aim of Chapter 2 was therefore fulfilled since it showed that generic PBK models, such as Httk, may be applied to analyse HBM data in the chemical risk assessment context. How to perform such an analysis was explained in detail. However, as outlined earlier, more studies with high confidence data are needed to further validate such models.

II. The second aim was to develop a human-relevant PBK model based on ordinary differential equations available in the public literature and which can be used to quantify the relationship between an administered dose and concentrations in key organs of the human body over time for a broad range of chemical substances (Chapter 3). The reason why a new PBK model was generated as opposed to using a publicly available one, such as Httk, for further analysis was to ensure full transparency and flexibility when using it in conjunction with a subsequently generated mechanistic kidney model (Chapter 4). Full transparency means knowing all parameter values and algorithms used in the model and, whenever an error occurred or an unexpected result was simulated, being able to get to rationalise and explain the issue and rectify it. Full flexibility characterises a model such that it may be easily amended and extended to fulfil the objective of a new study – in our case, the objective was to couple the PBK model to a mechanistic kidney model and apply both to predict concentration-time profiles in proximal tubular cells following oral exposure, in healthy and renally-compromised individuals.

   A literature review showed that, in comparison to the high number of publications on PBK models, only a small proportion of these include information on the model structure and ODEs in full detail. Therefore, the development, parameterisation and validation of the model generated in the frame of this thesis was described with an extensive level of detail so that researchers who intend to build a PBK model in the future may use it as

guidance. With increasing regulatory acceptance of PBK study results for the registration of pharmaceuticals and other chemicals (e.g. industrial, pesticidal), there is increasing demand for expert knowledge in this area. The information presented here offers a solid starting point to gain expert knowledge in PBK modelling. Also, transparent publication of PBK models and applied data is vital to build credibility in predicted results and confidence in using these for risk assessment and regulatory decision-making (Cohen Hubal et al., 2019).

The PBK model generated here contained compartments of 15 major human organs and tissues and included mathematical terms representing key physiological processes (e.g. tissue permeation, hepatic and renal elimination, oral absorption, enterohepatic recirculation and biliary elimination). In order to gauge whether the model predicted well over a significant applicability domain, the PBK model was parameterised and validated with nine substances covering a broad physico-chemical space. For each compound, a local sensitivity analysis of the impact of model parameters on the simulated venous blood concentration profile and fitting of most sensitive parameters were performed. Resulting simulations demonstrated a good representation of experimentally established data which were quantified with the calculation of goodness-of-fit parameters measuring model accuracy. According to the criteria outlined in the WHO/IPCS Guidance on the Characterisation and Application of Physiologically Based Pharmacokinetic Models in Risk Assessment (IPCS WHO, 2010), the level of confidence in the PBK model presented was considered to be good.

Limiting factors of the PBK model which were not considered in the current version of the model were transporter-driven kinetics, tissue-specific partition coefficients, differences in transit rates through the gastrointestinal tract, uptake through the skin or lungs and metabolism in tissues other than the liver. Also, since this PBK model was tested and validated to simulate the kinetics of small molecular weight chemicals, and the application of these models goes far beyond such chemical classes, there is a need to assess how well this model performs to predict the kinetics of, for instance, nanoparticles,

large biopharmaceuticals or even microbial pathogens. The kinetics of nanoparticles are driven by moving from the blood compartment into the interstitial spaces of organs by extravasation or transcytosis, opsonisation to facilitate phagocytotic uptake into macrophages and transport into the venous blood via the lymphatic system (Li et al., 2017; Aborig et al., 2019). Therefore, ODEs for nanoparticle PBK models are fundamentally different to those described in this thesis.

When applying this PBK model in further kinetics studies, the quality of simulation results depend strongly on the availability and quality of input data for the chemical under consideration. For data poor chemicals, PBK modelling results are typically used for rapid screening purposes while for data rich substances, the model may be refined to answer a specific research question (Cohen Hubal et al., 2019). In many cases, *in vitro* data are used to inform such models and scaling is needed to extrapolate to an *in vivo* activity. The *in vitro* value most typically used is intrinsic hepatic clearance established in liver microsomes, hepatocytes or liver slices. For this, scaling approaches have been established (Barter et al., 2007) but not necessarily for other *in vitro* data. This issue is discussed further in Chapter 4 with regard to metabolism in the kidney.

In summary, the aim of Chapter 3 was fulfilled since a human-relevant PBK model was successfully developed which can be used to quantify the relationship between an administered dose and concentrations in key organs of the human body over time for a broad range of chemical substances. This was shown in further detail in Chapter 4 where the PBK model was applied and extended.

III. The third aim was to develop a mechanistic model of the kinetics of drugs in the kidney with specific reference to salicylic acid (SA), a major metabolite of aspirin (ASA) (Chapter 4). Twenty-three renal blood, cellular and luminal compartments were defined resembling the structure of a nephron, connecting to a collecting duct and surrounded by vasculature. The quantification of all compartment volumes was described in sufficient detail to

enable them to be reproduced. However, since the distribution of the medullary volume among medullary compartments may need revising, it is appreciated that the data in the public literature may not be sufficient to quantify the medullary volumes with high confidence. A revision is needed in particular for assessments of toxicity endpoints which occur mainly in the medulla and for which the quantification of substance concentrations in medullary compartments are required. This highlighted one of the pressing issues in quantitative *in silico* toxicology: the lack of readily usable human-based quantitative data, in particular of high quality.

Studies such as those in this thesis help to identify data gaps so that they may be filled in the future. Computational methods may also be used to estimate certain parameter values but in cases where considerable uncertainty underlies these it will be difficult to estimate all of these values with high confidence.

ODEs were generated which include mathematical terms representing major renal kinetic processes for SA such as blood and luminal fluid flows, glomerular filtration, active and passive secretion and reabsorption processes, and metabolism to SU and glucuronides. Then, in line with the first objective (i) of Chapter 4, this sub-compartment kidney model was embedded in our previously developed PBK model, in order to be able to predict proximal tubular cell concentrations from an oral dose. The mechanistic kidney model, in conjunction with the full-body PBK model, was validated with data on the fractions of a dose excreted in urine as SA, ASA, SU and glucuronides.

In line with the "Toxicity Testing in the 21st Century" paradigm, a considerable proportion of data used for the mechanistic kidney model were based on alternative methods and, to a high degree, were human-based. However, the transporter related $J_{\max}$ value which had the most impact on all predicted proximal tubular cell concentrations in both higher dose scenarios for all three virtual individuals was generated in a mouse protein *in vitro* model. This value was also considerably higher than any other $J_{\max}$ value used in the kidney model. This is why we estimated that this value has much higher uncertainties

than much lower $J_{\max}$ values which were established in a human kidney cell line. The issue is that even though the model was based predominantly on human data, a single animal-based value may have a significant impact on the predicted outcome. This concern needs to be interpreted with care and validated with further data.

This study adds to the efforts of using *in vitro* sub-cellular level data (e.g. transporter or metabolism V_{max} and K_m), sub-organ level data (such as data used to define compartment volumes) and organism level data (e.g. the clinical kinetic data used for model validation) for the generation and validation of a multiscale model. In this context, an IVIVE approach was applied to scale sub-cellular level data to organism level data (assuming two kidneys per person). Limitations of this IVIVE approach were addressed in the context of scaling up glucuronidation *in vitro* data and it was highlighted that additional scaling factors (e.g. RAF, REF) are needed.

The second objective (ii) of this study was to investigate whether a quantitative relationship can be established between therapeutic doses of SA, predicted proximal tubular cell concentrations in young and elderly virtual individuals and toxicity events in proximal tubular cells. For this, key parameters of the model, which was initially set up for a young and healthy adult, were adjusted to simulate kinetics of two virtual elderly individuals (one at risk of CKD and one with signs of renal dysfunction). This objective addressed the issue of interindividual variability which is of particular importance since the vast majority of acute renal failures occurs in elderly patients. Since no significant difference in the results of the sensitivity analyses and predictions was noted for both elderly individuals, it is suggested to decrease certain parameter values (e.g. the GFR or renal blood flow) more for the elderly with signs of renal dysfunction to evaluate whether a greater difference in predicted results is observed. For this, it would be particularly beneficial to investigate whether additional data may be obtained from the public literature or elsewhere.

Due to the lack of human data, the toxicity threshold applied to discriminate between toxic and non-toxic concentrations in the proximal tubular cell

compartments was derived from an animal assay with rat liver mitochondria. Even though SA is a very data rich chemical, only a few quantitative toxicity data were identified which inform the AOP illustrated in Figure 4.1 for SA. This pathway is initiated by the interaction of a substance with organic anion transporters located in the basolateral membrane of proximal tubular cells. There, these substances subsequently accumulate and uncouple or inhibit mitochondrial oxidative phosphorylation. The mechanistic kidney model study in Chapter 4 simulated this part of the AOP and added information on different dosing and individual scenarios. Following the AOP, uncoupling or inhibition of mitochondrial oxidative phosphorylation may lead to acute tubular necrosis and acute renal failure. At this stage, it is typically unlikely to obtain data which clarify at which (internal or external) dose acute tubular necrosis is induced in humans. More attainable are data on the exposure level causing the adverse outcome, in this case acute renal failure, even though these are usually restricted to poisoning case reports or clinical data of patients. The quality and usability of these data need to be assessed carefully since case reports often do not contain a reliable quantification of the dose and as patients may have preconditions or various comorbidities. Reliable dosing/exposure information leading to adverse outcomes in humans is needed to bridge the knowledge gap between effects observed *in vitro* and adversities induced in the human *in vivo* context. This information may be in the form of HBM data or clinical information for individuals who have experienced, or are susceptible to develop, adverse renal effects, which are potentially more common in highly exposed residential or occupational areas. HBM data provide a distribution of exposure for selected substances and clinical information, which could include novel kidney disease biomarkers (Pletz et al., 2018b). Population-level HBM and kidney disease biomarker data may be used to establish probabilistic distributions of exposure-response relationships. For example, a probability distribution informs about the level of exposure at which, for instance, 5%, 50% or 95% of a population are expected to develop acute tubular necrosis; this may provide more confidence in a chosen toxicity threshold than one single (deterministic) value (Chiu and Slob, 2015). Overall, a probabilistic approach helps to quantify uncertainties, however, such probability distribution data are mostly unavailable.

In summary, the aim of Chapter 4 – to develop a mechanistic model of the kinetics of SA in the kidney – was achieved, along with both specific objectives: to embed the sub-compartment kidney model in our previously developed PBK model and validate it with full-body kinetic data; and to investigate the quantitative relationship between exposure to SA, predicted proximal tubular cell concentrations in young and elderly virtual individuals and toxicity events in proximal tubular cells. Both objectives (i and ii) are novel in the field of *in silico* nephrotoxicology as, to date, no study exists in the public literature which offers a mechanistic kidney model embedded in a full-body PBK model which was subsequently used to simulate concentrations at the site of toxicity for the young and healthy, as well as vulnerable individuals. This study adds to the efforts in toxicology to progress towards a more quantitative human pathway-based science. However, since not all parameter values are human-based and uncertainties underlying the data used in this model have not been quantified, e.g. through a distribution of dose-response relationships, there is still great potential for further improvement.

5.2 Conclusions related to mechanistic modelling in nephrotoxicology

Nephrotoxicity is a complex endpoint which often occurs gradually or as a result of other pathologies. Therefore, even sophisticated toxicity testing and clinical trials have not provided the mechanistic understanding needed to adequately quantify exposure-response relationships for chemical risk assessments. *In silico* models, including PBK and organ-level mechanistic models, have been evolving steadily and have the potential to contribute immensely to the field of nephrotoxicology.

If the development of AOPs and multi-scale models is currently considered to be the panacea of 21st century toxicology, knowledge and information spanning molecular to population levels are necessary to generate multi-scale models resembling the structure of kidney toxicity-related AOPs. In order to improve and expedite the development of *in silico* models for kidney toxicity, at least three – highly interrelated – problems have to be overcome. These are:

i) The identification and definition of effects to the kidney that may be brought about by chemical exposure.
ii) A full description of relevant mechanisms of action (and their translation to AOPs) relevant to kidney toxicity.
iii) Access to appropriate data ranging from *in vivo* through to *in vitro* and molecular responses.

The identification of effects to the kidney requires existing knowledge to be extended and unified. Networked AOPs may facilitate this, although these efforts may require a systematic evaluation of current knowledge and data. With regard to the data from which to develop the models, no assay exists which is specifically targeted towards renal toxicity endpoints. In addition, interspecies variability between rats and humans is known to be relevant for certain pathways (i.e. certain transporter-driven and α2μ-globulin related nephrotoxicity). Therefore, the usefulness of *in vivo* data in this area needs to be assessed carefully. Human and *in vitro* assay data are widely available but need to be utilised with care due to challenges related to their relevance to the known nephrotoxicity mechanisms, comparability of studies and other factors related to data interpretation. For instance, whilst providing the most human-relevant information, the quality and usability of poisoning case reports or patient adverse event reports need to be reviewed thoroughly, since case reports often do not contain a reliable quantification of the dose and patients may have various pre-existing comorbidities. Thus, a strategy to utilise existing data at different levels of AOPs may prove to be extremely effective to provide information relating to chemical toxicity and risk assessment as this does not require full testing of every compound and could be a solution to model development. In addition, as the lack of readily available data is considered to be a key limiting factor when it comes to the generation of future computational models in this field, the following recommendations may help to drive future modelling efforts forward:

(i) There is a need to improve understanding of mechanisms of nephrotoxicity, how novel, recently proposed, biomarkers relate to these mechanisms and how biomarker data are related quantitatively to each other at various dose levels. This will result in alternative sources of data and could be facilitated by appropriate statistical approaches such as Bayesian networks. With these, quantitative

relationships between KEs within an AOP from multiple biological levels may be established.

(ii) A global review of the quality of currently available kidney toxicity data is needed as well as an assessment of how these data relate to each other (e.g. cellular vs. tissue vs. organ-level effects). Information would be leveraged more readily if databases allowed for searches on both compounds and mechanistic data (including dosing information) enabling discrimination between the various nephrotoxicity endpoints.

(iii) Generation of more AOPs for nephrotoxicity with MIE and KE related data being searchable in a central database linked to respective mechanistic toxicological data would also assist the development of more computational models.

The development of a mechanistic model spanning an entire AOP requires an extensive amount of data, time and resources. Therefore, it appears inefficient to aim for a mechanistic model for each AOP that has been generated. Other *in silico* approaches which have been proposed to quantify an AOP apply dose-response modelling and dynamic Bayesian networks (Zgheib et al., 2019). The former defines empirical equations that fit the data which may, however, over-simplify underlying biology. The latter derives probabilistic relationships between components of an AOP, e.g. between KEs or the MIE and a KE. This method is less data-hungry than a mechanistic model. However, the data used to inform the model are ideally obtained using uniform dose and time schedules across experiments. In practice, this requires that data need to be experimentally generated for the model since it will be highly unlikely to source adequate data from the public literature. Also, it might not be achievable to observe various KEs within the same time frame since molecular reactions happen in seconds, cells react in hours and tissues within days (Zgheib et al., 2019).

5.3 Conclusions related to mechanistic modelling in chemical risk assessment

The work undertaken within this thesis covered several aspects of how PBK and organ-level mechanistic modelling may be used to assess the risk posed by chemicals. For all modelling efforts, compounds were selected which are considered data rich. However, as shown for the active transporter data for SA in Chapter 4, even for these

data rich compounds a full set of parameter values, based on human *in vitro* or clinical studies, could not be found. For the vast majority of substances, fewer data are available. For these substances, modelling needs to be feasible using fewer data and/or more data need to be generated in a systematic way to inform such models. Since PBK and mechanistic models have recently been used increasingly, these will continue to be applied with growing frequency in the field of chemical risk assessment. With the growing acceptance of AOPs, researchers are motivated to generate multi-scale *in silico* models which evaluate the quantitative relationships between two or more KEs. In cases where data allow it, these relationships may be investigated by applying mechanistic models. Alternatively, a combination of various approaches as described in Zgheib et al. (2019) may provide a valuable insight as all have different advantages. In other human health hazard assessment areas such as benchmark dose (BMD) estimation, results of a set of accepted dose-response models have been used to derive a Bayesian model averaging (BMA) BMD estimate (Shao and Gift, 2014). Potentially, a similar approach or strategy may be derived to leverage all results in a systematic way. In cases where data gaps prevent the application of a mechanistic model, other less data hungry methods may be applied and further extended once more data become available.

Researchers have increasingly been using IVIVE approaches, including PBK modelling, for screening and risk assessment on the basis of *in vitro* assay results (Wetmore et al., 2012; Martin et al., 2015; Fabian et al., 2019). Therefore, for data poor substances which are not addressed in any AOP but showed toxicity-related effects in *in vitro* assays, PBK models such as that generated in Chapter 3 may be used for initial screening purposes to predict an expected target organ concentration. This concentration may then be compared to the *in vitro* study results – potentially following a fingerprint method which is briefly outlined in the following and final subchapter (Yoon et al., 2012). If the predicted target organ concentration is below the effect concentration observed in the *in vitro* assay, it may be argued that no further assessment is necessary at this stage. If the predicted target organ concentration is above the *in vitro* effect concentration, a more detailed assessment should then be undertaken. Another aspect which has been discussed in the context of understanding the toxic concentration in an *in vitro* assay is the free and bioavailable concentration (Blaauboer, 2010; Kramer, 2010). The free concentration

can deviate greatly from the nominal concentration which has been added to the *in vitro* system due to binding to the plastic of the culture plate, binding to proteins in the medium or evaporation from the medium. Modelling approaches to calculate the free concentration exist (Kramer, 2010; Paini et al., 2017b) and would have to be considered where possible. Missing PBK parameter values for a data poor substance may be obtained from QSAR models (e.g. calculation of the absorption rate constant using Winiwarter et al. (1998), model 3b, and Peters (2008a) as performed in Chapters 2 and 3), QSPR models (such as those used in IndusChemFate as explained in Jongeneelen and ten Berge (2011)) or read-across (i.e. using parameter values of substances which are structurally similar based on which similar kinetics may be assumed). Again, the use of a set of computational methods to evaluate data poor substances is vital to shed light on data gaps or compensate for limitations of *in vitro* approaches. Since there is typically no agreement on which computational methods are best to use, using a set of models may add to variability of results which needs to be characterised and understood.

Initial screening to prioritise data poor substances based on *in vitro* toxicity data may even be improved if external exposure data are considered (Wetmore et al., 2012). HBM data are typically only generated for selected substances which implies that they may not be available for data poor (with regard to toxicity data) substances. However, external exposure data may be calculated from intake and inhalation rates, use or emission patterns and environmental concentrations, such as EDIs calculated from food, dust and air samples (Cequier et al., 2014; Sakhi et al., 2014; Liagkouridis et al., 2017) (see Chapter 2). These estimations bear more uncertainties than measured exposure data as many factors influence the extent an individual or population is exposed, e.g. distribution of a substance within food, estimation of amount ingested, weather conditions influencing environmental concentrations etc. (WHO, 2005). However, in the absence of more specific data, these estimations may be used for a crude risk assessment.

Overall, with respect to all modelling scenarios discussed in this thesis, an iterative approach is necessary, in particular if the dataset used for a model is incomplete or its underlying uncertainties have not been assessed. The challenge to reproduce a PBK model from one publication (as discussed in Chapter 3) highlighted the need for

uniform methods for the reporting of computational models to ensure that correct and complete information is captured and can be reused. Moving forward, it is clear that experimental and computational efforts have to go hand-in-hand, along with the development of mechanistic knowledge, to achieve much needed progress in this area.

5.4 Future work

Depending on the data available, topics in this thesis may be extended in many ways, for instance by testing the model(s) with different substances which principally requires the update of active and passive transport and metabolism parameter values. For the evaluation of distal tubular cell toxicity, it may be valuable to revisit medullary compartment volumes first, since the distal tubules follow the loop of Henle which is associated with the medulla.

No significant difference in the results of the sensitivity analyses and simulations was observed for both virtual elderly individuals. Therefore, the public literature and databases need to be searched for distributions of parameter values and dose-response relationships observed in individuals with renal dysfunction. Simulations can then be re-performed to assess how results for the elderly individual with signs of renal dysfunction differ from those of the elderly individual at risk of CKD or the young and healthy individual.

It would be more challenging to use the model to elucidate other mechanisms of nephrotoxicity, such as haemodynamic alteration, tubular obstruction and glomerular, tubulo- and/or interstitial nephritis (see Figure 1.1). As outlined in Chapter 1, the research need for a better understanding of nephrotoxicity pathways clearly exists. The most feasible option is to develop SAR profilers for each individual nephrotoxicity endpoint and couple the mechanistic kidney model with these profilers. Initial work has been performed for the generation of an "*in silico* profiler" for nephrotoxicity in general (Pletz et al., 2018a). The existing knowledge needs to be rationalised such that a robust set of structural alerts can be established. Such an "*in silico* profiler" will assist in the designing-out of toxicity as well as grouping, allowing for read-across, especially to estimate the chronic toxicity of data-poor

substances. A potentially rich source of information to develop further structural information are the data resultant from ToxCast. It has been shown that fingerprints using available ToxCast data on kidney tissue cell lines may be developed (Madden et al., 2017). Such fingerprints could consist of a defined number of *in vitro* assays reflecting the toxic mechanism of a specific group of known nephrotoxicants. If a new chemical is shown to generate hits according to one of the defined fingerprints, the likelihood of the chemical to cause nephrotoxic effects is considered to be high. A more mechanistic and data-demanding option would be to add toxicodynamic components to the mechanistic kidney model which help understand concentration-effect relationships in specific compartments of the kidney.

6.0 REFERENCES

Abbiati, R.A. and Manca, D., (2017) Enterohepatic circulation effect in physiologically based pharmacokinetic models: The sorafenib case. *Industrial and Engineering Chemistry Research*, 5612, pp.3156–3166.

Abdulkader, R.C.R.M., Burdmann, E.A., Lebrão, M.L., Duarte, Y.A.O. and Zanetta, D.M.T., (2017) Aging and decreased glomerular filtration rate: An elderly population-based study. *PLoS ONE*, 1212, pp.1–12.

Aborig, M., Malik, P.R. V., Nambiar, S., Chelle, P., Darko, J., Mutsaers, A., Edginton, A.N., Fleck, A., Osei, E. and Wettig, S., (2019) Biodistribution and physiologically-based pharmacokinetic modeling of gold nanoparticles in mice with interspecies extrapolation. *Pharmaceutics*, 114, p.179.

Agoram, B., Woltosz, W.S. and Bolger, M.B., (2001) Predicting the impact of physiological and biochemical processes on oral drug bioavailability. *Advanced Drug Delivery Reviews*, 50 Suppl 1, pp.S41–S67.

Aker, A.M., Watkins, D.J., Johns, L.E., Ferguson, K.K., Soldin, O.P., Anzalota Del Toro, L. V., Alshawabkeh, A.N., Cordero, J.F. and Meeker, J.D., (2016) Phenols and parabens in relation to reproductive and thyroid hormones in pregnant women. *Environmental Research*, 151, pp.30–37.

Al-Jahdari, W.S., Yamamoto, K., Hiraoka, H., Nakamura, K., Goto, F. and Horiuchi, R., (2006) Prediction of total propofol clearance based on enzyme activities in microsomes from human kidney and liver. *European Journal of Clinical Pharmacology*, 627, pp.527–533.

Al-Nasser, I.A., (1999) Salicylate-induced kidney mitochondrial permeability transition is prevented by cyclosporin A. *Toxicology Letters*, 1051, pp.1–8.

Alpern, R.J., Caplan, M.J. and Moe, O.W. eds., (2013) *Seldin and Giebisch's the kidney: Physiology and pathophysiology*. Fifth ed. Boston: Academic Press/Elsevier.

Alvan, G., Bergman, U. and Gustafsson, L., (1981) High unbound fraction of salicylate in plasma during intoxication. *British Journal of Clinical Pharmacology*, 116, pp.625–626.

Angerer, J., Aylward, L.L., Hays, S.M., Heinzow, B. and Wilhelm, M., (2011) Human

biomonitoring assessment values: Approaches and data requirements. *International Journal of Hygiene and Environmental Health*, 2145, pp.348–360.

Ankley, G.T., Bennett, R.S., Erickson, R.J., Hoff, D.J., Hornung, M.W., Johnson, R.D., Mount, D.R., Nichols, J.W., Russom, C.L., Schmieder, P.K., Serrrano, J.A., Tietge, J.E. and Villeneuve, D.L., (2010) Adverse outcome pathways: A conceptual framework to support ecotoxicology research and risk assessment. *Environmental Toxicology and Chemistry*, 293, pp.730–741.

Antal, E.J., Kramer, P.A., Mercik, S.A., Chapron, D.J. and Lawson, I.R., (1981) Theophylline pharmacokinetics in advanced age. *British Journal of Clinical Pharmacology*, 125, pp.637–45.

Aprea, C., Colosio, C., Mammone, T., Minoia, C. and Maroni, M., (2002) Biological monitoring of pesticide exposure: A review of analytical methods. *Journal of Chromatography B*, 769, pp.191–219.

Armstrong, J.S., (2006) The role of the mitochondrial permeability transition in cell death. *Mitochondrion*, 65, pp.225–234.

Arnold, S.M., Morriss, A., Velovitch, J., Juberg, D., Burns, C.J., Bartels, M., Aggarwal, M., Poet, T., Hays, S. and Price, P., (2015) Derivation of human Biomonitoring Guidance Values for chlorpyrifos using a physiologically based pharmacokinetic and pharmacodynamic model of cholinesterase inhibition. *Regulatory Toxicology and Pharmacology*, 712, pp.235–243.

Arundel, P.A., (1997) A multi-compartmental model generally applicable to physiologically-based pharmacokinetics. *IFAC Proceedings Volumes*, 302, pp.129–133.

Asimakopoulos, A.G., Thomaidis, N.S. and Kannan, K., (2014) Widespread occurrence of bisphenol A diglycidyl ethers, p-hydroxybenzoic acid esters (parabens), benzophenone type-UV filters, triclosan, and triclocarban in human urine from Athens, Greece. *Science of the Total Environment*, 470–471, pp.1243–1249.

Aslaksen, A., Bakke, O.M. and Vigander, T., (1981) Comparative pharmacokinetics of theophylline and aminophylline in man. *British Journal of Clinical Pharmacology*, 113, pp.269–273.

Bainbridge, T.R., (1985) The Committee on Standards: precision and bias. *ASTM Standardization News*, 13, pp.44–46.

Baker, R.E., Peña, J.-M., Jayamohan, J. and Jérusalem, A., (2018) Mechanistic models versus machine learning, a fight worth fighting for the biological community? *Biology Letters*, 145, pp.1–4.

Baley, J.E., Meyers, C., Kliegman, R.M., Jacobs, M.R. and Blumer, J.L., (1990) Pharmacokinetics, outcome of treatment, and toxic effects of amphotericin B and 5-fluorocytosine in neonates. *The Journal of Pediatrics*, 1165, pp.791–797.

Ball, K., Bouzom, F., Scherrmann, J.-M., Walther, B. and Declèves, X., (2013) Physiologically based pharmacokinetic modelling of drug penetration across the blood-brain barrier - Towards a mechanistic IVIVE-based approach. *AAPS Journal*, 154, pp.913–932.

Bang, D.Y., Kyung, M., Kim, M.J., Jung, B.Y., Cho, M.C., Choi, S.M., Kim, Y.W., Lim, S.K., Lim, D.S., Won, A.J., Kwack, S.J., Lee, Y., Kim, H.S. and Lee, B.M., (2012) Human risk assessment of endocrine-disrupting chemicals derived from plastic food containers. *Comprehensive Reviews in Food Science and Food Safety*, 115, pp.453–470.

Baraka, O.Z., Mahmoud, B.M., Marschke, C.K., Geary, T.G., Homeida, M.M.A. and Williams, J.F., (1996) Ivermectin distribution in the plasma and tissues of patients infected with Onchocerca volvulus. *European Journal of Clinical Pharmacology*, 505, pp.407–410.

Bartels, M., Rick, D., Lowe, E., Loizou, G., Price, P., Spendiff, M., Arnold, S., Cocker, J. and Ball, N., (2012) Development of PK- and PBPK-based modeling tools for derivation of biomonitoring guidance values. *Computer Methods and Programs in Biomedicine*, 1082, pp.773–788.

Barter, Z., Bayliss, M., Beaune, P., Boobis, A., Carlile, D., Edwards, R., Brian Houston, J., Lake, B., Lipscomb, J., Pelkonen, O., Tucke, G. and Rostami-Hodjegan, A., (2007) Scaling factors for the extrapolation of in vivo metabolic drug clearance from in vitro data: Reaching a consensus on values of human microsomal protein and hepatocellularity per gram of liver. *Current Drug Metabolism*, 81, pp.33–45.

Bernardi, P., Rasola, A., Forte, M. and Lippe, G., (2015) The mitochondrial permeability transition pore: Channel formation by F-ATP synthase, integration in

signal transduction, and role in pathophysiology. *Physiological Reviews*, 954, pp.1111–1155.

Bernareggi, A. and Rowland, M., (1991) Physiologic modeling of cyclosporin kinetics in rat and man. *Journal of Pharmacokinetics and Biopharmaceutics*, 191, pp.21–50.

Bertram, J.F., Douglas-Denton, R.N., Diouf, B., Hughson, M.D. and Hoy, W.E., (2011) Human nephron number: Implications for health and disease. *Pediatric Nephrology*, 269, pp.1529–1533.

Bessems, J.G., Loizou, G., Krishnan, K., Clewell, H.J., Bernasconi, C., Bois, F., Coecke, S., Collnot, E.M., Diembeck, W., Farcal, L.R., Geraets, L., Gundert-Remy, U., Kramer, N., Küsters, G., Leite, S.B., Pelkonen, O.R., Schröder, K., Testai, E., Wilk-Zasadna, I. and Zaldívar-Comenges, J.-M., (2014) PBTK modelling platforms and parameter estimation tools to enable animal-free risk assessment. Recommendations from a joint EPAA - EURL ECVAM ADME workshop. *Regulatory Toxicology and Pharmacology*, 681, pp.119–139.

Bhatt, K., Zhou, L., Mi, Q.-S., Huang, S., She, J.-X. and Dong, Z., (2010) MicroRNA-34a is induced via p53 during cisplatin nephrotoxicity and contributes to cell survival. *Molecular Medicine*, 169–10, pp.409–16.

Bhattacharya, S., Shoda, L.K.M., Zhang, Q., Woods, C.G., Howell, B.A., Siler, S.Q., Woodhead, J.L., Yang, Y., McMullen, P., Watkins, P.B. and Melvin, E.A., (2012) Modeling drug- and chemical-induced hepatotoxicity with systems biology approaches. *Frontiers in Physiology*, 3December, pp.1–18, article 462.

Björkman, S., (2002) Prediction of the volume of distribution of a drug: Which tissue-plasma partition coefficients are needed? *Journal of Pharmacy and Pharmacology*, 54, pp.1237–1245.

Blaauboer, B.J., (2010) Biokinetic modeling and in vitro-in vivo extrapolations. *Journal of Toxicology and Environmental Health - Part B: Critical Reviews*, 132–4, pp.242–252.

Blatt, A.E. and Liebman, S.E., (2013) Drug induced acute kidney injury. In: E.J. Alper and V.J. Lang, eds., *Hospital Medicine Clinics*. [online] Elsevier Inc., pp.e525–e541. Available at: http://dx.doi.org/10.1016/j.ehmc.2013.04.003.

Boas, M., Frederiksen, H., Feldt-Rasmussen, U., Skakkebæk, N.E., Hegedüs, L., Hilsted, L., Juul, A. and Main, K.M., (2010) Childhood exposure to phthalates: Associations with thyroid function, insulin-like growth factor I, and growth. *Environmental Health Perspectives*, 11810, pp.1458–1464.

Bochner, F., Graham, G.G., Cham, B.E., Imhoff, D.M. and Haavisto, T.M., (1981) Salicylate metabolite kinetics after several salicylates. *Clinical Pharmacology and Therapeutics*, 302, pp.266–275.

Boeniger, M.F., Lowry, L.K. and Rosenberg, J., (1993) Interpretation of urine results used to assess chemical exposure with emphasis on creatinine adjustments: A review. *American Industrial Hygiene Association Journal*, 5410, pp.615–627.

Bonora, M., Wieckowski, M.R., Chinopoulos, C., Kepp, O., Kroemer, G., Galluzzi, L. and Pinton, P., (2015) Molecular mechanisms of cell death: Central implication of ATP synthase in mitochondrial permeability transition. *Oncogene*, 3412, pp.1475–1486.

Bonventre, J. V, Vaidya, V.S., Schmouder, R., Feig, P. and Dieterle, F., (2010) Next-generation biomarkers for detecting kidney toxicity. *Nature Biotechnology*, 285, pp.436–440.

Bopp, S.K., Kienzler, A., Richarz, A.-N., van der Linden, Sander Parissis, N., Paini, A. and Worth, A., (2018) *JRC Technical Report: Cross-sector EU approach to combined exposures and effects – elements to consider*. Ispra, Italy.

Boroujerdi, M., (2015) *Pharmacokinetics and toxicokinetics*. Boca Raton: CRC Press, Taylor & Francis Group.

Bosgra, S., Van Eijkeren, J., Bos, P., Zeilmaker, M. and Slob, W., (2012) An improved model to predict physiologically based model parameters and their inter-individual variability from anthropometry. *Critical Reviews in Toxicology*, 429, pp.751–767.

Braithwaite, P.A., Roberts, M.S., Allan, R.J. and Watson, T.R., (1982) Clinical pharmacokinetics of high dose mebendazole in patients treated for cystic hydatid disease. *European Journal of Clinical Pharmacology*, 222, pp.161–169.

Van Breemen, R.B. and Li, Y., (2005) Caco-2 cell permeability assays to measure drug absorption. *Expert Opinion on Drug Metabolism and Toxicology*, 12, pp.175–185.

Breimer, D.D., (1977) Clinical pharmacokinetics of hypnotics. *Clinical*

Pharmacokinetics, 22, pp.93–109.

Breimer, D.D., Zilly, W. and Richter, E., (1975) Pharmacokinetics of hexobarbital in acute hepatitis and after apparent recovery. *Clinical Pharmacology and Therapeutics*, 184, pp.433–440.

Brody, T.M. and Fouts, W., (1956) Action of sodium salicylate and related compounds on tissue metabolism in vitro. *Journal of Pharmacology and Experimental Therapeutics*, 1171, pp.39–51.

Broom, A.J., (2015) *A systems approach to understanding mechanisms of drug induced mitochondrial toxicity*. Imperial College London.

Brown, N.J. and Vaughan, D.E., (1998) Angiotensin-converting enzyme inhibitors. *Circulation*, 9714, pp.1411–1420.

Brown, R.P., Delp, M.D., Lindstedt, S.L., Rhomberg, L.R. and Beliles, R.P., (1997) Physiological parameter values for physiologically based pharmacokinetic models. *Toxicology and Industrial Health*, 134, pp.407–484.

Brune, K., Nuernberg, B. and Schneider, H.T., (1993) Biliary elimination of aspirin after oral and intravenous administration in patients. *Agents and actions. Supplements*, 44, pp.51–7.

Burt, H.J., Neuhoff, S., Almond, L., Gaohua, L., Harwood, M.D., Jamei, M., Rostami-Hodjegan, A., Tucker, G.T. and Rowland-Yeo, K., (2016) Metformin and cimetidine: Physiologically based pharmacokinetic modelling to investigate transporter mediated drug-drug interactions. *European Journal of Pharmaceutical Sciences*, 88, pp.70–82.

Calzavacca, P., May, C.N. and Bellomo, R., (2014) Glomerular haemodynamics, the renal sympathetic nervous system and sepsis-induced acute kidney injury. *Nephrology Dialysis Transplantation*, 2912, pp.2178–2184.

Cattermole, G.N., Leung, P.Y.M., Ho, G.Y.L., Lau, P.W.S., Chan, C.P.Y., Chan, S.S.W., Smith, B.E., Graham, C.A. and Rainer, T.H., (2017) The normal ranges of cardiovascular parameters measured using the ultrasonic cardiac output monitor. *Physiological Reports*, 56, pp.1–9.

CDC (Centers for Disease Control and Prevention), (2018) *About child & teen BMI |*

Healthy weight | CDC. [online] Available at: https://www.cdc.gov/healthyweight/assessing/bmi/childrens_bmi/about_childrens_bmi.html [Accessed 6 Sep. 2019].

Cequier, E., Ionas, A.C., Covaci, A., Marcé, R.M., Becher, G. and Thomsen, C., (2014) Occurrence of a broad range of legacy and emerging flame retardants in indoor environments in Norway. *Environmental Science and Technology*, 4812, pp.6827–6835.

Cequier, E., Sakhi, A.K., Haug, L.S. and Thomsen, C., (2017) Exposure to organophosphorus pesticides in Norwegian mothers and their children: Diurnal variability in concentrations of their biomarkers and associations with food consumption. *Science of the Total Environment*, 590–591, pp.655–662.

Cequier, E., Sakhi, A.K., Marcé, R.M., Becher, G. and Thomsen, C., (2015) Human exposure pathways to organophosphate triesters - A biomonitoring study of mother-child pairs. *Environment International*, 75, pp.159–165.

Cha, S.H., Sekine, T., Fukushima, J., Kanai, Y., Kobayashi, Y., Goya, T. and Endou, H., (2001) Identification and characterization of human organic anion transporter 3 expressing predominantly in the kidney. *Molecular Pharmacology*, 595, pp.1277–1286.

Cha, S.H., Sekine, T., Kusuhara, H., Yu, E., Kim, J.Y., Kim, D.K., Sugiyama, Y., Kanai, Y. and Endou, H., (2000) Molecular cloning and characterization of multispecific organic anion transporter 4 expressed in the placenta. *Journal of Biological Chemistry*, 2756, pp.4507–4512.

Chai, T. and Draxler, R.R., (2014) Root mean square error (RMSE) or mean absolute error (MAE)? – Arguments against avoiding RMSE in the literature. *Geoscientific Model Development*, 73, pp.1247–1250.

Chandorkar, G., Xiao, A., Mouksassi, M.S., Hershberger, E. and Krishna, G., (2015) Population pharmacokinetics of ceftolozane/tazobactam in healthy volunteers, subjects with varying degrees of renal function and patients with bacterial infections. *Journal of Clinical Pharmacology*, 552, pp.230–239.

Chanu, P., Gieschke, R., Charoin, J.E., Pannier, A. and Reigner, B., (2010) Population pharmacokinetic/pharmacodynamic model for C.E.R.A. in both ESA-naïve and ESA-

treated chronic kidney disease patients with renal anemia. *Journal of Clinical Pharmacology*, 505, pp.507–520.

Chen, Y., Jin, J.Y., Mukadam, S., Malhi, V. and Kenny, J.R., (2012) Application of IVIVE and PBPK modeling in prospective prediction of clinical pharmacokinetics: Strategy and approach during the drug discovery phase with four case studies. *Biopharmaceutics & Drug Disposition*, 332, pp.85–98.

Cheng, W. and Ng, C.A., (2017) A permeability-limited physiologically based pharmacokinetic (PBPK) model for perfluorooctanoic acid (PFOA) in male rats. *Environmental Science and Technology*, 5117, pp.9930–9939.

Chevalier, R.L., (1996) Growth factors and apoptosis in neonatal ureteral obstruction. *Journal of the American Society of Nephrology*, 78, pp.1098–1105.

Chiu, W.A. and Slob, W., (2015) A unified probabilistic framework for dose–response assessment of human health effects. *Environmental Health Perspectives*, 12312, pp.1241–1254.

Choi, J., Aarøe Mørck, T., Polcher, A., Knudsen, L.E. and Joas, A., (2015) Review of the state of the art of human biomonitoring for chemical substances and its application to human exposure assessment for food safety. *EFSA Supporting Publications*, EN-724, pp.1–321.

Chrzanowski, F.A., Niebergall, P.J., Mayock, R.L., Taubin, J.M. and Sugita, E.T., (1977) Kinetics of intravenous theophylline. *Clinical Pharmacology and Therapeutics*, 222, pp.188–195.

Coecke, S., Pelkonen, O., Leite, S.B., Bernauer, U., Bessems, J.G.M., Bois, F.Y., Gundert-Remy, U., Loizou, G., Testai, E. and Zaldívar, J.M., (2013) Toxicokinetics as a key to the integrated toxicity risk assessment based primarily on non-animal approaches. *Toxicology in Vitro*, 275, pp.1570–1577.

Cohen Hubal, E.A., Wetmore, B.A., Wambaugh, J.F., El-Masri, H., Sobus, J.R. and Bahadori, T., (2019) Advancing internal exposure and physiologically-based toxicokinetic modeling for 21st-century risk assessments. *Journal of Exposure Science and Environmental Epidemiology*, 291, pp.11–20.

Collins, A.J., Foley, R.N., Gilbertson, D.T. and Chen, S.C., (2015) United States Renal

Data System public health surveillance of chronic kidney disease and end-stage renal disease. *Kidney International Supplements*, 51, pp.2–7.

Cook, J.D., Strauss, K.A., Caplan, Y.H., LoDico, C.P. and Bush, D.M., (2007) Urine pH: The effects of time and temperature after collection. *Journal of Analytical Toxicology*, 318, pp.486–496.

Cornish-Bowden, A., (2015) One hundred years of Michaelis–Menten kinetics. *Perspectives in Science*, 4, pp.3–9.

Council of Europe, (2009) *Consumer Health Protection Committee. Committee of Experts on Materials coming into Contact with Food. Policy Statement concerning Paper and Board Materials and Articles Intended to Come Into Contact with Foodstuffs. Version 4 – 12.02.2009*. [online] Available at: https://www.edqm.eu/sites/default/files/policy_statement_concerning_paper_and_board_materials_and_articles_intended_to_come_into_contact_with_foodstuffs_v4_february_2009.pdf.

Cronin, M.T.D., Enoch, S.J., Mellor, C.L., Przybylak, K.R., Richarz, A.-N. and Madden, J.C., (2017) In silico prediction of organ level toxicity: Linking chemistry to adverse effects. *Toxicological Research*, 333, pp.173–182.

Cronin, M.T.D. and Richarz, A.-N., (2017) Relationship between adverse outcome pathways and chemistry-based in silico models to predict toxicity. *Applied In Vitro Toxicology*, 34, pp.286–297.

Danlami, U., Odunola, M.T., Magaji, G. and Thomas, S.A., (2011) The effect of chloroquine on the pharmacokinetics of chlorpropamide in human volunteers. *African Journal of Pharmacy and Pharmacology*, 514, pp.1682–1686.

Davies, B. and Morris, T., (1993) Physiological parameters in laboratory animals and humans. *Pharmaceutical Research*, 107, pp.1093–1095.

Dawson, M., Braithwaite, P.A., Roberts, M.S. and Watson, T.R., (1985) The pharmacokinetics and bioavailability of a tracer dose of [3H]-mebendazole in man. *British Journal of Clinical Pharmacology*, 191, pp.79–86.

Dayan, A.D., (2003) Albendazole, mebendazole and praziquantel. Review of non-clinical toxicity and pharmacokinetics. *Acta Tropica*, 862–3, pp.141–159.

Deguchi, T., Ohtsuki, S., Otagiri, M., Takanaga, H., Asaba, H., Mori, S. and Terasaki, T., (2002) Major role of organic anion transporter 3 in the transport of indoxyl sulfate in the kidney. *Kidney International*, 615, pp.1760–1768.

Delanaye, P., Schaeffner, E., Ebert, N., Cavalier, E., Mariat, C., Krzesinski, J.M. and Moranne, O., (2012) Normal reference values for glomerular filtration rate: What do we really know? *Nephrology Dialysis Transplantation*, 277, pp.2664–2672.

Denic, A., Glassock, R.J. and Rule, A.D., (2016) Structural and functional changes with the aging kidney. *Advances in Chronic Kidney Disease*, 231, pp.19–28.

Denic, A., Lieske, J.C., Chakkera, H.A., Poggio, E.D., Alexander, M.P., Singh, P., Kremers, W.K., Lerman, L.O. and Rule, A.D., (2017) The substantial loss of nephrons in healthy human kidneys with aging. *Journal of the American Society of Nephrology : JASN*, 281, pp.313–320.

Derry, S., (2000) Risk of gastrointestinal haemorrhage with long term use of aspirin: meta-analysis. *BMJ*, 3217270, pp.1183–1187.

DG Health & Consumers, (2012) *SCHER, SCENIHR, SCCS on Toxicity and assessment of chemical mixtures*. Brussels, BE.

Diamond, G.L., Thayer, W.C. and Choudhury, H., (2003) Pharmacokinetics/pharmacodynamics (PK/PD) modeling of risks of kidney toxicity from exposure to cadmium: Estimates of dietary risks in the U.S. population. *Journal of Toxicology and Environmental Health - Part A*, 6622, pp.2141–2164.

Diaz Ochoa, J.G., Bucher, J., Péry, A.R.R., Zaldivar Comenges, J.M., Niklas, J. and Mauch, K., (2013) A multi-scale modeling framework for individualized, spatiotemporal prediction of drug effects and toxicological risk. *Frontiers in Pharmacology*, 3January, pp.1–11, article 204.

Dickenmann, M., Oettl, T. and Mihatsch, M.J., (2008) Osmotic nephrosis: acute kidney injury with accumulation of proximal tubular lysosomes due to administration of exogenous solutes. *American Journal of Kidney Diseases*, 513, pp.491–503.

Dressman, J.B., Amidon, G.L., Reppas, C. and Shah, V.P., (1998) Dissolution testing as a prognostic tool for oral drug absorption: Immediate release dosage forms. *Pharmaceutical Research*, 151, pp.11–22.

Drew, R., Priestly, B.G. and O'Reilly, W.J., (1977) Hexobarbital pharmacokinetics in rats after ligation of the common bile duct. *The Journal of Pharmacology and Experimental Therapeutics*, 2013, pp.534–540.

Drewe, W.C., Cayley, A., Benz, R.D., Kruhlak, N.L. and Surfraz, M.B., (2014) *Identification of adverse outcome pathways for the nephrotoxicity of nucleoside and nucleotide anti-viral drugs (Poster)*. *SOT, 27th March 2014, Phoenix, USA*.

Drewe, W.C. and Surfraz, M.B., (2015) *Adverse outcome pathways for the nephrotoxicity of non-steroidal anti-inflammatory drugs (Poster)*. *SOT, 22-26 March 2015, San Diego, USA*.

Droz, P.O., Wu, M.M., Cumberland, W.G. and Berode, M., (1989) Variability in biological monitoring of solvent exposure. I Development of a population physiological model. *British Journal of Industrial Medicine*, 467, pp.447–460.

Ducharme, M.P., (2016) Chapter 7: Drug elimination, clearance, and renal clearance. In: L. Shargel and A.B.C. Yu, eds., *Applied Biopharmaceutics & Pharmacokinetics*, 7th ed. New York, USA: McGraw-Hill Education, pp.149–175.

Eaton, D.C. and Pooler, J.P., (2013) *Vander's Renal Physiology*. Eighth ed. New York: McGraw-Hill Medical.

EFSA (European Food Safety Authority), (2005a) Opinion of the Scientific Panel on Food Additives, Flavourings, Processing Aids and Materials in Contact with Food (AFC) on a request from the Commission related to Butylbenzylphthalate (BBP) for use in food contact materials. Question N° EFSA-Q-2003-190. *The EFSA Journal*, 241, pp.1–14.

EFSA (European Food Safety Authority), (2005b) Opinion of the Scientific Panel on Food Additives, Flavourings, Processing Aids and Materials in Contact with Food (AFC) on a request from the Commission related to Di-Butylphthalate (DBP) for use in food contact materials. *The EFSA Journal*, 242, pp.1–17.

EFSA (European Food Safety Authority), (2018) *EFSA OpenFoodTox*. [online] Available at: https://dwh.efsa.europa.eu/bi/asp/Main.aspx?rwtrep=400 [Accessed 23 Nov. 2018].

EFSA Panel on Food Contact Materials, Enzymes, F. and P.A. (CEF), (2015) Scientific

Opinion on the risks to public health related to the presence of bisphenol A (BPA) in foodstuffs. *The EFSA Journal*, 131, p.3978.

Eipel, C., Abshagen, K. and Vollmar, B., (2010) Regulation of hepatic blood flow: The hepatic arterial buffer response revisited. *World Journal of Gastroenterology*, 1648, pp.6046–6057.

Eirin, A., Lerman, A. and Lerman, L.O., (2017) The emerging role of mitochondrial targeting in kidney disease. In: *Handbook of Experimental Pharmacology*. pp.229–250.

El-Sheikh, A.A.K., van den Heuvel, J.J.M.W., Koenderink, J.B. and Russel, F.G.M., (2007) Interaction of nonsteroidal anti-inflammatory drugs with multidrug resistance protein (MRP) 2/ABCC2- and MRP4/ABCC4-mediated methotrexate transport. *Journal of Pharmacology and Experimental Therapeutics*, 3201, pp.229–235.

Ellison, C.M., Piechota, P., Madden, J.C., Enoch, S.J. and Cronin, M.T.D., (2016) Adverse outcome pathway (AOP) informed modeling of aquatic toxicology: QSARs, read-across, and interspecies verification of modes of action. *Environmental Science and Technology*, 507, p.3995−4007.

Emami Riedmaier, A., Burt, H., Abduljalil, K. and Neuhoff, S., (2016) More power to OATP1B1: An evaluation of sample size in pharmacogenetic studies using a rosuvastatin PBPK model for intestinal, hepatic, and renal transporter-mediated clearances. *Journal of Clinical Pharmacology*, 56S7, pp.S132–S142.

Ericsson, J.L.E., Bergstrand, A., Andres, G., Buche, H. and Cinotti, G., (1965) Morphology of the renal tubular epithelium in young, healthy humans. *Acta path. et microbiol scandinav*, March, pp.361–384.

Eriksson, J.K., Neovius, M., Jacobson, S.H., Elinder, C.G. and Hylander, B., (2016) Healthcare costs in chronic kidney disease and renal replacement therapy: A population-based cohort study in Sweden. *BMJ Open*, 610, pp.1–9.

European Commission, (2006) Regulation (EC) No 1907/2006 of the European Parliament and of the Council of 18 December 2006 concerning the Registration, Evaluation, Authorisation and Restriction of Chemicals (REACH), establishing a European Chemicals Agency, amending Directive 1999/4. *Official Journal of the European Union*.

European Commission, (2009) Regulation (EC) No 1223/2009 of the European Parliament and of the Council. *Official Journal of the European Union*, November.

European Commission Scientific Committee on Consumer Safety (SCCS), (2009) *Opinion on Triclosan, COLIPA n° P32*.

European Medicines Agency (EMA), (2018) *Guideline on the reporting of physiologically based pharmacokinetic (PBPK) modelling and simulation, EMA/CHMP/458101/2016*.

Evenepoel, P., (2010) Toxic nephropathy due to drugs and poisons. In: A. Jörres, C. Ronco and J.A. Kellum, eds., *Management of acute kidney problems*. Heidelberg, Germany: Springer, pp.317–328.

Evers, R., Piquette-Miller, M., Polli, J.W., Russel, F.G.M., Sprowl, J.A., Tohyama, K., Ware, J.A., de Wildt, S.N., Xie, W. and Brouwer, K.L.R., (2018) Disease-associated changes in drug transporters may impact the pharmacokinetics and/or toxicity of drugs: A white paper from the International Transporter Consortium. *Clinical Pharmacology & Therapeutics*, 1045, pp.900–915.

Eyler, R.F. and Mueller, B.A., (2010) Antibiotic pharmacokinetic and pharmacodynamic considerations in patients with kidney disease. *Advances in Chronic Kidney Disease*, 175, pp.392–403.

Fabian, E., Gomes, C., Birk, B., Williford, T., Hernandez, T.R., Haase, C., Zbranek, R., van Ravenzwaay, B. and Landsiedel, R., (2019) In vitro-to-in vivo extrapolation (IVIVE) by PBTK modeling for animal-free risk assessment approaches of potential endocrine-disrupting compounds. *Archives of Toxicology*, 932, pp.401–416.

Fàbrega, F., Nadal, M., Schuhmacher, M., Domingo, J.L. and Kumar, V., (2016) Influence of the uncertainty in the validation of PBPK models: A case-study for PFOS and PFOA. *Regulatory Toxicology and Pharmacology*, 77, pp.230–239.

Fanos, V. and Cataldi, L., (2000) Amphotericin B-induced nephrotoxicity: A review. *Journal of Chemotherapy*, 126, pp.463–470.

FAO and WHO (Food and Agriculture Organization of the United Nations. World Health Organization), (2009) *Principles and methods for the risk assessment of chemicals in food*. World Health Organization.

Farooqi, S. and Dickhout, J.G., (2016) Major comorbid disease processes associated with increased incidence of acute kidney injury. *World Journal of Nephrology*, 52, pp.139–146.

Feher, J., (2017) *Quantitative human physiology: An introduction*. Second ed. Cambridge, MA, USA: Academic Press/Elsevier.

Felmlee, M.A., Dave, R.A. and Morris, M.E., (2013) Mechanistic models describing active renal reabsorption and secretion: A simulation-based study. *The AAPS Journal*, 151, pp.278–287.

Felmlee, M.A., Wang, Q., Cui, D., Roiko, S.A. and Morris, M.E., (2010) Mechanistic toxicokinetic model for γ-hydroxybutyric acid: Inhibition of active renal reabsorption as a potential therapeutic strategy. *The AAPS Journal*, 123, pp.407–416.

Fenton, R.A. and Praetorius, J., (2015) Chapter 2: Anatomy of the kidney. In: *Brenner and Rector's The Kidney, 2-Volume Set*, Tenth. Elsevier Inc., pp.42–80.

Ferguson, M.A., Vaidya, V. and Bonventre, J. V., (2008) Biomarkers of nephrotoxic acute kidney injury. *Toxicology*, 2453, pp.182–193.

Ferl, G.Z., Theil, F.-P. and Wong, H., (2016) Physiologically based pharmacokinetic models of small molecules and therapeutic antibodies: A mini-review on fundamental concepts and applications. *Biopharmaceutics & Drug Disposition*, 372, pp.75–92.

Fisher, D.M., Reynolds, K.S., Schmith, V.D., Hsu, J., Sokoll, M.D., Lennon, R.L. and Caldwell, J.E., (1999) The influence of renal function on the pharmacokinetics and pharmacodynamics and simulated time course of doxacurium. *Anesthesia and Analgesia*, 893, pp.786–795.

Fogo, A.B., Lusco, M.A., Najafian, B. and Alpers, C.E., (2017) AJKD Atlas of Renal Pathology: Osmotic tubular injury. *American Journal of Kidney Diseases*, 692, pp.e11–e12.

Folli, F., Guzzi, V., Perego, L., Coletta, D.K., Finzi, G., Placidi, C., La Rosa, S., Capella, C., Socci, C., Lauro, D., Tripathy, D., Jenkinson, C., Paroni, R., Orsenigo, E., Cighetti, G., Gregorini, L., Staudacher, C., Secchi, A., Bachi, A., Brownlee, M. and Fiorina, P., (2010) Proteomics reveals novel oxidative and glycolytic mechanisms in type 1 diabetic

patients' skin which are normalized by kidney-pancreas transplantation. *PloS one*, 53, p.e9923.

Frederiksen, H., Aksglaede, L., Sorensen, K., Nielsen, O., Main, K.M., Skakkebaek, N.E., Juul, A. and Andersson, A.M., (2013) Bisphenol A and other phenols in urine from Danish children and adolescents analyzed by isotope diluted TurboFlow-LC-MS/MS. *International Journal of Hygiene and Environmental Health*, 2166, pp.710–720.

Frederiksen, H., Jensen, T.K., Jørgensen, N., Kyhl, H.B., Husby, S., Skakkebæk, N.E., Main, K.M., Juul, A. and Andersson, A.M., (2014) Human urinary excretion of non-persistent environmental chemicals: An overview of Danish data collected between 2006 and 2012. *Reproduction*, 1474, pp.555–565.

Frederiksen, H., Skakkebæk, N.E. and Andersson, A.M., (2007) Metabolism of phthalates in humans. *Molecular Nutrition and Food Research*, 517, pp.899–911.

Fu, Q., Colgan, S.P. and Shelley, C.S., (2016) Hypoxia: The force that drives chronic kidney disease. *Clinical Medicine and Research*, 141, pp.15–39.

Fung, M., Thornton, A., Mybeck, K., Hsiao-hui Wu, J., Hornbuckle, K. and Muniz, E., (2001) Evaluation of the characteristics of safety withdrawal of prescription drugs from worldwide pharmaceutical markets - 1960 to 1999. *Drug Information Journal*, 351, pp.293–317.

Furst, D.E., Tozer, T.N. and Melmon, K.L., (1979) Salicylate clearance, the resultant of protein binding and metabolism. *Clinical Pharmacology and Therapeutics*, 263, pp.380–389.

Gaganis, P., Miners, J.O., Brennan, J.S., Thomas, A. and Knights, K.M., (2007) Human renal cortical and medullary UDP-Glucuronosyltransferases (UGTs): Immunohistochemical localization of UGT2B7 and UGT1A enzymes and kinetic characterization of S-naproxen glucuronidation. *Journal of Pharmacology and Experimental Therapeutics*, 3232, pp.422–430.

Gaohua, L., Wedagedera, J., Small, B.G., Almond, L., Romero, K., Hermann, D., Hanna, D., Jamei, M. and Gardner, I., (2015) Development of a multicompartment permeability-limited lung PBPK model and its application in predicting pulmonary pharmacokinetics of antituberculosis drugs. *CPT: Pharmacometrics & Systems Pharmacology*, 4October, pp.605–613.

Ghahramani, P., Rowland-Yeo, K., Yeo, W.W., Jackson, P.R. and Ramsay, L.E., (1998) Protein binding of aspirin and salicylate measured by in vivo ultrafiltration. *Clinical Pharmacology and Therapeutics*, 633, pp.285–295.

Giacomini, K.M., Huang, S.-M., Tweedie, D.J. and The International Transporter Consortium, (2010) Membrane transporters in drug development. *Nature Reviews Drug Discovery*, 93, pp.215–236.

González Canga, A., Sahagún Prieto, A.M., Diez Liébana, M.J., Fernández Martínez, N., Sierra Vega, M. and García Vieitez, J.J., (2008) The pharmacokinetics and interactions of ivermectin in humans—A mini-review. *The AAPS Journal*, 101, pp.42–46.

González Canga, A., Sahagún Prieto, A.M., Diez Liébana, M.J., Fernández Martínez, N., Sierra Vega, M. and García Vieitez, J.J., (2009) The pharmacokinetics and metabolism of ivermectin in domestic animal species. *Veterinary Journal*, 1791, pp.25–37.

Goutelle, S., Bourguignon, L., Maire, P.H., Van Guilder, M., Conte Jr., J.E. and Jelliffe, R.W., (2009) Population modeling and Monte Carlo simulation study of the pharmacokinetics and antituberculosis pharmacodynamics of rifampin in lungs. *Antimicrobial Agents and Chemotherapy*, 537, pp.2974–2981.

van der Graaff, M., Vermeulen, N.P.E., Heij, P., Boeijinga, J.K. and Breimer, D.D., (1986) Pharmacokinetics of orally administered hexobarbital in plasma and saliva of healthy subjects. *Biopharmaceutics & Drug Disposition*, 73, pp.265–272.

Grešner, P., Dolník, M., Waczulíková, I., Bryszewska, M., Šikurová, L. and Watala, C., (2006) Increased blood plasma hydrolysis of acetylsalicylic acid in type 2 diabetic patients: A role of plasma esterases. *Biochimica et Biophysica Acta - General Subjects*, 17602, pp.207–215.

Guo, Y., Ni, J., Chen, S., Bai, M., Lin, J., Ding, G., Zhang, Y., Sun, P., Jia, Z., Huang, S., Yang, L. and Zhang, A., (2018) MicroRNA-709 mediates acute tubular injury through effects on mitochondrial function. *Journal of the American Society of Nephrology*, 292, pp.449–461.

Gutknecht, J., (1992) Aspirin, acetaminophen and proton transport through phospholipid bilayers and mitochondrial membranes. *Molecular and Cellular*

Biochemistry, 1141–2, pp.3–8.

Haber, L.T., Dourson, M.L., Allen, B.C., Hertzberg, R.C., Parker, A., Vincent, M.J., Maier, A. and Boobis, A.R., (2018) Benchmark dose (BMD) modeling: Current practice, issues, and challenges. *Critical Reviews in Toxicology*, 485, pp.387–415.

Hakooz, N., Ito, K., Rawden, H., Gill, H., Lemmers, L., Boobis, A.R., Edwards, R.J., Carlile, D.J., Lake, B.G. and Houston, J.B., (2006) Determination of a human hepatic microsomal scaling factor for predicting in vivo drug clearance. *Pharmaceutical Research*, 233, pp.533–539.

Hall, S. and Rowland, M., (1984) Relationship between renal clearance, protein binding and urine flow for digitoxin, a compound of low clearance in the isolated perfused rat kidney. *Journal of Pharmacology and Experimental Therapeutics*, 2281, pp.174–179.

Hallow, K.M. and Gebremichael, Y., (2017) A quantitative systems physiology model of renal function and blood pressure regulation: Model description. *CPT: Pharmacometrics and Systems Pharmacology*, 66, pp.383–392.

Hammond, T.G., Meng, X., Jenkins, R.E., Maggs, J.L., Castelazo, A.S., Regan, S.L., Bennett, S.N.L., Earnshaw, C.J., Aithal, G.P., Pande, I., Kenna, J.G., Stachulski, A. V., Park, B.K. and Williams, D.P., (2014) Mass spectrometric characterization of circulating covalent protein adducts derived from a drug acyl glucuronide metabolite: Multiple albumin adductions in diclofenac patients. *Journal of Pharmacology and Experimental Therapeutics*, 3502, pp.387–402.

Han, X. and Ni, F., (2004) *United States patent, Patent No.: US 6,773,894 B1*.

Hansson, L., Zanchetti, A., Carruthers, S.G., Dahlöf, B., Elmfeldt, D., Julius, S., Ménard, J., Rahn, K.H., Wedel, H. and Westerling, S., (1998) Effects of intensive blood-pressure lowering and low-dose aspirin in patients with hypertension: Principal results of the Hypertension Optimal Treatment (HOT) randomised trial. *The Lancet*, 351, pp.1755–1762.

Haug, L.S., Huber, S., Becher, G. and Thomsen, C., (2011) Characterisation of human exposure pathways to perfluorinated compounds - Comparing exposure estimates with biomarkers of exposure. *Environment International*, 374, pp.687–693.

Hays, S.M., Becker, R.A., Leung, H.W., Aylward, L.L. and Pyatt, D.W., (2007) Biomonitoring equivalents: A screening approach for interpreting biomonitoring results from a public health risk perspective. *Regulatory Toxicology and Pharmacology*, 471, pp.96–109.

HBM4EU, (2019) *The project | HBM4EU - Science and policy for a healthy future*. [online] Available at: https://www.hbm4eu.eu/the-project/ [Accessed 6 Sep. 2019].

Herman, R.J. and Wilkinson, G.R., (1996) Disposition of diazepam in young and elderly subjects after acute and chronic dosing. *British Journal of Clinical Pharmacology*, 422, pp.147–155.

Hewitt, M. and Przybylak, K.R., (2016) In silico models for hepatotoxicity. In: E. Benfenati, ed., *In Silico Methods for Predicting Drug Toxicity. Methods in Molecular Biology*, Volume 142. New York, USA: Humana Press, pp.201–236.

Hinderling, P.H., (1997) Red blood cells: A neglected compartment in pharmacokinetics and pharmacodynamics. *Pharmacological Reviews*, 493, pp.279–295.

Hines, C.J., Hopf, N.B.N., Deddens, J.A., Silva, M.J. and Calafat, A.M., (2011) Estimated daily intake of phthalates in occupationally exposed groups. *Journal of Exposure Science and Environmental Epidemiology*, 212, pp.133–141.

Ho, L., Greene, C.L., Schmidt, A.W. and Huang, L.H., (2004) Cultivation of HEK 293 cell line and production of a member of the superfamily of G-protein coupled receptors for drug discovery applications using a highly efficient novel bioreactor. *Cytotechnology*, 453, pp.117–123.

Hoffman, T.E. and Hanneman, W.H., (2017) Physiologically-based pharmacokinetic analysis of benzoic acid in rats, guinea pigs and humans: Implications for dietary exposures and interspecies uncertainty. *Computational Toxicology*, 3, pp.19–32.

Den Hond, E., Govarts, E., Willems, H., Smolders, R., Casteleyn, L., Kolossa-Gehring, M., Schwedler, G., Seiwert, M., Fiddicke, U., Castaño, A., Esteban, M., Angerer, J., Koch, H.M., Schindler, B.K., Sepai, O., Exley, K., Bloemen, L., Horvat, M., Knudsen, L.E., Joas, A., Joas, R., Biot, P., Aerts, D., Koppen, G., Katsonouri, A., Hadjipanayis, A., Krskova, A., Maly, M., Mørck, T.A., Rudnai, P., Kozepesy, S., Mulcahy, M., Mannion, R., Gutleb, A.C., Fischer, M.E., Ligocka, D., Jakubowski, M., Fátima Reis, M.,

Namorado, S., Gurzau, A.E., Lupsa, I.R., Halzlova, K., Jajcaj, M., Mazej, D., Tratnik, J.S., López, A., Lopez, E., Berglund, M., Larsson, K., Lehmann, A., Crettaz, P. and Schoeters, G., (2015) First steps toward harmonized human biomonitoring in Europe: Demonstration project to perform human biomonitoring on a European scale. *Environmental Health Perspectives*, 1233, pp.255–263.

Houston, J. and Galetin, A., (2008) Methods for predicting in vivo pharmacokinetics using data from in vitro assays. *Current Drug Metabolism*, 99, pp.940–951.

Hoy, W.E., Douglas-Denton, R.N., Hughson, M.D., Cass, A., Johnson, K. and Bertram, J.F., (2003) A stereological study of glomerular number and volume: Preliminary findings in a multiracial study of kidneys at autopsy. *Kidney International*, 63, pp.S31–S37.

Hsu, V., Vieira, M.D.L.T., Zhao, P., Zhang, L., Zheng, J.H., Nordmark, A., Berglund, E.G., Giacomini, K.M. and Huang, S.M., (2014) Towards quantitation of the effects of renal impairment and probenecid inhibition on kidney uptake and efflux transporters, using physiologically based pharmacokinetic modelling and simulations. *Clinical Pharmacokinetics*, 533, pp.283–293.

Hsueh, C.H., Hsu, V., Zhao, P., Zhang, L., Giacomini, K.M. and Huang, S.M., (2018) PBPK modeling of the effect of reduced kidney function on the pharmacokinetics of drugs excreted renally by organic anion transporters. *Clinical Pharmacology and Therapeutics*, 1033, pp.485–492.

Huang, W. and Isoherranen, N., (2018) Development of a dynamic physiologically based mechanistic kidney model to predict renal clearance. *CPT: Pharmacometrics and Systems Pharmacology*, 79, pp.593–602.

Hudkins, K.L., Giachelli, C.M., Cui, Y., Couser, W.G., Johnson, R.J. and Alpers, C.E., (1999) Osteopontin expression in fetal and mature human kidney. *Journal of the American Society of Nephrology*, 103, pp.444–457.

Huupponen, R. and Lammintausta, R., (1981) Chlorpropamide bioavailability and pharmacokinetics. *International Journal of Clinical Pharmacology, Therapy and Toxicology*, 197, pp.331–333.

ICH, (2000) *ICH Harmonized Tripartite Guideline 'Safety Pharmacology Studies For Human Pharmaceuticals S7A'*. [online] International Conference on Harmonisation

of Technical Requirements for Registration of Pharmaceuticals for Human Use. Available at: http://www.ich.org/fileadmin/Public_Web_Site/ICH_Products/Guidelines/Safety/S7A/Step4/S7A_Guideline.pdf [Accessed 25 Jan. 2018].

Iharada, M., Miyaji, T., Fujimoto, T., Hiasa, M., Anzai, N., Omote, H. and Moriyama, Y., (2010) Type 1 sodium-dependent phosphate transporter (SLC17A1 protein) is a Cl- dependent urate exporter. *Journal of Biological Chemistry*, 28534, pp.26107–26113.

Ijaz, A., Bhatti, H.N., Rasheed, S., Sadaf, B. and Nawaz, R., (2003) Pharmacokinetic study of aspirin in healthy female volunteers. *Pakistan Journal of Biological Sciences*, 616, pp.1404–1407.

Imai, T., Taketani, M., Shii, M., Hosokawa, M. and Chiba, K., (2006) Substrate specificity of carboxylesterase isozymes and their contribution to hydrolase activity in human liver and small intestine. *Drug Metabolism and Disposition*, 3410, pp.1734–1741.

Ingalls, B.P. and Sauro, H.M., (2003) Sensitivity analysis of stoichiometric networks: An extension of metabolic control analysis to non-steady state trajectories. *Journal of Theoretical Biology*, 2221, pp.23–36.

IPCS WHO, (2010) *Characterization and application of physiologically based pharmacokinetic models in risk assessment*. World Health Organization.

IPCS WHO, (2014) *Harmonization Project Document 11: Guidance document on evaluating and expressing uncertainty in hazard characterization*. World Health Organization.

Ishimoto, Y. and Inagi, R., (2016) Mitochondria: A therapeutic target in acute kidney injury. *Nephrology Dialysis Transplantation*, 317, pp.1062–1069.

ITER, (2019) *International Toxicity Estimates for Risk (ITER) Database*. [online] Available at: https://toxnet.nlm.nih.gov/newtoxnet/iter.htm [Accessed 6 Sep. 2019].

Izzo, V., Bravo-San Pedro, J.M., Sica, V., Kroemer, G. and Galluzzi, L., (2016) Mitochondrial permeability transition: New findings and persisting uncertainties. *Trends in Cell Biology*, 269, pp.655–667.

Jakobsson, S. V and Cinti, D.L., (1973) Studies on the cytochrome P-450-containing

mono-oxygenase system in human kidney cortex microsomes. *Journal of Pharmacology and Experimental Therapeutics*, 1852, pp.226–234.

Jamei, M., Dickinson, G.L. and Rostami-Hodjegan, A., (2009) A framework for assessing inter-individual variability in pharmacokinetics using virtual human populations and integrating general knowledge of physical chemistry, biology, anatomy, physiology and genetics: A tale of 'bottom-up' vs 'top-down' recognition. *Drug Metabolism and Pharmacokinetics*, 241, pp.53–75.

Janků, I., (1993) Physiological modelling of renal drug clearance. *European Journal of Clinical Pharmacology*, 446, pp.513–519.

John, R. and Herzenberg, A.M., (2009) Renal toxicity of therapeutic drugs. *Journal of Clinical Pathology*, 626, pp.505–515.

Johnson, C.L., Dohrmann, S.M., Burt, V.L. and Mohadjer, L.K., (2014) National health and nutrition examination survey: Sample design, 2011-2014. *Vital and Health Statistics. Series 2, Data Evaluation and Methods Research*, 162, pp.1–33.

Jones, A.W. and Larsson, H., (2004) Distribution of diazepam and nordiazepam between plasma and whole blood and the influence of hematocrit. *Therapeutic Drug Monitoring*, 264, pp.380–385.

Jones, H.M., Gardner, I.B., Collard, W.T., Stanley, P.J., Oxley, P., Hosea, N.A., Plowchalk, D., Gernhardt, S., Lin, J., Dickins, M., Rahavendran, S.R., Jones, B.C., Watson, K.J., Pertinez, H., Kumar, V. and Cole, S., (2011) Simulation of human intravenous and oral pharmacokinetics of 21 diverse compounds using physiologically based pharmacokinetic modelling. *Clinical Pharmacokinetics*, 505, pp.331–347.

Jones, H.M., Parrott, N., Jorga, K. and Lave, T., (2006) A novel strategy for physiologically based predictions of human pharmacokinetics. *Clinical Pharmacokinetics*, 455, pp.511–542.

Jones, H.M. and Rowland-Yeo, K., (2013) Basic concepts in physiologically based pharmacokinetic modeling in drug discovery and development. *CPT: Pharmacometrics & Systems Pharmacology*, 2, pp.1–12.

Jongeneelen, F.J. and ten Berge, W., (2011a) A generic, cross-chemical predictive

PBTK model with multiple entry routes running as application in MS Excel; design of the model and comparison of predictions with experimental results. *Annals of Occupational Hygiene*, 558, pp.841–864.

Jongeneelen, F.J. and ten Berge, W., (2011b) *IndusChemFate: A multi-chemical PBTK-model in MS-Excel applicable for workers, consumers and experimental animals. User manual, version 2.00*. [online] Available at: http://cefic-lri.org/toolbox/induschemfate/ [Accessed 25 Oct. 2018].

Judson, R.S., Kavlock, R.J., Setzer, R.W., Cohen Hubal, E.A., Martin, M.T., Knudsen, T.B., Houck, K.A., Thomas, R.S., Wetmore, B.A. and Dix, D.J., (2011) Estimating toxicity-related biological pathway altering doses for high-throughput chemical risk assessment. *Chemical Research in Toxicology*, 244, pp.451–462.

Kaissling, B. and Kriz, W., (2011) Morphology of the loop of Henle, distal tubule, and collecting duct. In: R. Terjung, ed., *Comprehensive Physiology*. Hoboken, NJ, USA: John Wiley & Sons, Inc., pp.109–167.

Kaplan, S.A., Jack, M.L., Alexander, K. and Weinfeld, R.E., (1973) Pharmacokinetic profile of diazepam in man following single intravenous and oral and chronic oral administrations. *Journal of Pharmaceutical Sciences*, 6211, pp.1789–1796.

Katayama, K., Ohtani, H., Kawabe, T., Mizuno, H., Endoh, M., Kakemi, M. and Koizumi, T., (1990) Kinetic studies on drug disposition in rabbits. I. Renal excretion of iodopyracet and sulfamethizole. *Journal of Pharmacobio-Dynamics*, 132, pp.97–107.

Katsube, T., Wajima, T., Ishibashi, T., Arjona Ferreira, J.C. and Echols, R., (2017) Pharmacokinetic/pharmacodynamic modeling and simulation of cefiderocol, a parenteral siderophore cephalosporin, for dose adjustment based on renal function. *Antimicrobial Agents and Chemotherapy*, 611, pp.1–12, e01381-16.

Kawai, R., Lemaire, M., Steimer, J.-L., Bruelisauer, A., Niederberger, W. and Rowland, M., (1994) Physiologically based pharmacokinetic study on a cyclosporin derivative, SDZ IMM 125. *Journal of Pharmacokinetics and Biopharmaceutics*, 225, pp.327–365.

Kerr, M., Bray, B., Medcalf, J., O'Donoghue, D.J. and Matthews, B., (2012) Estimating the financial cost of chronic kidney disease to the NHS in England. *Nephrology Dialysis Transplantation*, 27Suppl. 3, pp.iii73–iii80.

Khamdang, S., Takeda, M., Noshiro, R., Narikawa, S., Enomoto, A., Anzai, N., Piyachaturawat, P. and Endou, H., (2002) Interactions of human organic anion transporters and human organic cation transporters with nonsteroidal anti-inflammatory drugs. *Journal of Pharmacology and Experimental Therapeutics*, 3032, pp.534–539.

Kienzler, A., Bopp, S.K., van der Linden, S., Berggren, E. and Worth, A., (2016) Regulatory assessment of chemical mixtures: Requirements, current approaches and future perspectives. *Regulatory Toxicology and Pharmacology*, 80, pp.321–334.

Kim, J.S., He, L. and Lemasters, J.J., (2003) Mitochondrial permeability transition: A common pathway to necrosis and apoptosis. *Biochemical and Biophysical Research Communications*, 3043, pp.463–470.

Kirch, W. and Görg, K.G., (1982) Clinical pharmacokinetics of atenolol - A review. *European Journal of Drug Metabolism and Pharmacokinetics*, 72, pp.81–91.

Klaassen, C.D. ed., (2008) *Casarett and Doull's toxicology: The basic science of poisons*. Seventh ed. New York, USA: McGraw-Hill Medical.

Knepper, M.A., Danielson, R.A., Saidel, G.M. and Post, R.S., (1977) Quantitative analysis of renal medullary anatomy in rats and rabbits. *Kidney International*, 125, pp.313–323.

Knights, K.M. and Miners, J.O., (2010) Renal UDP-glucuronosyltransferases and the glucuronidation of xenobiotics and endogenous mediators. *Drug Metabolism Reviews*, 421, pp.60–70.

Knights, K.M., Spencer, S.M., Fallon, J.K., Chau, N., Smith, P.C. and Miners, J.O., (2016) Scaling factors for the in vitro-in vivo extrapolation (IV-IVE) of renal drug and xenobiotic glucuronidation clearance. *British Journal of Clinical Pharmacology*, 816, pp.1153–1164.

Kodner, C.M. and Kudrimoti, A., (2003) Diagnosis and management of acute interstitial nephritis. *American Family Physician*, 6712, pp.2527–2534.

Kojima, S., Shida, M., Tanaka, K.E., Takano, H., Yokoyama, H. and Kuramochi, M., (2001) Renal macrostructure and cortical circulation in hypertension assessed by dynamic computed tomography. *American Journal of Hypertension*, 146 I, pp.516–

523.

Komiya, I., (1986) Urine flow dependence of renal clearance and interrelation of renal reabsorption and physicochemical properties of drugs. *Drug Metabolism and Disposition*, 142, pp.239–245.

Komiya, I., (1987) Urine flow-dependence and interspecies variation of the renal reabsorption of sulfanilamide. *Journal of Pharmacobio-Dynamics*, 101, pp.1–7.

Kramer, N.I., (2010) *Measuring, modeling, and increasing the free concentration of test chemicals in cell assays*. *Utrecht University*. Utrecht University.

Krishnan, K. and Andersen, M.E., (2001) Physiologically based pharmacokinetic modeling in toxicology. In: A.W. Hayes, ed., *Principles and Methods of Toxicology*, Fourth. Philadelphia, PA, USA: Taylor & Francis, pp.193–241.

Krishnan, K. and Andersen, M.E., (2007) Physiologically-based pharmacokinetic and toxicokinetic models. In: W.A. Hayes, ed., *Principles and Methods of Toxicology*, Fifth. New York, NY, USA: Informa Healthcare, pp.231–292.

Krishnan, K., Clewell III, H.J. and Andersen, M.E., (1994) Physiologically based pharmacokinetic analyses of simple mixtures. *Environmental Health Perspectives*, 102Suppl 9, pp.151–155.

Krishnan, K., Crouse, L.C.B., Bazar, M.A., Major, M.A. and Reddy, G., (2009) Physiologically based pharmacokinetic modeling of cyclotrimethylenetrinitramine in male rats. *Journal of Applied Toxicology*, 297, pp.629–637.

Krishnan, K., Gagné, M., Nong, A., Aylward, L.L. and Hays, S.M., (2010a) Biomonitoring Equivalents for bisphenol A (BPA). *Regulatory Toxicology and Pharmacology*, 581, pp.18–24.

Krishnan, K., Gagné, M., Nong, A., Aylward, L.L. and Hays, S.M., (2010b) Biomonitoring Equivalents for triclosan. *Regulatory Toxicology and Pharmacology*, 581, pp.10–17.

Krishnan, N. and Perazella, M.A., (2015) Drug-induced acute interstitial nephritis: Pathology, pathogenesis, and treatment. *Iranian Journal of Kidney Diseases*, 91, pp.3–13.

Kröning, R., Katz, D., Lichtenstein, A.K. and Nagami, G.T., (1999) Differential effects of cisplatin in proximal and distal renal tubule epithelial cell lines. *British Journal of Cancer*, 792, pp.293–299.

Kuehl, G.E., Bigler, J., Potter, J.D. and Lampe, J.W., (2006) Glucuronidation of the aspirin metabolite salicylic acid by expressed UDP-glucuronosyltransferases and human liver microsomes. *Drug Metabolism and Disposition*, 342, pp.199–202.

Kusuhara, H. and Sugiyama, Y., (2009) In vitro-in vivo extrapolation of transporter-mediated clearance in the liver and kidney. *Drug Metabolism and Pharmacokinetics*, 241, pp.37–52.

Kvalseth, T.O., (1985) Cautionary note about R-squared. *The American Statistician*, 394, pp.279–285.

Lagarias, J.C., Reeds, J.A., Wright, M.H. and Wright, P.E., (1998) Convergence properties of the Nelder–Mead simplex method in low dimensions. *SIAM Journal on Optimization*, 91, pp.112–147.

Lagas, M., Lerk, C.F. and Breimer, D.D., (1980) Increased gastro-intestinal absorption of hexobarbital by hydrophilization. *Pharmaceutisch Weekblad Scientific Edition*, 2, pp.541–547.

Lash, L.H., Putt, D.A. and Cai, H., (2008) Drug metabolism enzyme expression and activity in primary cultures of human proximal tubular cells. *Toxicology*, 2441, pp.56–65.

Layton, A.T., (2013) Mathematical modeling of kidney transport. *Wiley Interdisciplinary Reviews: Systems Biology and Medicine*, 55, pp.557–573.

Leahy, D.E., Lynch, J., Finney, R.E. and Taylor, D.C., (1994) Estimation of sieving coefficients of convective absorption of drugs in perfused rat jejunum. *Journal of Pharmacokinetics and Biopharmaceutics*, 225, pp.411–429.

Leahy, D.E., Lynch, J. and Taylor, D.C., (1989) Mechanisms of absorption of small molecules. In: L. Prescott and W. Nimmo, eds., *Novel drug delivery and its therapeutic applications*. Chichester, UK: John Wiley & Sons, Ltd.

Lee, S., Kang, Y.-M., Park, H., Dong, M.-S., Shin, J.-M. and No, K.T., (2013) Human nephrotoxicity prediction models for three types of kidney injury based on data sets

of pharmacological compounds and their metabolites. *Chemical Research in Toxicology*, 2611, pp.1652–1659.

Lemasters, J.J., Nieminen, A.-L., Qian, T., Trost, L.C., Elmore, S.P., Nishimura, Y., Crowe, R.A., Cascio, W.E., Bradham, C.A., Brenner, D.A. and Herman, B., (1998) The mitochondrial permeability transition in cell death: A common mechanism in necrosis, apoptosis and autophagy. *Biochimica et Biophysica Acta - Bioenergetics*, 13661–2, pp.177–196.

Leopold, G., Pabst, J., Ungethüm, W. and Bühring, K.-U., (1986) Basic pharmacokinetics of bisoprolol, a new highly beta 1-selective adrenoceptor antagonist. *Journal of Clinical Pharmacology*, 268, pp.616–621.

Leung, H.-W., (1992) Use of physiologically based pharmacokinetic models to establish biological exposure indexes. *American Industrial Hygiene Association Journal*, 536, pp.369–374.

Levy, G., (1965) Pharmacokinetics of salicylate elimination in man. *Journal of pharmaceutical sciences*, 547, pp.959–67.

Levy, G. and Tsuchiya, T., (1972) Salicylate accumulation kinetics in man. *New England Journal of Medicine*, 2879, pp.430–432.

Li, G., Wang, K., Chen, R., Zhao, H., Yang, J. and Zheng, Q., (2012) Simulation of the pharmacokinetics of bisoprolol in healthy adults and patients with impaired renal function using whole-body physiologically based pharmacokinetic modeling. *Acta Pharmacologica Sinica*, 3311, pp.1359–1371.

Li, M., Zou, P., Tyner, K. and Lee, S., (2017) Physiologically based pharmacokinetic (PBPK) modeling of pharmaceutical nanoparticles. *AAPS Journal*, 191, pp.26–42.

Liagkouridis, I., Cequier, E., Lazarov, B., Palm Cousins, A., Thomsen, C., Stranger, M. and Cousins, I.T., (2017) Relationships between estimated flame retardant emissions and levels in indoor air and house dust. *Indoor Air*, 273, pp.650–657.

Liao, K.H., Tan, Y.-M. and Clewell, H.J., (2007) Development of a screening approach to interpret human biomonitoring data on volatile organic compounds: Reverse dosimetry on biomonitoring data for trichloroethylene. *Risk Analysis*, 275, pp.1223–1236.

Lien, E.J., (1975) Chapter 3: Structure-absorption-distribution relationships: Significance for drug design. In: E.J. Ariëns, ed., *Drug design: Medicinal chemistry: A series of monographs, Volume V*. New York, USA: Acadmic Press, Inc., pp.81–132.

Lopez-Novoa, J.M., Quiros, Y., Vicente, L., Morales, A.I. and Lopez-Hernandez, F.J., (2011) New insights into the mechanism of aminoglycoside nephrotoxicity: An integrative point of view. *Kidney International*, 79, pp.33–45.

Louisse, J., de Jong, E., van de Sandt, J.J.M., Blaauboer, B.J., Woutersen, R.A., Piersma, A.H., Rietjens, I.M.C.M. and Verwei, M., (2010) The use of in vitro toxicity data and physiologically based kinetic modeling to predict dose-response curves for in vivo developmental toxicity of glycol ethers in rat and man. *Toxicological Sciences*, 1182, pp.470–484.

Low, Y., Uehara, T., Minowa, Y., Yamada, H., Ohno, Y., Urushidani, T., Sedykh, A., Muratov, E., Kuz'min, V., Fourches, D., Zhu, H., Rusyn, I. and Tropsha, A., (2011) Predicting drug-induced hepatotoxicity using QSAR and toxicogenomics approaches. *Chemical Research in Toxicology*, 248, pp.1251–1262.

Lukacz, E.S., Sampselle, C., Gray, M., MacDiarmid, S., Rosenberg, M., Ellsworth, P. and Palmer, M.H., (2011) A healthy bladder: A consensus statement. *International Journal of Clinical Practice*, 6510, pp.1026–1036.

Luque, Y., Louis, K., Jouanneau, C., Placier, S., Esteve, E., Bazin, D., Rondeau, E., Letavernier, E., Wolfromm, A., Gosset, C., Boueilh, A., Burbach, M., Frère, P., Verpont, M.-C., Vandermeersch, S., Langui, D., Daudon, M., Frochot, V. and Mesnard, L., (2017) Vancomycin-associated cast nephropathy. *Journal of the American Society of Nephrology*, 286, pp.1723–1728.

Madden, J.C., Pawar, G., Cronin, M.T.D., Webb, S.D., Tan, Y.-M. and Paini, A., (2019) In silico resources to assist in the development and evaluation of physiologically-based kinetic models. *Computational Toxicology*, 11, pp.33–49.

Madden, J.C., Pletz, J., Webb, S.D., Enoch, S.J. and Cronin, M.T.D., (2017) Identifying potential liver toxicants using in vitro and in silico methods in a weight-of-evidence based approach. *Toxicology Letters*, 280, p.S133.

Madsen, K.M., Clapp, W.L. and Verlander, J.W., (1988) Structure and function of the inner medullary collecting duct. *Kidney International*, 344, pp.441–454.

Margaillan, G., Rouleau, M., Fallon, J.K., Caron, P., Villeneuve, L., Turcotte, V., Smith, P.C., Joy, M.S. and Guillemette, C., (2015) Quantitative profiling of human renal UDP-glucuronosyltransferases and glucuronidation activity: A comparison of normal and tumoral kidney tissues. *Drug Metabolism and Disposition*, 434, pp.611–619.

Markowitz, G.S. and Perazella, M.A., (2005) Drug-induced renal failure: A focus on tubulointerstitial disease. *Clinica Chimica Acta*, 3511–2, pp.31–47.

Martens, M.E., Chang, C.H. and Lee, C.P., (1986) Reye's syndrome: Mitochondrial swelling and Ca2+ release induced by Reye's plasma, allantoin, and salicylate. *Archives of Biochemistry and Biophysics*, 2442, pp.773–786.

Martin, S.A., McLanahan, E.D., Bushnell, P.J., Hunter, E.S. and El-Masri, H., (2015) Species extrapolation of life-stage physiologically-based pharmacokinetic (PBPK) models to investigate the developmental toxicology of ethanol using in vitro to in vivo (IVIVE) methods. *Toxicological Sciences*, 1432, pp.512–535.

Martins, J., Kroo, I. and Alonso, J., (2000) An automated method for sensitivity analysis using complex variables. In: *38th Aerospace Sciences Meeting and Exhibit*. Reston, Virigina: American Institute of Aeronautics and Astronautics, pp.1–12.

Martins, J.R.R.A., Sturdza, P. and Alonso, J.J., (2001) The connection between the complex-step derivative approximation and algorithmic differentiation. In: *39th Aerospace Sciences Meeting and Exhibit*. Reno, NV, USA: American Institute of Aeronautics and Astronautics, pp.1–11.

Mason, W.D., Winer, N., Kochak, G., Cohen, I. and Bell, R., (1979) Kinetics and absolute bioavailability of atenolol. *Clinical Pharmacology and Therapeutics*, 254, pp.408–415.

MathWorks, (2019a) *Evaluating goodness of fit - MATLAB & Simulink*. [online] Available at: https://uk.mathworks.com/help/curvefit/evaluating-goodness-of-fit.html [Accessed 10 Jan. 2019].

MathWorks, (2019b) *ode15s*. [online] Available at: https://uk.mathworks.com/help/matlab/ref/ode15s.html [Accessed 28 Jan. 2019].

MathWorks, (2019c) *Pharmacokinetic/pharmacodynamic (PK/PD) model*. [online] Available at: https://www.mathworks.com/discovery/pharmacokinetic.html

[Accessed 28 Jan. 2019].

MathWorks, (2019d) *SimBiology*. [online] Available at: https://uk.mathworks.com/help/simbio/index.html [Accessed 28 Jan. 2019].

Matsson, P., Englund, G., Ahlin, G., Bergstrom, C.A.S., Norinder, U. and Artursson, P., (2007) A global drug inhibition pattern for the human ATP-binding cassette transporter breast cancer resistance protein (ABCG2). *Journal of Pharmacology and Experimental Therapeutics*, 3231, pp.19–30.

Maunsbach, A.B. and Christensen, E.I., (2011) Functional ultrastructure of the proximal tubule. In: R. Terjung, ed., *Comprehensive Physiology*. Hoboken, NJ, USA: John Wiley & Sons, Inc., pp.41–107.

Mayer, J.M., Hall, S.D. and Rowland, M., (1988) Relationship between lipophilicity and tubular reabsorption for a series of 5-alkyl-5-ethylbarbituric acids in the isolated perfused rat kidney preparation. *Journal of Pharmaceutical Sciences*, 774, pp.359–364.

Mayo Clinic, (2019) *Daily aspirin therapy: Understand the benefits and risks*. [online] Available at: https://www.mayoclinic.org/diseases-conditions/heart-disease/in-depth/daily-aspirin-therapy/art-20046797 [Accessed 13 Jul. 2019].

McDowell, A.J., (1971) The health and nutrition examination survey. *HSMHA health reports*, 867, pp.592–595.

McGinnity, D.F., Soars, M.G., Urbanowicz, R.A. and Riley, R.J., (2004) Evaluation of fresh and cryopreserved hepatocytes as in vitro drug metabolism tools for the prediction of metabolic clearance. *Drug Metabolism and Disposition*, 3211, pp.1247–1253.

MedicineNet, (2019) *Migraine a-z list: Aspirin*. [online] Available at: https://www.medicinenet.com/acetylsalicylic_acid/article.htm#which_drugs_or_supplements_interact_with_aspirin [Accessed 13 Jul. 2019].

Mehta, R.L., Pascual, M.T., Soroko, S., Savage, B.R., Himmelfarb, J., Ikizler, T.A., Paganini, E.P. and Chertow, G.M., (2004) Spectrum of acute renal failure in the intensive care unit: The PICARD experience. *Kidney International*, 664, pp.1613–1621.

Ménochet, K., Kenworthy, K.E., Houston, J.B. and Galetin, A., (2012a) Simultaneous assessment of uptake and metabolism in rat hepatocytes: A comprehensive mechanistic model. *Journal of Pharmacology and Experimental Therapeutics*, 3411, pp.2–15.

Ménochet, K., Kenworthy, K.E., Houston, J.B. and Galetin, A., (2012b) Use of mechanistic modeling to assess interindividual variability and interspecies differences in active uptake in human and rat hepatocytes. *Drug Metabolism and Disposition*, 409, pp.1744–1756.

Miller, N.A., Reddy, M.B., Heikkinen, A.T., Lukacova, V. and Parrott, N., (2019) Physiologically based pharmacokinetic modelling for first-in-human predictions: An updated model building strategy illustrated with challenging industry case studies. *Clinical Pharmacokinetics*, 586, pp.727–746.

Milne, M.D., Scribner, B.H. and Crawford, M.A., (1958) Non-ionic diffusion and the excretion of weak acids and bases. *The American Journal of Medicine*, 245, pp.709–729.

Min, J.S. and Bae, S.K., (2017) Prediction of drug–drug interaction potential using physiologically based pharmacokinetic modeling. *Archives of Pharmacal Research*, 4012, pp.1356–1379.

Miners, J., Grgurinovich, N., Whitehead, A., Robson, R. and Birkett, D., (1986) Influence of gender and oral contraceptive steroids on the metabolism of salicylic acid and acetylsalicylic acid. *British Journal of Clinical Pharmacology*, 222, pp.135–142.

Mingatto, F.E., Santos, A.C., Uyemura, S.A., Jordani, M.C. and Curti, C., (1996) In vitro interaction of nonsteroidal anti-inflammatory drugs on oxidative phosphorylation of rat kidney mitochondria: Respiration and ATP synthesis. *Archives of Biochemistry and Biophysics*, 3342, pp.303–308.

Mingeot-Leclercq, M.-P. and Tulkens, P.M., (1999) Aminoglycosides: Nephrotoxicity. *Antimicrobial Agents and Chemotherapy*, 435, pp.1003–1012.

Mofenson, H.C., Caraccio, T.R., McGuigan, M. and Greensher, J., (2016) Medical toxicology. In: E.T. Bope and R.D. Kellerman, eds., *Conn's Current Therapy 2016*, 2016th ed. Philadelphia, PA, USA: Elsevier, pp.1203–1255.

Moos, R.K., Angerer, J., Dierkes, G., Brüning, T. and Koch, H.M., (2016) Metabolism and elimination of methyl, iso- and n-butyl paraben in human urine after single oral dosage. *Archives of Toxicology*, 9011, pp.2699–2709.

Moos, R.K., Apel, P., Schröter-Kermani, C., Kolossa-Gehring, M., Brüning, T. and Koch, H.M., (2017) Daily intake and hazard index of parabens based upon 24 h urine samples of the German Environmental Specimen Bank from 1995 to 2012. *Journal of Exposure Science and Environmental Epidemiology*, 27, pp.591–600.

Mori, K., Saito, R., Nakamaru, Y., Shimizu, M. and Yamazaki, H., (2016) Physiologically based pharmacokinetic-pharmacodynamic modeling to predict concentrations and actions of sodium-dependent glucose transporter 2 inhibitor canagliflozin in human intestines and renal tubules. *Biopharmaceutics & Drug Disposition*, 378, pp.491–506.

Morita, N., Kusuhara, H., Sugiyama, Y., Sekine, T. and Endou, H., (2001) Functional characterization of rat organic anion transporter 2 in LLC-PK1 cells. *Journal of Pharmacology and Experimental Therapeutics*, 2983, pp.1179–1184.

Moss, D.M., Domanico, P., Watkins, M., Park, S., Randolph, R., Wring, S., Rajoli, R.K.R., Hobson, J., Rannard, S., Siccardi, M. and Owen, A., (2017) Simulating intestinal transporter and enzyme activity in a physiologically based pharmacokinetic model for tenofovir disoproxil fumarate. *Antimicrobial Agents and Chemotherapy*, 617.

Motojima, M., Hosokawa, A., Yamato, H., Muraki, T. and Yoshioka, T., (2002) Uraemic toxins induce proximal tubular injury via organic anion transporter 1-mediated uptake. *British Journal of Pharmacology*, 1352, pp.555–563.

Mulay, S.R. and Anders, H.-J., (2017) Crystal nephropathies: Mechanisms of crystal-induced kidney injury. *Nature Reviews Nephrology*, 134, pp.226–240.

Mundform, D.J., Schaffer, J., Kim, M.-J., Shaw, D., Thongteeraparp, A., Preecha, C. and Supawan, P., (2011) Number of replications required in Monte Carlo simulation studies: A synthesis of four studies. *Journal of Modern Applied Statistical Methods*, 101, pp.19–28.

Munger, K.A., Maddox, D.A., Brenner, B.M. and Kost Jr, C.K., (2015) Chapter 3: The renal circulations and glomerular ultrafiltration. In: K. Skorecki, G.M. Chertow, P.A. Marsden, M.W. Taal, A.S.L. Yu and V. Luyckx, eds., *Brenner and Rector's The Kidney, 2-Volume Set*, Tenth. Philadelphia, PA, USA: Elsevier Inc., pp.83–111.

Naesens, M., Kuypers, D.R.J. and Sarwal, M., (2009) Calcineurin inhibitor nephrotoxicity. *Clinical Journal of the American Society of Nephrology*, 42, pp.481–508.

Najafi, A., Sobhanardakani, S. and Marjani, M., (2013) Exploring QSAR for antimalarial activities and drug distribution within blood of a series of 4-aminoquinoline drugs using genetic-MLR. *Journal of Chemistry*, 2013, pp.1–12, article ID 560415.

National Research Council, (2009) *Science and decisions: Advancing risk assessment*. Washington, D.C.: National Academies Press.

Naughton, C.A., (2008) Drug-induced nephrotoxicity. *American Family Physician*, 786, pp.743–750.

Navar, L.G., (2009) Glomerular permeability: A never-ending saga. *American Journal of Physiology - Renal Physiology*, 2966, pp.F1266-1268.

Needs, C.J. and Brooks, P.M., (1985) Clinical pharmacokinetics of the salicylates. *Clinical Pharmacokinetics*, 102, pp.164–177.

Neuhoff, S., Artursson, P., Zamora, I. and Ungell, A.L., (2006) Impact of extracellular protein binding on passive and active drug transport across Caco-2 cells. *Pharmaceutical Research*, 232, pp.350–359.

Neuhoff, S., Gaohua, L., Burt, H., Jamei, M., Li, L., Tucker, G.T. and Rostami-Hodjegan, A., (2013) Accounting for transporters in renal clearance: Towards a mechanistic kidney model (Mech KiM). In: Y. Sugiyama and B. Steffansen, eds., *Transporters in drug development: Discovery, optimization, clinical study and regulation*. New York, USA: Springer, pp.155–177.

Neuvonen, P.J., Kärkkäinen, S. and Lehtovaara, R., (1987) Pharmacokinetics of chloropropamide in epileptic patients: Effects of enzyme induction and urine pH on chlorpropamide elimination. *European Journal of Clinical Pharmacology*, 323, pp.297–301.

NHS, (2018) *Medicines A to Z: Low-dose aspirin*. [online] Available at: https://www.nhs.uk/medicines/low-dose-aspirin/ [Accessed 13 Jul. 2019].

Nozaki, Y., Kusuhara, H., Kondo, T., Iwaki, M., Shiroyanagi, Y., Nakayama, H., Horita, S., Nakazawa, H., Okano, T. and Sugiyama, Y., (2007) Species difference in the

inhibitory effect of nonsteroidal anti-inflammatory drugs on the uptake of methotrexate by human kidney slices. *Journal of Pharmacology and Experimental Therapeutics*, 3223, pp.1162–1170.

NRC (National Research Council), (2007) *Toxicity testing in the 21st century: A vision and a strategy. Committee on toxicity testing and assessment of environmental agents*. Washington, D.C., USA.

Nyengaard, J.R. and Bendtsen, T.F., (1992) Glomerular number and size in relation to age, kidney weight, and body surface in normal man. *The Anatomical Record*, 2322, pp.194–201.

O'Flaherty, E.J., (1981) *Toxicants and drugs: Kinetics and dynamics*. 1st ed. New York, USA: John Wiley & Sons, Inc.

Oates, C.J. and Mukherjee, S., (2012) Network inference and biological dynamics. *Annals of Applied Statistics*, 63, pp.1209–1235.

Obach, R.S., (2011) Predicting clearance in humans from in vitro duniversity of ata. *Current Topics in Medicinal Chemistry*, 114, pp.334–339.

Obach, R.S., Lombardo, F. and Waters, N.J., (2008) Trend analysis of a database of intravenous pharmacokinetic parameters in humans for 670 drug compounds. *Drug Metabolism and Disposition*, 367, pp.1385–1405.

Oberle, R.L., Chen, T.-S., Lloyd, C., Barnett, J.L., Owyang, C., Meyer, J. and Amidon, G.L., (1990) The influence of the interdigestive migrating myoelectric complex on the gastric emptying of liquids. *Gastroenterology*, 995, pp.1275–1282.

OECD, (2011) *Report of the workshop on using mechanistic information in forming chemical categories. Series on Testing and Assessment No.138. ENV/JM/MONO(2011)8*. [online] Available at: http://www.oecd.org/officialdocuments/publicdisplaydocumentpdf/?cote=env/jm/mono(2011)8&doclanguage=en [Accessed 14 Oct. 2019].

OECD, (2017) *AOP Knowledge Base (AOP-KB)*. [online] Available at: http://aopkb.org [Accessed 20 Feb. 2018].

OECD, (2019) *Adverse outcome pathways, molecular screening and toxicogenomics - OECD*. [online] Available at: http://www.oecd.org/chemicalsafety/testing/adverse-

outcome-pathways-molecular-screening-and-toxicogenomics.htm [Accessed 14 Oct. 2019].

OECD, (2019) *AOP Wiki*. [online] Available at: https://aopwiki.org/ [Accessed 20 Sep. 2019].

Oh, D.-M., Curl, R.L. and Amidon, G.L., (1993) Estimating the fraction dose absorbed from suspensions of poorly soluble compounds in humans: A mathematical model. *Pharmaceutical Research*, 102, pp.264–70.

Ohtsu, N., Anzai, N., Fukutomi, T., Kimura, T., Sakurai, H. and Endou, H., (2010) [Human renal urate transpoter URAT1 mediates the transport of salicylate] [article in Japanese]. *Nihon Jinzo Gakkai Shi*, [online] 524, pp.499–504. Available at: http://www.ncbi.nlm.nih.gov/pubmed/20560471.

Okonkwo, P.O., Ogbuokiri, J.E., Ofoegbu, E. and Klotz, U., (1993) Protein binding and ivermectin estimations in patients with onchocerciasis. *Clinical Pharmacology and Therapeutics*, 534, pp.426–430.

Ozbek, E., (2012) Induction of oxidative stress in kidney. *International Journal of Nephrology*, 2012, pp.1–9, Article ID 465897.

Pabla, N. and Dong, Z., (2008) Cisplatin nephrotoxicity: Mechanisms and renoprotective strategies. *Kidney International*, 73, pp.994–1007.

Pacifici, G.M., Franchi, M., Bencini, C., Repetti, F., Di Lascio, N. and Muraro, G.B., (1988) Tissue distribution of drug-metabolizing enzymes in humans. *Xenobiotica*, 187, pp.849–856.

Paini, A., Joossens, E., Bessems, J., Desalegn, A., Dorne, J., Gosling, J., Heringa, M., Klaric, M., Kramer, N., Loizou, G., Louisse, J., Lumen, A., Madden, J., Patterson, E., Proença, S., Punt, A., Setzer, R., Suciu, N., Troutman, J., Yoon, M., Worth, A. and Tan, Y., (2017a) *EURL ECVAM workshop on new generation of physiologically-based kinetic models in risk assessment, EUR 28794 EN, Publications Office of the European Union, PUBSY No. JRC108231*. Luxembourg.

Paini, A., Mennecozzi, M., Horvat, T., Gerloff, K., Palosaari, T., Sala Benito, J. V. and Worth, A., (2017b) Practical use of the Virtual Cell Based Assay: Simulation of repeated exposure experiments in liver cell lines. *Toxicology in Vitro*, 45, pp.233–240.

Pallone, T.L. and Cao, C., (2013) Renal cortical and medullary microcirculations. In: R.J. Alpern, M.J. Caplan and O.W. Moe, eds., *Seldin and Giebisch's The Kidney*, Fifth. Boston, USA: Elsevier, pp.803–857.

Palm, F. and Nordquist, L., (2011) Renal tubulointerstitial hypoxia: Cause and consequence of kidney dysfunction. *Clinical and Experimental Pharmacology and Physiology*, 387, pp.474–480.

Palmer, B.F., (2002) Renal dysfunction complicating the treatment of hypertension. *The New England Journal of Medicine*, 34716, pp.1256–1261.

Parvez, M.M., Shin, H.J., Jung, J.A. and Shin, J.G., (2017) Evaluation of para-aminosalicylic acid as a substrate of multiple solute carrier uptake transporters and possible drug interactions with nonsteroidal antiinflammatory drugs in vitro. *Antimicrobial Agents and Chemotherapy*, 615, pp.e02392-16.

Pearce, D., Soundararajan, R., Trimpert, C., Kashlan, O.B., Deen, P.M.T. and Kohan, D.E., (2015) Collecting duct principal cell transport processes and their regulation. *Clinical Journal of the American Society of Nephrology : CJASN*, 101, pp.135–46.

Pearce, R.G., Setzer, R.W., Strope, C.L., Sipes, N.S. and Wambaugh, J.F., (2017) Httk: R package for high-throughput toxicokinetics. *Journal of Statistical Software*, 794, pp.1–26.

Pelkonen, O., Kaltiala, E.H., Larmi, T.K.I. and Kärki, N.T., (1973) Comparison of activities of drug-metabolizing enzymes in human fetal and adult livers. *Clinical Pharmacology & Therapeutics*, 145, pp.840–846.

Perazella, M.A., (2009) Renal vulnerability to drug toxicity. *Clinical Journal of the American Society of Nephrology*, 47, pp.1275–1283.

Perazella, M.A., (2010) Toxic nephropathies: Core curriculum 2010. *American Journal of Kidney Diseases*, 552, pp.399–409.

Perbellini, L., Mozzo, P., Olivato, D. and Brugnone, F., (1990) "Dynamic" biological exposure indexes for n-hexane and 2,5-hexanedione, suggested by a physiologically based pharmacokinetic model. *American Industrial Hygiene Association Journal*, 517, pp.356–362.

Peters, S.A., (2008a) Evaluation of a generic physiologically based pharmacokinetic

model for lineshape analysis. *Clinical Pharmacokinetics*, 474, pp.261–275.

Peters, S.A., (2008b) Identification of intestinal loss of a drug through physiologically based pharmacokinetic simulation of plasma concentration-time profiles. *Clinical Pharmacokinetics*, 474, pp.245–259.

Peters, S.A. and Dolgos, H., (2019) Requirements to establishing confidence in physiologically based pharmacokinetic (PBPK) models and overcoming some of the challenges to meeting them. *Clinical Pharmacokinetics*, 5811, pp.1355–1371.

Petersen, P., Godtfredsen, J., Boysen, G., Andersen, E. and Andersen, B., (1989) Placebo-controlled, randomised trial of warfarin and aspirin for prevention of thromboembolic complications in chronic atrial fibrillation. *The Lancet*, 3338631, pp.175–179.

Peyret, T. and Krishnan, K., (2011) QSARs for PBPK modelling of environmental contaminants. *SAR and QSAR in Environmental Research*, 221–2, pp.129–169.

Peyret, T., Poulin, P. and Krishnan, K., (2010) A unified algorithm for predicting partition coefficients for PBPK modeling of drugs and environmental chemicals. *Toxicology and Applied Pharmacology*, 2493, pp.197–207.

Pitts, R.F., (1968) *Physiology of the kidney and body fluids*. 2nd ed. Chicago, USA: Year Book Medical Publishers Inc.

Pletz, J., Ebbrell, D.J., Enoch, S.J., Firman, J.W., Madden, J.C., Webb, S.D. and Cronin, M.T.D., (2018a) Development of a robust in silico profiler to screen for nephrotoxicity endpoints. *Toxicology Letters*, 295S1, p.S97.

Pletz, J., Enoch, S.J., Jais, D.M., Mellor, C.L., Pawar, G., Firman, J.W., Madden, J.C., Webb, S.D., Tagliati, C.A. and Cronin, M.T.D., (2018b) A critical review of adverse effects to the kidney: Mechanisms, data sources, and in silico tools to assist prediction. *Expert Opinion on Drug Metabolism and Toxicology*, 1412, pp.1225–1253.

Poet, T.S., Schlosser, P.M., Rodriguez, C.E., Parod, R.J., Rodwell, D.E. and Kirman, C.R., (2016) Using physiologically based pharmacokinetic modeling and benchmark dose methods to derive an occupational exposure limit for N-methylpyrrolidone. *Regulatory Toxicology and Pharmacology*, 76, pp.102–112.

Polasek, T.M., Tucker, G.T., Sorich, M.J., Wiese, M.D., Mohan, T., Rostami-Hodjegan,

A., Korprasertthaworn, P., Perera, V. and Rowland, A., (2018) Prediction of olanzapine exposure in individual patients using physiologically based pharmacokinetic modelling and simulation. *British Journal of Clinical Pharmacology*, 843, pp.462–476.

Posada, M.M., Bacon, J.A., Schneck, K.B., Tirona, R.G., Kim, R.B., Higgins, J.W., Pak, Y.A., Hall, S.D. and Hillgren, K.M., (2015) Prediction of renal transporter mediated drug-drug interactions for pemetrexed using physiologically based pharmacokinetic modeling. *Drug Metabolism And Disposition*, 43, pp.325–334.

Price, P.S., Conolly, R.B., Chaisson, C.F., Gross, E.A., Young, J.S., Mathis, E.T. and Tedder, D.R., (2003) Modeling interindividual variation in physiological factors used in PBPK models of humans. *Critical Reviews in Toxicology*, 335, pp.469–503.

Price, P.S. and Han, X., (2011) Maximum cumulative ratio (MCR) as a tool for assessing the value of performing a cumulative risk assessment. *International Journal of Environmental Research and Public Health*, 86, pp.2212–2225.

Proudfoot, A.T., Krenzelok, E.P., Brent, J. and Vale, J.A., (2003) Does urine alkalinization increase salicylate elimination? If so, why? *Toxicological Reviews*, 223, pp.129–136.

Przybylak, K.R. and Cronin, M.T.D., (2012) In silico models for drug-induced liver injury - Current status. *Expert Opinion on Drug Metabolism & Toxicology*, 82, pp.201–217.

Punt, A., Paini, A., Spenkelink, A., Scholz, G., Schilter, B., Van Bladeren, P.J. and Rietjens, I.M.C.M., (2016) Evaluation of interindividual human variation in bioactivation and DNA adduct formation of estragole in liver predicted by physiologically based kinetic/dynamic and Monte Carlo modeling. *Chemical Research in Toxicology*, 294, pp.659–668.

Rajoli, R.K.R., Curley, P., Chiong, J., Back, D., Flexner, C., Owen, A. and Siccardi, M., (2019) Predicting drug-drug interactions between rifampicin and long-acting cabotegravir and rilpivirine using physiologically based pharmacokinetic modeling. *Journal of Infectious Diseases*, 21911, pp.1735–1742.

Ramesh Kumar, A. and Sivaperumal, P., (2016) Analytical methods for the determination of biomarkers of exposure to phthalates in human urine samples.

Trends in Analytical Chemistry, 75, pp.151–161.

Rang, H.P., Ritter, J.M., Flower, R.J. and Henderson, G. eds., (2016) *Rang & Dale's pharmacology*. 8th ed. Edinburgh: Elsevier/Churchill Livingstone.

Regan, S.L., Maggs, J.L., Hammond, T.G., Lambert, C., Williams, D.P. and Park, B.K., (2010) Acyl glucuronides: The good, the bad and the ugly. *Biopharmaceutics & Drug Disposition*, 317, pp.367–395.

Rietjens, I.M.C.M., Louisse, J. and Punt, A., (2011) Tutorial on physiologically based kinetic modeling in molecular nutrition and food research. *Molecular Nutrition & Food Research*, 556, pp.941–956.

Roberts, M.A., Rumble, R.H., Wanwimolruk, S., Thomas, D. and Brooks, P.M., (1983) Pharmacokinetics of aspirin and salicylate in elderly subjects and in patients with alcoholic liver disease. *European Journal of Clinical Pharmacology*, 252, pp.253–261.

Rodgers, T. and Rowland, M., (2007) Mechanistic approaches to volume of distribution predictions: Understanding the processes. *Pharmaceutical Research*, 245, pp.918–933.

Rostami-Hodjegan, A. and Tucker, G.T., (2007) Simulation and prediction of in vivo drug metabolism in human populations from in vitro data. *Nature Reviews Drug Discovery*, 62, pp.140–148.

Rouiller, C., (1969) General anatomy and histology of the kidney. In: C. Rouiller and A.F. Muller, eds., *The kidney: Morphology, biochemistry, physiology*, First. New York, USA: Elsevier, pp.61–156.

Rowland, M., (1984) Protein binding and drug clearance. *Clinical Pharmacokinetics*, 91, pp.10–17.

Roy, K., Das, R.N., Ambure, P. and Aher, R.B., (2016) Be aware of error measures. Further studies on validation of predictive QSAR models. *Chemometrics and Intelligent Laboratory Systems*, 152, pp.18–33.

Russel, F.G.M., Wouterse, A.C. and van Ginneken, C.A.M., (1987a) Physiologically based pharmacokinetic model for the renal clearance of phenolsulfonphthalein and the interaction with probenecid and salicyluric acid in the dog. *Journal of Pharmacokinetics and Biopharmaceutics*, 154, pp.349–368.

Russel, F.G.M., Wouterse, A.C. and van Ginneken, C.A.M., (1987b) Physiologically based pharmacokinetic model for the renal clearance of salicyluric acid and the interaction with phenolsulfonphthalein in the dog. *Drug Metabolism and Disposition*, 155, pp.695–701.

Russel, F.G.M., Wouterse, A.C., Hekman, P., Grutters, G.J. and van Ginneken, C.A.M., (1987c) Quantitative urine collection in renal clearance studies in the dog. *Journal of Pharmacological Methods*, 172, pp.125–136.

Sager, J.E., Yu, J., Ragueneau-Majlessi, I. and Isoherranen, N., (2015) Physiologically based pharmacokinetic (PBPK) modeling and simulation approaches: A systematic review of published models, applications, and model verification. *Drug Metabolism and Disposition*, 4311, pp.1823–1837.

Sakhi, A.K., Lillegaard, I.T.L., Voorspoels, S., Carlsen, M.H., Løken, E.B., Brantsæter, A.L., Haugen, M., Meltzer, H.M. and Thomsen, C., (2014) Concentrations of phthalates and bisphenol A in Norwegian foods and beverages and estimated dietary exposure in adults. *Environment International*, 73, pp.259–269.

Sakhi, A.K., Sabaredzovic, A., Papadopoulou, E., Cequier, E. and Thomsen, C., (2018) Levels, variability and determinants of environmental phenols in pairs of Norwegian mothers and children. *Environment International*, 114, pp.242–251.

Sarigiannis, D., Karakitsios, S.P., Handakas, E. and Gotti, A., (2020) Development of a generic lifelong physiologically based biokinetic model for exposome studies. *Environmental Research*, 185February, p.109307.

Sawada, Y., Hanano, M., Sugiyama, Y. and Iga, T., (1985) Prediction of the disposition of nine weakly acidic and six weakly basic drugs in humans from pharmacokinetic parameters in rats. *Journal of Pharmacokinetics and Biopharmaceutics*, 135, pp.477–492.

Schena, F.P., Serino, G. and Sallustio, F., (2014) MicroRNAs in kidney diseases: New promising biomarkers for diagnosis and monitoring. *Nephrology Dialysis Transplantation*, 29, pp.755–763.

Schmid, M., Dalela, D., Tahbaz, R., Langetepe, J., Randazzo, M., Dahlem, R., Fisch, M., Trinh, Q.-D. and Chun, F.K.-H., (2015) Novel biomarkers of acute kidney injury: Evaluation and evidence in urologic surgery. *World Journal of Nephrology*, 42,

pp.160–168.

Scotcher, D., (2016) *Physiological scaling factors and mechanistic models for prediction of renal clearance from in vitro data*. University of Manchester.

Scotcher, D., Jones, C., Posada, M., Galetin, A. and Rostami-Hodjegan, A., (2016) Key to opening kidney for in vitro-in vivo extrapolation entrance in health and disease: Part II: Mechanistic models and in vitro-in vivo extrapolation. *The AAPS Journal*, 185, pp.1082–1094.

Scotcher, D., Jones, C.R., Galetin, A. and Rostami-Hodjegan, A., (2017) Delineating the role of various factors in renal disposition of digoxin through application of physiologically based kidney model to renal impairment populations. *Journal of Pharmacology and Experimental Therapeutics*, 3603, pp.484–495.

Sedykh, A., Fourches, D., Duan, J., Hucke, O., Garneau, M., Zhu, H., Bonneau, P. and Tropsha, A., (2013) Human intestinal transporter database: QSAR modeling and virtual profiling of drug uptake, efflux and interactions. *Pharmaceutical Research*, 304, pp.996–1007.

Sekine, T., Tsuda, M., Apiwattanakul, N., Nakajima, N., Kanai, Y., Endou, H. and Cha, S.H., (1998) Identification of multispecific organic anion transporter 2 expressed predominantly in the liver. *FEBS Letters*, 4292, pp.179–182.

Shao, K. and Gift, J.S., (2014) Model uncertainty and Bayesian model averaged benchmark dose estimation for continuous data. *Risk Analysis*, 341, pp.101–120.

Shen, H., Liu, T., Morse, B.L., Zhao, Y., Zhang, Y., Qiu, X., Chen, C., Lewin, A.C., Wang, X.T., Liu, G., Christopher, L.J., Marathe, P. and Lai, Y., (2015) Characterization of organic anion transporter 2 (SLC22A7): A highly efficient transporter for creatinine and species-dependent renal tubular expression. *Drug Metabolism and Disposition*, 437, pp.984–993.

Siccardi, M., Olagunju, A., Seden, K., Ebrahimjee, F., Rannard, S., Back, D. and Owen, A., (2013) Use of a physiologically-based pharmacokinetic model to simulate artemether dose adjustment for overcoming the drug-drug interaction with efavirenz. *In Silico Pharmacology*, 11, pp.1–8.

Skerjanec, A., Berenson, J., Hsu, C.H., Major, P., Miller, W.H., Ravera, C., Schran, H.,

Seaman, J. and Waldmeier, F., (2003) The pharmacokinetics and pharmacodynamics of zoledronic acid in cancer patients with varying degrees of renal function. *Journal of Clinical Pharmacology*, 432, pp.154–162.

Slob, W., (2006) Probabilistic dietary exposure assessment taking into account variability in both amount and frequency of consumption. *Food and Chemical Toxicology*, 447, pp.933–951.

Sluka, J.P., Fu, X., Swat, M., Belmonte, J.M., Cosmanescu, A., Clendenon, S.G., Wambaugh, J.F. and Glazier, J.A., (2016) A liver-centric multiscale modeling framework for xenobiotics. *PLoS ONE*, 119, pp.1–40, e0162428.

Somogyi, A. and Gugler, R., (1983) Clinical pharmacokinetics of cimetidine. *Clinical Pharmacokinetics*, 86, pp.463–495.

Spiess, A.-N. and Neumeyer, N., (2010) An evaluation of R-squared as an inadequate measure for nonlinear models in pharmacological and biochemical research: A Monte Carlo approach. *BMC Pharmacology*, 10, p.6.

Sprandel, K.A., Drusano, G.L., Hecht, D.W., Rotschafer, J.C., Danziger, L.H. and Rodvold, K.A., (2006) Population pharmacokinetic modeling and Monte Carlo simulation of varying doses of intravenous metronidazole. *Diagnostic Microbiology and Infectious Disease*, 554, pp.303–309.

Stader, F., Penny, M.A., Siccardi, M. and Marzolini, C., (2019) A comprehensive framework for physiologically-based pharmacokinetic modeling in Matlab. *CPT: Pharmacometrics and Systems Pharmacology*, 8, pp.444–459.

Stangier, J., Rathgen, K., Stähle, H. and Mazur, D., (2010) Influence of renal impairment on the pharmacokinetics and pharmacodynamics of oral dabigatran etexilate: An open-label, parallel-group, single-centre study. *Clinical Pharmacokinetics*, 494, pp.259–268.

Sturla, S.J., Boobis, A.R., FitzGerald, R.E., Hoeng, J., Kavlock, R.J., Schirmer, K., Whelan, M., Wilks, M.F. and Peitsch, M.C., (2014) Systems toxicology: From basic research to risk assessment. *Chemical Research in Toxicology*, 273, pp.314–329.

Summerbell, J., (1992) *Plasma aspirin esterase and associated plasma esterases in old age and frailty*. University of Newcastle Upon Tyne.

Sushko, I., Novotarskyi, S., Körner, R., Kumar Pandey, A., Rupp, M., Teetz, W., Brandmaier, S., Abdelaziz, A., Prokopenko, V. V., Tanchuk, V.Y., Todeschini, R., Varnek, A., Marcou, G., Ertl, P., Potemkin, V., Grishina, M., Gasteiger, J., Schwab, C., Baskin, I.I., Palyulin, V.A., Radchenko, E. V., Welsh, W.J., Kholodovych, V., Chekmarev, D., Cherkasov, A., Aires-De-Sousa, J., Zhang, Q.-Y., Bender, A., Nigsch, F., Patiny, L., Williams, A., Tkachenko, V. and Tetko, I. V., (2011) Online chemical modeling environment (OCHEM): Web platform for data storage, model development and publishing of chemical information. *Journal of Computer-Aided Molecular Design*, 256, pp.533–554.

Sutaria, P.M. and Staskin, D.R., (2000) Hydronephrosis and renal deterioration in the elderly due to abnormalities of the lower urinary tract and ureterovesical junction. *International Urology and Nephrology*, 321, pp.119–126.

Takeda, M., Khamdang, S., Narikawa, S., Kimura, H., Hosoyamada, M., Cha, S.H., Sekine, T. and Endou, H., (2002) Characterization of methotrexate transport and its drug interactions with human organic anion transporters. *Journal of Pharmacology and Experimental Therapeutics*, 3022, pp.666–671.

Tang-Liu, D.D.-S., Tozer, T.N. and Riegelman, S., (1983) Dependence of renal clearance on urine flow: A mathematical model and its application. *Journal of Pharmaceutical Sciences*, 722, pp.154–158.

Tang, M., Mukundan, M., Yang, J., Charpentier, N., LeCluyse, E.L., Black, C., Yang, D., Shi, D. and Yan, B., (2006) Antiplatelet agents aspirin and clopidogrel are hydrolyzed by distinct carboxylesterases, and clopidogrel is transesterificated in the presence of ethyl alcohol. *Journal of Pharmacology and Experimental Therapeutics*, 3193, pp.1467–1476.

Tannenbaum, J. and Bennett, B.T., (2015) Russell and Burch's 3Rs then and now: The need for clarity in definition and purpose. *Journal of the American Association for Laboratory Animal Science*, 542, pp.120–132.

The Medical Research Council's General Practice Research Framework, (1998) Thrombosis prevention trial: randomised trial of low-intensity oral anticoagulation with warfarin and low-dose aspirin in the primary prevention of ischaemic heart disease in men at increased risk. The Medical Research Council's General Practice

Research. *The Lancet*, 3519098, pp.233–241.

The Salt Collaborative Group, (1991) Swedish Aspirin Low-dose Trial (SALT) of 75 mg aspirin as secondary prophylaxis after cerebrovascular ischaemic events. *The Lancet*, 3388779, pp.1345–1349.

Thomas, R.S., Bigelow, P.L., Keefe, T.J. and Yang, R.S.H., (1996) Variability in biological exposure indices using physiologically based pharmacokinetic modeling and Monte Carlo simulation. *American Industrial Hygiene Association Journal*, 571, pp.23–32.

Thomas, R.S., Black, M.B., Li, L., Healy, E., Chu, T.-M., Bao, W., Andersen, M.E. and Wolfinger, R.D., (2012) A comprehensive statistical analysis of predicting in vivo hazard using high-throughput in vitro screening. *Toxicological Sciences*, 1282, pp.398–417.

Thomas, S.E., Anderson, S., Gordon, K.L., Oyama, T.T., Shankland, S.J. and Johnson, R.J., (1998) Tubulointerstitial disease in aging: Evidence for underlying peritubular capillary damage, a potential role for renal ischemia. *Journal of the American Society of Nephrology : JASN*, 92, pp.231–242.

Thompkins, L. and Lee, K.H., (1969) Studies on the mechanism of action of salicylates IV: Effect of salicylates on oxidative phosphorylation. *Journal of Pharmaceutical Sciences*, 581, pp.102–105.

Thompson, M.D. and Beard, D.A., (2011) Development of appropriate equations for physiologically based pharmacokinetic modeling of permeability-limited and flow-limited transport. *Journal of Pharmacokinetics and Pharmacodynamics*, 384, pp.405–421.

Tojo, A. and Kinugasa, S., (2012) Mechanisms of glomerular albumin filtration and tubular reabsorption. *International Journal of Nephrology*, 2012, pp.1–9, Article ID 481520.

Tong, W., Xie, Q., Hong, H., Shi, L., Fang, H. and Perkins, R., (2004) Assessment of prediction confidence and domain extrapolation of two structure-activity relationship models for predicting estrogen receptor binding activity. *Environmental Health Perspectives*, 11212, pp.1249–1254.

Trost, L.C. and Lemasters, J.J., (1997) Role of the mitochondrial permeability

transition in salicylate toxicity to cultured rat hepatocytes: Implications for the pathogenesis of Reye's syndrome. *Toxicology and Applied Pharmacology*, 1472, pp.431–441.

Truchon, G., Tardif, R., Droz, P.-O., Charest-Tardif, G. and Pierrehumbert, G., (2006) Biological exposure indicators: Quantification of biological variability using toxicokinetic modeling. *Journal of Occupational and Environmental Hygiene*, 33, pp.137–143.

Tucker, G.T., (1981) Measurement of the renal clearance of drugs. *British Journal of Clinical Pharmacology*, 12, pp.761–770.

U.S. Environmental Protection Agency (EPA), (2012) *Benchmark Dose Technical Guidance*. Washington, D.C., USA.

U.S. EPA, (2019) *Chemistry Dashboard*. [online] Available at: https://comptox.epa.gov/dashboard/ [Accessed 6 Sep. 2019].

U.S. Food and Drug Administration (FDA), (2018) *Physiologically based pharmacokinetic analyses — Format and content. Guidance for industry*.

U.S. National Center for Biotechnology Information, (2018) *PubChem*. [online] U.S. National Library of Medicine. Available at: https://pubchem.ncbi.nlm.nih.gov/search/ [Accessed 9 Jul. 2018].

U.S. National Center for Biotechnology Information, (2019a) *PubChem - Aspirin*. [online] Available at: https://pubchem.ncbi.nlm.nih.gov/compound/aspirin [Accessed 12 Aug. 2019].

U.S. National Center for Biotechnology Information, (2019b) *PubChem - Salicylic acid*. [online] Available at: https://pubchem.ncbi.nlm.nih.gov/compound/salicylic_acid [Accessed 12 Aug. 2019].

Uchino, S., Kellum, J.A., Bellomo, R., Doig, G.S., Morimatsu, H., Morgera, S., Schetz, M., Tan, I., Bouman, C., Macedo, E., Gibney, N., Tolwani, A. and Ronco, C., (2005) Acute renal failure in critically ill patients: A multinational, multicenter study. *JAMA*, 2947, pp.813–818.

University of Cambridge, (2019) *Metrabase: Metabolism and transport database*. [online] Available at: http://www-metrabase.ch.cam.ac.uk/ [Accessed 11 Aug. 2019].

Ursem, C.J., Kruhlak, N.L., Contrera, J.F., MacLaughlin, P.M., Benz, R.D. and Matthews, E.J., (2009) Identification of structure-activity relationships for adverse effects of pharmaceuticals in humans. Part A: Use of FDA post-market reports to create a database of hepatobiliary and urinary tract toxicities. *Regulatory Toxicology and Pharmacology*, 541, pp.1–22.

Vaidya, V.S., Bonventre, J. V. and Ferguson, M.A., (2010) Biomarkers of acute kidney injury. In: C.A. McQeen and R.G. Schnellmann, eds., *Comprehensive Toxicology*, Volume 7. Oxford, UK: Elsevier, pp.197–211.

Vaidya, V.S., Ferguson, M.A. and Bonventre, J. V., (2008) Biomarkers of acute kidney injury. *Annual Review of Pharmacology and Toxicology*, 48, pp.463–493.

Veerasamy, R., Rajak, H., Jain, A., Sivadasan, S., Varghese, C.P. and Agrawal, R.K., (2011) Validation of QSAR models - Strategies and importance. *International Journal of Drug Design and Discovery*, 23, pp.511–519.

Veng Pedersen, P. and Miller, R., (1980) Pharmacokinetics and bioavailability of cimetidine in humans. *Journal of Pharmaceutical Sciences*, 694, pp.394–398.

Verbeeck, R.K., Cardinal, J.-A. and Wallace, S.M., (1984) Effect of age and sex on the plasma binding of acidic and basic drugs. *European Journal of Clinical Pharmacology*, 271, pp.91–97.

Verbeeck, R.K. and Musuamba, F.T., (2009) Pharmacokinetics and dosage adjustment in patients with renal dysfunction. *European Journal of Clinical Pharmacology*, 658, pp.757–773.

Vinken, M. and Blaauboer, B.J., (2017) In vitro testing of basal cytotoxicity: Establishment of an adverse outcome pathway from chemical insult to cell death. *Toxicology In Vitro*, 39, pp.104–110.

Van Vleet, T.R. and Schnellmann, R.G., (2003) Toxic nephropathy: Environmental chemicals. *Seminars in Nephrology*, 235, pp.500–508.

Walker, R.J. and Endre, Z.H., (2013) Cellular mechanisms of drug nephrotoxicity. In: R.J. Alpern, M.J. Caplan and O.W. Moe, eds., *Seldin and Giebisch's The Kidney: Physiology and pathophysiology*, Fifth. London, UK: Academic Press/Elsevier, pp.2889–2932.

Wallentin, L.C., (1991) Aspirin (75 mg/day) after an episode of unstable coronary artery disease: Long-term effects on the risk for myocardial infarction, occurrence of severe angina and the need for revascularization. *Journal of the American College of Cardiology*, 187, pp.1587–1593.

Walther, B.A. and Moore, J.L., (2005) The concepts of bias, precision and accuracy, and their use in testing the performance of species richness estimators, with a literature review of estimator performance. *Ecography*, 286, pp.815–829.

Wambaugh, J.F., Hughes, M.F., Ring, C.L., MacMillan, D.K., Ford, J., Fennell, T.R., Black, S.R., Snyder, R.W., Sipes, N.S., Wetmore, B.A., Westerhout, J., Setzer, R.W., Pearce, R.G., Simmons, J.E. and Thomas, R.S., (2018) Evaluating in vitro-in vivo extrapolation of toxicokinetics. *Toxicological Sciences*, 1631, pp.152–169.

Wei, G., Rosen, S., Dantzler, W.H. and Pannabecker, T.L., (2015) Architecture of the human renal inner medulla and functional implications. *American Journal of Physiology-Renal Physiology*, 3097, pp.F627–F637.

Weiner, I.M., Washington, J.A. and Mudge, G.H., (1960) On the mechanism of action of probenecid on renal tubular secretion. *Bulletin of the John Hopkins Hospital*, 106, pp.333–346.

Weinstein, J.R. and Anderson, S., (2010) The aging kidney: Physiological changes. *Advances in Chronic Kidney Disease*, 174, pp.302–307.

Wetmore, B.A., (2015) Quantitative in vitro-to-in vivo extrapolation in a high-throughput environment. *Toxicology*, 332, pp.94–101.

Wetmore, B.A., Wambaugh, J.F., Ferguson, S.S., Li, L., Clewell, H.J., Judson, R.S., Freeman, K., Bao, W., Sochaski, M.A., Chu, T.M., Black, M.B., Healy, E., Allen, B., Andersen, M.E., Wolfinger, R.D. and Thomas, R.S., (2013) Relative impact of incorporating pharmacokinetics on predicting in vivo hazard and mode of action from high-throughput in vitro toxicity assays. *Toxicological Sciences*, 1322, pp.327–346.

Wetmore, B.A., Wambaugh, J.F., Ferguson, S.S., Sochaski, M.A., Rotroff, D.M., Freeman, K., Clewell, H.J., Dix, D.J., Andersen, M.E., Houck, K.A., Allen, B., Judson, R.S., Singh, R., Kavlock, R.J., Richard, A.M. and Thomas, R.S., (2012) Integration of dosimetry, exposure, and high-throughput screening data in chemical toxicity assessment. *Toxicological Sciences*, 1251, pp.157–174.

Whitehouse, M.W. and Dean, P.D.G., (1965) Biochemical properties of anti-inflammatory drugs V. *Biochemical Pharmacology*, 14, pp.557–567.

WHO, (2015) *Human biomonitoring: Facts and figures*. Copenhagen, Denmark.

WHO, (2019) *Obesity and overweight*. [online] Available at: https://www.who.int/news-room/fact-sheets/detail/obesity-and-overweight [Accessed 6 Sep. 2019].

Wilkinson, G.R. and Shand, D.G., (1975) A physiological approach to hepatic drug clearance. *Clinical Pharmacology & Therapeutics*, 184, pp.377–390.

Willmann, S., Höhn, K., Edginton, A., Sevestre, M., Solodenko, J., Weiss, W., Lippert, J. and Schmitt, W., (2007) Development of a physiology-based whole-body population model for assessing the influence of individual variability on the pharmacokinetics of drugs. *Journal of Pharmacokinetics and Pharmacodynamics*, 343, pp.401–431.

Wilmes, A., Limonciel, A., Leonard, M.O. and Jennings, P., (2014) Translational biomarkers, in vitro and in vivo. In: A. Bal-Price and P. Jennings, eds., *In vitro toxicology systems, methods in pharmacology and toxicology*. New York: Springer Science+Business Media, pp.459–478.

Winiwarter, S., Bonham, N.M., Ax, F., Hallberg, A., Lennernäs, H. and Karlén, A., (1998) Correlation of human jejunal permeability (in vivo) of drugs with experimentally and theoretically derived parameters. A multivariate data analysis approach. *Journal of Medicinal Chemistry*, 4125, pp.4939–4949.

Wishart, D.S., Feunang, Y.D., Guo, A.C., Lo, E.J., Marcu, A., Grant, J.R., Sajed, T., Johnson, D., Li, C., Sayeeda, Z., Assempour, N., Iynkkaran, I., Liu, Y., Maciejewski, A., Gale, N., Wilson, A., Chin, L., Cummings, R., Le, D., Pon, A., Knox, C. and Wilson, M., (2018) DrugBank 5.0: a major update to the DrugBank database for 2018. *Nucleic Acids Research*, 46D1, pp.D1074–D1082.

Wolff, N.A., Burckhardt, B.C., Burckhardt, G., Oellerich, M. and Armstrong, V.W., (2007) Mycophenolic acid (MPA) and its glucuronide metabolites interact with transport systems responsible for excretion of organic anions in the basolateral membrane of the human kidney. *Nephrology Dialysis Transplantation*, 229, pp.2497–2503.

Wood, D.M., Dargan, P.I. and Jones, A.L., (2005) Measuring plasma salicylate concentrations in all patients with drug overdose or altered consciousness: Is it necessary? *Emergency Medicine Journal*, 226, pp.401–403.

Woodard, H.Q. and White, D.R., (1986) The composition of body tissues. *British Journal of Radiology*, 59708, pp.1209–1219.

World Health Organization (WHO), (1991) *IPCS Environmental Health Criteria 119: Principles and methods for the assessment of nephrotoxicity associated with exposure to chemicals*. [online] Available at: http://www.inchem.org/documents/ehc/ehc/ehc119.htm [Accessed 25 Jan. 2018].

World Health Organization (WHO), (2005) *Principles of characterizing and applying human exposure models - IPCS harmonization project document No. 3*. *World Health Organization*.

Wunnapuk, K., Liu, X., Peake, P., Gobe, G., Endre, Z., Grice, J.E., Roberts, M.S. and Buckley, N.A., (2013) Renal biomarkers predict nephrotoxicity after paraquat. *Toxicology Letters*, 2223, pp.280–288.

Yamane, T., (1967) *Statistics: An introductory analysis*. Second ed. New York, NY, USA: Harper and Row.

Yang, C.H., Glover, K.P. and Han, X., (2010) Characterization of cellular uptake of perfluorooctanoate via organic anion-transporting polypeptide 1A2, organic anion transporter 4, and urate transporter 1 for their potential roles in mediating human renal reabsorption of perfluorocarboxylates. *Toxicological Sciences*, 1172, pp.294–302.

Yang, J., Jamei, M., Yeo, K.R., Rostami-Hodjegan, A. and Tucker, G.T., (2007) Misuse of the well-stirred model of hepatic drug clearance. *Drug Metabolism and Disposition*, 353, pp.501–502.

Yang, Y., Zhao, Y., Yu, A., Sun, D. and Yu, L.X., (2017) Oral drug absorption: Evaluation and prediction. In: Y. Qiu, Y. Chen, G.G.Z. Zhang, L. Yu and R. V Mantri, eds., *Developing solid oral dosage forms: Pharmaceutical theory and practice*, Second. Academic Press, pp.331–354.

Yao, Y., Zhao, Y., Sun, H., Chang, S., Zhu, L., Alder, A.C. and Kannan, K., (2018) Per-

and polyfluoroalkyl substances (PFASs) in indoor air and dust from homes and various microenvironments in China: Implications for human exposure. *Environmental Science and Technology*, 525, pp.3156–3166.

Ye, M., Nagar, S. and Korzekwa, K., (2016) A physiologically based pharmacokinetic model to predict the pharmacokinetics of highly protein-bound drugs and impact of errors in plasma protein binding. *Biopharmaceutics & Drug Disposition*, 373, pp.123–141.

Yelland, C., Summerbell, J., Nicholson, E., Herd, B., Wynne, H. and Woodhouse, K.W., (1991) The association of age with aspirin esterase activity in human liver. *Age and Ageing*, 201, pp.16–18.

Yoon, M., Campbell, J.L., Andersen, M.E. and Clewell, H.J., (2012) Quantitative in vitro to in vivo extrapolation of cell-based toxicity assay results. *Critical Reviews in Toxicology*, 428, pp.633–652.

You, K., (1983) Salicylate and mitochondrial injury in Reye's syndrome. *Science*, 221July, pp.163–165.

Yu, L.X. and Amidon, G.L., (1998) Characterization of small intestinal transit time distribution in humans. *International Journal of Pharmaceutics*, 1712, pp.157–163.

Yu, L.X. and Amidon, G.L., (1999) A compartmental absorption and transit model for estimating oral drug absorption. *International Journal of Pharmaceutics*, 186, pp.119–125.

Zager, R.A., Johnson, A.C.M. and Becker, K., (2012) Plasma and urinary heme oxygenase-1 in AKI. *Journal of the American Society of Nephrology*, 236, pp.1048–1057.

Zamzami, N., Larochette, N. and Kroemer, G., (2005) Mitochondrial permeability transition in apoptosis and necrosis. *Cell Death and Differentiation*, 12S2, pp.1478–1480.

Zaza, G., Granata, S., Tomei, P., Dalla Gassa, A. and Lupo, A., (2015) Personalization of the immunosuppressive treatment in renal transplant recipients: The great challenge in 'omics' medicine. *International Journal of Molecular Sciences*, 162, pp.4281–4305.

Zgheib, E., Gao, W., Limonciel, A., Aladjov, H., Yang, H., Tebby, C., Gayraud, G., Jennings, P., Sachana, M., Beltman, J.B. and Bois, F.Y., (2019) Application of three approaches for quantitative AOP development to renal toxicity. *Computational Toxicology*, 11November 2018, pp.1–13.

Zhang, H., Gao, N., Tian, X., Liu, T., Fang, Y., Zhou, J., Wen, Q., Xu, B., Qi, B., Gao, J., Li, H., Jia, L. and Qiao, H., (2015) Content and activity of human liver microsomal protein and prediction of individual hepatic clearance in vivo. *Scientific Reports*, 5May, pp.1–12.

Zhang, L., Wang M and Wang, H., (2005) Acute renal failure in chronic kidney disease - clinical and pathological analysis of 104 cases. *Clinical Nephrology*, 635, pp.346–350.

7.0 APPENDICES

Appendix 2.A: Supplemental information on simulations with IndusChemFate and Httk

Table 2.A.1: Parameter values used for predictions on DnBP, BBzP, bisphenol A, triclosan and their metabolites with IndusChemFate, Part A

Abb.	Chemical name	Metabolite of	CAS	Molecular Weight (g/mol) (EPA)	Density (mg/cm3 or grams/litre)	Vapour Pressure (Pa)	Log(Kow) in blood pH 7.4	Water Solubility (mg/litre)
DnBP	Dibutyl phthalate	-/-	84-74-2	278	1,050 (av est)	2.68×10^{-3}	4.50	11.2
MnBP	Mono-n-butyl phthalate	DnBP	131-70-4	222	1,180 (av est)	1.88×10^{-3} (av est)	2.77 (av est)	769 (av est)
BBzP	Butylbenzyl phthalate	-/-	85-68-7	312	1,130 (av est)	1.01×10^{-3}	4.73	2.69
MBzP	Mono-benzyl phthalate	BBzP	2528-16-7	256	1,270 (av est)	1.26×10^{-4} (av est)	2.80 (av est)	119 (av est)
TCS	Triclosan	-/-	3380-34-5	289	1,510 (av est)	1.30×10^{-3} (av est)	4.76	9.99
TCS-glu	Triclosan glucuronide	TCS	63156-12-7	463	1,780 (av est)	3.80×10^{-8} (av est)	2.26 (av est)	73.7
BPA	Bisphenol A	-/-	80-05-7	228	1,170 (av est)	1.12×10^{-4} (av est)	3.32	120

Abb: abbreviations; -/- : not applicable; (av est): average estimate; Reference: All parameter values illustrated in Part A of this table are sourced from U.S. EPA, 2019; up to three significant figures are reported.

Table 2.A.1: Parameter values used for predictions on DnBP, BBzP, bisphenol A, triclosan and their metabolites with IndusChemFate, Part B

Abb.	Vmax Liver (parent[total] µmol/kg tissue/hr)	Km Liver (parent[total] µmol/litre)	Enterohepatic removal (relative to liver venous blood)	Polar Surface Area (PSA) (A^2)	Hydrogen Bond Donor (HBD)	Oral absorption rate k_a (1/h)	Elimination half-life ($t_{1/2}$) (h)	Time to steady state (estimated; $t_{1/2}$*5) (h)
DnBP	41,280[1]	99.7[1]	1[2]	52.6[3]	0[3]	9.85[4]	6[5]	30
MnBP	-/-	-/-	1[2]	-/-	-/-	-/-	2.6[6]	13
BBzP	173,040[7]	16.1[7]	1[8]	52.6[3]	0[3]	10.7[4]	24[9]	120
MBzP	-/-	-/-	1[8]	-/-	-/-	-/-	24[9]	120
TCS	34.35[10]	122.5[10]	0[11,12]	29.5[3]	1[3]	10.8[4]	29[11]	145
TCS-glu	-/-	-/-	0[11,12]	-/-	-/-	-/-	29[11]	145
BPA	11,304[13]	45.8[13]	0.2[14,15] (est)	40.5[3]	2[3]	2.8[4]	5.4[16]	27

Abb: abbreviations; -/- : not applicable; (est): estimated; For none of the chemicals selected, information on resorption in renal tubuli was found in the literature. Therefore, for all chemicals a question mark (?) was entered as input value which, according to the documentation in ICF, means that this value is unknown. The time to reach steady state was assessed using the equation $T_{ss}=5*t_{(1/2)}$, with $t_{(1/2)}$ being the elimination half-life. Properties of the BPA glucuronide used are those saved in the IndusChemFate model; hence BPA-glu is not included in this table.

References: [1]Hanioka et al., 2012; [2]ATSDR, 2018; [3]U.S. National Center for Biotechnology Information, 2018; [4]calculated using PSA, HBD and the Winiwarter et al. (1998) model 3b to derive the logarithm of the effective permeability (P_{eff}) and Peters (2008, Eq. 1) to then calculate the k_a; [5]Aylward et al., 2009; [6]Koch et al., 2012; [7]Takahara et al., 2014; [8]Eigenberg et al., 1986; [9]European Commission, 2007; [10]Ashrap et al., 2017; [11]European Commission Scientific Committee on Consumer Safety (SCCS), 2009; [12]ECHA, 2015; [13]Coughlin et al., 2012; [14]Teeguarden et al., 2005; [15]Yang et al., 2015; [16]Völkel et al., 2002.

Appendix 2.B: Mixture assessment results with the 95th percentile and median of measured urine concentrations and the 5th percentile of the BE_{TDI} distribution

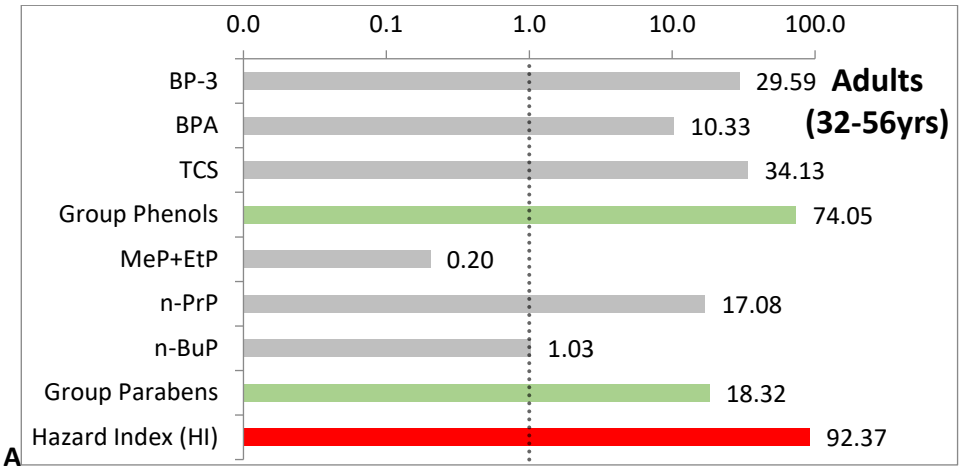

A

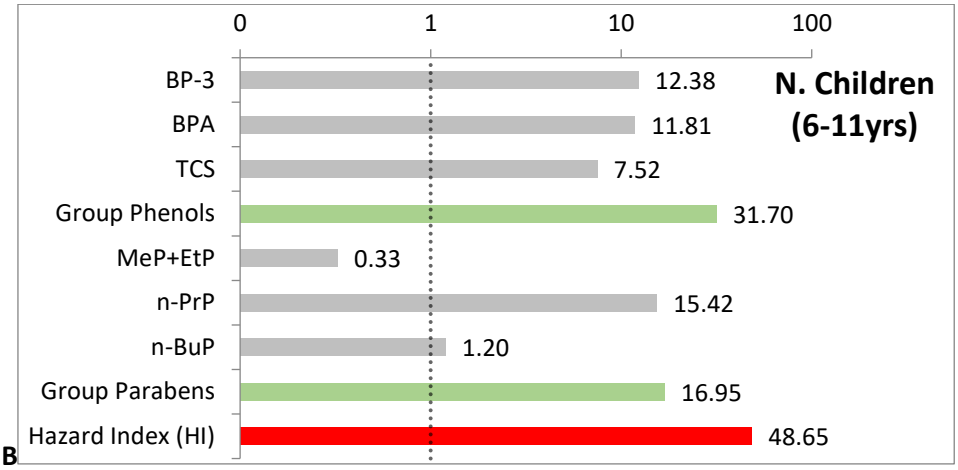

B

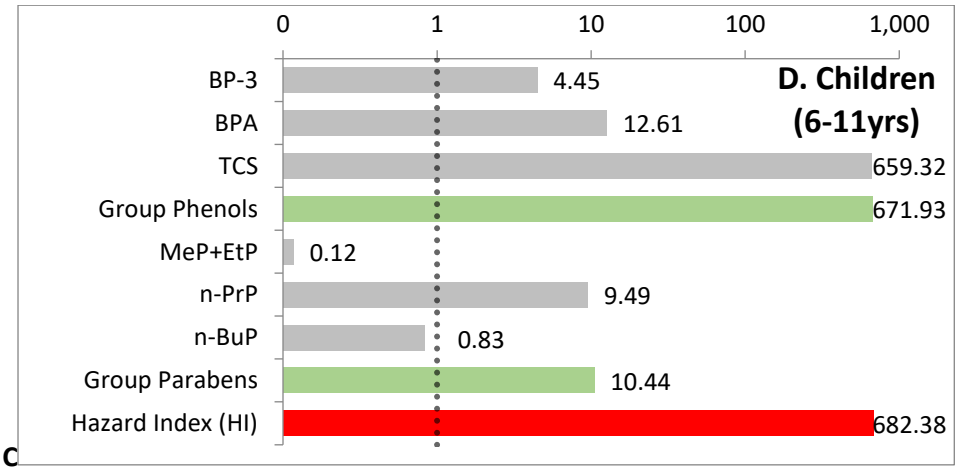

C

Figure 2.B.1: Hazard Index calculated with the 95th percentile concentration of a chemical in urine with respect to the BE value selected on the basis of the 5th percentile of the BE_{TDI} distribution. **A.** Norwegian female adults, **B.** Norwegian children, **C.** Danish children.

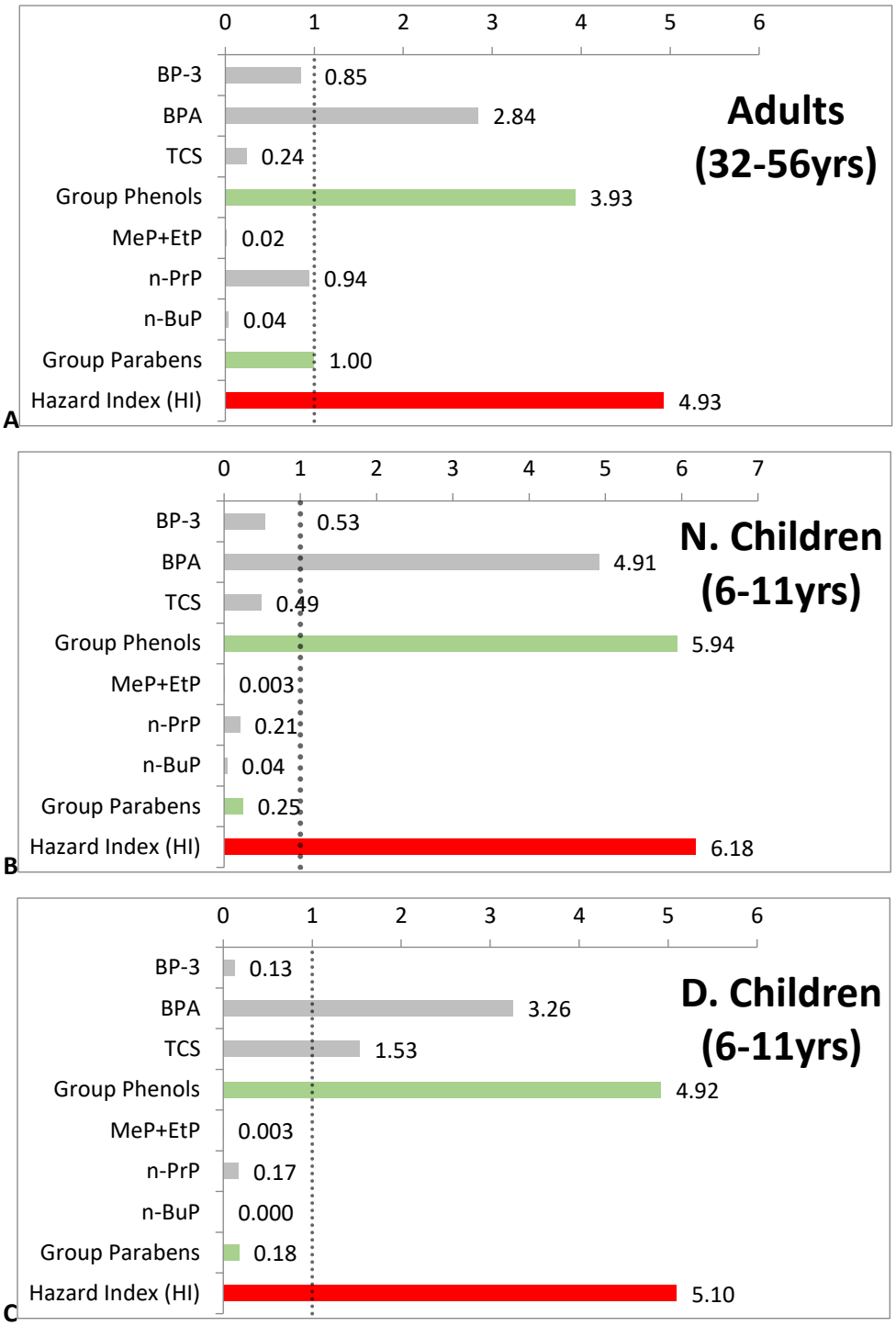

Figure 2.B.2: Hazard Index calculated with the median concentration of a chemical in urine with respect to the BE value selected on the basis of the 5th percentile of the BE_{TDI} distribution. **A.** Norwegian female adults, **B.** Norwegian children, **C.** Danish children.

Appendix 3.A: Ordinary differential equations (ODEs) to generate the PBK model

All terms presented here are defined in subchapters 3.1.1.1 and 3.1.1.2.

Somatic compartments: LU = lung; HE = heart; TH = thymus; AD = adipose tissue; MU = muscle; BR = brain; SK = skin; KI = kidney; SP = spleen; PA = pancreas; LI = liver; HA = hepatic artery; ST = stomach; GU = gut; VE = venous blood; AR = arterial blood; **Oral absorption compartments:** STL = stomach lumen; DUO = duodenum lumen; $JE1$ = jejunum 1 lumen; $JE2$ = jejunum 2 lumen; $IL1$ = ileum 1 lumen; $IL2$ = ileum 2 lumen; $IL3$ = ileum 3 lumen; CAE = caecum lumen; ACO = ascending colon lumen; **Parameters:** Q = blood flow rates corresponding to an organ or tissue compartment; K_p = tissue partition coefficient; R = whole blood to plasma concentration ratio; CL_{hep} = hepatic clearance rate; EHR = enterohepatic recirculation; k_{bil} = biliary elimination rate constant; CP = conversion of the metabolite to the parent compound; $k_{e(r)}$ = renal elimination rate constant; k_a = absorption rate constant in stomach *($k_{a(ST)}$)* and gut *($k_{a(GU)}$)*; k_{il} = intestinal loss rate constant; $f_{u(p)}$ = fraction unbound in plasma; K_D = dissolution rate constant; GER = gastric emptying rate; k_t = transit rate in small intestine *($k_{t(GU)}$)* and colon *($k_{t(CO)}$)*.

For each somatic compartment, the ODE represents the change in concentration within that tissue compartment over a concentration gradient between the capillary and tissue ($C_{blood} - C_{tissue}$; Boroujerdi, 2015). The binding to fatty acids (e.g. in plasma proteins or erythrocytes) as well as the perfusion rate (expressed as the tissue blood flow rate over the tissue volume) are considered. ODEs of eliminating tissues, e.g. liver and kidney, include a term representing processes of elimination or clearance. Compartments are located within the model and interlinked according to human physiology.

Throughout t is time and concentration is measured in the unit mM. All compartment volumes (e.g. $V_{compartment}$, for all compartments defined above), blood flow rates ($Q_{compartment}$) and other physiological parameters (including GER, $k_{t(GU)}$, $k_{t(CO)}$) are given in Table 3.1. All chemical-specific parameters used in Chapter 3 are presented in Tables 3.3-3.5.

3.A.1 Differential equations for somatic compartments:

1. Lungs *(LU)*

$$\frac{dC_{LU}}{dt} = \frac{Q_{LU}}{V_{LU}}\left(C_{VE} - \frac{(C_{LU} \times R)}{K_p}\right)$$

2. Non-eliminating organs and tissues

$$\frac{dC_T}{dt} = \frac{Q_T}{V_T}\left(C_{AR} - \frac{C_T \times R}{K_p}\right)$$

where T represents $HE =$ heart, $SP =$ spleen, $TH =$ thymus, $PA =$ pancreas, $AD =$ adipose, $MU =$ muscle, $BR =$ brain, $SK =$ skin.

3. Liver *(LI)*

$$\frac{dC_{LI}}{dt} = \frac{1}{V_{LI}}\left(Q_{HA} \times C_{AR} + \sum \frac{Q_i \times C_i \times R}{K_p} - \frac{Q_{LI} \times C_{LI} \times R}{K_p} - \frac{C_{LI} \times CL_{hep}}{K_p} \times f_{u(p)} - \frac{EHR \times k_{bil} \times C_{LI} \times V_{LI}}{K_p} - \frac{CP \times k_{bil} \times C_{LI} \times V_{LI}}{K_p}\right)$$

where i = *GU (gut)*, *ST (stomach)*, PA, SP; therefore:

$$\sum_i \frac{Q_i \times C_i \times R}{K_p} = \frac{Q_{GU} \times C_{GU} \times R}{K_p} + \frac{Q_{PA} \times C_{PA} \times R}{K_p} + \frac{Q_{SP} \times C_{SP} \times R}{K_p} + \frac{Q_{ST} \times C_{ST} \times R}{K_p}$$

Also, hepatic artery *(HA)* blood flow equals:

$$Q_{HA} = Q_{LI} - (Q_{GU} + Q_{PA} + Q_{SP} + Q_{ST})$$

4. Stomach *(ST)*

$$\frac{dC_{ST}}{dt} = \frac{Q_{ST}}{V_{ST}}\left(C_{AR} - \frac{C_{ST} \times R}{K_p}\right) + \frac{A_{ABS(ST)}}{V_{ST}}$$

5. Gut *(GU)*

$$\frac{dC_{GU}}{dt} = \frac{1}{V_{GU}} \left(Q_{GU} \left(C_{AR} - \frac{C_{GU} \times R}{K_p} \right) + A_{TIA} \right)$$

6. Kidney *(KI)*

$$\frac{dC_{KI}}{dt} = \frac{1}{V_{KI}} \times \left[Q_{KI} \left(C_{AR} - \frac{C_{KI} \times R}{K_p} \right) \right] - \frac{C_{KI} \times k_{e(r)}}{K_p} \; x \; f_{u(p)}$$

7. Venous blood *(VE)*

$$\frac{dC_{VE}}{dt} = \frac{1}{V_{VE}} \left(\sum \frac{Q_T \times C_T \times R}{K_p} - Q_{LU} \times C_{VE} \right)$$

Excluding the gut, pancreas, spleen, stomach, and lung; (no venous infusion rate (VIR) included)

$$\sum_i \frac{Q_T \times C_T \times R}{K_p} = \frac{Q_{HE} \times C_{HE} \times R}{K_p} + \frac{Q_{LI} \times C_{LI} \times R}{K_p} + \frac{Q_{KI} \times C_{KI} \times R}{K_p} + \frac{Q_{TH} \times C_{TH} \times R}{K_p} + \frac{Q_{AD} \times C_{AD} \times R}{K_p} + \frac{Q_{MU} \times C_{MU} \times R}{K_p} + \frac{Q_{BR} \times C_{BR} \times R}{K_p} + \frac{Q_{SK} \times C_{SK} \times R}{K_p}$$

8. Arterial blood *(AR)*

$$\frac{dC_{AR}}{dt} = \frac{1}{V_{AR}} \left(Q_{LU} \frac{C_{LU} \times R}{K_p} \right) - \sum \frac{Q_i \times C_{AR}}{V_{AR}}$$

where *i* = *HE, HA, ST, GU, SP, KI, TH, PA, AD, MU, BR, SK*; therefore:

$$\sum \frac{Q_i \times C_{AR}}{V_{AR}} = \frac{Q_{HE} \times C_{AR}}{V_{AR}} - \frac{Q_{HA} \times C_{AR}}{V_{AR}} - \frac{Q_{ST} \times C_{AR}}{V_{AR}} - \frac{Q_{GU} \times C_{AR}}{V_{AR}} - \frac{Q_{SP} \times C_{AR}}{V_{AR}} - \frac{Q_{KI} \times C_{AR}}{V_{AR}} - \frac{Q_{TH} \times C_{AR}}{V_{AR}} - \frac{Q_{PA} \times C_{AR}}{V_{AR}} - \frac{Q_{AD} \times C_{AR}}{V_{AR}} - \frac{Q_{MU} \times C_{AR}}{V_{AR}} - \frac{Q_{BR} \times C_{AR}}{V_{AR}} - \frac{Q_{SK} \times C_{AR}}{V_{AR}}$$

3.A.2 Differential equations for oral absorption compartments:

For each of the nine gastrointestinal compartments, the amounts undissolved (A_{UND}), dissolved (A_{DIS}), degraded (A_{DEG}) and absorbed (A_{ABS}) from that compartment are calculated over time. Only dissolved amounts are subject to absorption. Amounts absorbed from the stomach lumen ($A_{ABS(ST)}$) feed into the stomach compartment and amounts absorbed from any gut compartment including colon ($A_{ABS(GU1-7)}$ and $A_{ABS(CO}$)) feed into the gut compartment.

9. Undissolved Stomach

$$\frac{dA_{UND(ST)}}{dt} = -GER \times A_{UND(ST)} - \frac{3D}{prT} \times A_{UND(ST)} \left(K_{S(ST)} \times S - \frac{A_{DIS(ST)}}{V_{STL}}\right)$$

10. Dissolved Stomach

$$\frac{dA_{DIS(ST)}}{dt} = -GER \times A_{DIS(ST)} + \frac{3D}{prT} \times A_{UND(ST)} \left(K_{S(ST)} \times S - \frac{A_{DIS(ST)}}{V_{STL}}\right) - k_{il(ST)} \times A_{DIS(ST)} - k_{a(ST)} \times A_{DIS(ST)}$$

11. Degraded Stomach

$$\frac{dA_{DEG(ST)}}{dt} = k_{il(ST)} \times A_{DIS(ST)}$$

12. Absorbed Stomach

$$\frac{dA_{ABS(ST)}}{dt} = k_{a(ST)} \times A_{DIS(ST)}$$

13. Undissolved Gut 1

$$\frac{dA_{UND(GU1)}}{dt} = GER \times A_{UND(ST)} - k_{t(GU)} \times A_{UND(GU1)} - \frac{3D}{prT} \times A_{UND(GU1)} \times \left(K_{S(DUO)} \times S - \frac{A_{DIS(GU1)}}{V_{DUO}}\right)$$

14. Dissolved Gut 1

$$\frac{dA_{DIS(GU1)}}{dt} = GER \times A_{DIS(ST)} - k_{t(GU)} \times A_{DIS(GU1)} + \frac{3D}{prT} \times A_{UND(GU1)} \times \left(K_{S(DUO)} \times S - \frac{A_{DIS(GU1)}}{V_{DUO}}\right) - k_{il(GU)} \times A_{DIS(GU1)} - k_{a(GU)} \times A_{DIS(GU1)} + \frac{EHR \times k_{bil} \times C_{LI} \times V_{LI}}{K_p}$$

15. Degraded Gut 1

$$\frac{dA_{DEG(GU1)}}{dt} = k_{il(GU)} \times A_{DIS(GU1)}$$

16. Absorbed Gut 1

$$\frac{dA_{ABS(GU1)}}{dt} = k_{a(GU)} \times A_{DIS(GU1)}$$

17. Undissolved Gut 2-7

$$\frac{dA_{UND(GUi)}}{dt} = k_{t(GU)} \times A_{UND(GUi-1)} - k_{t(GU)} \times A_{UND(GUi)} - \frac{3D}{prT} \times A_{UND(GUi)} \times \left(K_{S(GUi)} \times S - \frac{A_{DIS(GUi)}}{V_{GUi}}\right)$$

18. Dissolved Gut 2-7

$$\frac{dA_{DIS(GUi)}}{dt} = k_{t(GU)} \times A_{DIS(GUi-1)} - k_{t(GU)} \times A_{DIS(GUi)} + \frac{3D}{prT} \times A_{UND(GUi)} \times \left(K_{S(GUi)} \times S - \frac{A_{DIS(GUi)}}{V_{GUi}}\right) - k_{il(GU)} \times A_{DIS(GUi)} - k_{a(GU)} \times A_{DIS(GUi)}$$

19. Degraded Gut 2-7

$$\frac{dA_{DEG(GUi)}}{dt} = k_{il(GU)} \times A_{DIS(GUi)}$$

20. Absorbed Gut 2-7

$$\frac{dA_{ABS(GUi)}}{dt} = k_{a(GU)} \times A_{DIS(GUi)}$$

Where *i* = 2-7 and V_{GUi} corresponds to V_{JE1}, V_{JE2}, V_{IL1}, V_{IL2}, V_{IL3}, and V_{CAE}.

21. Undissolved Colon

$$\frac{dA_{UND(CO)}}{dt} = k_{t(GU)} \times A_{UND(GU7)} - k_{t(CO)} \times A_{UND(CO)} - \frac{3D}{prT} \times A_{UND(CO)} \times \left(K_{S(CO)} \times S - \frac{A_{DIS(CO)}}{V_{ACO}}\right)$$

22. Dissolved Colon

$$\frac{dA_{DIS(CO)}}{dt} = k_{t(GU)} \times A_{DIS(GU7)} - k_{t(CO)} \times A_{DIS(CO)} + \frac{3D}{prT} \times A_{UND(CO)} \times \left(K_{S(CO)} \times S - \frac{A_{DIS(CO)}}{V_{ACO}}\right) - k_{il(CO)} \times A_{DIS(CO)} - k_{a(CO)} \times A_{DIS(CO)} + \frac{CP \times C_{LI} \times V_{LI} \times k_{bil}}{K_p}$$

23. Degraded Colon

$$\frac{dA_{DEG(CO)}}{dt} = k_{il(CO)} \times A_{DIS(CO)}$$

24. Absorbed Colon

$$\frac{dA_{ABS(CO)}}{dt} = k_{a(CO)} \times A_{DIS(GU7)}$$

25. Total Intestinal Absorption (TIA)

$$\frac{dA_{TIA}}{dt} = \sum \left[k_{a(i)} \times A_{DIS(i)}\right]$$

Where i = $GU1$ to $GU7$, and CO; therefore:

$$\frac{dA_{TIA}}{dt} = k_{a(GU)} \times A_{DIS(GU1)} + k_{a(GU)} \times A_{DIS(GU2)} + k_{a(GU)} \times A_{DIS(GU3)} + k_{a(GU)} \times A_{DIS(GU4)} + k_{a(GU)} \times A_{DIS(GU5)} + k_{a(GU)} \times A_{DIS(GU6)} + k_{a(GU)} \times A_{DIS(GU7)} + k_{a(CO)} \times A_{DIS(CO)}$$

Appendix 3.B: Results of the sensitivity analyses and fitting for bisoprolol, diazepam and theophylline

For each compound, a simulation with initial parameter values, the results of the sensitivity analysis and a simulation with the fitted parameter values are generated. For bisoprolol, diazepam and theophylline, results of the sensitivity analyses, the fitted plots and residual distributions are presented here. In the sensitivity analysis, the bar to the right of the bar chart indicates that the perturbation of parameters the venous blood concentration is most sensitive to have a yellow bar while those whose perturbation have the least effect have a dark blue bar. In the fitted plots, the orange fitted curves and data points relate to the IV route while the blue fitted curves and data points relate to the oral route. Residual distributions show the differences between measured data points and the fit to these at each predictor value (MathWorks, 2018). Ideally, residuals are equally distributed below and above zero indicating that the model describes the measure data well.

For bisoprolol, the renal elimination rate constant ($k_{e(r)}$) is calculated from the renal clearance (CL_r) and the volume of distribution (V_d). Therefore, these parameters are included in the sensitivity analysis. Primarily *R* and to a lower extent K_p are identified as sensitive parameters.

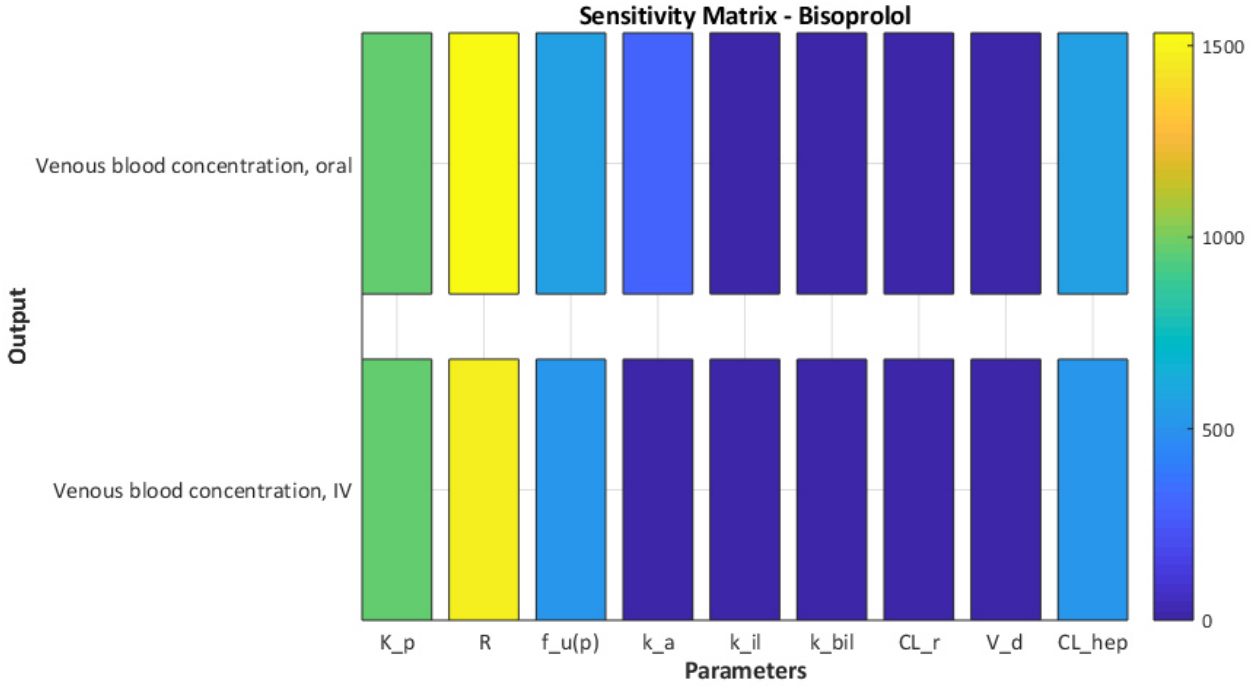

Figure 3.B.1: Time-integral sensitivity coefficients (S_q), giving an indication of the total sensitivity of the model parameters $K_{p(ad)}$, K_p, R, $f_{u(p)}$, k_a, k_{il}, k_{bil}, $k_{e(r)}$ and CL_{hep} on the predicted venous blood concentrations following oral and IV administration of bisoprolol

The fitted plot of bisoprolol shows that both predicted curves represent the observed data well. The predicted oral curve slightly overpredicts exposure at early time points.

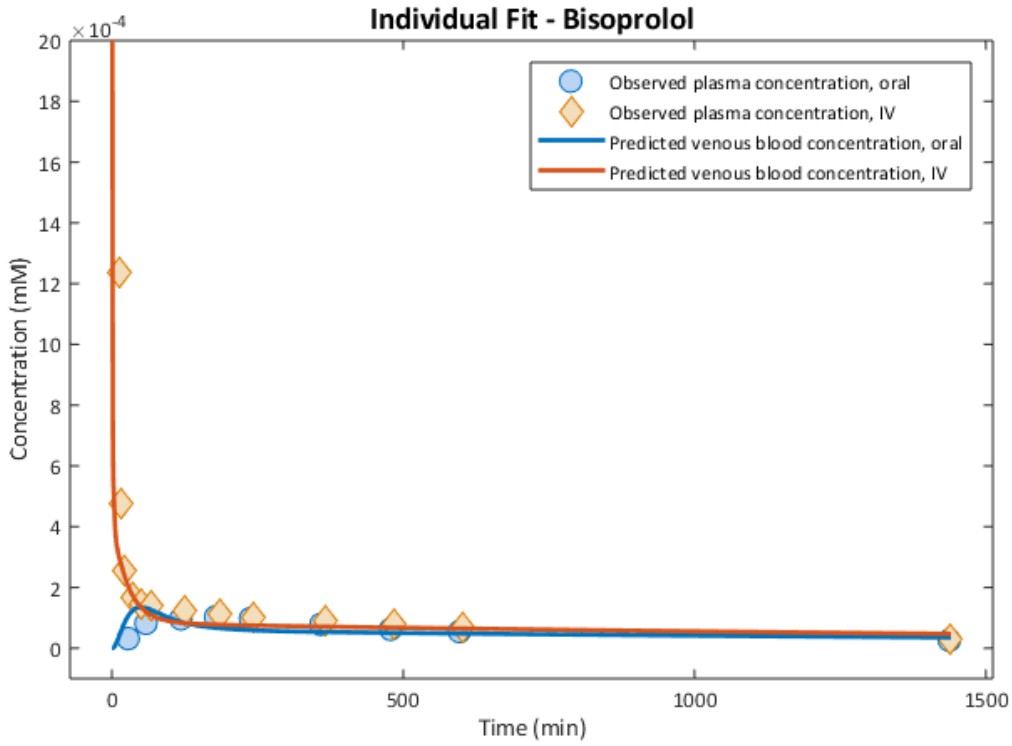

Figure 3.B.2: Bisoprolol fitted simulated curve fitted to observed pharmacokinetic data reported by Leopold et al. (1986)

The residual distribution of the bisoprolol fit shows that for the oral fit residuals are higher than for the IV fit. As oral residuals as equally distributed above and below zero the model is considered to describe the observed data well.

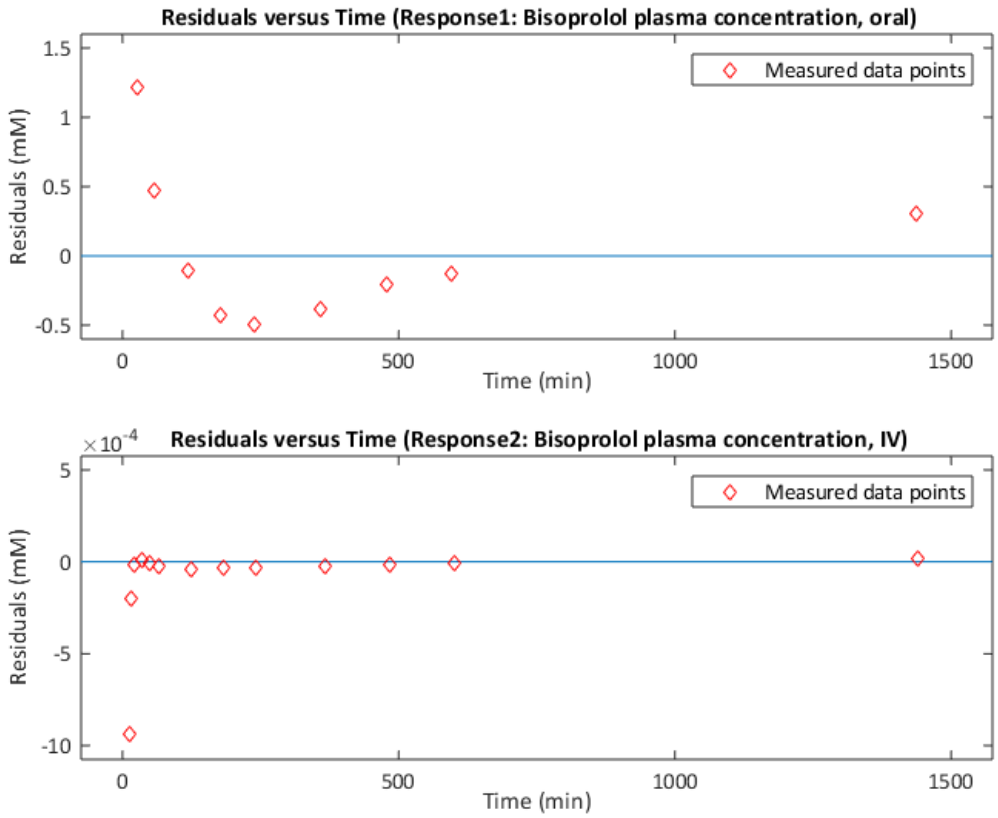

Figure 3.B.3: Residual distribution of bisoprolol fit (blue line) in relation to data points measured by Leopold et al. (1986)

For diazepam, since a partition coefficient for the adipose tissue ($K_{p(AD)}$) is included in the model, this parameter was also included in the sensitivity analysis. *R* is identified as most sensitive parameter followed by K_p.

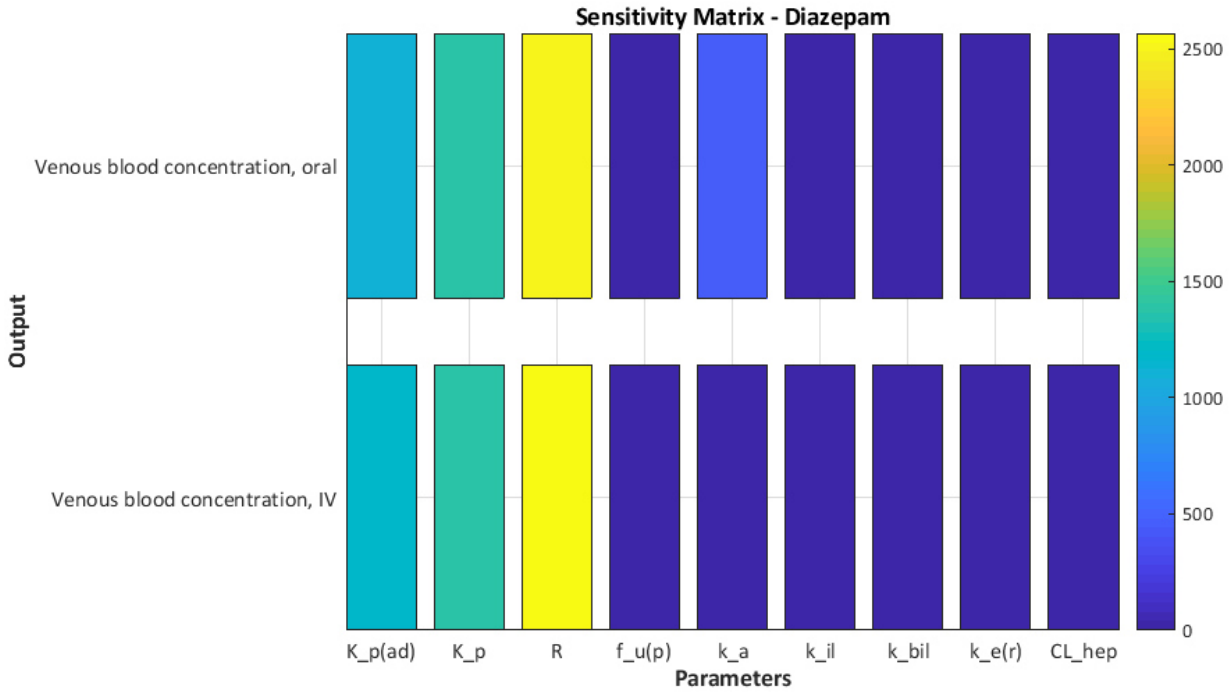

Figure 3.B.4: Time-integral sensitivity coefficients (S_q), giving an indication of the total sensitivity of the model parameters $K_{p(ad)}$, K_p, R, $f_{u(p)}$, k_a, k_{il}, k_{bil}, $k_{e(r)}$ and CL_{hep} on the predicted venous blood concentrations following oral and IV administration of diazepam

The fitted plot of diazepam shows that both predicted curves represent the observed data well. At early time poins, the oral fit slightly underpredicts measured data.

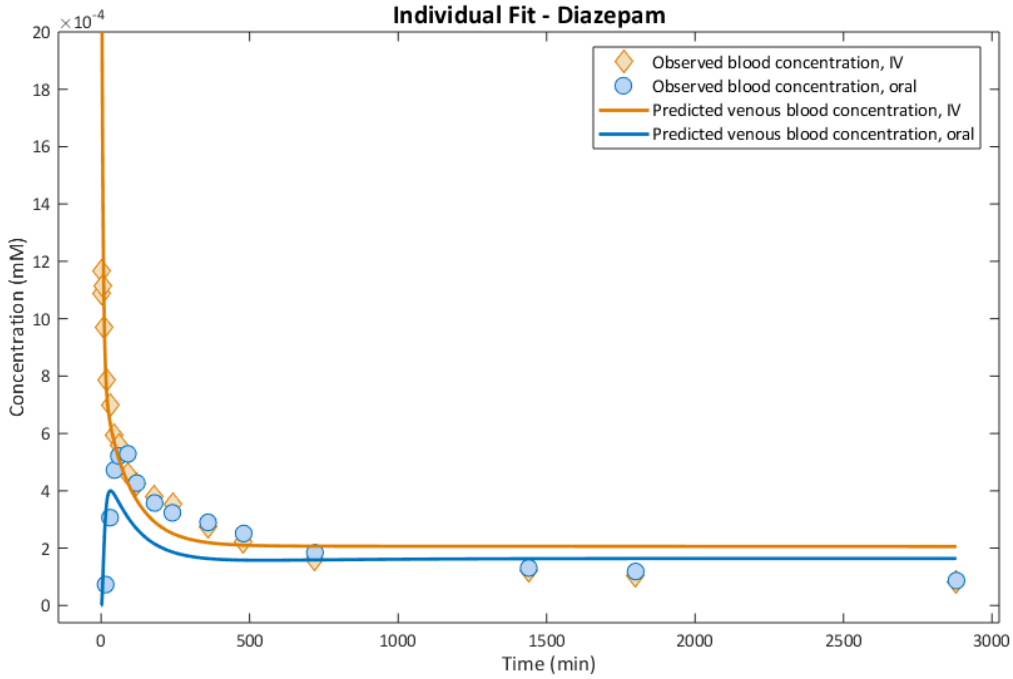

Figure 3.B.5: Diazepam fitted simulated curve fitted to observed pharmacokinetic data reported by Kaplan et al. (1973)

The residual distribution of the diazepam fit shows that residuals are fairly low and equally distributed around the zero line. Therefore, the model is considered to describe the observed data well.

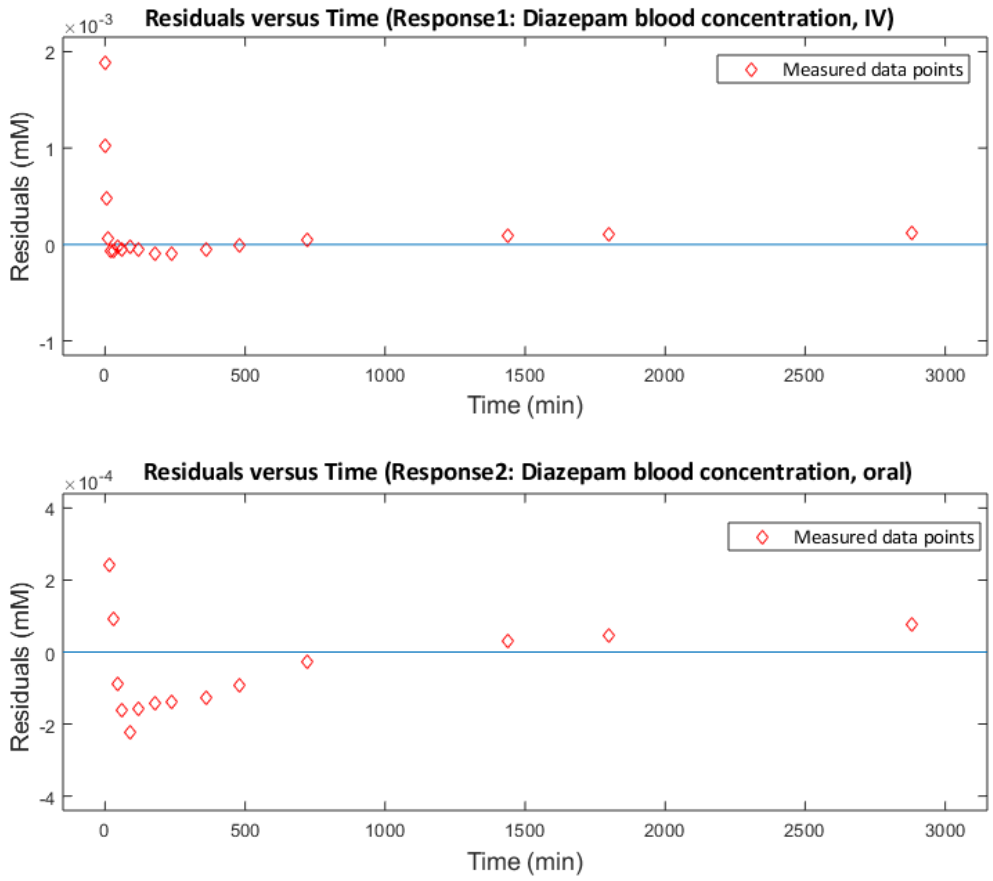

Figure 3.B.6: Residual distribution of diazepam fit (blue line) in relation to data points measured by Kaplan et al. (1973)

For theophylline, the most sensitive parameter is *R*, followed by K_p.

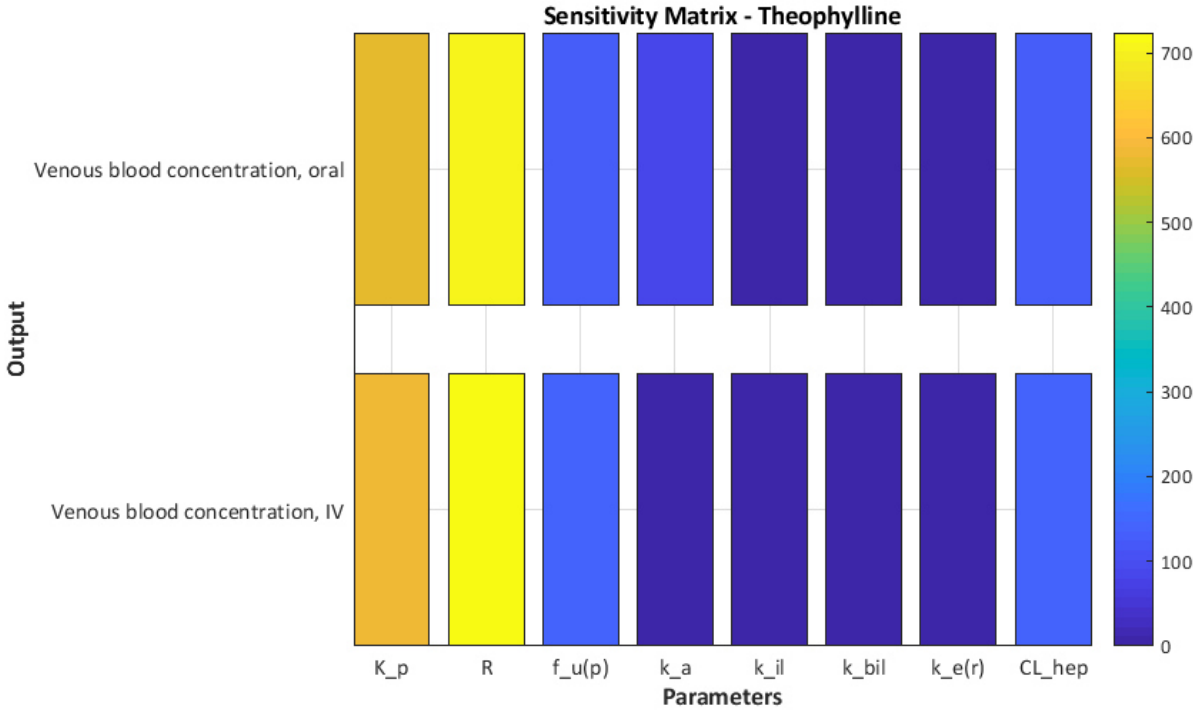

Figure 3.B.7: Time-integral sensitivity coefficients (S_q), giving an indication of the total sensitivity of the model parameters K_p, R, $f_{u(p)}$, k_a, k_{il}, k_{bil}, $k_{e(r)}$ and CL_{hep} on the predicted venous blood concentrations following oral and IV administration of theophylline

The fitted plot of theophylline shows that both predicted curves represent the observed data very well.

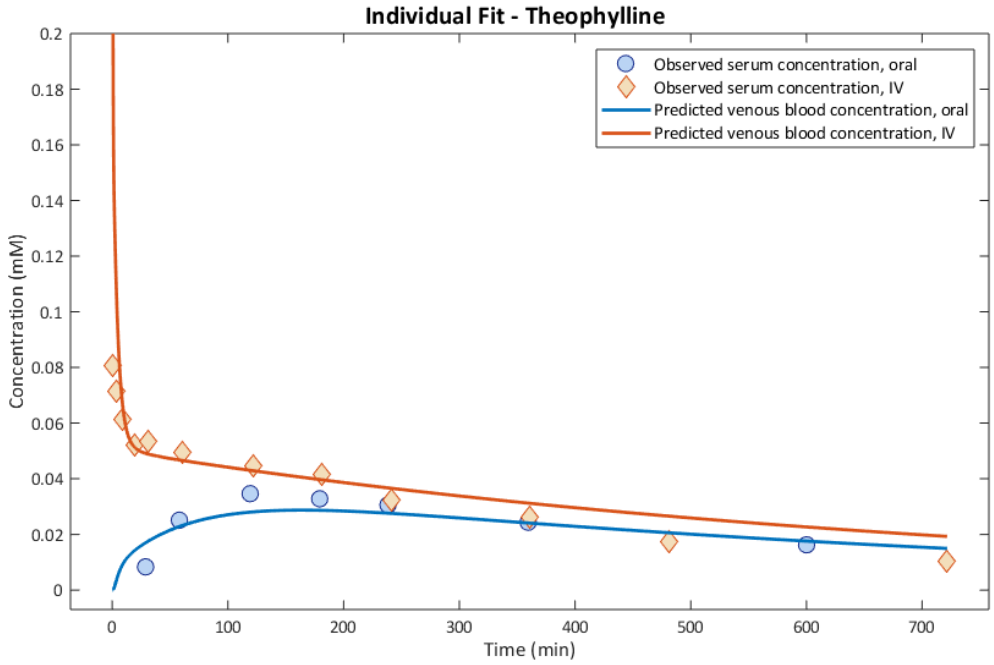

Figure 3.B.8: Theophylline fitted simulated curve fitted to observed pharmacokinetic data reported by Aslaksen et al. (1981)

The residual distribution of the theophylline fit shows that for the oral fit residuals are higher than for the IV fit. Overall, residuals of the oral fit are fairly low and equally distributed around the zero line. Hence, the model is considered to describe both observed datasets well.

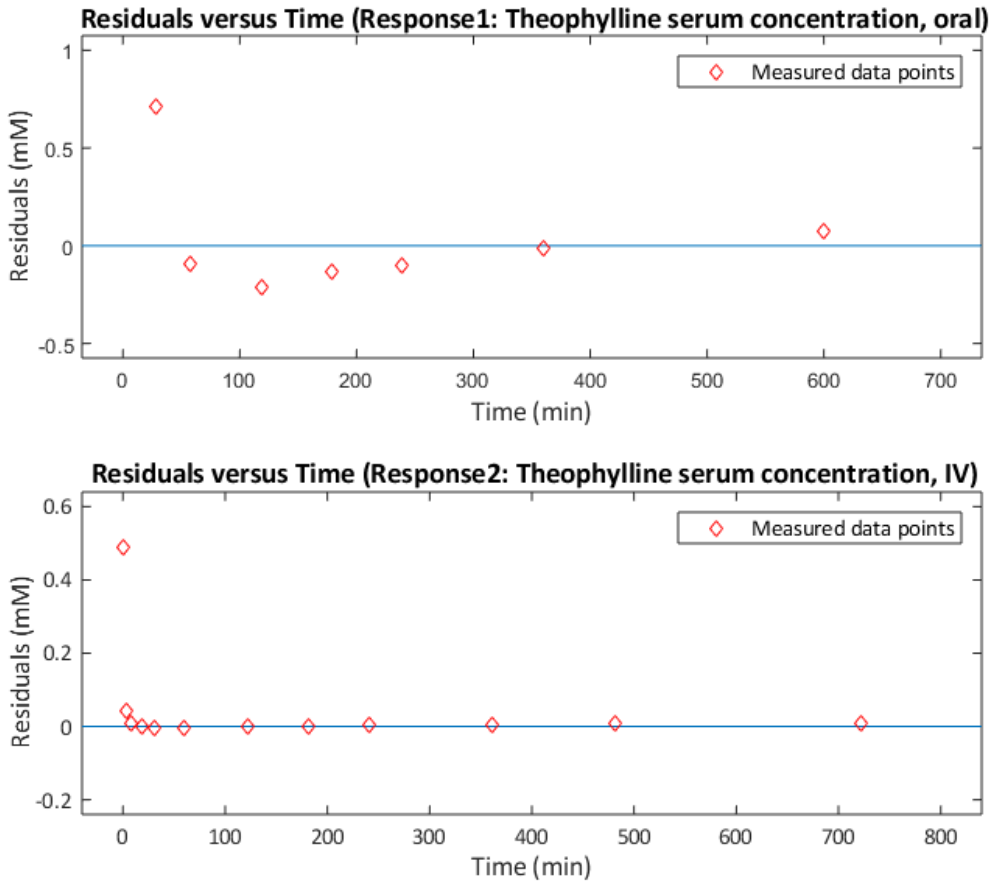

Figure 3.B.9: Residual distribution of theophylline fit (blue line) in relation to data points measured by Aslaksen et al. (1981)

Appendix 4.A: Ordinary differential equations (ODEs) for renal blood, cellular and luminal compartments of the mechanistic kidney model

All terms presented here are defined in subchapters 4.2.1.2 and 4.2.2.1 to 4.2.2.5. **Compartments**: GB = glomerular blood; GS = glomerular space; $PTB1-3$ = proximal tubular blood 1-3; HLB = Loop of Henle blood; DTB = distal tubular blood; CDB = collecting duct blood 1-2; $PTC1-3$ = proximal tubular cells 1-3; HLC = Loop of Henle cells; DTC = distal tubular cells; $CDC1-2$ = collecting duct cells 1-2; $PTL1-3$ = proximal tubular lumen 1-3; HLL = Loop of Henle lumen; DTL = distal tubular lumen; $CDL1-2$ = collecting duct lumen 1-2; KI = kidney; AR = arterial blood; VE = venous blood; BL = bladder; **Concentrations**: SA = SA concentration in respective compartment; SU = SU concentration in respective compartment; $glucs$ = glucuronide concentration in respective compartment; **Blood and fluid flows**: GFR = glomerular filtration rate; Q_{KI} = renal blood flow rate; Q_{HL-CD2} = blood flow in loop of Henle and collecting ducts; FF_{PT} = fluid flow leaving the glomerular space and proximal tubules; FF_{HL} = fluid flow leaving the loop of Henle; FF_{DT} = fluid flow leaving the distal tubules and collecting ducts.

For each blood compartment, the ODE represents the change in SA concentration within that compartment driven by blood flows (Q_{KI} and Q_{HL-CD2}), the glomerular filtration rate (GFR), and unidirectional active and bidirectional passive transport to cellular compartments. Active transport is expressed by the fraction unbound and Michaelis-Menten terms (e.g. $\frac{J_{max}\, C_{blood}\, f_{u(p)}}{K_m + C_{blood}}$) and passive transport occurs due to a concentration gradient between the capillary and cells ($P_{diff,u}\, C_{blood} - P_{diff,u}\, C_{cells}$).

In cellular compartments, the change in concentration of SA, SU and glucuronides (glucs), occurs due to a concentration gradient between the capillary and cells, and cells and the tubular lumen ($P_{diff,u}\, C_{blood} - P_{diff,u}\, C_{cells}$ and $P_{diff,u}\, C_{cells} - P_{diff,u}\, C_{lumen}$) and active transport between these compartments, expressed by Michaelis-Menten terms (e.g. $\frac{J_{max}\, C_{cells}}{K_m + C_{cells}}$).

Metabolism in cellular compartments is also expressed as Michaelis-Menten term (e.g. $\frac{V_{max}\, C_{cells}}{K_m + C_{cells}}$). For each luminal compartment, the ODE represents the change in

SA concentration within that compartment driven by fluid flow rates (FF_{PT}, FF_{HL} and FF_{DT}) determining the flow of filtrate through luminal compartments and into the bladder, and active transport and passive diffusion to and from cellular compartments. Throughout t is time and concentration is measured in the unit mM.

For the young and healthy adult, blood flow, fluid flow and GFR are defined in subchapters 4.2.1.2. All active transport related K_m and J_{max} values for the young and healthy adult are shown in Table 4.6 and in subchapter 4.2.2.4. Passive diffusion determining parameter values are outlined in Tables 4.7. Parameter values for metabolism related Michaelis-Menten terms are presented in Table 4.9 and 4.10.

For the elderly individuals, amended blood flow, fluid flow, GFR, J_{max}, $P_{diff,u}$ and V_{max} values are stated in Tables 4.16 to 4.19.

All compartment volumes (e.g. $V_{compartment}$, for all compartments defined above) are given in Table 4.3.

4.A.1 Blood compartments

1. Glomerular blood (GB)

$$\frac{dC_{GB}}{dt} = \frac{1}{V_{GB}}\left(Q_{KI}\left(C_{AR_{SA}} - C_{GB}\right) - GFR\, f_{u(p)}\, C_{GB}\right)$$

2. Proximal tubular blood 1 ($PTB1$)

$$\frac{dC_{PTB1}}{dt} = \frac{1}{V_{PTB1}}\Bigg(Q_{KI}\,(C_{GB} - C_{PTB1}) - C_{PTB1}\, f_{u(p)}\left(\frac{J_{\max(\mathrm{OCT2})}}{K_{m(OCT2)} + C_{PTB1}} + \frac{J_{\max(OAT1)}}{K_{m(OAT1)} + C_{PTB1}} + \frac{J_{\max(OAT2)}}{K_{m(OAT2)} + C_{PTB1}} + \frac{J_{\max(OAT3)}}{K_{m(OAT3)} + C_{PTB1}}\right) - \left(P_{diff,u(SA)}\, C_{PTB1} - P_{diff,u(SA)}\, C_{PTC1}\right)\Bigg)$$

3. Proximal tubular blood 2 ($PTB2$)

$$\frac{dC_{PTB2}}{dt} = \frac{1}{V_{PTB2}}\Bigg(Q_{KI}\,(C_{PTB1} - C_{PTB2}) - C_{PTB2}\,f_{u(p)}\Bigg(\frac{J_{\max(\mathrm{OCT2})}}{K_{m(OCT2)} + C_{PTB2}} + \frac{J_{\max(OAT1)}}{K_{m(OAT1)} + C_{PTB2}} + \frac{J_{\max(OAT2)}}{K_{m(OAT2)} + C_{PTB2}} + \frac{J_{\max(OAT3)}}{K_{m(OAT3)} + C_{PTB2}}\Bigg) - \left(P_{diff,u(SA)}\,C_{PTB2} - P_{diff,u(SA)}\,C_{PTC2}\right)\Bigg)$$

4. Proximal tubular blood 3 ($PTB3$)

$$\frac{dC_{PTB3}}{dt} = \frac{1}{V_{PTB3}}\Bigg(Q_{KI}\,(C_{PTB2} - C_{PTB3}) - Q_{HL-CD}\,C_{PTB3} - C_{PTB3}\,f_{u(p)}\Bigg(\frac{J_{\max(\mathrm{OCT2})}}{K_{m(OCT2)} + C_{PTB3}} + \frac{J_{\max(OAT1)}}{K_{m(OAT1)} + C_{PTB3}} + \frac{J_{\max(OAT2)}}{K_{m(OAT2)} + C_{PTB3}} + \frac{J_{\max(OAT3)}}{K_{m(OAT3)} + C_{PTB3}}\Bigg) - \left(P_{diff,u(SA)}\,C_{PTB3} - P_{diff,u(SA)}\,C_{PTC3}\right)\Bigg)$$

5. Loop of Henle blood (HLB)

$$\frac{dC_{HLB}}{dt} = \frac{1}{V_{HLB}}\Bigg(Q_{HL-CD2}\,(C_{PTB3} - C_{HLB}) - C_{HLB}\,f_{u(p)}\frac{J_{\max(OAT1)}}{K_{m(OAT1)} + C_{HLB}} - \left(P_{diff,u(SA)}\,C_{HLB} - P_{diff,u(SA)}\,C_{HLC}\right)\Bigg)$$

6. Distal tubular blood (DTB)

$$\frac{dC_{DTB}}{dt} = \frac{1}{V_{DTB}}\Bigg(Q_{KI}\,(C_{PTB3} - C_{DTB}) - C_{DTB}\,f_{u(p)}\frac{J_{\max(OAT1)}}{K_{m(OAT1)} + C_{DTB}} - \left(P_{diff,u(SA)}\,C_{DTB} - P_{diff,u(SA)}\,C_{DTC}\right)\Bigg)$$

7. Collecting duct blood 1 ($CDB1$)

$$\frac{dC_{CDB1}}{dt} = \frac{1}{V_{CDB1}}\Bigg(Q_{KI}\,(C_{DTB} - C_{CDB1}) - C_{CDB1}\,f_{u(p)}\frac{J_{\max(OAT1)}}{K_{m(OAT1)} + C_{CDB1}} - \left(P_{diff,u(SA)}\,C_{CDB1} - P_{diff,u(SA)}\,C_{CDC1}\right)\Bigg)$$

8. Collecting duct blood 2 ($CDB2$)

$$\frac{dC_{CDB2}}{dt} = \frac{1}{V_{CDB2}}\left(Q_{HL-CD2}\,(C_{HLB} - C_{CDB2}) - C_{CDB2}\,f_{u(p)}\frac{J_{\max(OAT1)}}{K_{m(OAT1)} + C_{CDB2}} - \left(P_{diff,u(SA)}\,C_{CDB2} - P_{diff,u(SA)}\,C_{CDC2}\right)\right)$$

4.A.2 Cellular compartments

9. Proximal tubular cells 1-3 ($PTC1, PTC2, PTC3$)

$$\frac{dC_{PTCi}}{dt} = \frac{1}{V_{PTCi}}\left(C_{PTBi}\,f_{u(p)}\left(\frac{J_{\max(\mathrm{OCT2})}}{K_{m(OCT2)} + C_{PTBi}} + \frac{J_{\max(OAT1)}}{K_{m(OAT1)} + C_{PTBi}} + \frac{J_{\max(OAT2)}}{K_{m(OAT2)} + C_{PTBi}} + \frac{J_{\max(OAT3)}}{K_{m(OAT3)} + C_{PTBi}}\right) + C_{PTLi}\left(\frac{J_{\max(OAT4)}}{K_{m(OAT4)} + C_{PTLi}} + \frac{J_{\max(URAT1)}}{K_{m(URAT1)} + C_{PTLi}}\right) - C_{PTCi}\left(\frac{J_{\max(OAT4)}}{K_{m(OAT4)} + C_{PTCi}} + \frac{J_{\max(NPT1)}}{K_{m(NPT1)} + C_{PTCi}} + \frac{V_{\max(SU)}}{K_{m(SU)} + C_{PTCi}} + \frac{V_{\max(PhenUGT1A6)PTCi}}{K_{m(PhenUGT1A6)} + C_{PTCi}} + \frac{V_{\max(AcylUGT1A6)PTCi}}{K_{m(AcylUGT1A6)} + C_{PTCi}} + \frac{V_{\max(PhenUGT1A9)PTCi}}{K_{m(PhenUGT1A9)} + C_{PTCi}} + \frac{V_{\max(AcylUGT1A9)PTCi}}{K_{m(AcylUGT1A9)} + C_{PTCi}} + \frac{V_{\max(PhenUGT2B7)PTCi}}{K_{m(PhenUGT2B7)} + C_{PTCi}} + \frac{V_{\max(AcylUGT2B7)PTCi}}{K_{m(AcylUGT2B7)} + C_{PTCi}}\right) + \left(P_{diff,u(SA)}\,C_{PTBi} - P_{diff,u(SA)}\,C_{PTCi}\right) - \left(P_{diff,u(SA)}\,C_{PTCi} - P_{diff,u(SA)}\,C_{PTLi}\right)\right)$$

$i = 1 - 3$; where i refers to the section of proximal tubule (see Figures 4.2 and 4.3).

10. SU in proximal tubular cells 1-3 ($PTC1_{SU}, PTC2_{SU}, PTC2_{SU}$)

$$\frac{dC_{PTCi_{SU}}}{dt} = \frac{1}{V_{PTC1}}\left(C_{PTCi}\left(\frac{V_{\max(SU)}}{K_{m(SU)} + C_{PTCi}}\right) - C_{PTCi_{SU}}\,\frac{J_{\max(OATmets)}}{K_{m(OATmets)} + C_{PTCi_{SU}}} - \left(P_{diff,u(SU)}\,C_{PTCi_{SU}} - P_{diff,u(SU)}\,C_{PTLi_{SU}}\right)\right)$$

$i = 1 - 3$; where i refers to the section of proximal tubule (see Figures 4.2 and 4.3).

11. Glucuronides in proximal tubular cells 1-3
$(PTC1_{glucs}, PTC2_{glucs}, PTC3_{glucs})$

$$\frac{dC_{PTCi_{glucs}}}{dt} = \frac{1}{V_{PTC1}}\Bigg(C_{PTCi}\left(\frac{V_{\max(PhenUGT1A6)PTCi}}{K_{m(PhenUGT1A6)} + C_{PTCi}} + \frac{V_{\max(AcylUGT1A6)PTCi}}{K_{m(AcylUGT1A6)} + C_{PTCi}} + \frac{V_{\max(PhenUGT1A9)PTCi}}{K_{m(PhenUGT1A9)} + C_{PTCi}} + \frac{V_{\max(AcylUGT1A9)PTCi}}{K_{m(AcylUGT1A9)} + C_{PTCi}} + \frac{V_{\max(PhenUGT2B7)PTCi}}{K_{m(PhenUGT2B7)} + C_{PTCi}} + \frac{V_{\max(AcylUGT2B7)PTCi}}{K_{m(AcylUGT2B7)} + C_{PTCi}}\right) - C_{PTCi_{glucs}}\frac{J_{\max(OATmets)}}{K_{m(OATmets)} + C_{PTCi_{glucs}}} - \left(P_{diff,u(glucs)}\, C_{PTCi_{glucs}} - P_{diff,u(glucs)}\, C_{PTLi_{glucs}}\right)\Bigg)$$

$i = 1 - 3$; where i refers to the section of proximal tubule (see Figures 4.2 and 4.3).

12. Loop of Henle cells (HLC)

$$\frac{dC_{HLC}}{dt} = \frac{1}{V_{HLC}}\Bigg(C_{HLB}\, f_{u(p)}\frac{J_{\max(OAT1)}}{K_{m(OAT1)} + C_{HLB}} - C_{HLC}\frac{J_{\max(OAT1)}}{K_{m(OAT1)} + C_{HLC}} + \left(P_{diff,u(SA)}\, C_{HLB} - P_{diff,u(SA)}\, C_{HLC}\right) - \left(P_{diff,u(SA)}\, C_{HLC} - P_{diff,u(SA)}\, C_{HLL}\right) - C_{HLC}\left(\frac{V_{\max(SU)}}{K_{m(SU)} + C_{HLC}} + \frac{V_{\max(PhenUGT1A6)HLC}}{K_{m(PhenUGT1A6)} + C_{HLC}} + \frac{V_{\max(AcylUGT1A6)HLC}}{K_{m(AcylUGT1A6)} + C_{HLC}} + \frac{V_{\max(PhenUGT1A9)HLC}}{K_{m(PhenUGT1A9)} + C_{HLC}} + \frac{V_{\max(AcylUGT1A9)HLC}}{K_{m(AcylUGT1A9)} + C_{HLC}} + \frac{V_{\max(PhenUGT2B7)HLC}}{K_{m(PhenUGT2B7)} + C_{HLC}} + \frac{V_{\max(AcylUGT2B7)HLC}}{K_{m(AcylUGT2B7)} + C_{HLC}}\right)\Bigg)$$

13. Distal tubular cells (DTC)

$$\frac{dC_{DTC}}{dt} = \frac{1}{V_{DTC}}\left(C_{DTB}\, f_{u(p)} \frac{J_{\max(OAT1)}}{K_{m(OAT1)} + C_{DTB}} - C_{DTC}\, \frac{J_{\max(OAT1)}}{K_{m(OAT1)} + C_{DTC}}\right.$$
$$+ \left(P_{diff,u(SA)}\, C_{DTB} - P_{diff,u(SA)}\, C_{DTC}\right)$$
$$- \left(P_{diff,u(SA)}\, C_{DTC} - P_{diff,u(SA)}\, C_{DTL}\right)$$
$$- C_{DTC}\left(\frac{V_{\max(SU)}}{K_{m(SU)} + C_{DTC}}\right.$$
$$+ \frac{V_{\max(PhenUGT1A6)DTC}}{K_{m(PhenUGT1A6)} + C_{DTC}} + \frac{V_{\max(AcylUGT1A6)DTC}}{K_{m(AcylUGT1A6)} + C_{DTC}}$$
$$+ \frac{V_{\max(PhenUGT1A9)DTC}}{K_{m(PhenUGT1A9)} + C_{DTC}} + \frac{V_{\max(AcylUGT1A9)DTC}}{K_{m(AcylUGT1A9)} + C_{DTC}}$$
$$\left.\left. + \frac{V_{\max(PhenUGT2B7)DTC}}{K_{m(PhenUGT2B7)} + C_{DTC}} + \frac{V_{\max(AcylUGT2B7)DTC}}{K_{m(AcylUGT2B7)} + C_{DTC}}\right)\right)$$

14. Collecting duct cells 1-2 ($CDC1, CDC2$)

$$\frac{dC_{CDCi}}{dt} = \frac{1}{V_{CDCi}}\left(C_{CDBi}\, f_{u(p)} \frac{J_{\max(OAT1)}}{K_{m(OAT1)} + C_{CDBi}} - C_{CDCi}\, \frac{J_{\max(OAT1)}}{K_{m(OAT1)} + C_{CDCi}}\right.$$
$$+ \left(P_{diff,u(SA)}\, C_{CDBi} - P_{diff,u(SA)}\, C_{CDCi}\right)$$
$$- \left(P_{diff,u(SA)}\, C_{CDCi} - P_{diff,u(SA)}\, C_{CDLi}\right)$$
$$- C_{CDCi}\left(\frac{V_{\max(SU)}}{K_{m(SU)} + C_{CDCi}}\right.$$
$$+ \frac{V_{\max(PhenUGT1A6)CDCi}}{K_{m(PhenUGT1A6)} + C_{CDCi}} + \frac{V_{\max(AcylUGT1A6)CDCi}}{K_{m(AcylUGT1A6)} + C_{CDCi}}$$
$$+ \frac{V_{\max(PhenUGT1A9)CDCi}}{K_{m(PhenUGT1A9)} + C_{CDCi}} + \frac{V_{\max(AcylUGT1A9)CDCi}}{K_{m(AcylUGT1A9)} + C_{CDCi}}$$
$$\left.\left. + \frac{V_{\max(PhenUGT2B7)CDCi}}{K_{m(PhenUGT2B7)} + C_{CDCi}} + \frac{V_{\max(AcylUGT2B7)CDCi}}{K_{m(AcylUGT2B7)} + C_{CDCi}}\right)\right)$$

$i = 1 - 2$; where i refers to the section of proximal tubule (see Figures 4.2 and 4.3).

15. SU in loop of Henle cells (HLC_{SU})

$$\frac{dC_{HLC_{SU}}}{dt} = \frac{1}{V_{HLC}}\left(C_{HLC}\, \frac{V_{\max(SU)}}{K_{m(SU)} + C_{HLC}} - C_{HLC_{SU}}\, \frac{J_{\max(OATmets)}}{K_{m(OATmets)} + C_{HLC_{SU}}}\right.$$
$$\left. - \left(P_{diff,u(SU)}\, C_{HLC_{SU}} - P_{diff,u(SU)}\, C_{HLL_{SU}}\right)\right)$$

16. Glucuronides in loop of Henle cells (HLC_{glucs})

$$\frac{dC_{HLC_{glucs}}}{dt} = \frac{1}{V_{HLC}}\Bigg(C_{HLC}\left(\frac{V_{\max(PhenUGT1A6)HLC}}{K_{m(PhenUGT1A6)}+C_{HLC}}+\frac{V_{\max(AcylUGT1A6)HLC}}{K_{m(AcylUGT1A6)}+C_{HLC}}+\frac{V_{\max(PhenUGT1A9)HLC}}{K_{m(PhenUGT1A9)}+C_{HLC}}+\frac{V_{\max(AcylUGT1A9)HLC}}{K_{m(AcylUGT1A9)}+C_{HLC}}+\frac{V_{\max(PhenUGT2B7)HLC}}{K_{m(PhenUGT2B7)}+C_{HLC}}+\frac{V_{\max(AcylUGT2B7)HLC}}{K_{m(AcylUGT2B7)}+C_{HLC}}\right) - C_{HLC_{glucs}}\frac{J_{\max(OATmets)}}{K_{m(OATmets)}+C_{HLC_{glucs}}} - \left(P_{diff,u(glucs)}\,C_{HLC_{glucs}} - P_{diff,u(glucs)}\,C_{HLL_{glucs}}\right)\Bigg)$$

17. SU in distal tubular cells (DTC_{SU})

$$\frac{dC_{DTC_{SU}}}{dt} = \frac{1}{V_{DTC}}\Bigg(C_{DTC}\frac{V_{\max(SU)}}{K_{m(SU)}+C_{DTC}} - C_{DTC_{SU}}\frac{J_{\max(OATmets)}}{K_{m(OATmets)}+C_{DTC_{SU}}} - \left(P_{diff,u(SU)}\,C_{DTC_{SU}} - P_{diff,u(SU)}\,C_{DTL_{SU}}\right)\Bigg)$$

18. Glucuronides in distal tubular cells (DTC_{glucs})

$$\frac{dC_{DTC_{glucs}}}{dt} = \frac{1}{V_{DTC}}\Bigg(C_{DTC}\left(\frac{V_{\max(PhenUGT1A6)DTC}}{K_{m(PhenUGT1A6)}+C_{DTC}}+\frac{V_{\max(AcylUGT1A6)DTC}}{K_{m(AcylUGT1A6)}+C_{DTC}}+\frac{V_{\max(PhenUGT1A9)DTC}}{K_{m(PhenUGT1A9)}+C_{DTC}}+\frac{V_{\max(AcylUGT1A9)DTC}}{K_{m(AcylUGT1A9)}+C_{DTC}}+\frac{V_{\max(PhenUGT2B7)DTC}}{K_{m(PhenUGT2B7)}+C_{DTC}}+\frac{V_{\max(AcylUGT2B7)DTC}}{K_{m(AcylUGT2B7)}+C_{DTC}}\right) - C_{DTC_{glucs}}\frac{J_{\max(OATmets)}}{K_{m(OATmets)}+C_{DTC_{glucs}}} - \left(P_{diff,u(glucs)}\,C_{DTC_{glucs}} - P_{diff,u(glucs)}\,C_{DTL_{glucs}}\right)\Bigg)$$

19. SU in collecting duct cells 1-2 ($CDC1_{SU}, CDC2_{SU}$)

$$\frac{dC_{CDCi_{SU}}}{dt} = \frac{1}{V_{CDCi}}\Bigg(C_{CDCi}\frac{V_{\max(SU)}}{K_{m(SU)}+C_{CDCi}} - C_{CDCi_{SU}}\frac{J_{\max(OATmets)}}{K_{m(OATmets)}+C_{CDCi_{SU}}} - \left(P_{diff,u(SU)}\,C_{CDCi_{SU}} - P_{diff,u(SU)}\,C_{CDLi_{SU}}\right)\Bigg)$$

$i = 1 - 2$; where i refers to the section of proximal tubule (see Figures 4.2 and 4.3).

20. Glucuronides in collecting duct cells 1-2 ($CDC1_{glucs}, CDC2_{glucs}$)

$$\frac{dC_{CDCi_{glucs}}}{dt} = \frac{1}{V_{CDCi}}\Bigg(C_{CDCi}\left(\frac{V_{\max(PhenUGT1A6)CDCi}}{K_{m(PhenUGT1A6)} + C_{CDCi}} + \frac{V_{\max(AcylUGT1A6)CDCi}}{K_{m(AcylUGT1A6)} + C_{CDCi}} + \frac{V_{\max(PhenUGT1A9)CDCi}}{K_{m(PhenUGT1A9)} + C_{CDCi}} + \frac{V_{\max(AcylUGT1A9)CDCi}}{K_{m(AcylUGT1A9)} + C_{CDCi}} + \frac{V_{\max(PhenUGT2B7)CDCi}}{K_{m(PhenUGT2B7)} + C_{CDCi}} + \frac{V_{\max(AcylUGT2B7)CDCi}}{K_{m(AcylUGT2B7)} + C_{CDCi}}\right) - C_{CDCi_{glucs}} \frac{J_{\max(OATmets)}}{K_{m(OATmets)} + C_{CDCi_{glucs}}} - \left(P_{diff,u(glucs)}\, C_{CDCi_{glucs}} - P_{diff,u(glucs)}\, C_{CDLi_{glucs}}\right)\Bigg)$$

$i = 1 - 2$; where i refers to the section of proximal tubule (see Figures 4.2 and 4.3).

4.A.3 Luminal compartments

21. Glomerular space (GS)

$$\frac{dC_{GS}}{dt} = \frac{1}{V_{GS}}\left(GFR\, f_{u(p)}\, C_{GB} - FF_{PT}\, C_{GS}\right)$$

22. Proximal tubular lumen 1-3 ($PTL1, PTL2, PTL3$)

$$\frac{dC_{PTLi}}{dt} = \frac{1}{V_{PTLi}}\Bigg(FF_{PT}\,(C_{PTLi-1} - C_{PTLi}) - C_{PTLi}\left(\frac{J_{\max(OAT4)}}{K_{m(OAT4)} + C_{PTLi}} + \frac{J_{\max(URAT1)}}{K_{m(URAT1)} + C_{PTLi}}\right) + C_{PTCi}\left(\frac{J_{\max(OAT4)}}{K_{m(OAT4)} + C_{PTCi}} + \frac{J_{\max(NPT1)}}{K_{m(NPT1)} + C_{PTCi}}\right) + \left(P_{diff,u(SA)}\, C_{PTCi} - P_{diff,u(SA)}\, C_{PTLi}\right)\Bigg)$$

$i = 1 - 3$; where i refers to the section of proximal tubule (see Figures 4.2 and 4.3).

C_{PTLi-1} refers to the concentration of SA in the segment preceding the current proximal tubular lumen section, i.e $PTL1 - 1 = GS; PTL2 - 1 = PTL1;\ PTL3 - 1 = PTL2$.

23. SU in proximal tubular lumen 1 ($PTL1_{SU}$)

$$\frac{dC_{PTL1_{SU}}}{dt} = \frac{1}{V_{PTL1}}\left(C_{PTC1_{SU}}\ \frac{J_{\max(OATmets)}}{K_{m(OATmets)} + C_{PTC1_{SU}}} + \left(P_{diff,u(SU)}\ C_{PTC1_{SU}} - P_{diff,u(SU)}\ C_{PTL1_{SU}}\right) - FF_{PT}\ C_{PTL1_{SU}}\right)$$

24. SU in proximal tubular lumen 2-3 ($PTL2_{SU}, PTL3_{SU}$)

$$\frac{dC_{PTLi_{SU}}}{dt} = \frac{1}{V_{PTLi}}\left(C_{PTCi_{SU}}\ \frac{J_{\max(OATmets)}}{K_{m(OATmets)} + C_{PTCi_{SU}}} + \left(P_{diff,u(SU)}\ C_{PTCi_{SU}} - P_{diff,u(SU)}\ C_{PTLi_{SU}}\right) + FF_{PT}\ \left(C_{PTLi-1_{SU}} - C_{PTLi_{SU}}\right)\right)$$

$i = 2 - 3$; where i refers to the section of proximal tubule (see Figures 4.2 and 4.3).

$C_{PTLi-1_{SU}}$ refers to the concentration of SU in the previous proximal tubular lumen section, i.e. $PTL2 - 1 = PTL1;\ PTL3 - 1 = PTL2$.

25. Glucuronides in proximal tubular lumen 1 ($PTL1_{glucs}$)

$$\frac{dC_{PTL1_{glucs}}}{dt} = \frac{1}{V_{PTL1}}\left(C_{PTC1_{glucs}}\ \frac{J_{\max(OATmets)}}{K_{m(OATmets)} + C_{PTC1_{glucs}}} + \left(P_{diff,u(glucs)}\ C_{PTC1_{glucs}} - P_{diff,u(glucs)}\ C_{PTL1_{glucs}}\right) - FF_{PT}\ C_{PTL1_{glucs}}\right)$$

26. Glucuronides in proximal tubular lumen 2-3 ($PTL2_{glucs}, PTL3_{glucs}$)

$$\frac{dC_{PTLi_{glucs}}}{dt} = \frac{1}{V_{PTLi}}\left(C_{PTCi_{glucs}}\ \frac{J_{\max(OATmets)}}{K_{m(OATmets)} + C_{PTCi_{glucs}}} + \left(P_{diff,u(glucs)}\ C_{PTCi_{glucs}} - P_{diff,u(glucs)}\ C_{PTLi_{glucs}}\right) + FF_{PT}\ \left(C_{PTLi-1_{glucs}} - C_{PTLi_{glucs}}\right)\right)$$

$i = 2 - 3$; where i refers to the section of proximal tubule (see Figures 4.2 and 4.3).

$C_{PTLi-1_{glucs}}$ refers to the concentration of glucuronides in the previous proximal tubular lumen section, i.e. $PTL2 - 1 = PTL1;\ PTL3 - 1 = PTL2$.

27. Loop of Henle lumen (HLL)

$$\frac{dC_{HLL}}{dt} = \frac{1}{V_{HLL}}\left(FF_{PT}\ C_{PTL3} - FF_{HL}\ C_{HLL} + C_{HLC}\ \frac{J_{\max(OAT1)}}{K_{m(OAT1)} + C_{HLC}} + \left(P_{diff,u(SA)}\ C_{HLC} - P_{diff,u(SA)}\ C_{HLL}\right)\right)$$

28. Distal tubular lumen (DTL)

$$\frac{dC_{DTL}}{dt} = \frac{1}{V_{DTL}}\left(FF_{HL}\ C_{HLL} - FF_{DT}\ C_{DTL} + C_{DTC}\ \frac{J_{\max(OAT1)}}{K_{m(OAT1)} + C_{DTC}} + \left(P_{diff,u(SA)}\ C_{DTC} - P_{diff,u(SA)}\ C_{DTL}\right)\right)$$

29. Collecting duct lumen 1-2 $(CDL1, CDL2)$

$$\frac{dC_{CDLi}}{dt} = \frac{1}{V_{CDLi}}\left(FF_{DT}\ (C_{CDLi-1} - C_{CDLi}) + C_{CDCi}\ \frac{J_{\max(OAT1)}}{K_{m(OAT1)} + C_{CDCi}} + \left(P_{diff,u(SA)}\ C_{CDCi} - P_{diff,u(SA)}\ C_{CDLi}\right)\right)$$

$i = 1 - 2$; where i refers to the section of collecting duct (see Figures 4.2 and 4.3).

C_{CDLi-1} refers to the concentration of SA in the segment preceding the current collecting duct lumen section, i.e. $CDL1 - 1 = DTL;\ CDL2 - 1 = CDL1$.

30. SU in loop of Henle lumen (HLL_{SU})

$$\frac{dC_{HLL_{SU}}}{dt} = \frac{1}{V_{HLL}}\left(FF_{PT}\ C_{PTL3_{SU}} - FF_{HL}\ C_{HLL_{SU}} + C_{HLC_{SU}}\ \frac{J_{\max(OATmets)}}{K_{m(OATmets)} + C_{HLC_{SU}}} + \left(P_{diff,u(SU)}\ C_{HLC_{SU}} - P_{diff,u(SU)}\ C_{HLL_{SU}}\right)\right)$$

31. Glucuronides in loop of Henle lumen (HLL_{glucs})

$$\frac{dC_{HLL_{glucs}}}{dt} = \frac{1}{V_{HLL}}\left(FF_{PT}\ C_{PTL3_{glucs}} - FF_{HL}\ C_{HLL_{glucs}} + C_{HLC_{glucs}}\ \frac{J_{\max(OATmets)}}{K_{m(OATmets)} + C_{HLC_{glucs}}} + \left(P_{diff,u(glucs)}\ C_{HLC_{glucs}} - P_{diff,u(glucs)}\ C_{HLL_{glucs}}\right)\right)$$

32. SU in distal tubular lumen (DTL_{SU})

$$\frac{dC_{DTL_{SU}}}{dt} = \frac{1}{V_{DTL}}\left(FF_{HL}\ C_{HLL_{SU}} - FF_{DT}\ C_{DTL_{SU}} + C_{DTC_{SU}}\ \frac{J_{\max(OATmets)}}{K_{m(OATmets)} + C_{DTC_{SU}}} + \left(P_{diff,u(SU)}\ C_{DTC_{SU}} - P_{diff,u(SU)}\ C_{DTL_{SU}}\right)\right)$$

33. Glucuronides in distal tubular lumen $\left(DTL_{glucs}\right)$

$$\frac{dC_{DTL_{glucs}}}{dt} = \frac{1}{V_{DTL}}\left(FF_{HL}\ C_{HLL_{glucs}} - FF_{DT}\ C_{DTL_{glucs}} + C_{DTC_{glucs}}\ \frac{J_{\max(OATmets)}}{K_{m(OATmets)} + C_{DTC_{glucs}}} + \left(P_{diff,u(glucs)}\ C_{DTC_{glucs}} - P_{diff,u(glucs)}\ C_{DTL_{glucs}}\right)\right)$$

34. SU in collecting duct lumen 1-2 ($CDL1_{SU}, CDL2_{SU}$)

$$\frac{dC_{CDLi_{SU}}}{dt} = \frac{1}{V_{CDLi}}\left(FF_{DT}\left(C_{CDLi-1_{SU}} - C_{CDLi_{SU}}\right) + C_{CDCi_{SU}}\ \frac{J_{\max(OATmets)}}{K_{m(OATmets)} + C_{CDCi_{SU}}} + \left(P_{diff,u(SU)}\ C_{CDCi_{SU}} - P_{diff,u(SU)}\ C_{CDLi_{SU}}\right)\right)$$

$i = 1 - 2$; where i refers to the section of collecting duct (see Figures 4.2 and 4.3).

$C_{CDLi-1_{SU}}$ refers to the concentration of SU in the segment preceding the current collecting duct lumen section, i.e. $CDL1 - 1 = DTL;\ CDL2 - 1 = CDL1$.

35. Glucuronides in collecting duct lumen 1-2 $\left(CDL1_{glucs}, CDL2_{glucs}\right)$

$$\frac{dC_{CDLi_{glucs}}}{dt} = \frac{1}{V_{CDLi}}\left(FF_{DT}\ \left(C_{CDLi-1_{glucs}} - C_{CDLi_{glucs}}\right) + C_{CDCi_{glucs}}\ \frac{J_{\max(OATmets)}}{K_{m(OATmets)} + C_{CDCi_{glucs}}} + \left(P_{diff,u(glucs)}\ C_{CDCi_{glucs}} - P_{diff,u(glucs)}\ C_{CDLi_{glucs}}\right)\right)$$

$i = 1 - 2$; where i refers to the section of collecting duct (see Figures 4.2 and 4.3).

$C_{CDLi-1_{glucs}}$ refers to the concentration of glucuronides in the segment preceding the current collecting duct lumen section, i.e. $CDL1 - 1 = DTL;\ CDL2 - 1 = CDL1$.

36. Urine

$$\frac{dC_{urine}}{dt} = \frac{1}{V_{BL}}\ (FF_{DT}\ C_{CDL2})$$

37. SU in urine

$$\frac{dC_{urine_{SU}}}{dt} = \frac{1}{V_{BL}}\ \left(FF_{DT}\ C_{CDL2_{SU}}\right)$$

38. Glucuronides in urine

$$\frac{dC_{urine_{glucs}}}{dt} = \frac{1}{V_{BL}}\ \left(FF_{DT}\ C_{CDL2_{glucs}}\right)$$

39. SA arterial blood (AR_{SA})

$$\frac{dC_{AR_{SA}}}{dt} = \frac{1}{V_{AR}}\left(Q_{LU}\frac{C_{LU_{SA}} \times R_{SA}}{K_{p_{SA}}}\right) - \sum_i \frac{Q_i \times C_{AR_{SA}}}{V_{AR}} - Q_{KI}\frac{\left(C_{AR_{SA}} - C_{GB}\right)}{V_{AR}}$$

where *i* = *HE, HA, ST, GU, SP, TH, PA, AD, MU, BR, SK*; therefore:

$$\sum_i \frac{Q_i \times C_{AR_{SA}}}{V_{AR}} = \frac{Q_{HE} \times C_{AR_{SA}}}{V_{AR}} - \frac{Q_{HA} \times C_{AR_{SA}}}{V_{AR}} - \frac{Q_{ST} \times C_{AR_{SA}}}{V_{AR}} - \frac{Q_{GU} \times C_{AR_{SA}}}{V_{AR}} - \frac{Q_{SP} \times C_{AR_{SA}}}{V_{AR}} - \frac{Q_{TH} \times C_{AR_{SA}}}{V_{AR}} - \frac{Q_{PA} \times C_{AR_{SA}}}{V_{AR}} - \frac{Q_{AD} \times C_{AR_{SA}}}{V_{AR}} - \frac{Q_{MU} \times C_{AR_{SA}}}{V_{AR}} - \frac{Q_{BR} \times C_{AR_{SA}}}{V_{AR}} - \frac{Q_{SK} \times C_{AR_{SA}}}{V_{AR}}$$

40. SA venous blood (VE_{SA})

$$\frac{dC_{VE_{SA}}}{dt} = \frac{1}{V_{VE}}\left(\sum_i \frac{Q_T \times C_{T_{SA}} \times R_{SA}}{K_{p_{SA}}} + Q_{HL-CD2}\ C_{CDB2} + Q_{KI}\ C_{CDB1} - Q_{LU} \times C_{VE_{SA}}\right)$$

Excluding the kidney, gut, pancreas, spleen, stomach, and lung; (no venous infusion rate (VIR) included)

$$\sum_i \frac{Q_T \times C_{T_{SA}} \times R_{SA}}{K_{p_{SA}}} = \frac{Q_{HE} \times C_{HE_{SA}} \times R_{SA}}{K_{p_{SA}}} + \frac{Q_{LI} \times C_{LI_{SA}} \times R_{SA}}{K_{p_{SA}}} + \frac{Q_{TH} \times C_{TH_{SA}} \times R_{SA}}{K_{p_{SA}}} + \frac{Q_{AD} \times C_{AD_{SA}} \times R_{SA}}{K_{p_{SA}}} + \frac{Q_{MU} \times C_{MU_{SA}} \times R_{SA}}{K_{p_{SA}}} + \frac{Q_{BR} \times C_{BR_{SA}} \times R_{SA}}{K_{p_{SA}}} + \frac{Q_{SK} \times C_{SK_{SA}} \times R_{SA}}{K_{p_{SA}}}$$

Appendix 4.B: ODEs and calculations related to the extended PBK model which is coupled to the mechanistic kidney model

4.B.1 Amendments to gut, liver compartments to account for hydrolysis of ASA to SA, and amendments to arterial blood and venous blood compartment ODEs of the full-body PBK model to account for hydrolysis of ASA to SA and terms connecting to the mechanistic kidney model

All terms are defined in Chapter 3 and subchapter 4.2.3. All parameter values for ASA and SA are stated in Tables 4.11 to 4.14. Please note that all chemical-specific parameters stated in 4.B.1.1 to 4.B.1.4 are those of ASA.

4.B.1.1 Gut compartment (GU)

$$\frac{dC_{GU}}{dt} = \frac{1}{V_{GU}} \left(Q_{GU} \left(C_{AR} - \frac{C_{GU} \times R}{K_p} \right) - C_{GU} \frac{V_{max_{hydro(GU)}}}{K_{m_{hydro(GU)}} + C_{GU}} + A_{TIA} \right)$$

where A_{TIA} is defined in equation 25 of Appendix 3.A.2.

4.B.1.2 Liver compartment (LI)

$$\frac{dC_{LI}}{dt} = \frac{1}{V_{LI}} \left(Q_{HA} \times C_{AR} + \sum_i \frac{Q_i \times C_i \times R}{K_p} - \frac{Q_{LI} \times C_{LI} \times R}{K_p} - \frac{C_{LI} \times CL_{int}}{K_p} \times f_{u(p)} - \frac{EHR \times k_{bil} \times C_{LI} \times V_{LI}}{K_p} - \frac{CP \times k_{bil} \times C_{LI} \times V_{LI}}{K_p} - C_{LI} \frac{V_{max_{hydro(LI)}}}{K_{m_{hydro(LI)}} + C_{LI}} \right)$$

where i = *GU* (gut), *ST* (stomach), *PA*, *SP*; therefore:

$$\sum_i \frac{Q_i \times C_i \times R}{K_p} = \frac{Q_{GU} \times C_{GU} \times R}{K_p} + \frac{Q_{PA} \times C_{PA} \times R}{K_p} + \frac{Q_{SP} \times C_{SP} \times R}{K_p} + \frac{Q_{ST} \times C_{ST} \times R}{K_p}$$

4.B.1.3 Arterial blood compartment (AR)

$$\frac{dC_{AR}}{dt} = \frac{1}{V_{AR}} \left(Q_{LU} \frac{C_{LU} \times R}{K_p} - C_{AR} \frac{V_{max_{hydro(AR)}}}{K_{m_{hydro(AR-VE)}} + C_{AR}} \right) - \sum_i \frac{Q_i \times C_{AR}}{V_{AR}}$$

where *i* = *HE*, *HA*, *ST*, *GU*, *SP*, *KI*, *TH*, *PA*, *AD*, *MU*, *BR*, *SK*; therefore:

$$\sum_i \frac{Q_i \times C_{AR}}{V_{AR}} = \frac{Q_{HE} \times C_{AR}}{V_{AR}} - \frac{Q_{HA} \times C_{AR}}{V_{AR}} - \frac{Q_{ST} \times C_{AR}}{V_{AR}} - \frac{Q_{GU} \times C_{AR}}{V_{AR}} - \frac{Q_{SP} \times C_{AR}}{V_{AR}} - \frac{Q_{KI} \times C_{AR}}{V_{AR}} - \frac{Q_{TH} \times C_{AR}}{V_{AR}} - \frac{Q_{PA} \times C_{AR}}{V_{AR}} - \frac{Q_{AD} \times C_{AR}}{V_{AR}} - \frac{Q_{MU} \times C_{AR}}{V_{AR}} - \frac{Q_{BR} \times C_{AR}}{V_{AR}} - \frac{Q_{SK} \times C_{AR}}{V_{AR}}$$

4.B.1.4 Venous blood compartment (VE)

$$\frac{dC_{VE}}{dt} = \frac{1}{V_{VE}} \left(\sum_i \frac{Q_T \times C_T \times R}{K_p} - Q_{LU} \times C_{VE} - C_{VE} \frac{V_{max_{hydro(VE)}}}{K_{m_{hydro(AR-VE)}} + C_{VE}} \right)$$

Excluding the gut, pancreas, spleen, stomach, and lung; (no venous infusion rate (VIR) included)

$$\sum_i \frac{Q_T \times C_T \times R}{K_p} = \frac{Q_{HE} \times C_{HE} \times R}{K_p} + \frac{Q_{LI} \times C_{LI} \times R}{K_p} + \frac{Q_{KI} \times C_{KI} \times R}{K_p} + \frac{Q_{TH} \times C_{TH} \times R}{K_p} + \frac{Q_{AD} \times C_{AD} \times R}{K_p} + \frac{Q_{MU} \times C_{MU} \times R}{K_p} + \frac{Q_{BR} \times C_{BR} \times R}{K_p} + \frac{Q_{SK} \times C_{SK} \times R}{K_p}$$

4.B.2: Conversion factors to scale ASA-hydrolysis related V_{max} values from in nmol/min/mg protein to micromol/min

Conversion factors were derived to convert V_{max} values sourced from Imai et al. (2006) for the rate of hydrolysis of ASA in the liver and gut from nmol/min/mg protein to the *in vivo* rates $V_{max_{hydro(LI)}}$ and $V_{max_{hydro(GU)}}$ in µmol/min. Both conversion factors and all values used to derive these are presented in Table 4.B.2.1.

Table 4.B.2.1: Derivation of conversion factors to scale *in vitro* V_{max} values to the *in vivo* rates $V_{max_{hydro(LI)}}$ and $V_{max_{hydro(GU)}}$

Parameters	Liver[1]	Gut[2]	Reference
mg microsomal protein/g organ	40	NA	[1] Hakooz et al., 2006; Zhang et al., 2015
Organ weight (g)	1400	NA	[1] Johnson et al., 2005
Conversion factor (mg microsomal protein/organ)	56000	2977	[2] Paine et al., 1997